

CHEMIA

**STUDIA
UNIVERSITATIS BABEȘ-BOLYAI
CHEMIA**

3/2017

EDITORIAL BOARD OF STUDIA UNIVERSITATIS BABEȘ-BOLYAI CHEMIA

ONORARY EDITOR:

IONEL HAIDUC - Member of the Romanian Academy

EDITOR-IN-CHIEF:

LUMINIȚA SILAGHI-DUMITRESCU

EXECUTIVE EDITOR:

CASTELIA CRISTEA

EDITORIAL BOARD:

PAUL ȘERBAN AGACHI, Babeș-Bolyai University, Cluj-Napoca, Romania

LIVAIN BREAU, UQAM University of Quebec, Montreal, Canada

HANS JOACHIM BREUNIG, Institute of Inorganic and Physical Chemistry,
University of Bremen, Bremen, Germany

MIRCEA DIUDEA, Babeș-Bolyai University, Cluj-Napoca, Romania

JEAN ESCUDIE, HFA, Paul Sabatier University, Toulouse, France

ION GROSU, Babeș-Bolyai University, Cluj-Napoca, Romania

EVAMARIE HEY-HAWKINS, University of Leipzig, Leipzig, Germany

FLORIN DAN IRIMIE, Babeș-Bolyai University, Cluj-Napoca, Romania

FERENC KILAR, University of Pecs, Pecs, Hungary

BRUCE KING, University of Georgia, Athens, Georgia, USA

ANTONIO LAGUNA, Department of Inorganic Chemistry, ICMA, University of
Zaragoza, Zaragoza, Spain

JURGEN LIEBSCHER, Humboldt University, Berlin, Germany

KIERAN MOLLOY, University of Bath, Bath, UK

IONEL CĂȚĂLIN POPESCU, Babeș-Bolyai University, Cluj-Napoca, Romania

CRISTIAN SILVESTRU, Babeș-Bolyai University, Cluj-Napoca, Romania

<http://chem.ubbcluj.ro/~studiachemia/>; studiachemia@chem.ubbcluj.ro

http://www.studia.ubbcluj.ro/serii/chemia/index_en.html

YEAR
MONTH
ISSUE

Volume 62 (LXII) 2017
SEPTEMBER
3

STUDIA UNIVERSITATIS BABEȘ-BOLYAI CHEMIA

3

ISSUE DOI:10.24193/subbchem.2017.3

STUDIA UBB EDITORIAL OFFICE: B.P. Hasdeu no. 51, 400371 Cluj-Napoca, Romania,
Phone + 40 264 405352

CUPRINS – CONTENT – SOMMAIRE – INHALT

SIMONA CODRUTA COBZAC, In Memoriam prof.dr. Simion Gocan.....	7
NELI-KINGA OLAH, DANIELA HANGANU, EDE BODOKI, RADU OPREAN, CLAUDIA TOMA, CLAUDIU MORGOVAN, ELISABETA CHIȘE, ANDREEA BRAȘOVAN, SIMONA CODRUȚA AURORA COBZAC, <u>SIMION GOCAN</u> , Characterization of <i>Orthosiphon Stamineus</i> Benth Extracts by Reversed-Phase Thin Layer Chromatographic Methods.....	9
ADELA MEGHESAN-BREJA, CLAUDIA CIMPOIU, ANAMARIA HOSU, Identification and Quantification of Some Pesticide Metabolites from Vegetables by GC-TOF-MS and LC-MS-QQQ.....	19
MIHAIL SIMION BELDEAN-GALEA, DIDIER THIEBAUT, JEROME VIAL, VIRGINIA COMAN, Identification of Complex Volatile Organic Compounds in Municipal Landfill Leachate by Head-Space Solid Phase Microextraction and GCXGC-qMS Analysis	35

DORINA CASONI, NELI OLAH, LOREDANA SORAN, SIMONA CODRUTA AURORA COBZAC, Comparison of Different Extraction Techniques for the Evaluation of Polyphenols Content in Summer Savory Extracts	45
NELI-KINGA OLAH, RAMONA BURTESCU, SORINA PETRESCU, ANDREEA BRAȘOVAN, ELISABETA CHIȘE, SIMONA CODRUȚA AURORA COBZAC, DANIELA HANGANU, Phytochemical Screening of Different <i>Crataegus Oxyacantha</i> Extracts	57
TEODORA NEAG, CLAUDIA-CRINA TOMA, NELI OLAH, AUREL ARDELEAN, Polyphenols Profile and Antioxidant Activity of Some Romanian <i>Ranunculus</i> Species	75
DORINA CASONI, MIHAELA BADEA, ILDIKO BROS, SIMONA CODRUTA AURORA COBZAC, Investigation on Image Processing Parameters for Plate Evaluation in TLC Analysis of Mycotoxins	89
LUCA RIVOIRA, MOJCA ZORZ, MITJA MARTELANC, SARA BUDAL, DAVIDE CARENA, MLADEN FRANKO, MARIA CONCETTA BRUZZONITI, Novel Approaches for the Determination of Biogenic Amines in Food Samples.....	103
RAMONA BLEIZIFFER, SONIA SUVAR, PAULA PODEA, CORNELIA MESAROS, MONICA CULEA, Blaj White Wines Characterization	123
ENIKŐ COVACI, EUGEN DARVASI, MICHAELA PONTA, Simultaneous Determination of Zn, Cd, Pb and Cu in Mushrooms by Differential Pulse Anodic Stripping Voltammetry	133
ANA-MARIA SĂCARĂ, LIANA MARIA MUREȘAN, Electrochemical Sensors for Malachite Green Based on Carbonaceous Nanomaterials	145
IOAN BRATU, CONSTANTIN MARUTOIU, DANA POSTOLACHE, CLAUDIU TANASELIA, OLIVIA FLORENA NEMEȘ, The Analysis of Constituent Materials of the Naos Doors Belonging to the Wooden Church from Petrindu, Salaj County.....	157
THOMAS DIPPONG, FIRUTA GOGA, ALEXANDRA AVRAM, Influence of the Cobalt Nitrate:Ethylene Glycol Molar Ratio on the Formation of Carboxylate Precursors and Cobalt Oxides.....	165
SORIN-AUREL DORNEANU, Electrochemical Recycling of Waste Printed Circuit Boards in Bromide Media. Part I: Preliminary Leaching and Dismantling Tests	177
LILIANA BIZO, ADRIANA VULPOI, FIRUȚA GOGA, Enhancement of Physical Properties in ZrO ₂ /Ga ₂ O ₃ Co-Substituted Indium Oxide ...	187

CLAUDIU LUNGU, SARA ERSALI, BEATA SZEFLER, ATENA PÎRVAN-MOLDOVAN, SUBHASH BASAK, MIRCEA V. DIUDEA, Dimensionality of Big Data Sets Explored by Cluj Descriptors	197
ANDREEA ROTARU, EDINA REIZER, VLAD PĂNESCU, SORIN POP, MIHAIL SIMION BELDEAN-GALEA, The Occurrence and Source Evaluation of Polycyclic Aromatic Hydrocarbons in Urban Atmosphere Using Moss as Biomonitor and GC-MS Analysis	205
OLGA HILDA ORASAN, ANDREA MARIA CHISNOIU, MONICA LAURA DASCĂLU (RUSU), OVIDIU PĂSTRAV, MIHAELA PĂSTRAV, MARIOARA MOLDOVAN, RADU CHISNOIU, Optical Properties and Microstructural Changes of Hard Dental Tissues in Gastro-Esophageal Reflux Disease Patients.....	215
SEBASTIAN RADU CRISTIAN PLUGARU, TUDOR RUSU, KATALIN MOLNAR, LASZLO FODORPATAKI, Chromium Removal from Polluted Water And Its Influence on Biochemical and Physiological Parameters in Algal Cells Used for Phytoremediation	225
SEBASTIAN RADU CRISTIAN PLUGARU, LASZLO FODORPATAKI, MIHAELA ORBAN, ANCA SARB, BERNAT TOMPA, BALAZS KOVACS, Comparative Study on Growth and Photosynthetic Pigment Dynamics of Two Microalgae Under the Influence of Water Pollution with the Herbicide Glufosinate	239
AURA RUSU, GABRIEL HANCU, LAVINIA BERȚA, CAMIL EUGEN VARI, Determination of Letrozole, Anastrozole and Exemestane by Capillary Zone Electrophoresis.....	251
ÉVA MOLNÁR, DÓRA RIPPEL-PETHŐ, GÉZA HORVÁTH, JANKA BOBEK, RÓBERT BOCSI, ZOLTÁN HODAI, Removal of Hydrogen Sulphide Content from Biogas by Atomizing of Alkali Solution.....	265
ÉVA MOLNÁR, DÓRA RIPPEL-PETHŐ, GÉZA HORVÁTH, JANKA BOBEK, RÓBERT BOCSI, ZOLTÁN HODAI, Study of Selective Hydrogen Sulfide Absorption by Comparing Two Different Alkali Absorbents by Using Atomization Method.....	273
RÉKA KERESZTES, ESZTER RÁPÓ, Statistical Analysis of Air Pollution with Specific Regard to Factor Analysis in the Ciuc Basin, Romania..	283
ANDREA VARGA, ZSÓFIA BATA, PÁL CSUKA, DIANA MONICA BORDEA, BEÁTA G. VÉRTESSY, ADRIANA MARCOVICI, FLORIN DAN IRIMIE, LÁSZLÓ POPPE, LÁSZLÓ CSABA BENCZE, A Novel Phenylalanine Ammonia-Lyase from <i>Kangiella Koreensis</i>	293

Studia Universitatis Babes-Bolyai Chemia has been selected for coverage in Thomson Reuters products and custom information services. Beginning with V. 53 (1) 2008, this publication is indexed and abstracted in the following:

- Science Citation Index Expanded (also known as SciSearch®)
- Chemistry Citation Index®
- Journal Citation Reports/Science Edition



1930 - 2015

Professor Simion Gocan, Ph.D. one of the most important personalities in separation sciences in Romania, was born in the village of Berindu, Cluj County, on 26 December 1930. After having graduated from the Pedagogical High School from Cluj-Napoca in 1950, he studied at the Faculty of Chemistry of “Babeş-Bolyai” University till 1954. In 1969 he defended his doctoral thesis entitled “*Paper Thermography*” under the supervision of Prof. Candin Liteanu, Ph.D.

After graduating from “Victor Babeş” University, he began his didactic activity at the Department of Physics of the Polytechnic Institute in Cluj-Napoca in 1954, and then he taught at the Pedagogical Institute. He became assistant professor in 1962 and lecturer in 1963. In 1973 he accepted a position of associated professor at the Department of Analytical Chemistry of the Faculty of Chemistry and Chemical Engineering, “Babeş-Bolyai” University. From 1990 till 1995, when he retired, he was full professor and head of the Analytical Chemistry Department. After having retired, he continued to keep in touch with research as consulting professor and in 2009 he was appointed honorary consulting professor.

Professor Simion Gocan is one of the first Romanian researchers who understood the importance of the separation methods in analytical chemistry. He introduced the course on *Separation Methods* in the faculty curriculum, particularly developing the chromatographic techniques.

All along his career he advised numerous students on their graduation papers. In 1990 he was accredited as a Ph.D. advisor and he tackled numerous aspects of fundamental and applied research in analytical chemistry. He advised thirteen doctoral students, seven of them

“stepped into his shoes” and followed an academic career. He trained researchers and he formed characters as well. He taught his disciples about the “Sisyphus work” to find the accurate scientific information and encouraged them “bond” with one another. He himself never turned down giving a helping hand when needed. This is how he laid the foundation of the Quality Control Laboratory for homeopathic and plant extracts analysis at PlantExtrakt Company in Cluj-Napoca.

Professor Gocan paid special attention to his didactic activity and to the necessity of transmitting the scientific information. He published numerous courses, practical guides, and collections of problems: *Guide for the Electronics and Radiotechnical Laboratories* (1964); *General Physics Course* (1971); *Analytical Methods of Separation - A Practical Guide* (1977); *Analytical Chemistry Course - Separation Methods* which had several editions: 1981, 1989, and 1995.

Professor Gocan authored or co-authored ten scientific books which were published in Romania. Mention must be made of: *The Fundamentals of Adsorption Column Chromatography* (1971); *Liquid Chromatography* (1974); *Analytical Immunochemistry* (1995); *Modern Methods for Organic Samples Processing* (2006). To these one must add three volumes in the series entitled *High Performance Chromatography: Gas Chromatography* (1998), *Liquid Chromatography* (2002), and *Thin-Layer Chromatography* (2005). Professor Gocan co-authored the ninth edition of *The Romanian Pharmacopoeia* (1976) as well.

He co-authored the book *Gradient Liquid Chromatography* (1974) and also authored chapters in “*Modern Thin Layer Chromatography*” (1990), “*Water Analysis*” (2000), “*Encyclopedia of Chromatography On-Line*” (2001) and “*Advances in Chromatography*” (2006), published by prestigious scientific publishing houses from abroad (Ellis Horwood, Marcel Dekker, and CRC Press).

Professor Gocan’s scientific activity resulted in 105 papers published in Romania (the first one was published in 1959) and 40 papers published in prestigious international journals (*Talanta*, *Pure and Applied Chemistry*, *Reviews in Analytical Chemistry*, *Journal of Chromatography A*, *Chromatographia*, *Planar Chromatography - Modern TLC*, *Journal of Pharmacology and Biomedical Analysis*, and many others). He got seventeen patents and eight research contracts. Due to his research activity, he became a member of numerous scientific societies of Chemistry and Analytical Chemistry in Romania and abroad.

Professor Simion Gocan left behind not only a very valuable and rich scientific work, but also many people who pay a respectful tribute to his memory.

Fama semper vivat!
Lector Dr. Simona Codruta Cobzac

CHARACTERIZATION OF *ORTHOSIPHON STAMINEUS* BENTH EXTRACTS BY REVERSED-PHASE THIN LAYER CHROMATOGRAPHIC METHODS

NELI-KINGA OLAH^{a,b}, DANIELA HANGANU^{c*}, EDE BODOKI^c, RADU
OPREAN^c, CLAUDIA TOMA^a, CLAUDIU MORGOVAN^a, ELISABETA CHIȘE^a,
ANDREEA BRAȘOVAN^d, SIMONA CODRUȚA AURORA COBZAC^{e*},
SIMION GOCAN^e

ABSTRACT. TLC is a powerful method used for separation of complex mixtures such as plant extracts. Employing different TLC techniques the separations can be improved. This paper presents a study of the *Orthosiphon stamineus* Benth extracts using isocratic reversed-phase thin layer chromatography (RP-TLC) and reversed-phase automated multiple development technique (RP-AMD). Methanol (SI) and a mixture of methanol–water–methyl acetate (SII) were used as extraction agents. *Orthosiphon stamineus* Benth. belongs to the Lamiaceae family. Its leaves contain rosmarinic acid, sinesetine and eupatorine as main compounds. After TLC separation the bioactive compounds from plant extracts were identified by comparison of the R_f values and *in situ* UV-Vis spectra with those of the standards and quantified using the calibration method. The rosmarinic acid was better extracted in the solvent mixture methanol–water–methyl acetate (10:10:80, v/v), while the sinesetine and eupatorine, which are more lipophilic, were better extracted in methanol. The study revealed the AMD technique superiority in comparison with the isocratic one.

Keywords: RP-TLC; RP-AMD; *Orthosiphon stamineus* Benth. extracts; rosmarinic acid; sinesetine; eupatorine.

^a "Vasile Goldis" Western University of Arad, Faculty of Pharmacy, 86 L. Rebreanu str., Arad, Romania

^b SC PlantExtrakt SRL, 407059 Rădaia. Cluj, Romania

^c "Iuliu Hațieganu" University of Medicine and Pharmacy from Cluj-Napoca, Faculty of Pharmacy, 8 Victor Babeș str., Cluj-Napoca, Romania

* Corresponding authors: danahcluj@gmail.com, csimona@chem.ubbcluj.ro

^d Babeș-Bolyai University of Cluj-Napoca, 1 Kogălniceanu Str., Cluj-Napoca, Romania

^e Babeș-Bolyai University of Cluj-Napoca, Faculty of Chemistry and Chemical Engineering, 11 Arany Janos Str., Cluj-Napoca, Romania

INTRODUCTION

Orthosiphon stamineus Benth. belongs to the Lamiaceae family and it is originary from Southeast Asia. *Orthosiphonis folium* was used from long time in different kidney diseases. The vegetal product contains caffeic acid derivatives (rosmarinic acid, cichoric acid, etc) and polymethoxylated flavonoids (sinesetine, eupatorine) [1,2]. Their structure is presented in figure 1.

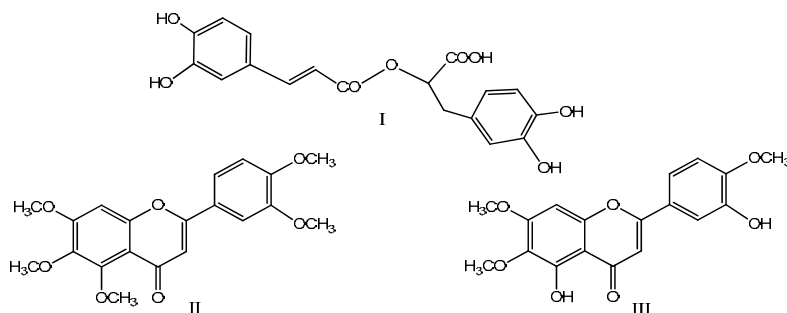


Figure 1. Structure of rosmarinic acid (I), sinesetin (II) and eupatorin (III)

Different techniques are used for identification and determination of these compounds. Usually separation methods using both, column [3-5] and planar [6-9] chromatography are preferred. Generally thin layer analyses are carried out on silica plates. Spectrophotometric methods for determination of caffeic acid derivatives are also used [3].

TLC is a versatile method for separating multicomponent mixtures. The separating power of isocratic TLC can be enhanced by two-dimensional development, multiple or automated multiple development (ADM). The AMD technique uses a solvent gradient and several development steps to separate compounds of widely different polarity. Most reported AMD applications have used gradients on normal phase plates [10-19].

This paper presents the qualitative and quantitative determination of rosmarinic acid, sinesetine and eupatorine from two extracts of *Orthosiphon stamineus* Benth. using isocratic RP-TLC and RP-AMD techniques. The identification of the separated compounds was performed based on chromatographic (R_f values) and non-chromatographic (*in situ* UV-Vis spectra) parameters. The efficiency of RP-TLC and RP-AMD separation techniques was achieved by comparison of R_f values. On the other hand, based on quantitative analyses, the efficiency of the extraction systems was correlated with analytes polarity.

RESULTS AND DISCUSSION

The chromatograms of developed plates using both chromatographic development methods RP-TLC and RP-AMD are presented in figure 2 and figure 3 respectively.

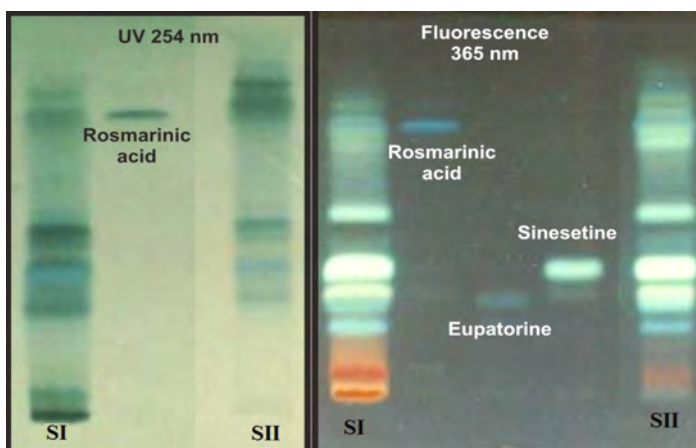


Figure 2. The chromatograms obtained using the isocratic technique

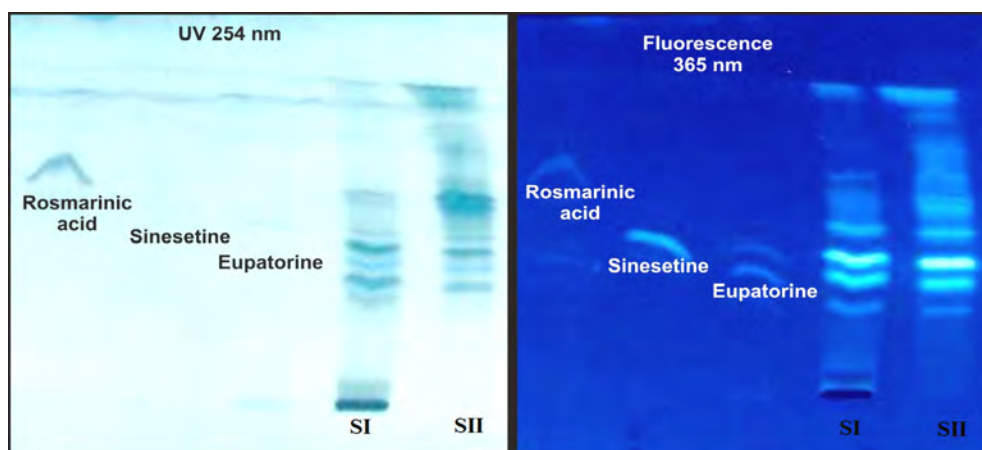


Figure 3. The chromatograms obtained using the AMD technique

The photodesitograms obtained by scanning the plates at 254 nm in reflectance mode and at 400 nm in fluorescence mode (excitation wavelength at 365 nm) are presented in Figures 4 – 6.

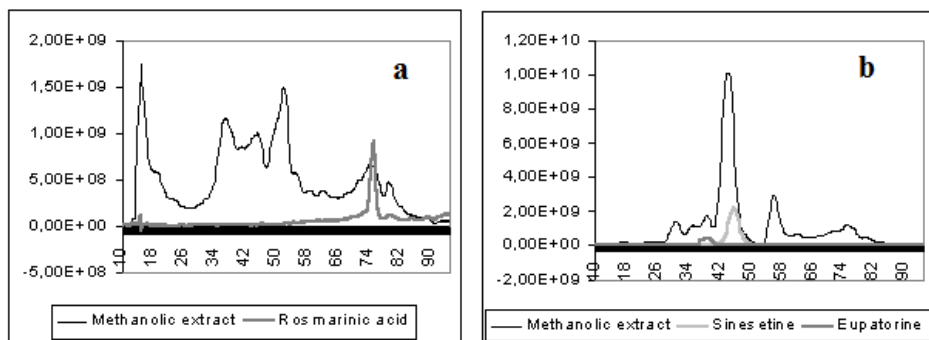


Figure 4. The densitogram of the methanolic extract (SI) separated by RP-TLC development. Visualization mode: (a) UV at 254 nm; (b) fluorescence at 400 nm.

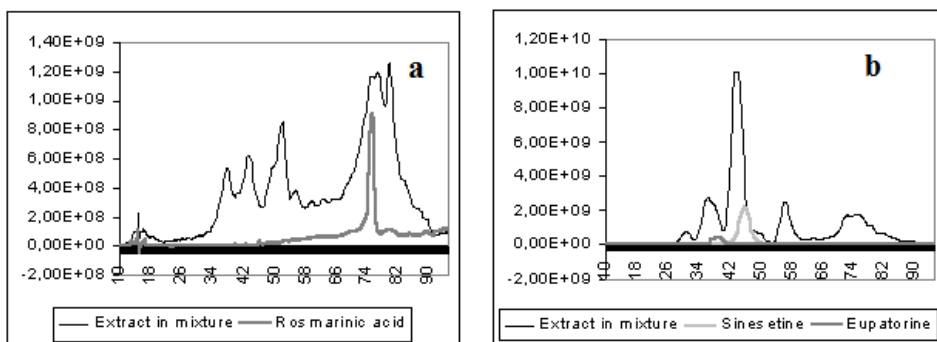


Figure 5. The densitogram of the solvent mixture extract (SII) separated by RP-TLC development. Visualization mode: (a) UV at 254 nm, (b) fluorescence at 400 nm.

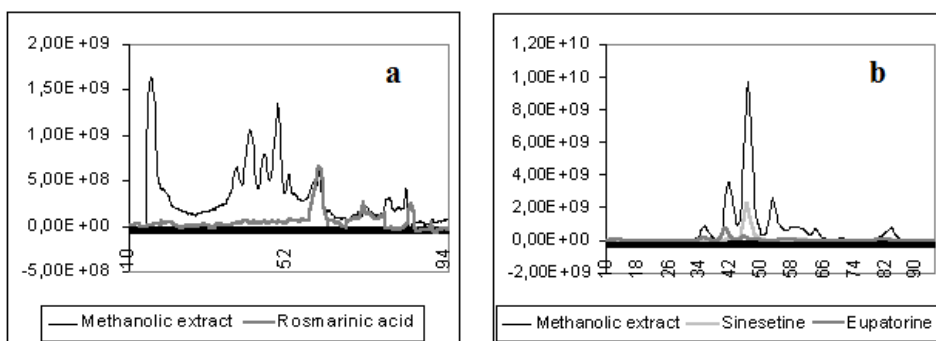


Figure 6. The densitogram of the methanolic extract (SI) separated by RP-AMD development. Visualization mode: (a) UV at 254 nm; (b) fluorescence at 400 nm.

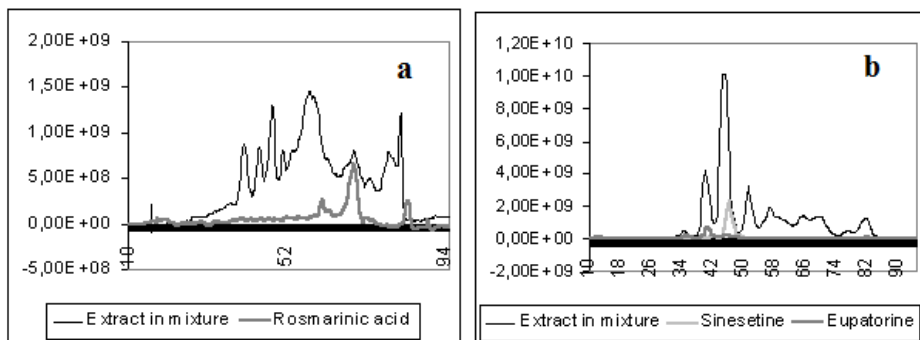


Figure 7. The densitogram of the solvent mixture extract (SII) separated by RP-AMD development. Visualization mode: (a) UV at 254 nm, (b) fluorescence at 400nm.

Comparing the photodensitograms from Figure 4a with Figure 5a and Figure 6a with Figure 7a, respectively, it can be observed a difference between the polarities of extracted compounds. In methanol (SI) were extracted most non-polar compounds than by using the solvent mixture methanol – water – methyl acetate (10:10:80, v/v), which extracted more polar compounds. This observation is confirmed by a pronounced peak at the start line and also by decreasing the concentration of the more polar compounds that are located in the top area of the plate. Furthermore, it can be observed a good separation of rosmarinic acid, a more polar compound having a higher R_f value, from sinesetine and eupatorine - less polar compounds that are situate in the middle zone of the plate.

On the other hand, comparing photodensitograms obtained by RP-AMD developing method with than obtained by RP-TLC, it can be observed a better separation efficiency achieved with the first mentioned technique.

Moreover, comparison of figures 4a with 6a and 5a with 7a, respectively, it can be observed an increased number of separated compounds obtained by RP-AMD vs RP-TLC method. The RP-AMD method gives a more specific fingerprint for plant extracts.

Another important observation is that fluorescence densitometry at 400 nm has a higher specificity than UV at 254 nm. Having natural fluorescence, sinesetine and eupatorine can be selectively identified by fluorescence photodensitometry.

The interest compounds from extracts were identified based on chromatographic parameter - R_f , which are similar with the standards ones, in both visualization modes – fluorescence and fluorescence quenching (Table 1).

Table 1. The R_f value of the separated compounds

Compound	Extract type	RP-TLC	RP-AMD
Rosmarinic acid	Standard	0.94	0.73
	Methanolic extract	0.93	0.73
	Extract in solvent mixture	0.94	0.73
Sinesetine	Standard	0.54	0.43
	Methanolic extract	0.53	0.44
	Extract in solvent mixture	0.54	0.43
Eupatorine	Standard	0.45	0.35
	Methanolic extract	0.46	0.36
	Extract in solvent mixture	0.45	0.34

Moreover, *in situ* UV-Vis spectra between 200 - 500 nm were register for spots having the same R_f . The spectra of the standards (rosmarinic acid, sinesetine and eupatorine) and their corresponding spots from both extracts are showing similar shapes (Figures 8-10).

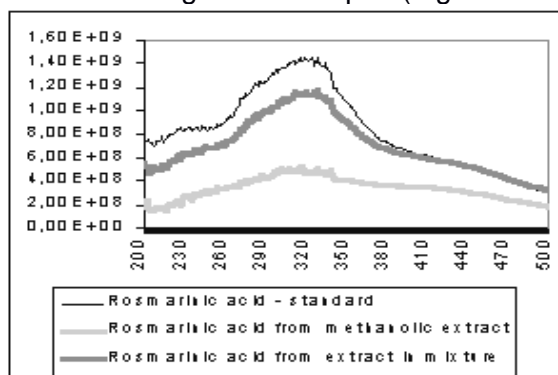


Figure 8. *In situ* UV-Vis spectra for rosmarinic acid (RP-AMD separation)

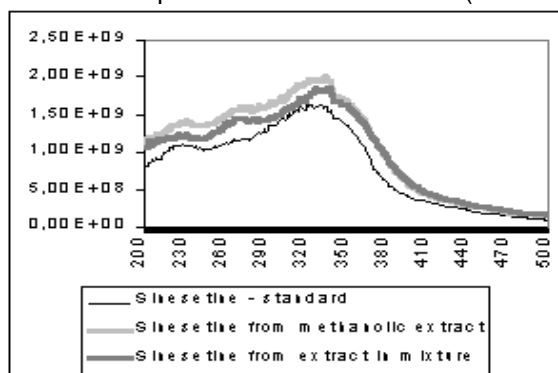


Figure 9. *In situ* UV-Vis spectra for sinesetine (RP-AMD separation)

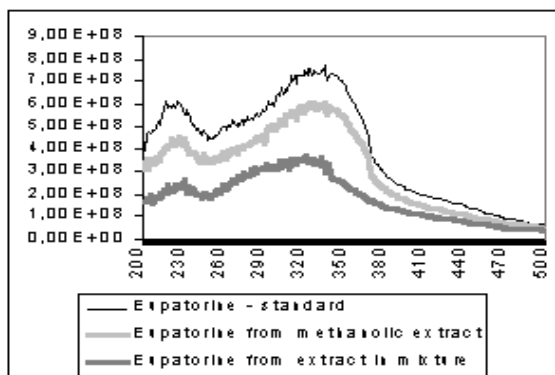


Figure 10. *In situ* UV-Vis spectra for eupatorine (RP-AMD separation)

Quantitative determination of the analytes was carried out by scanning the RP-TLC plates at 254 nm. The calibration functions were obtained by linear regression. Linear relationships between area (Y) and analyte quantity/spot (X) were obtained (Table 2).

Table 2. Calibration curves parameters

Compound	Rosmarinic acid	Sinesetin	Eupatorin
Working range - concentration (mg/ml)	0.108-0.540	1.500-6.000	1.050-4.200
Working range ($\mu\text{g}/\text{spot}$)	1.1 – 5.5	15.0 - 60.0	10.5 – 42.0
Slope($\pm t^*s/n^{1/2}$)	3914.80(± 947.62)	2690.90(± 109.75)	576.84(± 100.91)
Intercept($\pm t^*s/n^{1/2}$)	714.32(± 339.44)	3134.50(± 416.25)	207.72(± 267.85)
r	0.989	0.999	0.994

The percent content (% mg/g) of rosmarinic acid, sinesetin, and eupatorin in the studied plant, computed based on measured spot area and the equation of calibration curve, taking in account the extract volume and the analyzed quantity of the dry plant are presented in Table 3.

The extraction yield of rosmarinic acid - a hydrophilic compound, was higher when SII extraction system was used. On the other hand, when methanol was used, more lipophilic compounds like sinesetin and eupatorin are favored.

Table 3. The content of rosmarinic acid, sinesetine, and eupatorine in *Orthosiphon stamineus* Benth.

Rosmarinic acid % mg/g($\pm t^*s/n^{1/2}$)	Sinesetine % mg/g($\pm t^*s/n^{1/2}$)	Eupatorine % mg/g($\pm t^*s/n^{1/2}$)
Methanolic extract (SI)		
0,021 \pm (0,0004)	0,852 \pm (0,0154)	0,424 \pm (0,0071)
Extract in solvent mixture (SII) methanol – water – methyl acetate (1:1:8, v/v)		
0,031 \pm (0,0006)	0,837 \pm (0,0154)	0,405 \pm (0,0071)

CONCLUSIONS

The two studied *Orthosiphon stamineus* Benth. extracts can be characterized using reversed phase – thin layer chromatography and automated multiple development on reversed phase, because the RP-TLC and RP-AMD techniques show good separation of the main compounds from *Orthosiphon stamineus* Benth. leaves. The separations with AMD technique were better than those with isocratic RP-TLC. The characterization of the studied extracts was performed by separation and identification of two main compound classes: the caffeic acid derivatives (rosmarinic acid) respectively the polymethoxylated flavonoids (sinesetine and eupatorine).

EXPERIMENTAL SECTION

Materials, reagents and apparatus

The experiment was performed using acetonitrile and methyl acetate obtained from Roth, (Germany), methanol supplied from Euromedica (Romania) and acetic acid from Chimopar (Romania). Rosmarinic acid (I) was supplied from Roth (Germany), sinesetine (II) and eupatorine (III) were obtained from Extrasynthese (France). *Orthosiphon stamineus* Benth. leaves were obtained from Caesar & Loretz (Germany).

TLC RP18-Kieselgel F₂₅₄ (20x20 cm) plate used for chromatographic separation were purchased from Merck (Germany).

There were used a Desaga AS-30 automated applicator (Germany), a Camag AMD instrument (Muttentz Switzerland) and a Desaga CD 60 photodensitometer (Germany).

Sample Preparation

Bioactive compounds from 20 g crushed leaves of *Orthosiphon stamineus Benth* were extracted by cold extraction (10 days) with 100 mL extraction solvent. Two different systems were used for extraction: methanol (SI) and methanol-water-methyl acetate (10:10:80, v / v) mixture (SII). The second extraction system has already been optimized for a high yield of polyphenols extraction [20,21]. Both extracts were concentrated to 10 ml.

Experimental Conditions for Isocratic RP-TLC and RP-AMD Separation

Both separations were carried out on RP-silicagel plates. Methanolic solutions of rosmarinic acid (1.08 mg/mL), sinesetine (6.00 mg/mL) and eupatorine (4.20 mg/mL) were used as standards. 20 μ L of each sample and 10 μ L from each standard solution were applied as bands (1 cm) using an

automated applicator. Isocratic elution was performed in normal chamber using the mixture acetonitrile – water – acetic acid (55:44:1, v/v) as mobile phase. The developing distance was 8 cm. Gradient elution for RP-AMD was performed in 12 steps, on 8 cm (final developing distance), with acetonitrile – water – acetic mixtures of different composition, starting with the most polar one (Table 4).

Table 4. Mobile phase for AMD

Bottle no.	1	2	3	4	5
Steps no.	1-2	3-4	5-6	7-9	10-12
Water	79	69	59	49	39
Acetonitrile	20	30	40	50	60
Acetic acid	1	1	1	1	1

The scanning densitometry of the plates was performed at 254 nm and at 400 nm in fluorescence mode (excitation wavelength - 365 nm). The *in situ* UV-Vis spectra of sinesetin, eupatorin and rosmarinic acid spots from standards and extracts were obtained in the range of 200 - 500 nm.

The quantitative analyses were performed using calibration curves of three standards determined in the same chromatographic conditions as the isocratic analyses were performed. All determinations were made in triplicate and the result is the average of the individual values.

REFERENCES

1. H. List, L. Horhammer, „Hagers Handbuch der Pharmazeutischen Praxis“, Springer Verlag, Berlin, Vol. 5: Drogen E-O, **1993**, 967.
2. M. Wichtl, „Herbal Drugs and Phytopharmaceuticals“, Medpharm Scientific Publishers, Stuttgart, **1994**, 358.
3. P. Gorecki, E. Segiet-Kujawa, A. Mscisz, B. Zygmunt, *Herba Polonica*, **1999**, 45(3), 179.
4. W. Sumaryono, P. Proksch, V. Wray, L. Witte, T. Hartmann T., *Planta Medica*, **1991**, 57, 176.
5. P.G. Pietta, P. L. Mauri, C. Gardana, A. Bruno, *Journal of Chromatography*, **1991**, 547, 439.
6. H. Wagner, S. Bladt, E.M. Zgainski, „Drogenanalyse“, Springer-Verlag, Berlin, **1983**, 169.
7. L. Gracza, P. Ruff, *Archive Pharmazie (Weinheim)*, **1984**, 17, 339.
8. E. Wollenweber, K. Mann, *Planta Medica*, **1985**, 51, 459.

9. K.E. Malterud, I.M. Hanche-Olsen, I. Smith-Kielland, *Planta Medica*, **1989**, *55*, 569.
10. K. Burger, *Fresenius Zeitung Analytische Chemie*, **1984**, *318*, 228.
11. D.E. Jänchen, "Instrumental Multiple Development of High-Performance Thin-Layer Chromatograms", Kaiser, R. E. Ed.; Proc. Of the 3rd Int. Symp. on Instr. HPLC, Würzburg, Bad Dürkheim. **1985**, 83.
12. D.E. Jänchen, H.J. Issaq, *Journal of Liquid Chromatography*, **1988**, *11*, 1941.
13. M.F.M. Trysteen, R.G.e. Van Severen, B.M.J. De Spiegeleer, *Analyst*, **1989**, *114*, 1021.
14. S. Ebel, S. Völkl, *Deutsche Apotheke Zeitung*, **1990**, *130*, 2162.
15. S. Gocan, G. Cîmpan, L. Mureşan, *Journal of Pharmaceutical and Biomedical Analysis*, **1996**, *14*, 1221.
16. G. Matysik, E. Wojtasik, *Journal of Planar Chromatography*, **1994**, *7*, 34.
17. G. Matysik, *Journal of Planar Chromatography*, **1992**, *5*, 146.
18. J. Pothier, N. Galand, *Journal of Chromatography A*, **2005**, *1080(2)*, 186.
19. C. Poole, Chapter 4. Automated Multiple Development, "Instrumental Thin-Layer Chromatography", Elsevier, Amsterdam, Boston, Heidelberg, London, New York, Oxford, Paris, San Diego, San Francisco, Singapore, Sydney, Tokyo, **2015**, 73.
20. Sz. Nyiredy, *Chromatographia*, **2000**, *51*, S-288.
21. N.K. Olah, D. Hanganu, R. Oprean, C. Mogoşan, N. Dubei, S. Gocan, *Journal of Planar Chromatography*, **2004**, *17(1)*, 18.

In memory of prof. dr. Simion Gocan

IDENTIFICATION AND QUANTIFICATION OF SOME PESTICIDE METABOLITES FROM VEGETABLES BY GC-TOF-MS AND LC-MS-QQQ

ADELA MEGHESAN-BREJA^{a,b}, CLAUDIA CIMPOIU^b, ANAMARIA HOSU^{b,*}

ABSTRACT. Considering the international situation regarding the residues of pesticides in vegetables and fruits and the requirement for sensitive and reliable analytical methods that are able to ensure the compliance of marketed food commodities with the law on food safety, the aim of this paper was the identification and determination of some degradation products and metabolites of ten most often used pesticides. Two analytical approaches are proposed and used for the development of reliable screening, quantification and confirmation of pesticides metabolites in different vegetables. The proposed methods have different approaches than the other multi-residue methods for vegetables allowing the extensive investigation of previously undetectable or unknown pesticide metabolites in vegetables. These methods were tested on cherry tomato, cucumber, and chili pepper, some of the most widely consumed vegetables. The results suggests that spraying pesticides in high doses lead to high levels of pesticide residues in the case of some studied vegetables and the concentration of metabolites together concentration of parent pesticide must be taken into account in order to establish the MRL's in vegetables and fruits.

Keywords: *pesticides metabolites, GC-TOF-MS, LC-MS-QQQ, vegetables*

^a *Regional Laboratory for Control of Pesticide Residues in Plants and Plant Products, 80 Dezrobirii, str., RO-540243, Targu-Mures, Romania*

^b *Babes-Bolyai University, Faculty of Chemistry and Chemical Engineering, 11 Arany Janos, str., RO-400082 Cluj-Napoca, Romania*

* *Corresponding author ahosu@chem.ubbcluj.ro*

INTRODUCTION

The pesticides are widespread used in modern agriculture leading to the contamination of waters, soil or vegetables. In the European Union (EU) the approval of pesticides and their use are strictly regulated [1, 2], the authorities trying to reduce the number of such permitted products. Any formulated pesticide product includes active ingredients and passive ingredients, the active ingredients being the toxic components. The active ingredients of some pesticides are absorbed by plants and animals and are converted by biotransformation in lethal substances. These substances, known as metabolites, are produced by chemical reactions that naturally occur in the cell metabolism, which in case of vegetables may depend on type of plant, plant vigour and temperature [3, 4]. Also, these metabolites can appear not only in metabolic pathway, but also during the analysis of pesticides as a result of the setting of some instruments parameters. Although these compounds are actually degradation products, in some research papers they have been included in the same category with metabolism metabolites [5-11].

Usually, after separation and identification of compounds by specific analytical methods, especially chromatographic methods, the authentication of metabolites and degradation products is made by isotopic marking. The manufacturer must specify in the safety sheet of each pesticide any confirmed metabolites that may occur, together with the technical characteristics and the metabolic pathway in plants, animals, soil, air, water [4]. However, an important challenge is to detect untargeted compounds and to determine their identity in foods. Therefore, the development of advanced analytical techniques is expected to play a crucial role [12]. Moreover, in order to establish the MRL-s the European Food Safety Authority (EFSA) take into account that no information regarding the storage stability of pesticides, and their metabolism and residues in crops. The MRL of different pesticides are reposted as sum of parent pesticide and its metabolites or isomers. Thus, in the case of no availability of validated analytical methods for degradation products, only the concentration of parent pesticide is reported, those of degradation products being not counted.

Based on the information available on safety sheets and other articles on this topic [4, 5, 13-17] the most common metabolites and degradation products of ten most used pesticides for plant protection treatments in Romania were selected for development of multi-methods for analysis of various representative matrices. The chosen pesticides were the following: azoxystrobin, iprodione, captan, thiophanate-methyl, carbendazim, folpet, dicofol, dimethoate, fenarimol and bromopropylate.

Considering the international situation regarding the residues of pesticides in vegetables and fruits, the aim of this paper was the identification

and determination of some degradation products and metabolites of ten most often used pesticides, therewith answering to the important requirements in approaching of exposure to pesticides and health risk. Also, sensitive and reliable analytical methods for the determination of pesticide residues are required to ensure the compliance of marketed food commodities with the law on food safety [18]. The proposed methods allow the extensive investigation of previously undetectable or unknown pesticide metabolites in vegetables. Because only a limited number of these metabolites have been analyzed before and they have a great structural diversity, the general aspects concerning chromatographic separation and the specific conditions for analysis of target compounds were deduced.

The developed methods were tested on cherry tomato, cucumber, and chili pepper, some of the most widely consumed vegetables. Although the crops are suited for pesticide free or organic cultivation efficient and profitable crop protection most often relies on the use of synthetic pesticides [19].

RESULTS AND DISCUSSION

This study aims to analyse metabolites of various pesticides from quite different classes, namely fungicides, insecticides/acaricides. The used pesticides exert specific effects on all selected vegetables. The studied pesticides and their metabolites have different physical and chemical properties, some of them (i.e. captan, folpet, and dicofol) being a real challenge for any analyst due to their sensitivity to certain pH and high temperature values. The metabolites are from the so-called “relevant and non-relevant metabolites”, relevancy based upon a risk assessment as prescribed in Directive 91/414/EEC [2]. The metabolites of the following pesticides are analysed using either GC-MS or LC-MS techniques.

Captan ((3*aR*,7*aS*)-2-[(trichloromethyl) sulfanyl] -3*a*,4,7,7*a*-tetrahydro-1*H*-isoindole-1,3(2*H*)-dione) is quickly decomposed in plants, but its fungitoxic activity does not disappear because one of its metabolites seems to have antifungal properties [4]. The main degradation products of captan are **tetrahydrophthalimide (THPI)** and **thiophosgene**, which can be identified and quantified by GC. Besides these compounds, due to thermo-sensitivity of captan other degradation products may occur during analysis [8, 9]. The MRL for captan is reported as sum of captan and THPI quantities. Any validated analytical method does not exist for THPI and analytical standard is commercial available only from 2016.

Dicofol (2,2,2-trichloro-1,1-bis(4-chlorophenyl) ethanol) is an analogue of dichlorodiphenyltrichloroethane (DDT), but the replacing of the hydrogen atom from the first position with a hydroxyl group lead to essential

changes in chemical properties of the molecule and to the increasing of their volatility. The molecule is quickly degraded under temperature or by hydrolysis, resulting **4,4'-dichlorobenzophenone**, the major metabolite of dicofol. This metabolite was identified and quantified in plants by GC-MS [4, 8]. The MRL is reported as sum of isomers.

The main metabolite of **folpet** (*N*-(trichloormethylthio) ftalimide), produced in plants as a result of photolysis, is **phthalimide**, which was identified and determined by GC-MS [4, 8, 9]. The MRL for folpet is given as sum of quantities of folpet and phtalimide, for phtalimide being no analytical standard available on the market.

Iprodione (3-(3,5-dichlorophenyl)-*N*-isopropyl-2,4-dioxoimidazoli dine-1-carboxamide) is stable only at pH below 5, being rapidly degraded in aqueous or alcaline solution [7]. Its structure is similar to procymidone and vinclozolin, so it may be metabolized like these pesticides to **3,5-dichloroaniline** (3,5-DCA), a metabolites that can be determined by GC-MS [8]. The MRL for iprodione is given as sum of quantities of iprodion and all its metabolites that contain 3,5-dicloroaniline moiety.

Regarding **fenarimol** ((*RS*)-2,4'-dichloro- α -(pyrimidin-5-yl) benzhydrl alcohol), the main metabolites identified in vegetables and fruits were **dehidroxyfenarimol** and **2,4'-dichlorobenzophenone** that could be analyzed so far only by LC-MS due to their thermo-sensitivity [10]. In the establishing of MRL only the parent pesticide is taken into account although its degradation product almost always is present with this.

The metabolism pathway of **bromopropylate** (*iso*-propyl bis(4-bromophenyl)(hydroxy) acetate) in plants shows that it slightly penetrates the leaves or fruit, its identified metabolite being **4,4'-dibromobenzophenone** [11]. Only the parent pesticide is taken into account for MRL establishing.

3,4-Dichlophenyl isocyanate is known as metabolite of diuron, but is also used for some pesticide synthesis so that is very likely to be encountered in the analysis of these pesticides.

The most known metabolite of **dimethoate** (*O,O*-dimethyl *S*-[2-(methylamino)-2-oxoethyl] dithiophosphate) is **omethoate** (dimethoate Oxon), but on the plant metabolic pathway dimethoate carboxylic acid, omethoate carboxylic acid and des-*O*-methyl-dimethoate carboxylic acid are also obtained. These metabolites can be analyzed by TLC, HPLC-UV or LC-MS [4, 8]. The omethoate can be determined by validated analytical methods because it is available as analytical standard and the MRL is reported as the sum of dimethoate and omethoate expressed as dimethoate.

Carbendazim ((methyl 2- benzimidazole carbamate) or MBC) is the primary metabolite of **thiophanate-methyl** (dimethyl 4,4'-(*o*-phenylene)bis(3-thioallophanate)) whose conversion speed depends on the pH and

temperature of environment. This conversion is fast in plants, being catalyzed by sunlight, the metabolism being also accelerated by fungus [4, 9]. Most residual analysis of thiophanate-methyl and carbendazim was done by HPLC-UV, derivated spectrophotometric methods or LC-MS-MS with different pre-treatment of the samples [8]. In the case of some vegetables and fruits the MRL for carbendazim is reported as sum of carbendazim and benomil and in for other vegetables and fruits as sum of carbendazim and thiophanate-methyl, being expressed in both cases as carbendazim.

Azoxystrobin (methyl (2*E*)-2-(2-[[6-(2-cyanophenoxy)pyrimidin-4-yl]oxy]phenyl)-3-methoxyacrylate) is degraded both on leaf surface by photolysis and by metabolic pathway of treated plant, resulting compounds that have not toxicological effect and significant antifungal activity. At least fifteen metabolites of azoxystrobin were identified in plant, the most important being the **azoxystrobin acid** and the **azoxystrobin metabolite Z** that occur more often in water. Other metabolites, such as **metabolite M** (4-(2 cyanophenoxy)-6- hydroxypyrimidine), **metabolite B** (E (2-{2-[6-(2-cianofenoxi)pirimidin-4-iloxi]fenil}-3-metoxiacrilat), **metabolite D** (isomer of metabolite B), **metabolite F** (2- hydroxybenzonitrile) and metabolite L (2-{2-[6-(2- cyanophenoxy) pyrimidin-4-yloxy] phenyl} glycolic acid) were identified in rice, wheat, grapes and peanuts by TLC, HPLC, LC-MS or GC [6]. The MRL is established using only the parent pesticides, its metabolites being not considered.

The choice of the extraction method

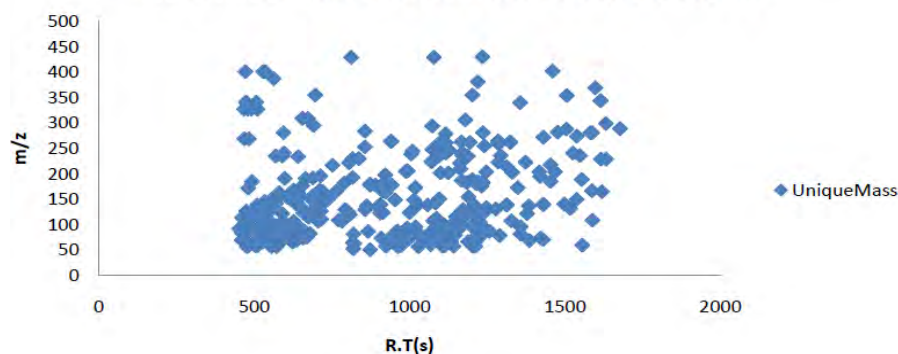
The extraction of target compounds is the most important step of pesticides residues and metabolites determination. Therefore, the finding an appropriate extraction method which provide an almost "clean" extract that not influence the sensibility and selectivity of determination is absolutely necessary. Also, the extraction method must be able to remove most of the co-extractable compounds and can be applied to wide variety of pesticides [20, 21]. Co-extractable compounds, such as lipids, dyes and non-polar compounds are always present when pesticides are extracted from vegetables. The presence of these compounds cause different problems in the further analysis, including the emulsifying, turbidity, the contamination of devices and, the most important one being the masking of the target compounds. Commonly, the co-extractable compounds are removed from the extract by different methods.

The extraction method is chosen on the basis of the recoveries obtained on a control spiked samples (**Table 1**). The values of recoveries are statistically compared (t-test for pair values) using GraphPad InStat statistical program.

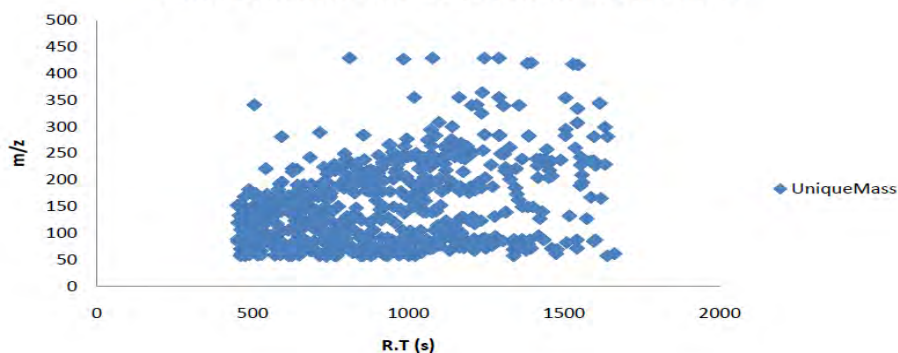
Table 1. Recovery rates of pesticides and their metabolites in spiked samples

Vegetables	Recovery rate (%)					
	Cucumbers		Cherry tomatoes		Chili peppers	
Extraction method Pesticide	QuEChERS modified	Mini-Luke modified	QuEChERS modified	Mini-Luke modified	QuEChERS modified	Mini-Luke modified
Tetrahydro- phthalimide	45	60	47	57	64	72
Thiophosgene	32	99	30	102	34	106
4,4'-Dichloro- benzophenone	74	44	113	42	92	40
Phthalimide	57	70	41	73	54	62
2,4'-Dichloro- benzophenone	66	58	69	59	67	56
Omethoate	75	82	35	60	20	39
Carbendazim	74	136	50	100	78	154
Azoxystrobin acid	75	103	75	85	116	83

Modified QueChERS extraction method



MiniLuke modified extraction method

**Figure 1.** Co-extractive compounds found in the cucumber extracts

Also, the LOQ values and the chromatographic peak shapes are taken into account for certain decisions. The main goal is to provide adequate and reproducible recovery rates for analyzed metabolites and to improve the extraction and stability of challenging compounds. Moreover, the presence of co-extractable compounds must be taken into account because lot of them may appear in the extracts obtained after both methods (e.g. **Figure 1**).

Thus, modified QuEChERS method gives higher recoveries than modified MINILUKE method in the case of 4,4'-dichlorobenzophenone and azoxystrobin acid, while for thiophosgene and phthalimide the most efficient extraction method has been found to be the modified MINILUKE. In some cases (e.g. tetrahydrophthalimide and omethoate) both method give comparable recovery rates for all spiked samples and the characteristics of chromatographic peaks are taken into account for choosing the appropriate extraction method. In these cases the modified QuEChERS method is preferable to be used because the chromatographic peaks are well resolved and the matrix background is almost non-existent (**Figure 2**). For 2,4-dichlorobenzophenone both methods give similar results in terms of recovery rate and peak shapes. Unlike these metabolites, the 4,4'-dibromobenzophenone and 3,4-dichlorophenyl isocyanate can be extracted only by modified MINILUKE method and for 3,5-dichloroaniline merely buffered QUECHERS method has been proven to be effective. These three compounds do not appear in the resulting extract, being extractable only by specified method. Regarding carbendazim, the buffered QUECHERS method is preferred although the MINILUKE method provides better results, but that can be influenced by co-extractable compounds, especially chlorophyll.

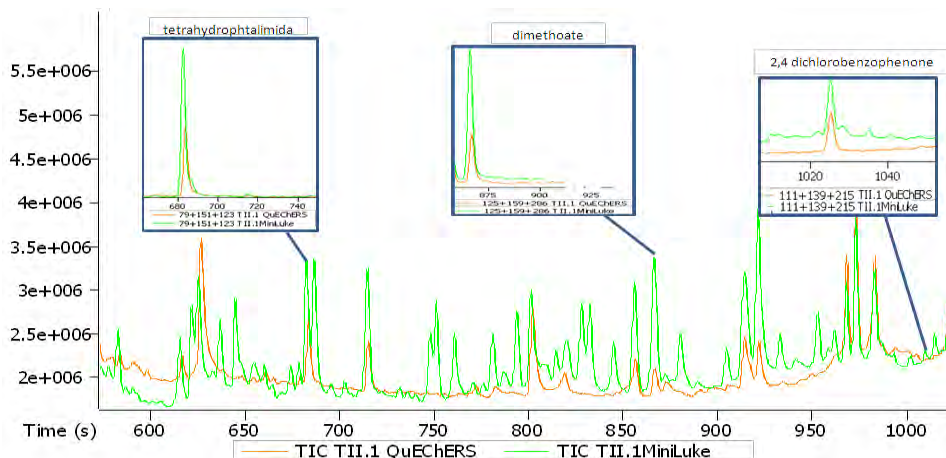


Figure 2. GC separation of pesticides standards

GC-TOF-MS analysis

The metabolites analyzed by GC-TOF-MS are the following: tetrahydrophthalimide, thiophosgene, 4,4'-dichlorobenzophenone, phthalimide, 3,5-dichloroaniline, 4,4'-dibromobenzophenone, 2,4-dichlorobenzophenone and 3,4-dichlorophenyl isocyanate. These metabolites are the most important as a result of the metabolic pathways of tested pesticides. The GC separation also shows other degradation products, but their similarities with mass spectra from libraries were below the relevant limit values imposed by the regulations in force.

The GC-TOF-MS assay is performed using the previously developed and validated method for 85 pesticides analysis from various fruits and vegetables, including the parent pesticides of the target metabolites [22]. Each compound is identified and quantified using the retention times, by monitoring three selected m/z ions (**Table 2**) and by comparing registered mass spectra with those from ten spectra libraries (overlap of at least 70%).

Table 2. The analyzed metabolites, retention time (RT), and specific ions/MRM transitions used for quantification (m/z)

Technique	Metabolite	Retention time (s)	Ions (m/z)/Transitions
GC-TOF-MS	Tetrahydrophthalimide	634.98	79, 123, 151
	Thiophosgene	953.00	79, 114
	4,4'-Dichlorobenzophenone	881.88	75, 111, 139
	Phthalimide	668.63	76, 104, 147
	3,5-Dichloroaniline	464.38	121, 161
	4,4'-Dibromobenzophenone	1024.50	76, 183, 340
	2,4-Dichlorobenzophenone	821.75	75, 111, 139
	3,4-Dichlorophenylisocyanate	390.13	113, 159, 187
LC-MS-QQQ	Omethoate	60.60	214 → 125, 214 → 183
	Carbendazim	66.00	192 → 160, 192 → 132
	Azoxystrobin acid	1041.00	404 → 372, 404 → 344

Tetrahydrophthalimide is the most important metabolite of captan and occurs due to thermal degradation of the parent pesticide that is also favored by the increasing temperature in GC analysis and by the pH of analyzed extract. Thiophosgene is a metabolite of captan too, but not so well known and analyzed as tetrahydrophthalimide. Unfortunately, for these metabolites has not been regulated as residues in vegetables and fruits, none Maximum Residue Limits (MRL) being specified. The 4,4'-dichlorobenzophenone, primary metabolite of dicofol, can be identified and quantified only by GC. This compound appears in all GC analysis of dicofol together with its isomer 2,4'-dichlorobenzophenone, which is the main

metabolite of fenarimol as well. Phthalimide is the most important metabolite of folpet and, as in the case of metabolites of captan, it appears in the GC analysis of the parent active substance. In the last years a growing interest is dedicated to this degradation product of captan. International regulations do not assign any MRL for phthalimide and, moreover, this metabolite is not included in the maximum permissible limit of folpet as its degradation product. Nevertheless, in the reports for European Food Safety Authority (EFSA) these compounds must be mentioned as metabolites of the parent pesticides. The 3,5-dichloroaniline is the main metabolite of iprodione, occurring also as a degradation product of vinclozolin and procymidone. Recently, this compound is used as a biomarker of iprodione and vinclozolin in human urine [23], thus the possibility to be included on the regulations of pesticides in vegetables in the near future is forthcoming. The 2,4-dichlorobenzophenone is the main metabolite of fenarimol and a secondary metabolite of dicofol, but it is not always identified from samples in which one of parent pesticide are determined. Literature indicates [24] that 3,4-dichlorophenylisocyanate is the metabolite of diuron, but this compound is also used as an intermediate substance for the pesticides manufacture, so is difficult to determine with accuracy its provenance.

LC-MS-QQQ analysis

Nowadays, a high-performance liquid chromatography coupled with a QQQ tandem mass spectrometer, working in the multiple reaction monitoring (MRM) mode, is the most frequently platform used in the analysis of pesticide residues in food [18].

The following metabolites are analyzed by LC-MS-QQQ: omethoate, carbendazim and azoxystrobin acid. The target compounds are identified and quantified on the basis of retention time and two Multiple Reaction Monitoring (MRM) transitions (**Table 2**). The target metabolites cannot be analysed by GC-TOF-MS.

Omethoate is the main and most common metabolite of dimethoate. Although the dimethoate can be successfully quantified by GC-TOF-MS, its metabolite, omethoate, cannot be easily analyzed by same technique and its identification can be made only at certain concentration levels. The carbendazim, a pesticid that is not approved for vegetables, is at the same time a metabolite or degradation product of thiophanate methyl and benomyl, two pesticides often used for the vegetables protection treatments. Carbendazim, a very polar compound determined only by LC [8, 13], could generate some problems in the multiresidue analysis on reverse phase. The azoxystrobin acid occurs by degradation of azoxystrobin, being his major identified metabolite.

Determination of metabolites in real samples

For testing the applicability of the developed multiresidues methods to a variety of vegetable matrices, three different vegetables from “high content water” commodity of food were selected: cherry tomato, cucumber, and chili pepper.

The quantification of metabolites on samples was done on the basis of calibration curves that are presented in **Table 3**. The compounds that do not fulfill the criteria of quantification are declared “only identified”. The results were expressed as mg of pesticide/kg of vegetable.

Tetrahydrophthalimide is identified in cherry tomatoes, cucumber and chili peppers, the overlapping of the obtained spectrum with that of library being 83.7%, 95.1% and 91.4% respectively.

Table 3. The obtained quantities of target compounds found in the analyzed real samples (mg/kg)

Metabolite	Calibration curve	r	Cherry tomatoes				Cucumbers				Chili peppers			
			T1		T2		T1		T2		T1		T2	
			3d	10d	3d	10d	3d	10d	3d	10d	3d	10d	3d	10d
Tetrahydrophthalimide	$y=776.042x-7642.850$	0.9974	0.558	0.286	0.283	0.168	0.319	0.138	1.741	1.140	1.988	1.061	1.915	0.172
Thiophosgene	$y=65.340x-1841.630$	0.9959	0.521	0.181	2.089	1.330	2.161	0.966	1.127	0.309	0.272	-	0.335	-
4,4'-Dichlorobenzophenone	$y=453.338x+624.167$	0.9971	0.127	0.060	0.196	0.068	0.425	0.250	0.317	0.103	0.208	0.088	0.310	0.065
Phthalimide	$y=874.344x-30363.200$	0.9961	3.569	1.823	1.937	1.200	5.168	1.450	1.509	0.812	4.833	1.163	4.670	1.110
3,5-Dichloroaniline	Only identified	-	yes	yes	yes	yes	-	-	-	-	-	-	-	-
4,4'-Dibromobenzophenone	Only identified	-	yes	yes	yes	yes	-	-	-	-	-	-	-	-
2,4-Dichlorobenzophenone	Only identified	-	yes	yes	yes	yes	-	-	-	-	yes	yes	yes	yes
3,4-Dichlorophenylisocyanate	Only identified	-	yes	yes	yes	yes	-	-	-	-	-	-	-	-
Omethoate	$y=650.488x+805.569$	0.9987	<LOQ	<LOQ	<LOQ	<LOQ	0.057	0.013	0.068	0.011	0.040	0.020	0.032	0.038
Carbendazim	$y=333.652x+1573.087$	0.9972	<LOQ	<LOQ	<LOQ	<LOQ	0.020	0.000	0.040	0.000	0.090	0.060	0.080	0.060
Azoxystrobin acid	Only identified	-	yes	yes	yes	yes	yes	-	-	-	yes	-	-	-

The degradation of captan is fast being facilitated by humidity and moderate temperature of soil and air. This can explain the higher concentrations of tetrahydrophthalimide, especially in chili peppers.

In this study, thiophosgene was identified and subsequently quantified in cherry tomatoes, cucumber and chili peppers (91.0%, 87.2%

and 90.4% overlap of the spectra). It must be mentioned that this metabolite disappears from chili pepper after 10 days.

It is interesting to compare the degradation of pesticide and its metabolites. For example, **Figure 3** represented the degradation curves of captan, tetrahydrophthalimide and thiophosgene, where it can be seen that thiophosgene tends to accumulate much more than the other metabolite from one treatment to another. This trend was not maintained in the case of cucumbers, concentration of tetrahydrophthalimide being higher than the thiophosgene. In chili peppers, it seems that the metabolism and elimination is rapid, so that after 10 days the parent pesticide and its metabolites are not present in the sample.

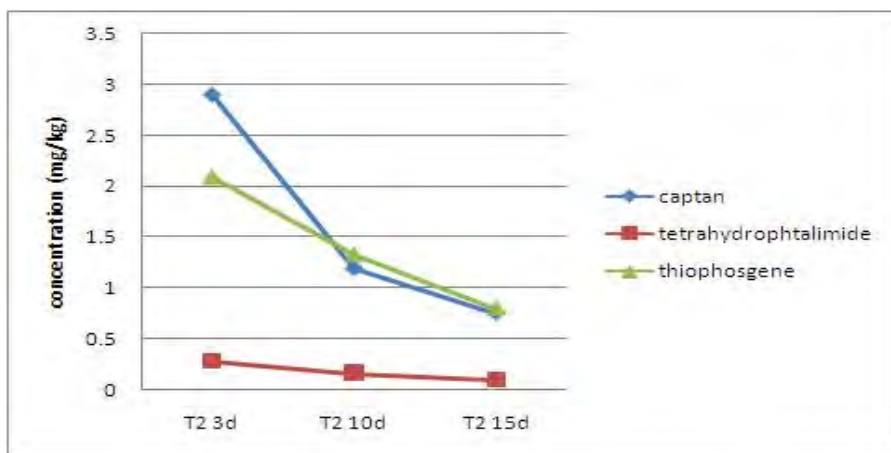


Figure 3. The degradation curves of captan, tetrahydrophthalimide and thiophosgene

The 4,4'-dichlorobenzophenone is determined in cherry tomatoes, cucumber and chili peppers, the spectra similarities being between 87.7% and 96.6%. The concentrations of 4,4'-dichlorobenzophenone are much smaller than those of dicofol proving once again the persistence of this pesticide.

The phthalimide is determined in all analyzed real samples with probability of 80.9% - 97.3%. The degradation shows the same descending trend as pesticide whose metabolite is and is more rapid in cucumbers and chili peppers than in cherry tomatoes. The most important factors that influence its determination can be the organic extract composition and the pH value.

The 3,5-dichloroaniline, 4,4'-dibromobenzophenone and 3,4-dichlorophenylisocyanate are identified by proposed GC method only in cherry tomatoes. This fact is probably due to the more acidic pH of cherry

tomatoes and/or to the different metabolic pathway of parent pesticides in the studied vegetables. According to the Center for Food Safety and Applied Nutrition at the U.S. Food and Drug Administration, the pH of fresh vegetables is into the range of 4.3-4.9 for tomatoes, 5.1-5.7 for cucumbers and 4.9 - 6.1 for chili peppers.

The 2,4-dichlorobenzophenone is identified in cherry tomatoes and chili peppers with a probability of 85.1%.

Omethoate is determined only in cucumbers and chili pepper, while in cherry tomatoes being below LOQ.

Carbendazim as metabolite, is determined in the cucumbers and the chili peppers, but its degradation is more accelerated in cucumbers being absent after ten days from both treatments. The situation of carbendazim in chili pepper must be mention. It is well known that the LMA for thiophanate-methyl is expressed as sum of thiophanate-methyl and carbendazim, while in the EFSA reports the carbendazim can be reported as stand-alone substance. The LMA is 0.1mg/kg after the release time of 3 days. The experimental value obtained after three days subsequent to treatment II is below LMA ($0.08 < 0.1$), but if the quantity of thiophanate-methyl is taken into consideration, the resulted value exceed LMA ($0.136 > 0.1$).

As in the situation of omethoate, the residue of this metabolite within the cherry tomatoes is minor being below LOQ.

Azoxystrobin acid is identified in all real samples, but unlike cherry tomatoes, in which is present in all samples, in the cucumbers and the chili peppers is identified only in the samples taken after three days from treatment. This fact leads us to conclude that the azoxystrobin acid is rapidly eliminated from cucumbers and chili peppers.

Concluding, in the cherry tomatoes six metabolites can be quantified, but all of them are below LMA values. Besides these, other five metabolites are identified. In the case of the cucumbers, six metabolites are quantified, all being below LMA, and another one metabolite is only identified. Regarding chili pepper, six pesticides have been determined and two other metabolites have been only identified. The concentration of metabolites in studied vegetables is lower than that is considered safe.

CONCLUSIONS

Two analytical approaches are used for the development of reliable screening, quantification and confirmation of pesticides metabolites in different vegetables. The proposed methods have different approaches than the other multi-residue methods for vegetables. A combination between proper extraction method and gas and liquid chromatography coupled with

mass spectrometry detection ensure a quick, cheap, effective, rugged, and safe multi-residue method for the analysis of pesticide metabolites.

The results suggests that spraying pesticides in high doses lead to high levels of pesticide residues in the case of some studied vegetables and should be discouraged because it may facilitate the emergence of various diseases.

The results suggest that the concentration of metabolites together concentration of parent pesticide must be taken into account in order to establish the LMA in vegetables and fruits.

EXPERIMENTAL SECTION

Materials and reagents

The cherry tomatoes, cucumbers and chili pepper were selected as representative matrices. The vegetables used in this study were grown in our garden. Two treatments for plant protection with solution of chosen pesticides were applied when the fruits of vegetables were grown at a rate of 10%. The solutions of each pesticide were prepared according to the instructions given by manufacturers for each type of plant culture. The plants were treated with pesticides by spraying with a hand pump dispenser just as the practice of small producers. The time between treatments was twenty days and the samples were taken after three and ten after each treatment. The sampling times were chosen according to the release time of tested pesticides.

All pesticides standards were of analytical grade and were purchased from Sigma-Aldrich (Munich, Germany). The stock solution of standards (1000 $\mu\text{g}/\text{mL}$ of each pesticide) was prepared in toluene for GC analysis and in acetonitrile for LC analysis and was stored at -18°C . A standards solution of intermediary concentration (5 $\mu\text{g}/\text{mL}$) and the working standards solutions were prepared by dilution of stock solutions with *iso*-octane - toluene, 9:1 (v/v) for GC analysis and with acetonitrile - water, 1:1 (v/v) for LC analysis. Solution of hexachlorobenzene (HCB) (0.2 $\mu\text{g}/\text{mL}$) was prepared in *iso*-octane - toluene, 9:1 (v/v) and was used as internal standard (IS) for GC-MS analysis. In the case of LC-MS analysis no internal standard was used.

GC calibration curves were constructed at seven levels of concentration, namely 0.01-0.03-0.06-0.09-0.27-0.54-0.81 $\mu\text{g}/\text{mL}$ and LC calibration curves were made at five levels of calibration between 0.01 and 0.4 $\mu\text{g}/\text{mL}$. The calibrations were made on equally standard solutions and fortified samples (cherry tomatoes, cucumber and peppers) subjected to both extraction methods.

All solvents of analytical grade (acetonitrile, acetone, dichloromethane, petroleum ether, methanol, toluene, *iso*-octane, acetic acid, formic acid) and anhydrous magnesium sulphate, sodium chloride, sodium acetate were purchased from Sigma-Aldrich (Munich, Germany). Primary-secondary amine (PSA) and PSA dispersive SPE Clean-up tubes (dSPE) were purchased from Supelco, USA and 0.2 µm RC filters were purchased from Whatman, Germany.

Sample preparation

Modified MINILUKE method

Into a 150mL polypropylene centrifuge tube, 10mL acetone, 10mL dichloromethane and 10mL petroleum ether were added to 10g of each sample accurately weighted. The sample was extracted for 2min at 15.000rpm using an Ultraturax homogenizer and then it was centrifuged for 5min at 4000rpm. The entire upper organic phase was evaporated near to dryness on vacuum evaporator at 40°C. The residue was re-dissolved in 2mL *iso*-octane - toluene, 9:1 (v/v) together with HCB (0.2µg/mL) and analyzed by GC-TOF/MS after filtered through RC 0.2 µm. In the case of LC- MS/MS method, the residue obtained after evaporation procedure was re-dissolved in 2 mL acetonitrile - water, 1:1 (v/v) and filtered through RC 0.2µm before analysis.

Buffered QUECHERS method

Into a 100mL polypropylene centrifuge tube, 10mL acetonitrile acidified with 1% acetic acid was added to 10g of each sample. In the case of GC analysis 200µL of HCB solution (10µg/mL) was also added as internal standard. To the extracted sample obtained using an Ultraturax homogenizer (15.000rpm for 1min), 4g MgSO₄, 1g NaCl and 1g CH₃COONa were added. Then, the resulting mixture was shaken for 1min and centrifuged for 5min at 4000rpm. An aliquot of 6mL extract was transfer into a 20mL PSA cartridge tube which 150mg PSA and 900mg MgSO₄ were previously added. The resulting mixture was shacked for few seconds, centrifuged for 5min at 4000rpm and then 1 mL of extract was evaporated under N₂ steam. The obtained residue was re-dissolved in *iso*-octane - toluene, 9:1 (v/v) for GC-TOF/MS analysis and in 1mL acetonitrile - water, 1:1 (v/v) for LC analysis. In both cases the re-dissolved residues were filtered through RC 0.2 µm before analysis.

Chromatographic analysis

GC-TOF-MS

An Agilent 6890 series gas chromatograph with two ovens, Agilent 7683 series Autosampler and a split/splitless capillary injector port equipped

with a LECO Pegasus Time-of-Flight Mass Spectrometer (TOF-MS) (USA) was used for GC-MS analysis. Chromatographic separation was achieved on two capillary columns, first RXi-MS 30m x 0.25mm x 0.25 μ m (Restek, USA) and second BPX50 1.6m x 0.1mm x 0.1 μ m (SGE Analytical Science, Australia). The injector temperature was 250°C and splitless injection was performed using helium as carrier gas with a flow rate of 1.2 mL/min. The ovens temperatures were programmed without modulation as follow: oven 1-80°C initial temperature for 2 min, increasing rate of 20°C/min to 180°C, 5°C/min to 220° C, 25°C/min to 300°C where is held for 10min; oven 2-110°C initial temperature for 2 min, 20°C/min to 210°C, 5°C/min to 250°C, 25°C/min to 330°C and held at this temperature for 10min. The injection volume was 1 μ L. The mass spectrometer was operated in electron ionization mode (EI) and full scan mode monitoring between m/z 40 and m/z 450, with ionization energy of 70eV and acquisition rate of 10spectra/second. The transfer line temperature was kept at 280°C.

LC-MS-QQQ

For LC-MS analysis, an AGILENT liquid chromatograph equipped with a quaternary pump model 1200, autosampler and a mass spectrometer triple quadrupole AGILENT 6410A, ionization source type Multi mode ionization (MMI), with electrospray ionization (ESI) in the positive mode were used.

Separation was performed at 25°C on a Zorbax Eclipse XDB-C18, 1.8 μ m, 4.6x50mm column (Agilent). 10 μ L of sample was injected and the mobile phases consisting of 0.1% formic acid in water (A) and acetonitrile (B) with a flow rate of 0.4 mL/min were used. The elution gradient was: 20-80% B at 0-28min, 80-100% B at 28-30min, kept this for 1min, 100-20% B at 31-33min and then kept 20% B for 2min. The fragmentation energy and the collision energy were between 70-120V and 5-20eV, respectively, being specific of each pesticide. Working parameters were set as follow: capillary voltage 2500V, the temperature of the gas in the ion source 350°C, the nebulizer pressure 60psi and the drying gas flow 5L/min. Nitrogen was used as nebulization, desolvation and collision gas.

REFERENCES

1. European Commission, Off. J. L 230 (1) EU (1991) Council Directive (EEC) No 414/1991of 15 July 1991 concerning the placing of plant protection products on the market Off J L 230, 19/08/1991.
2. European Union, Off. J. L 309 (1), **2009**.

3. European Commission, Health and Consumers Directorate-General, Regulation (EC) No 1107/2009 concerning the placing of plant protection product on the market.
4. <http://www.inchem.org/>
5. J. J. Menn, *Environmental Health Perspectives*, **1978**, 27, 113.
6. S. Klimmek, Analytical Method Development and Validation of the DFG Method S19 for the Determination of Residues of Azoxystrobin and the Metabolite R230310 in Plant Matrices. Chemische und Biologische Laboratorien AG, **2004**.
7. O. Belafdal, M. Bergon, J. P. Calmon, *Pesticide Science*, **1986**, 17, 335.
8. T. R. Roberts, D. H. Hutson, P. W. Lee, P. H. Nicholls, J. R. Plimmer, "Metabolic Pathways of Agrochemicals: Part 2, Insecticides and fungicides", The Royal Society of Chemistry, Cambridge, **1999**.
9. A. Hiroyasu, "Metabolic Maps of Pesticides (Ecotoxicology and Environmental Quality Series)", Academic Press, Inc., **1982**.
10. European Commission Directorate D, Food Safety: production and distribution chain, D3 - Chemicals, Contaminants and Pesticides, Review report for the active substance fenarimol, **2007**.
11. E. Corta, A. Bakkali, A. Barranco, L. A. Berrueta, B. Gallo, F. Vicente, S. Bogdanov, *Talanta*, **2000**, 52, 169.
12. A. Cifuentes, *ISRN Analytical Chemistry*, **2012**, 2012, 1.
13. L. L. van Eerd, R. E. Hoagland, J. C. Hall, *Weed Science*, **2003**, 51, 472.
14. R. Schöning, R. Schmuck, *Bulletin of Insectology*, **2003**, 56, 41.
15. Conclusion on the peer review of the pesticide risk assessment of the active substance myclobutanil, *EFSA Journal*, **2010**, 8, 1682.
16. A. Vanni, L. Anfossi, A. Cignetti, A. Baglieri, M. Gennari, *Journal of Environmental Science and Health, Part B*, **2006**, 41, 67.
17. World Health Organization, The Joint FAO/WHO Meeting on Pesticide residues in food 2011, FAO (Ed.), Rome, **2012**.
18. A. Stachniuk, E. Fornal, *Food Analytical Methods*, **2016**, 9, 1654.
19. S. Walorczyk, I. Kopeć, E. Szyrka, *Food Analytical Methods*, **2016**, 9, 1155.
20. J. L. Tadeo, "Analysis of Pesticides in Food and Environmental Samples", CRC Press, Taylor & Francis Group, Boca Raton, 2008. chapter 6.
21. M. Stoytcheva, "Pesticides – Strategies for Pesticides Analysis", InTech, Rijeka, **2011**, chapter 8.
22. A. Meghesan-Breja, C. Cimpoi, A. Hosu, *Acta Chromatographica*, **2015**, 27, 657.
23. C. H. Lindh, M. Littorin, A. Amilon, B. A. Jönsson, *Rapid Communication in Mass Spectrometry*, **2007**, 21, 536.
24. C. Ciscato, C. Barbosa, A. Gebara, "Analysis of Pesticide Residues in Mango by GC/MS/MS With Bond Elut QuEChERS EN Kits - Application Note", Agilent Technologies, Inc., **2015**.

In memory of prof. dr. Simion Gocan

IDENTIFICATION OF COMPLEX VOLATILE ORGANIC COMPOUNDS IN MUNICIPAL LANDFILL LEACHATE BY HEAD-SPACE SOLID PHASE MICROEXTRACTION AND GCXGC-qMS ANALYSIS

MIHAIL SIMION BELDEAN-GALEA^{a*}, DIDIER THÉBAUT^b,
JÉRÔME VIAL^b, VIRGINIA COMAN^c

ABSTRACT. A method for the identification of different classes of volatile organic compounds in the municipal landfill leachate using solid phase microextraction and comprehensive two dimensional gas chromatography coupled with mass spectrometry (SPME-GCxGC-qMS) is elaborated. The results showed that the proposed protocol is able to separate and identify in a single run different classes of volatile organic compounds responsible for the odor of leachate such as carbonyl compounds, aromatic compounds, terpenes, phenolic compounds and nitrogen and sulfur containing compounds. The use of solid phase microextraction not only eliminate the solvent from the samples processing step but also considerably reduces the time and the volume of the sample necessary for this step, being a viable green alternative for this type of analysis. The use of mass spectrometry gives the possibility to indentify many other compounds responsible for municipal landfill leachate odor, creating the premises for a better assessment of chemical composition of leachate. The developed protocol shows good performances in term of repeatability, linearity, limit of detection and limit of quantification being applicable for the real municipal landfill leachate analysis.

Keywords: *Volatile organic compounds, municipal landfill leachate, solid phase microextraction, GCxGC-qMS*

^a Babeş-Bolyai University, Faculty of Environmental Science and Engineering, 30 Fântânele street, RO-400294, Cluj-Napoca, Romania.

* Corresponding author simion.beldean@yahoo.com

^b École Supérieure de Physique et de Chimie Industrielles, 10 rue Vauquelin, 75231 Paris Cedex 05, France.

^c Babeş-Bolyai University, Raluca Ripan Institute for Research in Chemistry, 30 Fântânele street, RO-400294 Cluj-Napoca, Romania.

1. INTRODUCTION

Leachate is the liquid generated by the percolation of rainwater through the layers of wastes in municipal landfill site. This product can contain both organic and inorganic substances, released from the material deposited or as the result of biotic and abiotic reactions [1-2].

The basal composition of leachates is characterized by dissolved organic matter, xenobiotic organic compounds, inorganic salts, ammonia, heavy metals and other toxicants which are potentially harmful to human and animal health [1, 3].

More than 200 organic compounds have been identified as being dissolved in municipal landfill leachate with upwards of 35 compounds having the potential to cause harm to the environment and human health [4].

The most organic hazardous classes of compounds identified in the municipal landfill leachate are aromatic compounds, chlorinated aliphatic compounds, aliphatic and aromatic acids, polycyclic aromatic hydrocarbons, aldehydes, ketones, terpenes, phenols, phthalates, pesticides, nitrogen containing compounds, organo-phosphoric flame retardants, mercaptans etc. [5-7].

Near the dissolved chemical compounds, municipal landfills are also a potential source of offensive odors which make the areas in the proximity of landfills vulnerable not only to the emissions of potential toxic compounds but also to the nuisance such as odor pollution [8]. The odorous compounds generated by municipal landfill contain generally six classes of substances such as: saturated and unsaturated hydrocarbons, acidic hydrocarbons and organic alcohols, aromatic hydrocarbons, halogenated compounds, sulfur compounds (carbon disulfide and mercaptans), and inorganic compounds [7, 9]. Some of these compounds represent odors causing annoyance for the population, other compounds can be toxic for human and animal health (psychological stress, irritation of mucous membranes, long-term toxic reactions) [10] or can be precursors of photochemical smog formation [9]. From these reasons in the last decades many scientists have been paid attention to the characterization of volatile organic compounds emitted from the municipal landfill.

Over 500 compounds have been reported in landfill gas, these compounds including alkanes and alkenes, cycloalkanes and cycloalkenes, aromatic and polycyclic aromatic hydrocarbons and their derivatives, aldehydes, alcohols, ketones, esters, organohalogens and organosulphur compounds, trichlorethylene, tetrachlorethylene, *b*-pinenes, limonene, *p*-cymene etc. [11-13].

Usually the concentrations of the odorous compounds are very low, but their olfactory thresholds are in some cases lower. Hence, sensitive analytical methods are required for the identification and quantification of odorous substances taking into account that their concentrations are often below the detection limit of measuring equipment [14].

The aim of this study was to develop a sensitive and, in the same time, a comprehensive method for the identification of some classes of compounds responsible for the odor in municipal landfill leachate which may pose health concerns to nearby neighborhoods.

2. RESULTS AND DISCUSSION

2.1. Analytical performances of the SPME-GCxGC-qMS method

The performances of developed method were evaluated in term of repeatability (intra-day precision), linearity, limit of detection (LOD) and limit of quantification (LOQ) calculated based on the ratio of standard deviation (SD) and the slope of calibration curves (Table 1).

Table 1. The performances of developed SPME-GCxGC-MS method

Compound name	Linear curve equations	R ²	SD	Slope	LOD (ng mL ⁻¹)	LOQ (ng mL ⁻¹)	RSD (%)
Methyl isobutyl ketone	y=805869x+5E+07	0.9463	10026208	8058691	0.74	2.48	0.9
2-Heptanone	y=5E+06x + 3E+08	0.9785	2623366	5.00E+06	0.32	1.05	0.2
Dimethylbenzene	y=1E+07x + 4E+08	0.9835	310653	1E+07	0.02	0.06	4.0
Isopropylbenzene	y=6E+06x + 3E+08	0.9544	29827885	6.00E+06	3.00	9.94	5.5
Trimethylbenzene	y=2E+07x + 7E+08	0.984	681651	2.00E+07	0.02	0.07	2.9
Phenol	y=7591881x-2E+07	0.9892	15207533	7591881	1.20	4.00	6.6
<i>tert</i> -Butylbenzene	y=6E+06x + 2E+08	0.9855	42115421	6.00E+06	4.20	14.04	9.5
<i>alpha</i> -Terpinene	y=1E+07x + 1E+08	0.9647	47849916	1.00E+07	2.80	9.56	9.8
Limonene	y=2E+07x + 3E+08	0.9599	136306146	2.00E+07	4.00	13.64	10.5
Ocimene	y=9E+06x + 8E+07	0.9827	19865104	9.00E+06	1.32	4.42	6.3
Acetophenone	y=1E+07x - 1E+07	0.9944	42166192	1,00E+07	2.60	8.44	2.2
Cresol	y=3E+06x - 5E+07	0.9554	8847603	3,00E+06	1.76	5.90	2.2
1,3,5-Triisopropyl benzene	y=1E+07x + 2E+08	0.9883	12613977	1.00E+07	3.78	12.6	2.64
5-Nonanone	y=2E+07x + 5E+08	0.9938	62313078	2.00E+07	1.86	6.24	2.6
Terpinolene	y=1E+07x + 2E+08	0.9783	10613977	1.00E+07	0.64	2.12	2.1
Isophorone	y=5E+06x - 5E+06	0.9981	10035259	5.00E+06	1.20	4.02	0.9
Camphor	y=1E+07x + 4E+08	0.9894	76927561	1.00E+07	4.60	15.38	2.4
Benzothiazole	y=1E+07x - 9E+07	0.9888	89652655	1.00E+07	5.40	17.94	5.2

Repeatability was expressed by means of six replicates (n=6) of the standard mixture in concentration of 25 ng mL⁻¹. The results showed a good repeatability, the relative standard deviation RSD being situated under 15-16%, the maximum accepted at the concentration level less than 100 ppb [15]. The method provide also a good linearity with a coefficient of determination

(R^2) ranging between 0.95 and 0.99, a low LOD (0.02-54 ng mL⁻¹) and LOQ (0.05-17.94 ng mL⁻¹) respectively.

The combination of columns chosen for the separation provides a good resolution between the standard compound mixture (Figure 1).

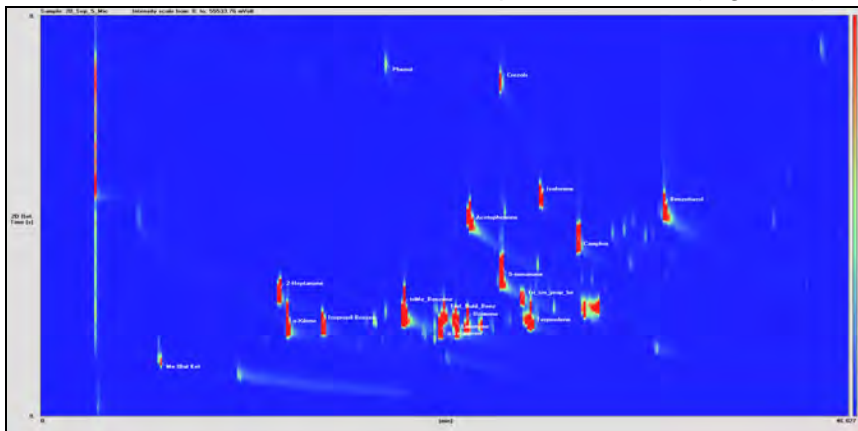


Figure 1. GCxGC chromatogram of the standard mixture

2.2. Analysis of municipal landfill leachate samples

The extraction and the analysis of volatile organic compounds in municipal landfill leachate samples were done under the conditions described in the Experimental part. The results of the performed experiment showed that the landfill leachate contains a huge number of volatile organic compounds with different polarities which are well distributed on the GCxGC chromatogram (Figure 2).

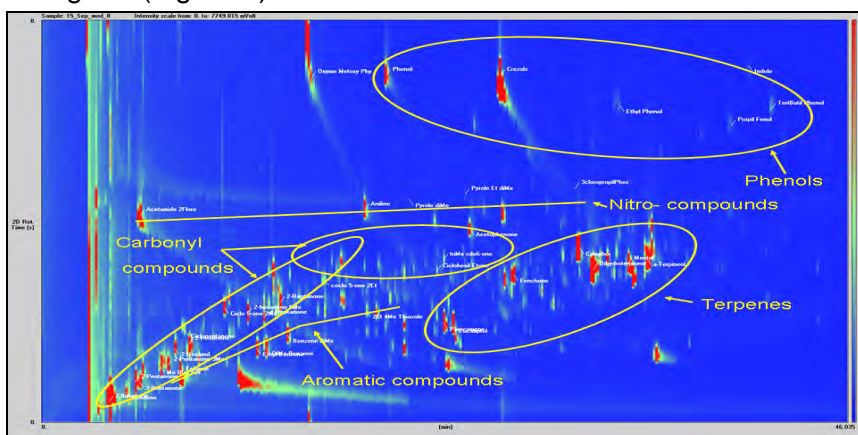
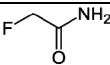
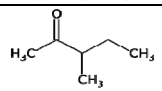
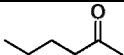
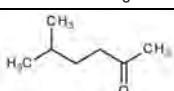


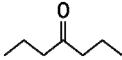
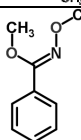
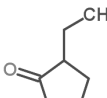
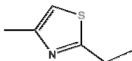
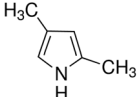
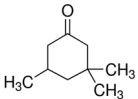
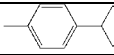
Figure 2. GCxGC chromatogram of the municipal landfill leachate sample and the classes of the identified compounds

It can be observed that the compounds are grouped on the families according to their physical and chemical proprieties.

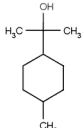
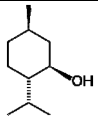
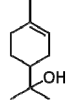
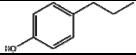
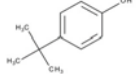
Using the standard mixtures, the retention parameters (retention time in the first dimension (RT 1st D) and retention time in the second dimension (RT 2nd D)) and the mass spectra, in the leachate sample 40 compounds were identified. Their name, molecular formula and retention parameters are presented in Table 2. It should be mention that only the compounds with similarity of mass spectra compared with NIST mass spectra library exceeding 70% were taken into consideration.

Table 2. Compounds identified according to standard mixture, their mass spectra and retention parameters

Component name/abbreviation	Molecular formula	RT 1st D (min)	RT 2nd D (sec)
2-Butanone		3.733	0.50
Benzene		4.872	0.64
2-Pentanone		5.333	0.82
3-Pentanone		5.412	0.93
Fluoroacetamide / (Acetamide 2Floro)		5.467	4.09
Methyl isobutyl ketone / (Me IBut Ket)		6.800	1.09
3-Methyl-2-pentanone / (2-Pentanone 3Me)		7.200	1.07
Hexanal		7.600	1.55
Toluene		8.000	1.00
2-Hexanone		8.400	1.55
2-Methylcyclopentanone / (Ciclo 5-one 2Me)		10.667	2.52
5-Methyl-2-hexanone / (2-hexanone 5Me)		11.600	2.02
Ethylbenzene / (Ethyl Benzene)		12.267	1.43

Component name/abbreviation	Molecular formula	RT 1st D (min)	RT 2nd D (sec)
4-Heptanone		12.667	2.14
1, 2-dimethylbenzene / (DiMe Benzene)		12.800	1.45
2-Heptanone		13.600	2.55
1, 3-dimethylbenzene / (Benzene diMe)		14.000	1.84
Methyl N- hydroxybenzenecarboximidoate/ (Oxyme Metoxy Phy)		15.067	7.25
2-Ethylcyclopentanone / (coclo 5-one 2Et)		16.000	2.86
Aniline		18.400	4.41
2-Ethyl-4-methylthiazole / (2Et 4Me Thiazole)		18.533	2.25
Phenol		19.600	6.93
2,4-Dimethylpyrrole / (Pyrole diMe)		21.200	4.82
Cyclohexyl Ethanone / (Ciclohexil Etone)		22.987	3.02
3,3,5-Trimethylcyclohexanone/ (triMe cilo6-one)		22.933	3.27
p-cymene / (Paracimene)		23.600	1.77
Eucalyptol / (Eucaliptol)		24.267	1.82

IDENTIFICATION OF COMPLEX VOLATILE ORGANIC COMPOUNDS IN MUNICIPAL LANDFILL ...

Component name/abbreviation	Molecular formula	RT 1st D (min)	RT 2nd D (sec)
Acetophenone		24.400	3.91
3-Ethyl-2,4-dimethylpyrrole / (Pyrole Et diMe)		24.400	4.57
Cresol / (Crezols)		26.133	6.61
Fenchone		26.833	2.84
Camphor		30.667	3.43
Dihydroterpineol		31.467	3.16
Ethyl Phenol		32.800	6.25
Menthol / (Mentol)		33.600	3.07
α -Terpineol		34.400	3.50
Propyl Phenol / (Propil Fenol)		39.067	5.95
Indole		40.000	7.11
4-tert Butylphenol / (TertButil Phenol)		41.923	6.12

It can be also observed that in the analyzed sample the most prevalent compounds are carbonyl group compounds, phenolic compounds, terpenes and aromatic and alkyl aromatic hydrocarbons. Also, nitrogen

containing compounds such as fluoroacetamide, aniline, 2,4-dimethylpyrrole, 3-ethyl-2,4-dimethylpyrrole, 2-ethyl-4-methylthiazole, methyl N-hydroxybenzenecarboximidoate have been identified.

Many other compounds could not be identified due to the technical limitation of the instrument. However, the developed method has a big potential and provides information that are difficult to obtain using classical chromatographic methods.

Moreover, the obtained results are in agreement with other studies referring to the odorants of municipal landfill leachate [8-12], but this study provides a better identification of the compounds due to their GCxGC arrangement.

3. CONCLUSIONS

The developed procedure provides a very sensitive method for the analysis of volatile organic compounds in municipal landfill leachate.

Identification of the compounds is improved due to the grouping of the compounds on the families according their physical and chemical proprieties.

The most prevalent families of the identified compounds are carbonyl group compounds, phenolic compounds, terpenes, aromatic and alkyl aromatic hydrocarbons and nitrogen-containing compounds.

SPME-GCxGC-qMS could be a good and green alternative for the screening of volatile organic compounds in municipal landfill leachate, being able to provide better information about the compounds responsible for odors.

4. EXPERIMENTAL SECTION

4.1. Reagents and solutions

For the qualitative and quantitative analysis a standard mixture containing different classes of organic compounds in concentration of $100 \mu\text{g mL}^{-1}$ dissolved in a solvent mixture of *n*-hexane:acetone (1:1 v/v) was used. The composition of the standard mixture is given in Table 1. The standard mixture was prepared from pure substances, of analytical grade purity, purchased from Sigma Aldrich, Supelco and Fluka. The calibration standard solutions in concentration of 10, 25, 50, 100 and 150 ng mL^{-1} were prepared by dilution of different volumes of standard mixture in 5 mL of Milli-Q water. Acetone and *n*-hexane (99.99% purity) were provided from Merck (Germany) and helium in purity of 99.9999% from Air Liquide, France. The Milli-Q water was prepared using a Milli-Q Plus water system from Millipore (USA).

4.2. Instrumentation, chromatographic and SPME conditions

For the analysis of volatile organic compounds in municipal landfill leachate, a Thermo Trace GC×GC gas chromatograph equipped with a dual CO₂ cryogenic modulator and coupled to a quadrupole mass spectrometer (qMS) model ThermoISQ (Courtaboeuf, France) was used. Helium of high purity at a constant pressure of 156 kPa was used as carrier gas. The mass spectrometer frequency of acquisition was 50 Hz, and the SCAN mode was used for data collection, setting a mass range from 45 to 250 m/z. The ionization was performed by Electron Impact Ionization using a voltage of 70 eV. The ion source temperature was 210°C and 280°C for the transfer line. The inlet temperature was set at 280°C and the injection was made in split mode using a split ration of 10.

For the separation, a Factor Four VF-1 ms column (100% dimethylpolysiloxane), 30 m × 0.25 mm ID, 0.25 µm film thickness (Varian) was used in the first dimension and a DB-1701 column ((14%-cyanopropyl-phenyl)-methylpolysiloxane), 1.5 m × 0.10 mm ID, 0.10 µm film thickness (Agilent) was used for the second dimension. The separation of compounds was performed with a gradient temperature program, by a heating of 2.0°C/min from 40 to 120°C, with 5 minutes final hold time. The modulation period was 8 seconds and the initial off-set was 0.5 second.

The data acquisition was performed using the X-Calibur software and the GC×GC representation was realized by the Chrom-Card software. The identification of the compounds was done comparing the obtained mass spectra with those from NIST (classical) mass spectral library.

The solid phase microextraction (SPME) of the target compounds was performed using a SDVB/carbowax/pdms fiber, 20 mm length using a TriPlus Autosampler. For the extraction, the following conditions were used: incubation temperature 60°C in constant mode, extraction time 10 minutes and desorption time 15 minutes.

For the analysis of volatile organic compounds in real samples, 5 mL of municipal landfill leachate collected from a municipal solid waste landfill from Romania was used. The extraction was done according to the protocol described above.

ACKNOWLEDGEMENTS

This work was performed in the frame of the Romania - France Bilateral Cooperation, Program Brâncuși, Project no. 774/2014 funded by UEFISCDI - Roumania and Project no 32654NJ funded by Campus-France.

REFERENCES

1. S. Budi, B.A. Suliasih, M.S. Othman, L.Y. Heng, S. Surif, *Waste Management*, **2016**, 55, 231.
2. C. Oman, P.-A. Hynning, *Environmental Pollution*, **1993**, 80, 265.
3. T.H. Christensen, P. Kjeldsen, H.J. Albrechtsen, H.J. Heron, P.H. Nielsen, P.L. Bjerg, P.E. Holm, *Critical Reviews in Environmental Science and Technology*, **1994**, 24, 119.
4. R.J. Slack, J.R. Gronow, N. Voulvoulis, *Science of the Total Environment*, **2005**, 337, 119.
5. D. Kulikowska, E. Klimiuk, *Bioresource Technology*, **2008**, 99, 5981.
6. M.S. Beldean-Galea, J. Vial, D. Thiébaud, *Central European Journal of Chemistry*, **2013**, 11(10), 1563.
7. E. Borrás, L.A. Tortajada-Genaro, A. Muñoz, *Talanta*, **2016**, 148, 472.
8. M. Palmiotto, E. Fattore, V. Paiano, G. Celeste, A. Colombo, E. Davoli, *Environment International*, **2014**, 68, 16.
9. D. Ying, C. Chuanyu, H. Bin, X. Yuen, Z. Xuejuan, C. Yingxu, W. Weixiang, *Waste Management*, **2012**, 32, 317.
10. B. Scaglia, V. Orzi, A. Artola, X. Font, E. Davoli, A. Sanchez, F. Adani, *Bioresource Technology*, **2011**, 102, 4638.
11. R. Chiriac, J. Carré, Y. Perrodin, L. Fine, J.-M. Letoffe, *Journal of Hazardous Materials*, **2007**, 149, 249.
12. R. Chiriac, J. Carré, Y. Perrodin, H. Vaillant, S. Gasso, P. Miele, *Atmospheric Environment*, **2009**, 43, 1926.
13. E. Davoli, M.L. Gangai, L. Morselli, D. Tonelli, *Chemosphere*, **2003**, 51, 357.
14. J.-J. Fang, N. Yang, D.-Y. Cen, L.-M. Shao, P.-J. He, *Waste Management*, **2012**, 32, 1401.
15. European Community Document, SANCO No. 3030/99, rev. 4, 11/07/2000 - https://ec.europa.eu/food/sites/food/files/plant/docs/pesticides_ppp_appproc_guide_phys-chem-ana_tech-mat-preps.pdf

In memory of prof. dr. Simion Gocan

COMPARISON OF DIFFERENT EXTRACTION TECHNIQUES FOR THE EVALUATION OF POLYPHENOLS CONTENT IN SUMMER SAVORY EXTRACTS

DORINA CASONI^a, NELI OLAH^{b, c}, LOREDANA SORAN^d
SIMONA CODRUTA AURORA COBZAC^{a*}

ABSTRACT. Efficiency of conventional solvent extraction (maceration and normal refluxing) and novel extraction techniques (ultrasound-assisted extraction-UAE and microwave-assisted extraction-MAE) were compared in order to obtain an enhanced content of total flavonoid, total phenolic compounds and rosmarinic acid from the *Satureja hortensis* L. (Summer savory) herb. Different mixtures of ethanol-water ratio were used for extraction of these compounds from dry plant material. High level of total flavonoid content was determined for a solvent system consisted of 40% respectively 50% ethanol (extraction systems ES6 and ES5) while the most efficient techniques were normal refluxing (R) and ultrasound-assisted extraction when sweep mode (UAE1) was selected. For the same solvent systems (ES6 and ES5), a high content of total phenolic compounds was determined when the normal refluxing (R) and microwave-assisted extraction (MAE1, with a duty coefficient of 40% and microwave action time 1 min) were used for the extraction procedure. For the rosmarinic acid extraction, the maceration technique (M) combined with an ethanol-water system consisted of 60% ethanol (ES4) was found as the most efficient procedure.

Keywords: *Satureja hortensis* L., flavonoids, phenolic compounds, rosmarinic acid, maceration, reflux extraction, ultrasound assisted extraction, microwave assisted extraction

^a Babeş-Bolyai University, Faculty of Chemistry and Chemical Engineering 11 Arany Janos Street, RO-400028, Cluj-Napoca, Romania

^b PlantExtract, Radaia, Cluj-Napoca, Romania

^c Vasile Goldiș Western University from Arad, Faculty of Pharmacy, 86 L. Rebreanu Street, 310414 Arad, Romania

^d National Institute for Research and Development of Isotopic and Molecular Technologies, 65–103 Donath Street, 400293, Cluj-Napoca, Romania

* Corresponding author: codruta.cobzac@yahoo.com

INTRODUCTION

Summer savory or Garden savory (*Satureja hortensis* L.), a widely used culinary herb belonging to the *Lamiaceae* family, has been used as spice for food flavouring and as traditional medicinal tea as remedy to treat various diseases and their symptoms [1]. The most recent studies suggest that the use of some savory species, are effective in body protecting against oxidative stress, free radical damage, inflammation or microbial infections, providing a natural prevention or treatment for some chronic and serious illnesses such as cancer, diabetes, cardiovascular and Alzheimer's diseases [2-5].

Many species of the *Lamiaceae* family are reported as plants with high content of phenolic compounds and antioxidant capacities [6]. Extensive studies on different *Satureja* species carried out in the last years demonstrated a remarkable diversity of classes of compounds such as volatile oils, polyphenolic acids, flavonoids - especially derivatives of apigenin and luteolin, tannins, steroids and pyrocatechols existing into [7, 8]. The major components of the essential oils of *Satureja* species are carvacrol, thymol, phenols [1] while the rosmarinic acid was found to be the major component of the alcoholic extracts [9].

Separation, identification and quantification of flavonoids and phenolic compounds in various *Laminaceae* family plants (including Savory species) are based especially on chromatographic techniques [10-13]. Most of the extraction procedures of these compounds are based on solvent extraction which is efficient, easy to use and have a wide applicability [14]. The type of the solvents and the composition of the used extraction system is one of the most influential variables on both extraction yield and classes of extracted constituents. Methanol, ethanol, and water are widely employed for extracting different classes of phenols. Despite methanol exhibits the highest capacity to extract polyphenols [15], due to its toxicity is less preferred than ethanol-water mixtures. Studies on extraction of natural antioxidants proved that the ethanol-water mixtures are suited to penetrate the hydrophobic areas of the vegetal matrix facilitating further extraction processes [16, 17]. Methods used for extracting phenolic compounds include both conventional techniques (maceration, reflux) and alternative one using high pressure solvents or the benefits of ultrasounds or microwaves [12, 18].

In context of abound studies on volatile oil of *Satureja hortensis* L existing in scientific literature, the aim of this study is to evaluate the effectiveness of different extraction techniques and systems with respect to the total content of flavonoids, phenolic compounds and rosmarinic acid to obtain high quality hydroalcoholic extracts from the Summer savory cultivated in Romania.

RESULTS AND DISCUSSION

Conventional solvent extraction and some of the novel extraction procedures have been used for the flavonoids, phenolic compounds and rosmarinic acid extraction from dry *Satureja hortensis* L. herb.

Based on the consideration that extraction solvent composition is one of the most influential variables on both extraction yield and classes of extracted compounds, various ethanol-water mixtures (ES1-ES6) were investigated. The evaluation of the applied extraction procedures was made based on extracted content of total flavonoids, phenolic compounds and rosmarinic acid content determined by UV-Vis absorption spectrometry and high performance liquid chromatography respectively.

Evaluation of total flavonoids

The concentration of flavonoids in hydroalcoholic extracts was determined based the rutoside calibration curve $Y=1.9372x+0.0043$ ($R^2=0.9990$; $LOD=0.6072 \mu\text{g/mL}$; $LOQ=1.202 \mu\text{g/mL}$) on $20 \mu\text{g/mL}$ - $400 \mu\text{g/mL}$ working range.

Table 1. Total flavonoids content expressed in rutoside ($\mu\text{g/mL}$) determined in *Satureja hortensis* L. extracts

Extraction procedure	Total flavonoids expressed as rutoside* ($\mu\text{g/mL}$ extract)					
	Extraction system composition ethanol-water (v/v)					
	100:0 (ES1)	80:20 (ES2)	70:30 (ES3)	60:40 (ES4)	50:50 (ES5)	40:60 (ES6)
M	13.66 (± 7.4)	77.9 (± 3.6)	113.40 (± 2.3)	125.04 (± 1.3)	129.53 (± 2.1)	108.57 (± 1.1)
R	15.44 (± 6.4)	99.28 (± 3.9)	128.45 (± 1.9)	143.08 (± 3.1)	149.55 (± 2.4)	151.49 (± 0.2)
UAE1	9.34 (± 4.0)	83.87 (± 4.1)	134.72 (± 2.6)	147.37 (± 2.6)	152.63 (± 2.1)	151.65 (± 2.2)
UAE2	10.76 (± 4.1)	88.72 (± 3.7)	122.41 (± 3.9)	132.60 (± 1.5)	136.27 (± 1.9)	128.81 (± 1.3)
MAE1	9.42 (± 5.9)	51.06 (± 4.2)	79.14 (± 2.7)	118.84 (± 3.1)	142.57 (± 2.3)	141.56 (± 1.3)
MAE2	12.98 (± 4.7)	45.97 (± 3.9)	107.64 (± 3.2)	128.58 (± 2.7)	140.14 (± 3.1)	1.38.02 (± 1.4)
MAE3	13.37 $\pm(8.2)$	68.46 (± 2.5)	106.07 (± 3.7)	116.86 (± 2.2)	140.63 (± 1.9)	134.62 (± 2.6)

* results are mean of three experimental determinations \pm relative standard deviation value; M - maceration; R - normal refluxing; UAE1 - ultrasound assisted extraction (sweep mode); UAE2 - ultrasound-assisted extraction (clean mode); MAE1-microwave-assisted extraction: duty coefficient 40%, 1 min microwave action time; MAE2 - microwave-assisted extraction: duty coefficient 40%, 2 min microwave action time; MAE3 - microwave-assisted extraction: duty coefficient 60%, 1 min microwave action time

The determined total flavonoids content expressed in rutoside, ranged from 11 µg/ml extract to 151 µg/ml extract, depending on the composition of the extraction system and extraction technique (Table 1).

Based on the obtained results it could be observed that for all applied extraction techniques, the flavonoids concentration increases with the polarity of the extraction system. High extraction yields were determined for the ES5 and ES6 (Figure 1). Regarding the extraction techniques, the best extraction yields were obtained using UAE1 due to continues action of ultrasonic waves which contribute to cell membrane breaking and R due to high extraction temperature that increases the solubility and diffusion coefficient respectively.

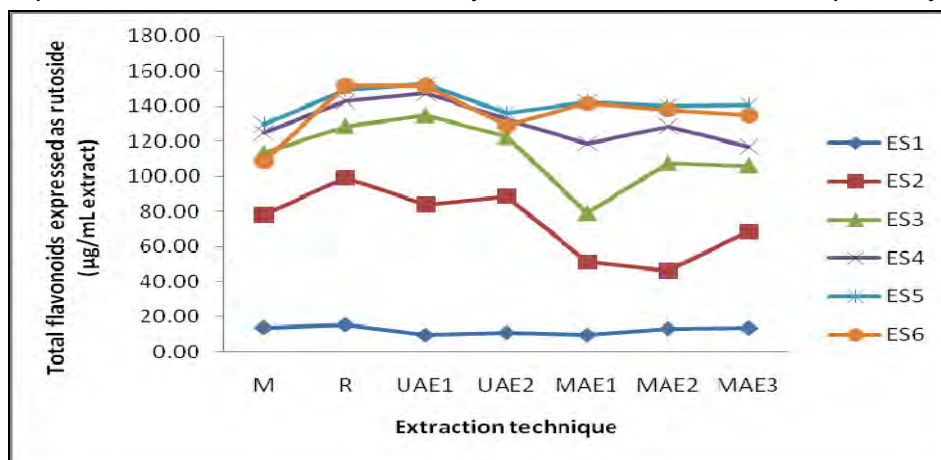


Figure 1. Influence of extraction system composition and extraction technique on total flavonoid content

Evaluation of polyphenols

Evaluation of polyphenols is based on the caffeic acid calibration curve $Y=1.245x+0.0033$ ($R^2=0.9990$; $LOD=0.2894$ µg/mL; $LOQ=0.5571$ µg/mL) determined on the 0.05 – 0.50 mg/mL working range. The determined values of total polyphenols, expressed in caffeic acid, lies between 0.53 – 6.85 mg/mL extract (Table 2).

The extraction yield of polyphenols is strongly influenced both by the extraction technique and by the extraction system composition (Figure 2). Best results were obtained by using ES5 and ES6 systems and R and MAE1 as extraction techniques.

Having a close look to Figure 2 it can be observed that extraction efficiency for R and MAE1 increases with solvent polarity. Moreover for UAE technique, both procedures show a similar trend lines, UAE1 being slightly more efficient. A different situation is encountered in the case of the MAE. Thus, for MAE3 the yield increase with extraction system polarity, from SE1 to SE3 when a maximum yield is obtained, after which the growth of the solvent's polarities

induce a decrease of the yield. For MAE2 there is an intermediate trend, common with MAE1 in the first part and in the second part common with MAE3.

Table 2. Total polyphenols content, expressed in caffeic acid, determined in *Satureja hortensis L.* extracts

Extraction procedure	Total polyphenols content expressed as caffeic acid (mg/mL extract)					
	Extraction system composition ethanol-water (v/v)					
	100:0 (ES1)	80:20 (ES2)	70:30 (ES3)	60:40 (ES4)	50:50 (ES5)	40:60 (ES6)
M	1.10 (±5.8)	2.80 (±4.3)	5.44 (±3.3)	5.56 (±3.5)	4.55 (±4.0)	3.51 (±5.4)
R	0.98 (±3.4)	5.70 (±2.8)	6.28 (±2.4)	6.36 (±3.4)	6.56 (±1.4)	6.85 (±3.0)
UAE1	0.79 (±2.6)	5.24 (±3.0)	5.83 (±3.1)	5.96 (±3.5)	6.47 (±3.0)	5.55 (±3.6)
UAE2	0.67 (±2.4)	5.22 (±3.1)	5.39 (±2.7)	5.26 (±3.1)	6.05 (±3.5)	5.63 (±6.8)
MAE1	0.53 (±3.7)	4.40 (±3.5)	6.06 (±3.2)	6.48 (±2.8)	6.59 (±2.5)	6.71 (±3.1)
MAE2	0.74 (±3.3)	4.38 (±14.4)	5.87 (±1.6)	5.39 (±3.6)	5.22 (±4.4)	4.52 (±2.5)
MAE3	0.75 (±7.5)	5.49 (±3.7)	6.19 (±3.2)	6.01 (±3.3)	5.78 (±3.1)	5.16 (±5.0)

* results are mean of three experimental determinations ± relative standard deviation value; M - maceration; R - normal refluxing; UAE1 - ultrasound assisted extraction (sweep mode); UAE2 – ultrasound-assisted extraction (clean mode); MAE1-microwave-assisted extraction: duty coefficient 40%, microwave action time:1 min; MAE2 - microwave-assisted extraction: duty coefficient 40%, microwave action time: 2 min; MAE3 - microwave-assisted extraction: duty coefficient 60%, 1 min microwave action time

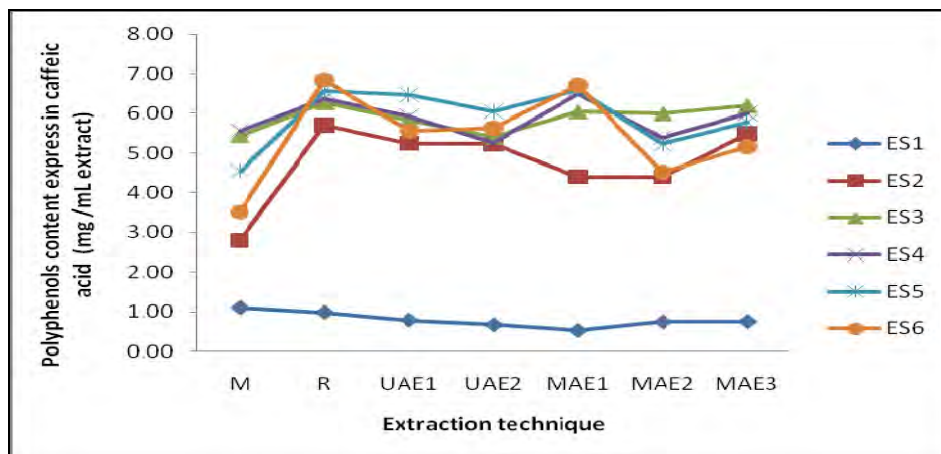


Figure 2. Influence of extraction system composition and extraction technique on total polyphenols content

Rosmarinic acid determination

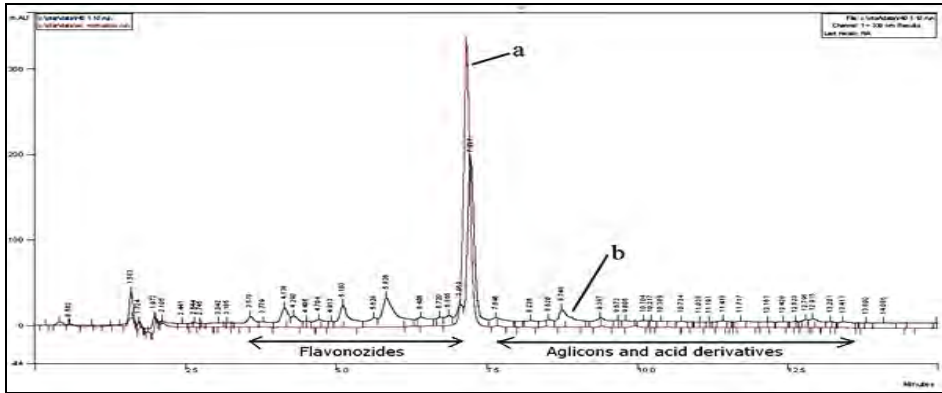


Figure 3. RP-HPLC Chromatogram of rosmarinic acid standard solution (a) and *Satureja hortensis* L extract obtained by reflux and ES6 (b)

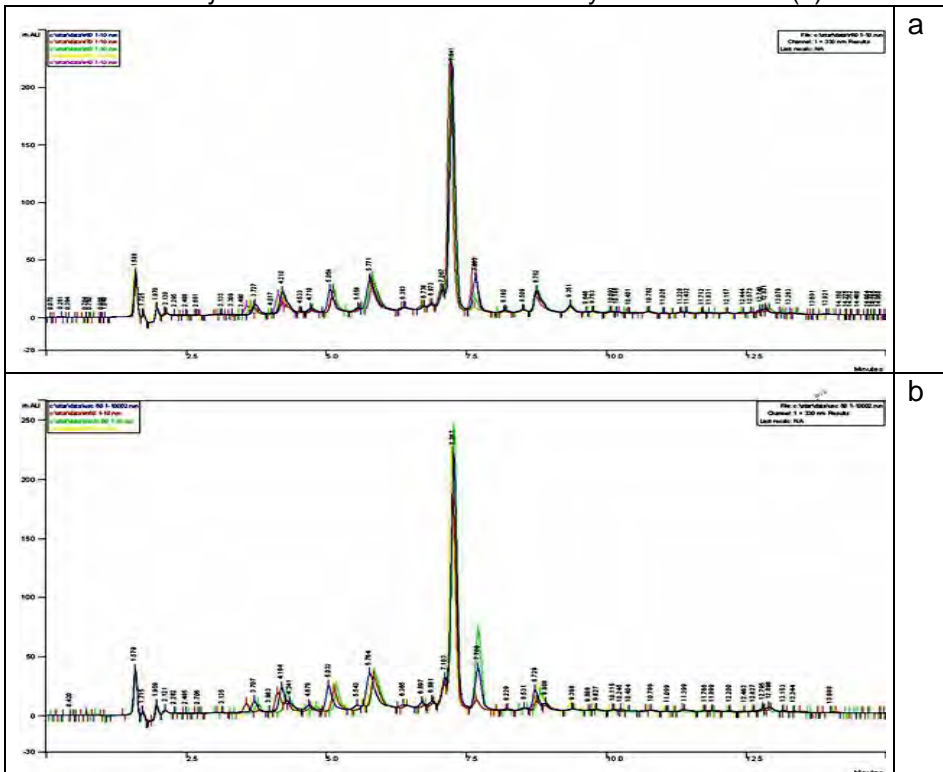


Figure 4. RP-HPLC chromatogram of the extracts obtained by (a) reflux with extraction systems ES2-ES6 and (b) using extraction system ES4 and different techniques - M, R, UAE1 and MAE1.

Rosmarinic acid separation was performed by RP-HPLC with gradient elution. Its identification in extracts was performed by comparison the retention time (17.24 min) and UV-spectra with a standard solution (Figure 3).

From qualitative point of view, the chromatograms obtained for the same technique and different extraction systems as well as for the same extraction system and different techniques have the same number of peaks, differing only in the area of peaks (Figure 4).

A linear calibration curve of rosmarinic acid ($Y=179672x+476900$; $R^2=0.9997$) on the working range 25 – 200 $\mu\text{g/mL}$ was obtained. The content of rosmarinic acid determined in extracts ranged between 50 – 118 $\mu\text{g/mL}$ extract (Table 3).

Table 3. Rosmarinic acid content ($\mu\text{g/mL}$ extract) determined in extracts of *Satureja hortensis* L.

Extraction procedure	Rosmarinic acid content in extracts ($\mu\text{g/mL}$)*				
	Extraction system composition ethanol-water (v/v)				
	80:20 (ES2)	70:30 (ES3)	60:40 (ES4)	50:50 (ES5)	40:60 (ES6)
M	75.17 (± 3.9)	108.42 (± 3.1)	152.58 (± 3.6)	143.92 (± 2.6)	50.34 (± 3.8)
R	96.35 (± 2.5)	97.43 (± 3.3)	118.15 (± 2.9)	109.25 (± 2.8)	77.84 (± 3.6)
UAE1	93.74 (± 2.8)	88.94 (± 4.9)	102.43 (± 3.2)	100.24 (± 3.1)	101.07 (± 2.4)
MAE1	81.22 (± 3.1)	102.21 (± 2.5)	102.79 (± 3.4)	101.93 (± 3.2)	100.70 (± 2.6)

* results are mean of three experimental determinations \pm relative standard deviation value; M - maceration; R - normal refluxing; UAE1 – ultrasound-assisted extraction (sweep mode); MAE1-microwave-assisted extraction: duty coefficient 40%, 1 min microwave action time

The amount of extracted rosmarinic acid is influenced by the extraction procedure (Figure 5). Thus, the extraction profiles showed that the systems ES4, ES5 and ES6 (in case of UAE1 and MAE1) were most effective and no significant variations due to variations in the ethanol-water ratio for R, UAE1 and MAE1 were observed.

A higher content of rosmarinic acid was determined using systems ES4 and ES5 when maceration was applied as extraction technique. Combination of the maceration technique (M) with the ethanol-water ratio (60:40, v/v) extraction system (ES4) was found as the most efficient procedure for extraction of an enhanced amount of rosmarinic acid from dry *Satureja hortensis* L. plant.

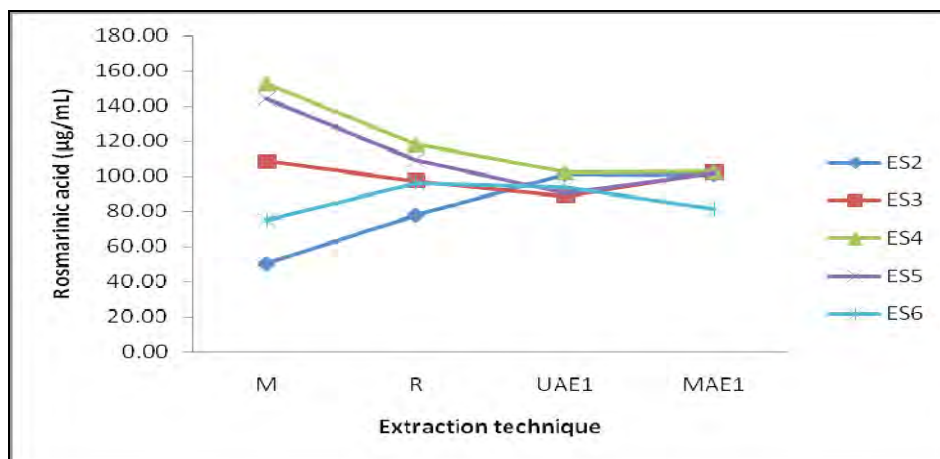


Figure 5. Influence of extraction system composition and extraction technique on rosmarinic acid content

CONCLUSIONS

Among the solvent extraction techniques investigated in this study, the ultrasound-assisted extraction with sweep mode selection (UAE1) and normal refluxing procedure (R) were found as the most efficient for the total flavonoids extraction from *Satureja hortensis* L. dry plant material. Normal refluxing (R) and also the microwave-assisted extraction using a duty coefficient of 40% and 1 minute microwave action time (MAE1) were found as the most suitable procedures for extraction of high content of polyphenolic compounds. For both of the investigated classes of compounds (flavonoids and polyphenols), combination of these techniques with the ethanol-water extraction system consisting of 50-60% ethanol were found to be the most efficient extraction procedures. Instead of this, the ethanol-water extraction system consisted of 60% ethanol combined with the maceration technique (M) was found as the most efficient procedure for the extraction of an enhanced content of rosmarinic acid from *Satureja hortensis* L. dry plant material.

EXPERIMENTAL SECTION

Equipment, reagents and plant material

The experiments were carried out using a Zass electric mill, a Soxhlet extractor, an Elmasonic S15H (Germany) ultrasonic bath, a homemade microwave extractor (PATENT H-OSIM NO 6/065 on 30.06.2008,

INCDTIM, Cluj-Napoca, Romania), a Jasco V 550 UV-Vis spectrophotometer (Japan) and a Varian Prostar HPLC system with quaternary pump, autosampler and DAD detector (Varian, USA). Organic solvents chloroform, ethanol and methanol were purchased from Chemical Company (Romania); acetonitril and acetic acid HPLC grade were from Merck (Germany). Sodium acetate, aluminium chloride, sodium carbonate, sodium tungstenate, sodium molybdate and phosphoric acid reagents were supplied from Merck (Germany). Rutoside, caffeic acid and rosmarinic acid standards were from Merck (Germany). For the experimental determinations, dried leaves of *Satureja hortensis* L. (*Viola Tricolor*, Romania) were purchased from local specialized store.

Sample preparation and extraction procedure

The plant material (dried leaves) was minced with the electrical mill to reduce the particle size and increase the solid-liquid contact surface for the solvent extraction procedure. The obtained powder was sieved and the fraction with the dimension below 400 μ m was used for further investigations. Prior to the solvent extraction procedure, chlorophylls and fatty compounds were removed from by Soxhlet extraction with chloroform until a colourless extract was obtained. The resulted plant material was dried at room temperature and accurately weighted portions were used for the extraction procedure. The applied conventional extraction methods included both room temperature maceration for 14 days (M) and normal refluxing for 30 min (R). Alternative solvent extraction techniques including the microwave-assisted (MAE) and ultrasound-assisted (UAE) extraction were used as modern extraction procedures. UAE was carried out for 30 min at 37 kHz and 95W. There were selected two types of wave action: sweep mode (UAE1) when a uniform ultrasound field was assured and clean mode (UAE2) when a pulsed field was generated. MAE was performed in close vessel with cooling system at atmospheric pressure and bellow 70°C. The extraction was carried out at 900W with different values of duty coefficient and action time (Table 4).

Table 4. The experimental parameters used for the microwave-assisted extraction (MAE) procedure

Duty coefficient (%)	Microwave action time (min)	Extraction time (min)	Symbol
40	1	1-2	MAE1
40	2	4-6	MAE2
60	2	20-25	MAE

In all cases, different extraction systems consisting of various proportions of ethanol–water (v/v): 100:0 (ES1); 80:20 (ES2), 70:30 (ES3); 60:40 (ES4), 50:50 (ES5) and 40:60 (ES6) were used. A ratio of 0.5:40 of dry plant/extraction solvent volume was used each time. The resulted extracts were filtered and used as stock samples for further quantitative investigations. Triplicate samples were obtained for each extraction method.

Evaluation of total flavonoid content

Total flavonoids content was determined using aluminium chloride method, when a yellowish soluble complex is formed [19]. An aliquot of stock sample was 1:5 diluted with methanol. Volume of 1 ml of diluted extract was mixed with 1.5 ml sodium acetate (100 g/L) and 2.5 ml aluminium chloride (25 g/L) and brought with methanol up to 10 ml (volumetric flask). After 15 minutes, the absorbance was measured at 430 nm, using a blank solution prepared from 1 ml diluted extract, 5 ml water and methanol up to 10 ml. The total flavonoids content was calculated based on calibration curve, the results being expressed as rutoside ($\mu\text{g}/\text{mL}$ plant extract). Calibration curve was determined on the range of 0.02 – 0.40 mg/ml, using rutoside standard solution prepared in methanol (1 mg/mL).

Evaluation of total polyphenols

The phenolic content was determined using Folin–Ciocalteu reagent [19]. Briefly, 1 mL of stock extract was diluted up to 5 mL with distilled water. Two-hundred microlitres of the obtained extract were mixed with 2 mL of Folin–Ciocalteu reagent and brought with sodium carbonate (15%) up to 10 mL. The absorbance of the coloured blue samples was measured at 715 nm. Calibration curve was determined on the range of 0.05 – 0.50 mg/ml, using caffeic acid standard solution prepared in methanol (1 mg/mL). The phenolic content was calculated based on the caffeic acid calibration curve and the results were given as total polyphenols expressed in caffeic acid (mg/mL plant extract).

Quantitative analysis of rosmarinic acid by HPLC-DAD

Rosmarinic acid content was determined by high-performance liquid chromatography (HPLC) method using a Varian ProStar HPLC system equipped with gradient pump unit, DAD detector and

autosampler (1-100 μ L). Separation was achieved using a Microsorb-MV 100-5 C18 (150 mm x 4.6 mm, 5 μ m) (Agilent Technologies) analytical column and the mixture acetic acid (10%) – acetonitrile – water as mobile phase. Gradient elution (from 10:15:75 (v/v/v) to 10:45:45 (v/v/v) in 10 minutes and 10:45:45 (v/v/v) for 5 minutes) at a flow rate of 1.0 mL/min at room temperature (25°C) was carried out. UV detection was performed at 330 nm.

REFERENCES

1. S. Momtaz, M. Abdollahi, *International Journal of Pharmacology*, **2010**, *6*, 454.
2. A. Alizadeh, M. Khoshkhui, K. Javidnia, O. Firuzi, E. Tafazoli, A. Khalighi, *Journal of Medicinal Plants Research*, **2010**, *4*, 40.
3. R. Hamidpour, S. Hamidpour, M. Hamidpour, M. Shahlari, M. Sohraby, *Journal of Traditional and Complementary Medicine*, **2014**, *4*, 140.
4. A.M. Abd El Tawab, N.N. Shahin, M.M. Abdel Mohsen, *Chemico-Biological Interactions*, **2014**, *224*, 196.
5. N. Alonso-Carrillo, M.Á. Aguilar-Santamaría, E.J. Vernon-Carter, R. Jiménez-Alvarado, F. Cruz-Sos, A. Roman-Guerrero, *Industrial Crops & Products*, **2017**, *103*, 213.
6. W. Yi, H.Y. Wetzstein, *Journal of the Science of Food and Agriculture*, **2010**, *90*, 1063.
7. M. Mahmoodreza, K. Forough, T. Hossein, G. Younes, *Iranian Journal of Pharmaceutical Sciences*, **2012**, *8*, 277.
8. M.M.J. Saharkhiz, K. Zomorodian, A. Taban, K. Pakshir, K. Heshmati, M.J. Rahimi, *Journal of Essential Oil Bearing Plants*, **2016**, *19*, 1984
9. S.E.Moghadam, S.N. Ebrahimi, F. Gafner, J.B. Ochola, M. Hamburger, *Industrial Crops and Products*, **2015**, *76*, 892
10. A. Ziakova, E. Brandsteterova, *Journal of Liquid Chromatography & Related Technologies*, **2003**, *26*, 443.
11. G.S. Cétković, A.Mandić, J.M. Cănadanović-Brunet, S.M. Djilas, V.T. Tumbas, *Journal of Liquid Chromatography & Related Technologies*, **2007**, *30*, 293.
12. I. Bros, M.L. Soran, R.D. Briciu, S.C. Cobzac, *Journal of Planar Chromatography*, **2009**, *22*, 25.
13. J. Hadian, S.N. Ebrahimi, P. Salehi, *Industrial Crops and Products*, **2010**, *32*, 62.
14. J. Dai, R.J. Mumper, *Molecules*, **2010**, *15*, 7313.
15. M. Pinelo, P. Del Fabbro, L. Manzocco, M.J. Nuñez, M.C. Nicoli, *Food Chemistry*, **2005**, *92*, 109.
16. D.P. Xu, Y. Li, X. Meng, T. Zhou, Y. Zhou, J. Zheng, J.J. Zhang, H.B. Li, *International Journal of Molecular Sciences*, **2017**, *18*, 96.

17. E. Conde, A. Moure, H. Domínguez, J. C. Parajó, "Separation, Extraction and Concentration Processes in the Food, Beverage and Nutraceutical Industries", Woodhead Publishing Limited, 2010.
18. H.K. Kala, R. Mehta, K.K. Sen, R. Tandey, V. Mandal, *Trends in Analytical Chemistry*, **2016**, *85*, 140.
19. "Farmacopeea Română", ed. X, Editura Medicală, București, **1993**.

In memory of prof. dr. Simion Gocan

PHYTOCHEMICAL SCREENING OF DIFFERENT *CRATAEGUS OXYACANTHA* EXTRACTS

NELI-KINGA OLAH^{a, b}, RAMONA BURTESCU^b, SORINA PETRESCU^b,
ANDREEA BRAȘOVAN^c, ELISABETA CHIȘE^a, SIMONA CODRUȚA
AURORA COBZAC^{d*}, DANIELA HANGANU^{e*}

ABSTRACT. *Crataegus oxyacantha* L., the hawthorn, is a well-known medicinal plant with cardiotonic effect. This paper presents a complex phytochemical screening of polyphenols profile, both qualitatively and quantitatively, in three different extracts obtained from fresh berries, flowers with leaves and young shoots. There were used spectral (UV-Vis) and chromatographic (TLC, HPLC) methods to evaluate the total flavonoids, total phenolic acids and qualitative polyphenols profile of the extracts. The antioxidant capacity was evaluated by DPPH, FRAP and NO radical inhibition methods, by UV-Vis spectrophotometry. The total flavonoid content expressed in rutoside ranges from 0.49 to 1.33 mg/ml, the total phenolic acids expressed in caffeic acid from 0.02 to 0.10 mg/ml, the most concentrated being the berries extract. In flowers with leaves extract can be identified and quantified a special flavonoid, the vitexine, 0.37 mg/ml. All three extracts present important antioxidant activity, both on ROS and RNS species. By FRAP method the berries extract was determined as most powerful, having also the best inhibition effect on NO radicals. The DPPH method indicates the special young shoots extract, used in gemmotherapy, as being the most powerful, with significant inhibiting effect on NO radicals. This indicates that the young shoots gemmotherapeutic extract is a good candidate for a powerful therapeutic tool.

Keywords: *Crataegus oxyacantha* extracts, spectral assays, TLC, HPLC-DAD, antioxidant capacity

^a "Vasile Goldis" Western University of Arad, Faculty of Pharmacy, 86 L. Rebreanu str., Arad, Romania

^b SC PlantExtrakt SRL, 407059 Rădaia. Cluj, Romania

^c Babeș-Bolyai University of Cluj-Napoca, 1 Kogălniceanu Str., Cluj-Napoca, Romania

^d Babeș-Bolyai University of Cluj-Napoca, Faculty of Chemistry and Chemical Engineering, 11 Arany Janos Str., Cluj-Napoca, Romania

* Correspondent authors: danahcluj@gmail.com, csimona@chem.ubbcluj.ro

^e "Iuliu Hațieganu" University of Medicine and Pharmacy from Cluj-Napoca, Faculty of Pharmacy, 8 Victor Babeș str., Cluj-Napoca, Romania

INTRODUCTION

Crataegus oxyacantha L. or *Crataegus monogyna* Jacq., the hawthorn, is one of the most known and used vegetal remedy for different cardiovascular disturbances. It belongs to Rosaceae family, being a shrub with white flowers grouped in corymb and intensive red berries as fruits with one stony seed. Traditionally, for medicinal purposes are used the flowers with leaves respectively the fruits. The vegetal material or the extracts, obtained both from dried or fresh plants, are standardized in flavonoids or / and oligomeric proanthocyanidines [1-3].

The phytochemical researches using different spectral and chromatographic methods identified in the hawthorn oligomeric proanthocyanidines, flavonoids of flavone and flavonole types, phenolic acids, triterpenes, fatty acids, sterols [3,4]. The studies were conducted on vegetal materials, but also on hydroalcoholic extracts. The alcoholic extracts from berries and flowers with leaves contain vitexine, hyperoside, rutoside, luteoline, apigenin and different vitexine, luteoline and apigenin derivatives from class of flavonoids; catechine and epicatechine derivatives from oligomeric proanthocyanidines; ursolic, oleanolic and crategolic acids from class of triterpenes; chlorogenic and caffeic acids from class of phenolic acids, respectively amines. The quantitative analyses identified 14.3 $\mu\text{g/g}$ respectively 1.65 $\mu\text{g/g}$ flavonols in the leaves respectively berries and 5.11 mg/g oligomeric proanthocyanidines into berries [5-7]. Another study evidenced in berries extracts 3.54 % phenolics expressed in gallic acid, 0.18 % flavonoids aglyca, 0.14 % hyperoside and 0.44 % oligomeric proanthocyanidines [4]. A comparative study performed on tinctures obtained from dried and fresh flowers with leaves highlight that the freshly processed vegetal material contains higher quantity of oligomeric proanthocyanidines, with reduced stability into alcoholic extracts and with 1.5 times less flavonoids like the extract obtained from dried vegetal product [8]. A recent study evidenced in flowers and leaves originary from Pakistan a lot of sterols and triterpenes: β -sitosterol-3-O- β -D-glucopyranoside, lupeol, β -sitosterol, betuline, betulinic acid, oleanolic acid and from flavonoids class the chrysine. From these compounds the sitosterol derivative was linked to the anticholinesterase effect with potential benefit into the improvement of Alzheimer disease's symptoms [9].

Due by the high content in polyphenols the hawthorn has high antioxidant capacity correlated also with cardioprotector and anti-inflammatory effects [3,9,10]. The antioxidant effect is expressed in the improvement and activation of the antioxidant enzymes status, like superoxide dismutase, catalase, glutathione peroxidase, glutathione, respectively in the inhibition of lipids peroxidation. Studies revealed, by

DPPH method, that the berries have a 1000 times more elevated antioxidant capacity than the quercetine, a powerful antioxidant flavonoid, while the leaves have 10 times more elevated this effect. The antioxidant and lipid lowering effects are due mainly by the high content in flavonoids [3,5,11-12]. It was proved that the anti-inflammatory effect is due by inhibition of different enzymes and cytokines, like COX2, α TNF, IL-1 β , IL-6 and iNOS [5].

At cardiovascular level were proved the beneficial effects in heart failure, stage I and II according to NYHA, angina pectoris, hypertension, mild arrhythmia and atherosclerosis [3,13,14]. The hawthorn berries and flowers with leaves lower the blood pressure, dilating the vessels, have endothelium protector effect, decrease the migration and proliferation of smooth muscle cells, protect in case of ischemia and determine a better use of the oxygen by the myocardium due by its positive inotropic and negative chronotropic activity, by improving the coronary stream and by inhibition of the angiotensin converting enzyme respectively the phosphodiesterase. Additionally have anxiolytic, antihyperlipidic, antihyperglycemic, immunomodulating and antimutagenic effects [3,5,15]. The flavonoids and oligomeric proanthocyanidines are responsible for the inhibition of angiotensin converting enzyme [16].

Clinical trials proved the efficacy of hawthorn products in case of stable angina pectoris by lowering the intercellular adhesive molecules, like ICAM-1 and the E-selectine, responsible by the coronary atherosclerosis development [17]. A randomized double blind clinical trial performed on a tincture obtained from fresh hawthorn berries evidenced its efficacy in stage II hearth failure, in long term administration [18].

The hawthorn berries and flowers with leaves have a good antimicrobial activity on *Pseudomonas aeruginosa* and mild effect on *Escherichia coli* [11].

Local traditions use hawthorn also in case of digestive disturbances, dyspnea, respectively in case of renal lithiasis [5,15]

The hawthorn is used in therapy mostly as hydroalcoholic extracts or dry extracts, on tablets or capsules form. Recent phytochemical, pharmacological and clinical studies are performed on extracts obtained from fresh plants. The use of fresh plants is characteristic for the new phytotherapy branches, like gemmotherapy is, that use the part of plants containing meristematic tissues. Because all type, classical and modern, extracts from hawthorn are used mainly as cardiotionic it worth to study comparatively to determine the differences in phytochemical profile that can indicate some differences also in efficacy.

This paper presents a comparative study of phytochemical profile of the tinctures obtained from fresh hawthorn berries and fresh hawthorn flowers with leaves respectively the glycerol macerate obtained from fresh hawthorn young shoots, used in gemmotherapy, performed by different spectral and chromatographic methods.

RESULTS AND DISCUSSION

In figures 1 and 2 are presented the calibration curve of rutoside respectively of caffeic acid used for the determination of total flavonoids respectively total phenolic acids content.

In figures 3-6 are presented the TLC respectively the HPLC chromatograms of the three studied extracts.

In figure 7 is presented the calibration curve for vitexine used for determination of the content by HPLC.

In tables 1 and 2 are presented the obtained results.

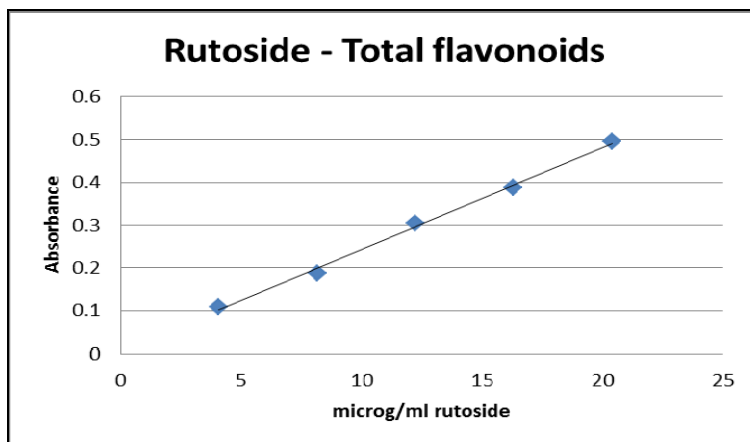


Figure 1. The calibration curve of rutoside for total flavonoids content determination $\text{Absorbance} = 0.024 \times \text{Conc} [\mu\text{g/ml}] + 0.0031$; $R^2 = 0.9970$

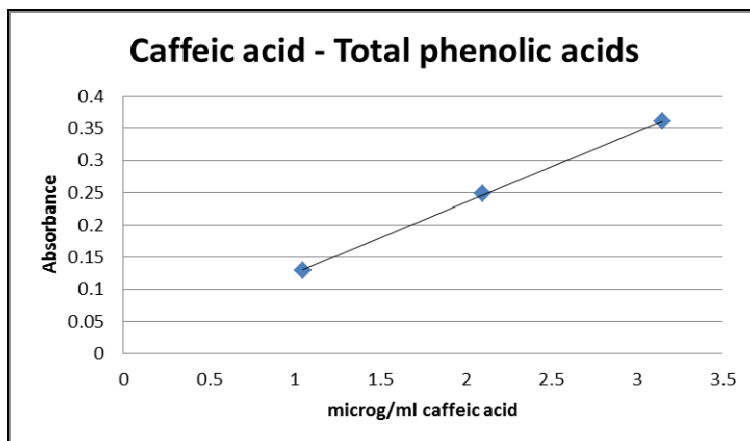


Figure 2. The calibration curve of caffeic acid for total phenolic acids content determination $\text{Absorbance} = 0.1098 \times \text{Conc} [\mu\text{g/ml}] + 0.0157$; $R^2 = 0.9997$

PHYTOCHEMICAL SCREENING OF DIFFERENT *CRATAEGUS OXYACANTHA* EXTRACTS

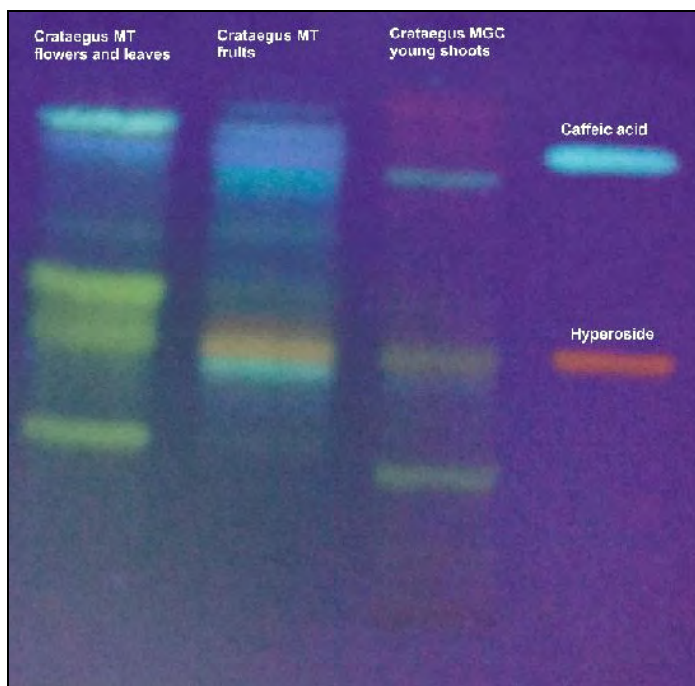


Figure 3. The TLC chromatogram in fluorescence at 365 nm.

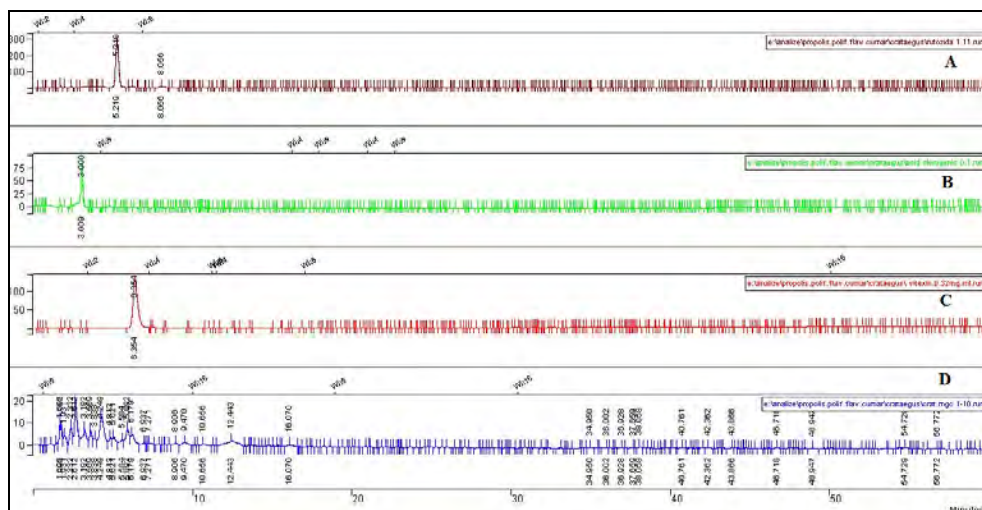
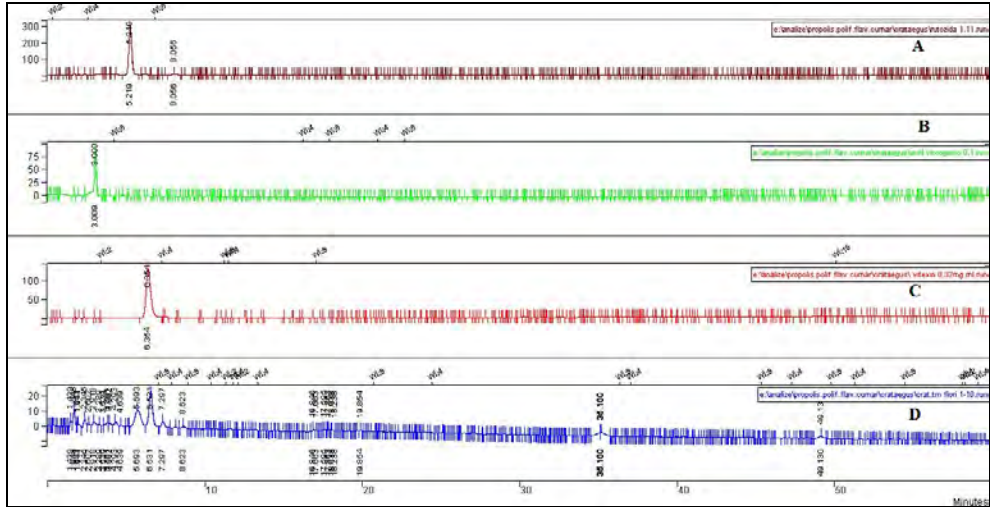


Figure 4. The HPLC chromatogram for glycerol macerate from hawthorn young shoots.
A – rutoside, B – chlorogenic acid, C – vitexine, D – extract



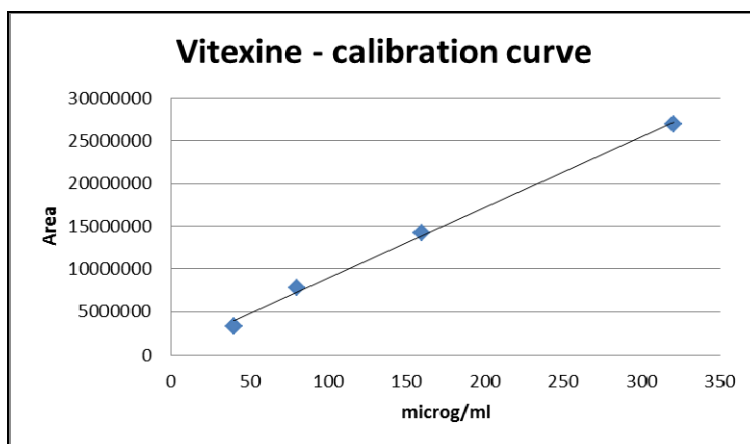


Figure 7. The calibration curve for dosing the vitexine by HPLC
 $\text{Area} = 83194 \times \text{Conc } [\mu\text{g/ml}] + 585207$; $R^2 = 0.9977$

Table 1. The results from TLC and HPLC analyses

Hawthorn extract from	Number of compounds separated by TLC	Number of compounds separated by HPLC
Young shoots	6 (2 chlorophylls)	16
Flowers with leaves	6	11
Berries	10	10

Table 2. The quantitative results from spectral and chromatographic analyses

Hawthorn extract from	Total flavonoids expressed in rutoside, mg/ml	Total phenolic acids expressed in caffeic acid, mg/ml	Vitexine content, mg/ml
Young shoots	0.87 ± 0.003	0.07 ± 0.001	-
Flowers with leaves	0.49 ± 0.001	0.02 ± 0.001	0.37 ± 0.005
Berries	1.33 ± 0.059	0.10 ± 0.002	-

The spectral analyses indicate that the highest concentration of polyphenols, flavonoids and phenolic acids are in berries tincture, and the lowest in the flowers with leaves extract. These are in correlation with the results obtained at TLC analysis where the flower with leaves extract show compounds with different yellow color. The quantitative spectral results can be correlated with those obtained by Tadic *et al.* in the berries extracts from Serbia [12].

The TLC analysis revealed the separation of 4 phenolic compounds in young shoots, 6 in flowers with leaves and 10 in berries. These compounds have yellow, orange-yellow, blue and greenish-blue fluorescence. The yellow

and orange-yellow colors indicate flavonoids, while the blue and greenish-blue colors the phenolic acids. The separated active compounds profile is different at flowers with leaves extract comparing with the others. This extract present three intensive yellow band corresponding to flavonoids, while the other two extracts have a yellow, a blue, an orange-yellow and an orange band in the same positions. The orange band is present more intensively in the berries extract and could be interpreted as being hyperoside. There are similarities between the young shoots and berries extracts also in the presence of a blue band around the caffeic acid. Just in the young shoots extract can be observed the red bands characteristic for chlorophylls. The TLC analysis evidenced the similarities and also the differences in phytochemical profile of the different hawthorn vegetal materials respectively extracts from these parts, but the results are according with the provisions of pharmacopoeias monographs respectively with the known scientific references that highlights the presence of flavonoids and phenolic acids in this species [1,2,19].

The HPLC analysis evidenced the same similarities and differences like were observed at TLC analysis. The number of separated compounds is similar in all extracts. From the berries and flowers with leaves extracts are separated 10 or 11 compounds, from young shoots 16 compounds. The table 3 shows the position of each separated compound and the maximum absorbance of their UV-Vis spectra.

It can be identified caffeic acid derivatives in young shoots extract at 1.65, 2.60 and 3.20 minutes based on absorption maximums and the shape of the UV-Vis spectra. The compound from 2.60 minutes could be chlorogenic acid according the UV-Vis spectra data, but is separated at 0.4 minutes difference in comparison with the standard. The compounds separated at 4.25, 5.90, 6.20 and 9.50 could be flavonoids according the UV-Vis spectra shape and maximum absorption wavelengths. It could not be identified any of them as rutoside, neither the retention time, neither the maximum absorption wavelengths do not correspond.

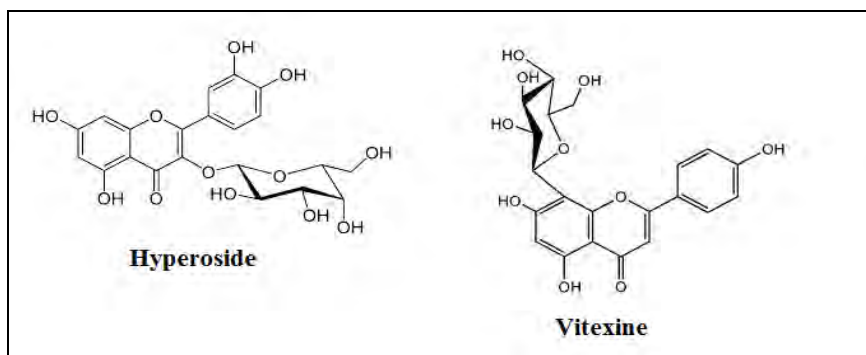
In the flower with leaves extract can not be identified any caffeic acid derivatives, but the compounds separated at 5.70 and 6.50 minutes could be flavonoids. It can be identified the vitexine, separated at similar retention time and with similar shape and absorption maximums like the standard. This corresponds with those mentioned in scientific references [5]. This extract contains 0.37 mg/ml vitexine, representing 75.5 % from total flavonoids.

The berries extracts contains possible flavonoids separated at 4.40, 6.20 respectively 6.60 minutes, but it could not be identified the rutoside. This is according with the references that mentioned the lower flavonoid content in fresh berries [8]. The higher total flavonoid content determined by spectral method using aluminum chloride could be explained by the possible interference of oligomeric proanthocyanidines.

Table 3. The retention time and the UV-Vis absorption maxims of the separated compounds by HPLC

Young shoots extract		Flowers with leaves extract		Berries extract	
t _r , min	UV-Vis absorption maxims, nm	t _r , min	UV-Vis absorption maxims, nm	t _r , min	UV-Vis absorption maxims, nm
1.65	237+328	1.65	234	1.65	233+280
2.30	233+293	2.30	296	2.30	294
2.60	238+325	2.60	236+268+296	2.70	263+298
-	-	2.90	234+263+298	-	-
3.20	234+328	-	-	3.20	236+288
3.60	352	3.60	234+268+318	3.60	234+308
4.25	267+343	4.30	258+332	4.40	236+271+349
5.00	236+268+346	-	-	-	-
5.90	260+357	5.70	234+268+343	-	-
6.20	263+355	-	-	6.20	265+359
-	-	6.50	268+343	6.60	240+360
8.90	242	-	-	-	-
9.50	238+357	-	-	9.60	240
10.70	243	-	-	-	-
12.45	240+269+346	-	-	-	-
-	-	-	-	13.00	241
16.00	242	-	-	-	-
35.00	241	35.10	240+318	-	-
49.00	240+304+357	49.10	240+268+310+356		
Chlorogenic acid		Rutoside		Vitexine	
3.00	239+325	5.20	264+355	6.20	267+344

The HPLC results are in concordance with the TLC and spectral results, explaining the difference in color of the flavonoids from flower and leaves due by the presence of vitexine that have a different structure like the rutoside or hyperoside (figure 8).

**Figure 8.** The structures of hyperoside and vitexine

The antioxidant capacity evaluation results are presented in table 4. In figure 9 are presented the extracts curve for IC₅₀ determination by DPPH method respectively in figure 10 the Trolox calibration curve for FRAP method.

Table 4. The results of antioxidant capacity evaluation

Extracts from	DPPH, IC ₅₀ , μl	FRAP, μM TE /100 ml extract	NO radical inhibition, %
Young shoots	6	848 ± 1.12	70.3
Flowers with leaves	80	278 ± 0.50	65.5
Berries	93	1255 ± 3.28	74.3
Trolox (standard)	50 μg	-	-

The results show a good correlation of the antioxidant activity determined by FRAP and the content in polyphenols determined by spectral methods (see figure 11). The DPPH method show a better antioxidant activity of young shoots extract, the other two extracts having similar values and approximately 1.5-2 times less than the standard trolox. These results are according to that obtained by Benmalek *et al.*, reference that mention a more effective antioxidant capacity of berries extract in comparison with the leaves or flowers extracts [7].

The results obtained with DPPH method can not be correlated with the extracts' polyphenols content. This leads us to conclude that the different hawthorn extracts will contain different type of antioxidant compounds which will act specifically on different radicals. This explains also the different results by different evaluation methods. On other hand to the antioxidant effect could contribute also other compounds types near polyphenols.

The DPPH evaluation shows that the young shoots extract is more powerful, even that the polyphenols content is lower as the berries extract and the extraction ratio, 1:20, lead to a more diluted extract like the berries' is. This result indicates that the young shoot hawthorn extract used in gemmotherapy could have a more powerful effect like the classical hawthorn extracts.

All three extracts have important NO radical inhibition effect. The value are similar, the most effective being the berries and young shoots extracts. Even that the values are similar, there is a concordance between the NO radical inhibition and the extracts polyphenols content (see figure 11). This explain the beneficial effect of the hawthorn extracts on endothelium, by inhibiting the transformation of endothelium factor NO into radicals and the damaging of vessels wall.

PHYTOCHEMICAL SCREENING OF DIFFERENT *CRATAEGUS OXYACANTHA* EXTRACTS

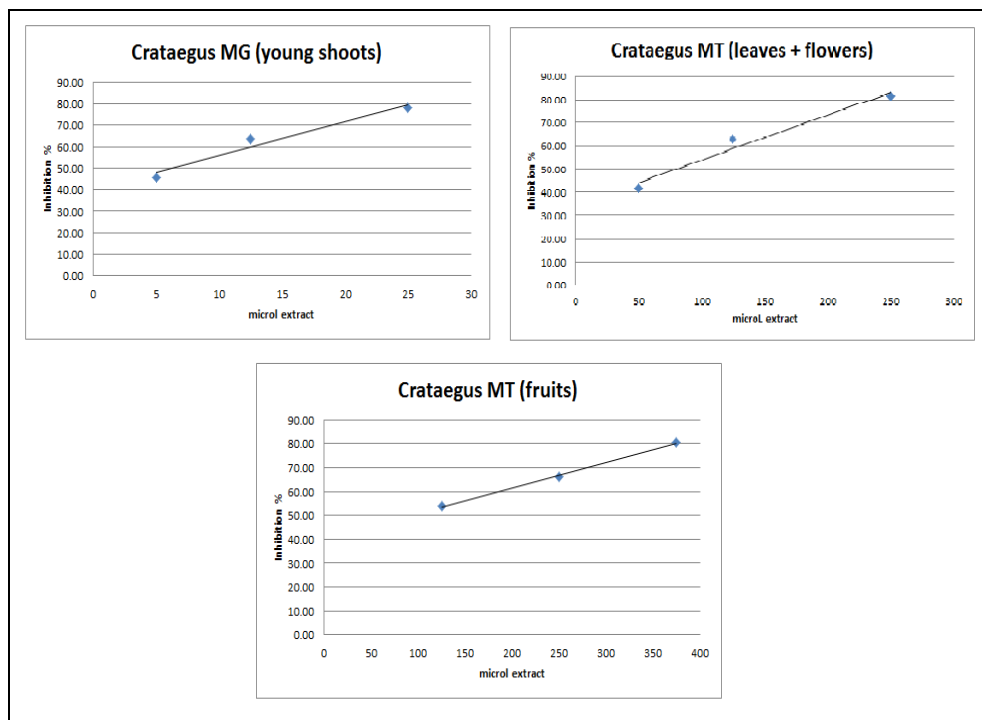


Figure 9. The inhibition curves for determination of IC_{50} by DPPH method; Young shoots: $I \% = 1.5774 \times \text{Conc } [\mu] + 40.164$; $R^2 = 0.9619$; Flowers with leaves: $I \% = 0.1943 \text{ Conc } [\mu] + 34.461$; $R^2 = 0.9657$; Berries: $I \% = 0.1067 \times \text{Conc } [\mu] + 40.079$; $R^2 = 0.9989$

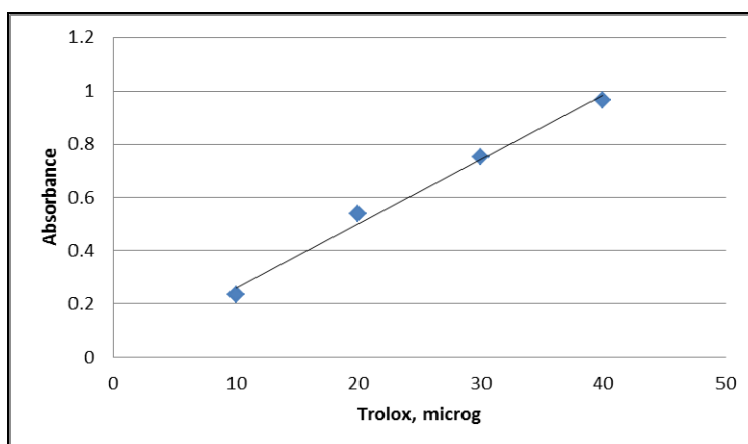


Figure 10. The calibration curve for Trolox by FRAP method

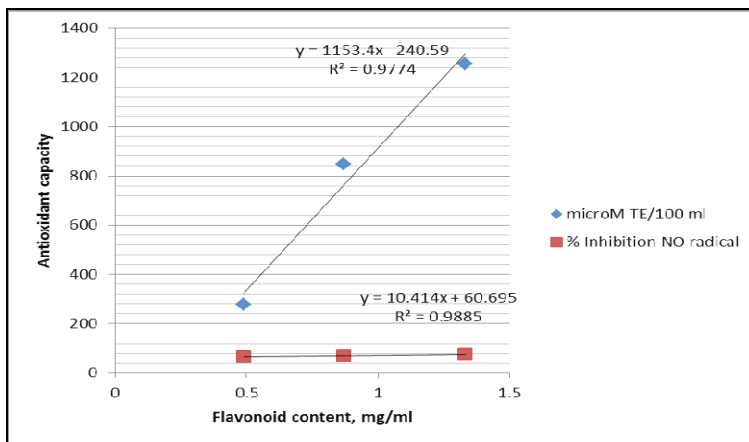


Figure 11. The correlation curves of antioxidant capacity with total flavonoid content

CONCLUSIONS

This paper highlights the differences and the similarities between the phytochemical profiles of different hawthorn vegetal materials respectively extracts. It can be observed a difference regarding the polyphenols types contained by flowers with leaves in comparison with the berries and young shoots. This will lead to an efficacy difference sustained also by the antioxidant capacity evaluations.

The berries extract was observed to have the highest concentration in polyphenols with important antioxidant effect, both on reactive oxygen species (ROS) and reactive nitrogen species (RNS).

In this paper was presented for first time a complex phytochemical analysis of young shoots hawthorn extract, used in gemmotherapy, that proved to have a similar polyphenols profile like the berries extract, the most used in cardiovascular diseases, but in less concentration, with comparative or higher antioxidant activity with berries extract, both on ROS and RNS. These results lead us to conclude that the young shoots extract, with its complete phytochemical profile, including also the polyphenols, can be therapeutically more valuable as other hawthorn extracts, obtained from other parts of this specie.

EXPERIMENTAL SECTION

Materials, reagents and apparatus

Crataegus oxyacantha L. young shoots, flowers with leaves and berries were collected from wild flora, in the woods near Cluj, in the springtime and autumn of year 2016. The fresh vegetal material was immediately processed after the collection. A voucher specimen was sampled, retained in herbarium, each time and the botanical identification was performed by the specialists from PlantExtrakt quality control laboratories.

The extracts were obtained according to provision of European and German Homeopathic Pharmacopoeias. There were obtained on GMP certified production flow mother tinctures from berries and flowers with leaves using 90 % vol. ethanol, the extraction ratio being 1:0.75 (plant-solvent) respectively glycerol macerate from young shoots using 96 % vol. ethanol – 100 % glycerol mixture (1:1), the extraction ratio being 1:20 (dry part of the plant – solvent). The extraction was made at cold, by maceration 10-20 days, with daily mixing followed by pressing and filtering [1,19].

The silicagel plate (Kieselgel F₂₅₄) was purchased from– Merck, (Germany). The HPLC column, type Luna 5 µm C18 (2) 100 A of 150 x 4.6 mm was purchased from Phenomenex, USA. The Sil-C18 SPE columns were purchased from Merck, Germany.

The Teflon Millex filters were purchased from Merck-Millipore, USA.

Solvents and reagents: sodium acetate, aluminum chloride, methanol, sodium carbonate, sodium tungstenate, phosphoric acid, ferric chloride, TPTZ, DPPH, hydrochloric acid, sodium nitroprusside, sodium phosphate, sulfanilamide, N-1-naphtylethylenediamine, ethyl acetate, ethyl-methyl ketone, formic acid and acetonitrile was supplied from Merck (Germany); PEG 400 was obtained from Roth, (Germany); diphenylboric acid aminoethyl ester was supplied from LGC (Germany).

The standards: rutoside, caffeic acid and trolox supplied from Merck (Germany), hyperoside, vitexine and chlorogenic acid were obtained from Phytolab (Germany).

Apparatus: Cintra 101 UV-Vis spectrophotometer, GBC Australia; Varian Prostar HPLC system with quaternary pump, autosampler and DAD detector, Varian USA.

Assay for total flavonoid content determination [20]

Samples: 1 ml from each extract was mixed with 5 ml of 10 % sodium acetate and 3 ml of 2.5 % aluminum chloride. These mixtures were filled with methanol until 25 ml.

Blank: 1 ml from each extract was mixed with 8 ml of water and filled to 25 ml with methanol.

After 15 minutes the samples were read at 430 nm. There were made 3 determinations and at every determination were made 3 repeated readings. The results are the average of the 3 determinations.

In the same conditions were built a calibration curve in rutoside, using solutions in methanol with a concentration of 4.08 to 20.4 $\mu\text{g/ml}$.

Assay for total phenolic acids content determination [21]

Samples: 1 ml from each extract was mixed with 0,5 ml of phosphotungstic reagent and filled with 15 % sodium carbonate until 25 ml.

Blank: 1 ml from each extract was filled to 25 ml with 15 % sodium carbonate.

After 2 minutes the samples were read at 715 nm. There were made 3 determinations and at every determination were made 3 repeated readings. The results are the average of the 3 determinations.

In the same conditions were built a calibration curve in caffeic acid, using solutions in methanol with a concentration of 1.05 to 3.15 $\mu\text{g/ml}$.

Antioxidant capacity determination by DPPH method [22]

Samples – berries extract: 0.25; 0.50 respectively 0.75 ml of extracts were diluted with methanol at 10 ml. From each solution an aliquot of 5 ml was mixed with 5 ml of DPPH reagent, then all were maintained at 40°C 30 minutes.

Samples – flowers with leaves extract: 0.10; 0.25 respectively 0.50 ml of extracts were diluted with methanol at 10 ml. From each solution an aliquot of 5 ml was mixed with 5 ml of DPPH reagent, then all were maintained at 40°C 30 minutes.

Samples – young shoot extract: 1 ml of extract was diluted with methanol at 10 ml, then aliquots of 0.25; 0.50 respectively 0.75 ml were diluted with methanol at 10 ml. From each solution an aliquot of 5 ml was mixed with 5 ml of DPPH reagent, then all were maintained at 40°C 30 minutes.

Control: 5 ml methanol mixed with 5 ml of DPPH reagent, maintained at 40°C 30 minutes.

Blank: methanol.

The samples were read at 517 nm. There were made 3 determinations and at every determination were made 3 repeated readings. The results are the average of the 3 determinations.

For each sample was determined the inhibition percentage using the following formula:

$$I \% = (A_{\text{control}} - A_{\text{sample}}) * 100 / A_{\text{control}}$$

For each extract was built a curve and from its equation was determined the IC₅₀, meaning the quantity of extract that will neutralize 50 % of radicals.

Antioxidant capacity determination by FRAP method [22]

Samples: 0.50 ml of each extract was diluted with methanol at 10 ml. From each solution an aliquot of 0.2 ml was mixed with 0.6 ml water and 6 ml of FRAP reagent.

Blank: 0.8 ml water mixed with 6 ml of FRAP reagent.

After 5 minutes the samples were read at 593 nm. There were made 3 determinations and at every determination were made 3 repeated readings. The results are the average of the 3 determinations.

A trolox calibration curve was built in same condition using 10 to 40 µg of trolox.

Antioxidant capacity determination by NO radical inhibition method [23]

Samples: 0.50 ml of each extract is mixed with 3 ml 10 mM sodium nitroprusside in 0.2 mM phosphate buffer at pH of 7.4. These mixtures were maintained at 30°C 150 minutes. Than is added 0.5 ml Griess reagent.

Control: 0.50 ml of solvent used for extraction is mixed with 3 ml 10 mM sodium nitroprusside in 0.2 mM phosphate buffer at pH of 7.4. These mixtures were maintained at 30°C 150 minutes. Than is added 0.5 ml Griess reagent.

Blank: 3 ml of 0.2 mM phosphate buffer at pH of 7.4 with 0.5 ml extract were maintained at 30°C 150 minutes. Than is added 0.5 ml Griess reagent.

The samples were read at 546 nm. There were made 3 determinations and at every determination were made 3 repeated readings. The results are the average of the 3 determinations.

For each sample was determined the inhibition percentage using the following formula:

$$I \% = (A_{\text{control}} - A_{\text{sample}}) * 100 / A_{\text{control}}$$

Experimental Conditions for TLC Separation [19]

The separations were performed on silicagel plates. As standards were used methanolic solutions of: hyperoside (1.00 mg/mL) and caffeic acid (1.00 mg/mL). On plates were applied 20 μ L from tinctures and 30 μ L from solution obtained after SPE separation of glycerol [24] from young shoots extract respectively 10 μ L from each standard solution. The samples and standard solutions were applied as bands of 2 cm. The plates were developed ascendant in normal chamber. The mobile phase was: ethyl acetate – ethyl-methyl ketone - water – formic acid (50:30:10:10, v/v) and development distance was 10 cm. After drying of plate it was sprayed with diphenylboric acid aminoethyl ester 1 % in methanol and PEG-400 5 % in methanol. The plate was visualized after 30 minutes in fluorescence, at 365 nm.

Experimental Conditions for HPLC Separation [25]

The separations were performed on Sil-C18 column. As standards were used methanolic solutions of: vitexine (40-320 μ g/mL), chlorogenic acid (0.1 mg/ml) and rutoside (1.11 mg/mL). The mobile phase is presented in table 5. It was used 1 ml/min flow rate and a DAD UV-Vis detector at 280 nm. There were injected 10 μ L from each sample and standard solution. Each extract was diluted 1 to 10 with methanol prior injection and filtered through 0.45 μ m Teflon filter.

Table 5. The mobile phase composition for HPLC separation

Time, min	Water – phosphoric acid, pH = 2.5	Methanol	Acetonitrile
0	75	10	15
30	75	10	15
35	69	12	19
40	67	12	21
60	54	15	81

REFERENCES

1. *** “European Pharmacopoeia”, 9th edition, EDQM, **2017**.
2. *** “French Pharmacopoeia”, 11th edition, ANSM, **2007**.
3. I.E. Orhan, *Current Medicinal Chemistry*, **2016**, 23.
4. A. Karioti, E. Giocaliere, C. Guccione, G. Pieraccini, E. Gallo, A. Vannacci, A.R. Bilia, *Journal of Pharmaceutical and Biomedical Analysis*, **2014**, 88, 7.

5. J. Wang, X. Xiong, B. Feng, *Evidence Based Complementary and Alternative Medicine*, **2013**, 2013.
6. P. Ficarra, R. Ficarra, A. de Pasquale, M.T. Monforte, M.L. Calabro, *Farmaco*, **1990**, 45(2), 247.
7. Y. Benmalek, O.A. Yahia, A. Belkebir, M.L. Fardeau, *Bioengineered*, **2013**, 4(4), 244.
8. A.R. Bilia, F. Eterno, M.C. Bergonzi, G. Mazzi, F.F. Vinceri, *Journal of Pharmaceutical and Biomedical Analysis*, **2007**, 44(1), 70.
9. A. Mumtaz, M. Sultan, R.S. Muhammad, K. Ajmal, R. Umer, F. Umar, U. Farhat, S. Abdul, A. Muhammad, A. Majid, A. Manzoor, L. Abdul, *Frontiers in Pharmacology*, **2017**, 8, 327.
10. I.E. Orhan, A. Gokbulut, F.S. Senol, *Current Pharmaceutical Design*, **2017**, 23(7), 1051.
11. M. Akila, H. Devaraj, *Vascular Pharmacology*, **2008**, 49(4-6), 173.
12. V.M. Tadic, S. Dobric, G.M. Markovic, S.M. Dordevic, I.A. Arsic, N.R. Menkovic, T. Stevic, *Journal of Agricultural and Food Chemistry*, **2008**, 56(17), 7700.
13. S. Rastogi, M.M. Pandey, A.K. Rawat, *Phytomedicine*, **2016**, 23(11), 1082.
14. H. Alp, B.C. Soner, T. Baysal, A.S. Sahin, *Anatolian Journal of Cardiology*, **2016**, 15(12), 970.
15. J.M. Rigelsky, B.V. Sweet, *American Journal of Health System Pharmacy*, **2002**, 59(5), 417.
16. Lacaille-Dubois, U. Franck, H. Wagner, *Phytomedicine*, **2001**, 8(1), 47.
17. L. Jalaly, G. Sharifi, M. Faramarzi, A. Nematollahi, M. Rafieian-Kopaei, M. Amiri, F. Moattar, *Daru*, **2015**, 23, 54.
18. F.H. Degenring, A. Suter, M. Weber, R. Saller, *Phytomedicine*, **2003**, 10(5), 363.
19. *** "German Homeopathic Pharmacopoeia", ed. 2016, MedPharm Scientific Publishers, **2016**.
20. *** "Farmacopeea Română", ed. X, Editura Medicală, București, **1993**.
21. *** "Farmacopeea Română", ed. IX, Editura Medicală, București, **1976**.
22. K. Thaipong, U. Boonprakob, K. Crosby, L. Cisneros-Zevallos, D. Hawkins Byrne, *Journal of Food Composition and Analysis*, **2006**, 19, 669.
23. M.N. Alam, N.J. Bristi, M. Rafiqzaman, *Saudi Pharmaceutical Journal*, **2013**, 21, 143.
24. S. Cobzac, G. Cimpan, N. Olah, S. Gocan, *Journal of Planar Chromatography – Modern TLC*, **1999**, 12(1), 26.
25. A. Dărăban, N.K.Olah, R.F. Câmpean, F. Furtuna, C. Cobzac, Gh. Dehelean, M. Bojiță, D. Hanganu, *Studia UBB Chemia*, **2015**, 60 (2), 125.

In memory of prof. dr. Simion Gocan

POLYPHENOLS PROFILE AND ANTIOXIDANT ACTIVITY OF SOME ROMANIAN *RANUNCULUS* SPECIES

TEODORA NEAG^a, CLAUDIA-CRINA TOMA^{a*}, NELI OLAH^{a,b*},
AUREL ARDELEAN^a

ABSTRACT. The *Ranunculus* species are mostly known for their toxic effect due to the anemonine and protoanemonine content. This paper studies the polyphenols and the antioxidant activity of four different spontaneous species from *Ranunculus* genus (*Ranunculaceae* family) harvested from Western Romania's spontaneous flora. The polyphenols profile was established by TLC and UV-Vis spectrophotometric methods. The antioxidant capacity was evaluated by different *in vitro* methods: DPPH, TEAC, FRAP, CUPRAC and SNP. From the studied species were prepared two different extracts: hydroalcoholic extracts (HA) respectively glycerol-ethanol extracts (GE). The study indicates that the highest total flavonoid content is in *R. ficaria* herb HA extract (23 % mg/ml), while the total phenolic acids are the highest in *R. bulbosus* herb GE extract (14,88 % mg/ml). The most important antioxidant activity was observed at GE extracts obtained from herb of *R. ficaria*, *R. sardous* and *R. bulbosus*. With the less antioxidant effect are the *R. sceleratus* extracts.

Keywords: *Ranunculus ficaria*, *Ranunculus bulbosus*, *Ranunculus sardous*, *Ranunculus sceleratus*, antioxidant activity, total flavonoids and total phenolic acids content, rutoside

^a Vasile Goldis Western University of Arad, Faculty of Pharmacy ,86 L. Rebreanu str., RO-310414, Arad, Romania

^{*} Corresponding authors: claudiatoma2004@yahoo.com, neliolah@yahoo.com

^b SC PlantExtrakt SRL, 407059-Rădaia, Jud. Cluj, Romania

INTRODUCTION

Species of the *Ranunculus* genus are spread in the aquatic environment, wetlands and meadows. They grow as ornamental plants in parks and gardens or on the waterfront. Almost all species are considered to be toxic, especially during flowering, due to their protoanemonine content. [1,2]

Ranunculus ficaria L. (*Ficaria verna* Huds.) is a perennial plant that flourishes in the early spring [1]. It is used in folk medicine and in homeopathy for anti-inflammatory, astringent, antibiotic and anti-haemorrhagic actions [2]. The tuberous and dry roots of this herbaceous plant with oval, cordate and glossy leaves is used in the pharmacy. Tubers are rich in starch and contain saponosides which are heterosides of hederagenin and oleanolic acid [3]. *R. ficaria* extracts and β -cyclodextrin complexes exhibit antioxidant activity even at very low concentrations and could be used in pharmaceutical formulations with improved bioactivity [4]. There are used to treat haemorrhoids by topical application as an ointment or suppositories.

Ranunculus bulbosus L. is used in traditional medicine in gout pain, arthritic pain and neuralgia, being the most used *Ranunculus* specie in medicine, mainly by its roots. The whole plant has astringent, calming, antispasmodic, diaforetic, rubefiant effects. The chemical constituents present in *Ranunculus bulbosus* L. are hexadecanoic acid, β -sitosterol, anemonine and protoanemonine [6].

Ranunculus sardous Crantz has irritating action and is not used in therapy. In the spontaneous flora of Arad county the species *Ranunculus sardous* grows on halomorphic soils [7].

Ranunculus sceleratus L. has pharmacological effects, such as antibiotic, antiphlogistic, and the relief of articular effusion [8].

The aim of these investigations was to determine the polyphenol profile and antioxidant activity of different *Ranunculus* extracts using 5 methods: DPPH, FRAP (ferric reducing ability of plasma), TEAC (trolox equivalent antioxidant capacity), CUPRAC (cupric reducing antioxidant capacity) and SNP (silver nanoparticle assay). Herbs have been harvested from the spontaneous flora of the west of Romania, Arad county. Two types of extractive solutions were prepared: mother tinctures (MT) and glycerol macerates (GM).

RESULTS AND DISCUSSION

In the figures 1-3 are presented the TLC chromatograms of the studied extracts. There were used chromatographic conditions that separate specifically the polyphenols like flavonoids, phenolic acids, tannins, etc. and it can be observed that all *Ranunculus* extracts are poor in polyphenols, being separated just 2-4 bands next to the start and immediately below the front. Generally the polyphenols profiles of the extracts are very similar. At *R. ficaria* and *R. sardous* could be observed in HA extracts 1-2 bands more than in GE extracts.

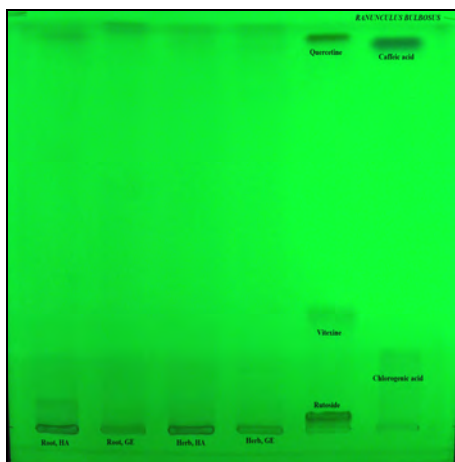


Figure 1. The TLC chromatograms of *R. bulbosus* extracts

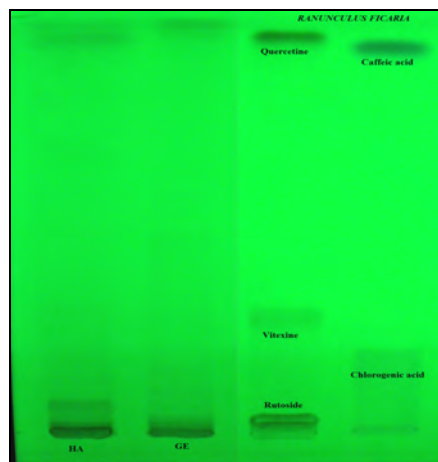


Figure 2. The TLC chromatograms of *R. ficaria* extracts

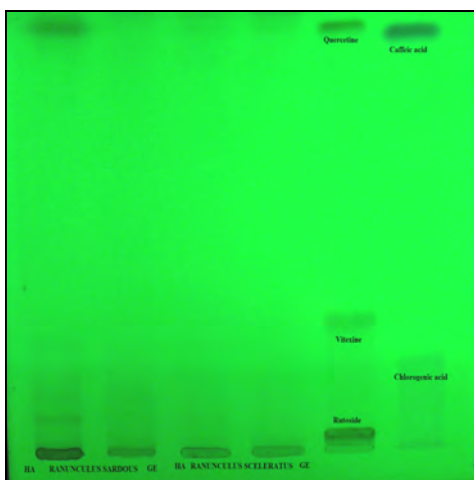


Figure 3. The TLC chromatograms of *R. sardous* and *R. sceleratus* extracts

In different amounts could be identified the rutoside in all extracts, more intensive bands being in the *R. bulbosus* roots and herba HA extracts respectively in *R. ficaria* herb HA and GE extracts. In *R. bulbosus* extracts can be identified in trace also the chlorogenic acid.

In figures 4 and 5 are presented the calibration curves of rutoside and caffeic acid for total flavonoids and total phenolic acids determination. The calibration curves equations and correlation factors are:

- Rutoside: Absorbance = 0,024xConcentration + 0,0031, $R^2 = 0,9970$.
- Caffeic acid: Absorbance = 0,0534xConcentration + 0,221, $R^2 = 0,9867$.

It can be observed that the highest total phenolic acids content is in GE extracts of *R. bulbosus* roots and herb respectively *R. sardous*, while the *R. ficaria* herb HA respectively *R. sardous* herb HA extracts are the richest in flavonoids (table 1).

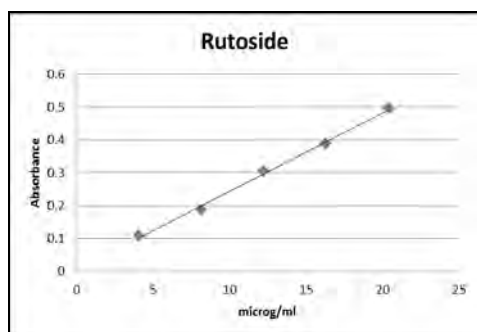


Figure 4. The calibration curve of rutoside

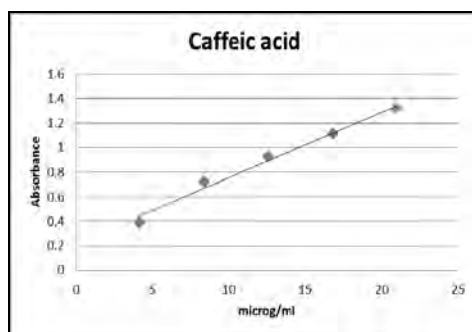


Figure 5. The calibration curve of caffeic acid

These results lead us to conclude that the herb (aerial part) of *Ranunculus* species is richer in flavonoids. The results can be correlated with the chromatographic analysis result at *R. ficaria* and *R. sardous* where in the region of flavonoids separation are more bands in HA extracts like in GE extracts. The higher phenolic acids content in *R. bulbosus* extract can be also correlated with the identification of chlorogenic acid only in these extracts.

Table 1. The assays and antioxidant capacity determinations results

Extract	Total flavonoids content, expressed in rutoside % mg/ml	Total phenolic acids content, expressed in caffeic acid % mg/ml	DPPH, IC ₅₀ , μ l	TEAC, IC ₅₀ , μ l
R. bulb. roots HA	7.61	9.63	169.5	47.1
R. bulb. roots GE	0.41	13.44	180.5	71.2
R. bulb. herb HA	9.34	6.76	220.1	58.3
R. bulb. herb GE	8.20	14.88	117.2	58.9
R. fic. herb HA	23.00	5.70	243.4	45.6
R. fic. herb GE	16.65	11.00	1.9	28.8
R. sard. herb HA	20.13	8.75	235.4	48.7
R. sard. herb GE	15.53	13.51	10.2	35.1
R. scel. herb HA	10.16	0.03	872.1	186.7
R. scel. herb GE	3.45	1.01	988.4	250.7
	FRAP, μ M ET/100 ml extract	CUPRAC, μ M ET/100 ml extract	SNP, μ M ET/100 ml extract	
R. bulb. roots HA	150	155	357	
R. bulb. roots GE	178	259	374	
R. bulb. herb HA	160	188	405	
R. bulb. herb GE	163	278	578	
R. fic. herb HA	108	205	570	
R. fic. herb GE	154	219	596	
R. sard. herb HA	129	195	472	
R. sard. herb GE	139	198	569	
R. scel. herb HA	103	61	297	
R. scel. herb GE	60	49	161	

In figures 6-8 are presented the inhibition curves of the extracts by DPPH and TEAC methods respectively for Trolox by FRAP, CUPRAC and SNP methods. The results obtained by different methods for antioxidant activity are presented in table 1.

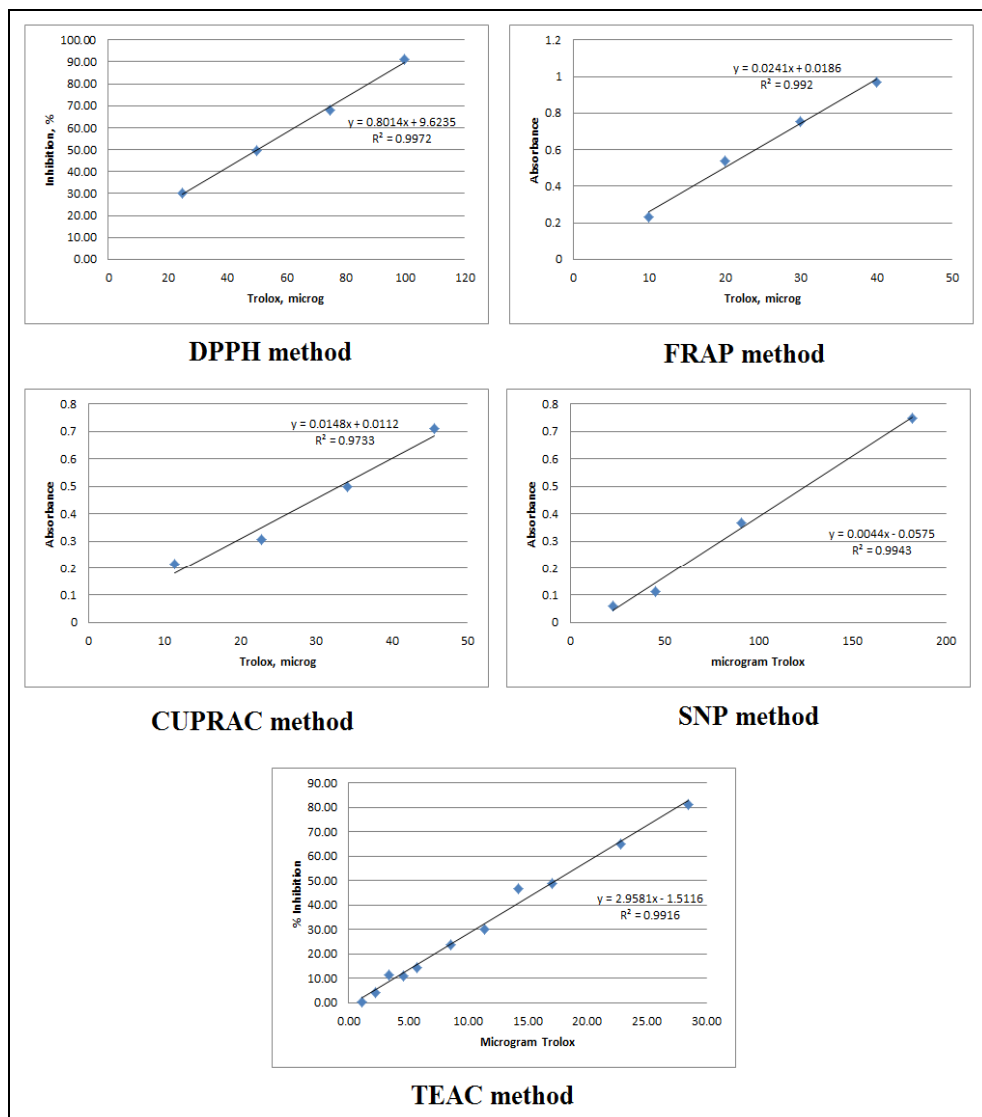


Figure 6. The Trolox inhibition curves obtained by different methods

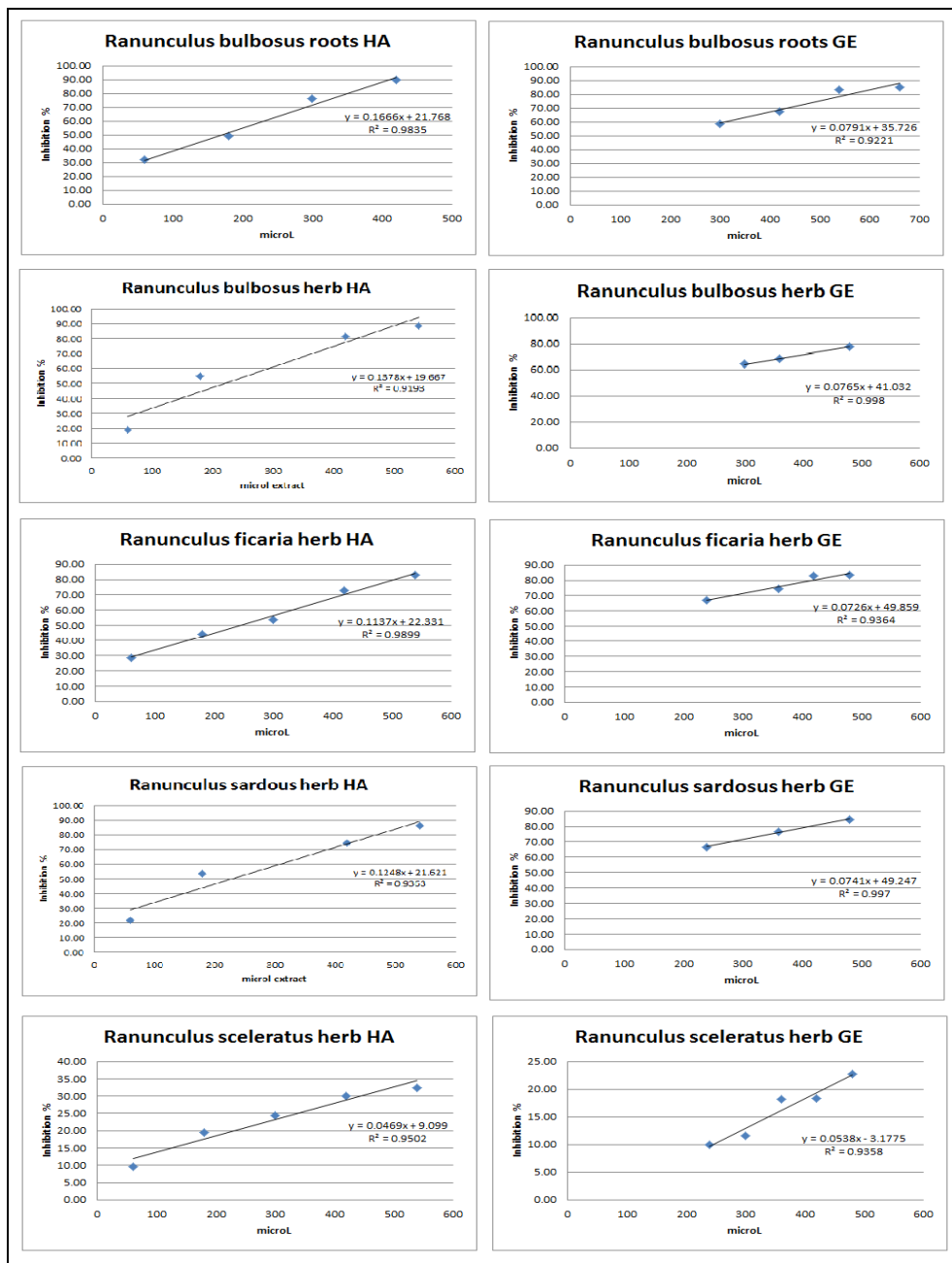


Figure 7. The inhibition curves of *Ranunculus* extracts obtained by DPPH method

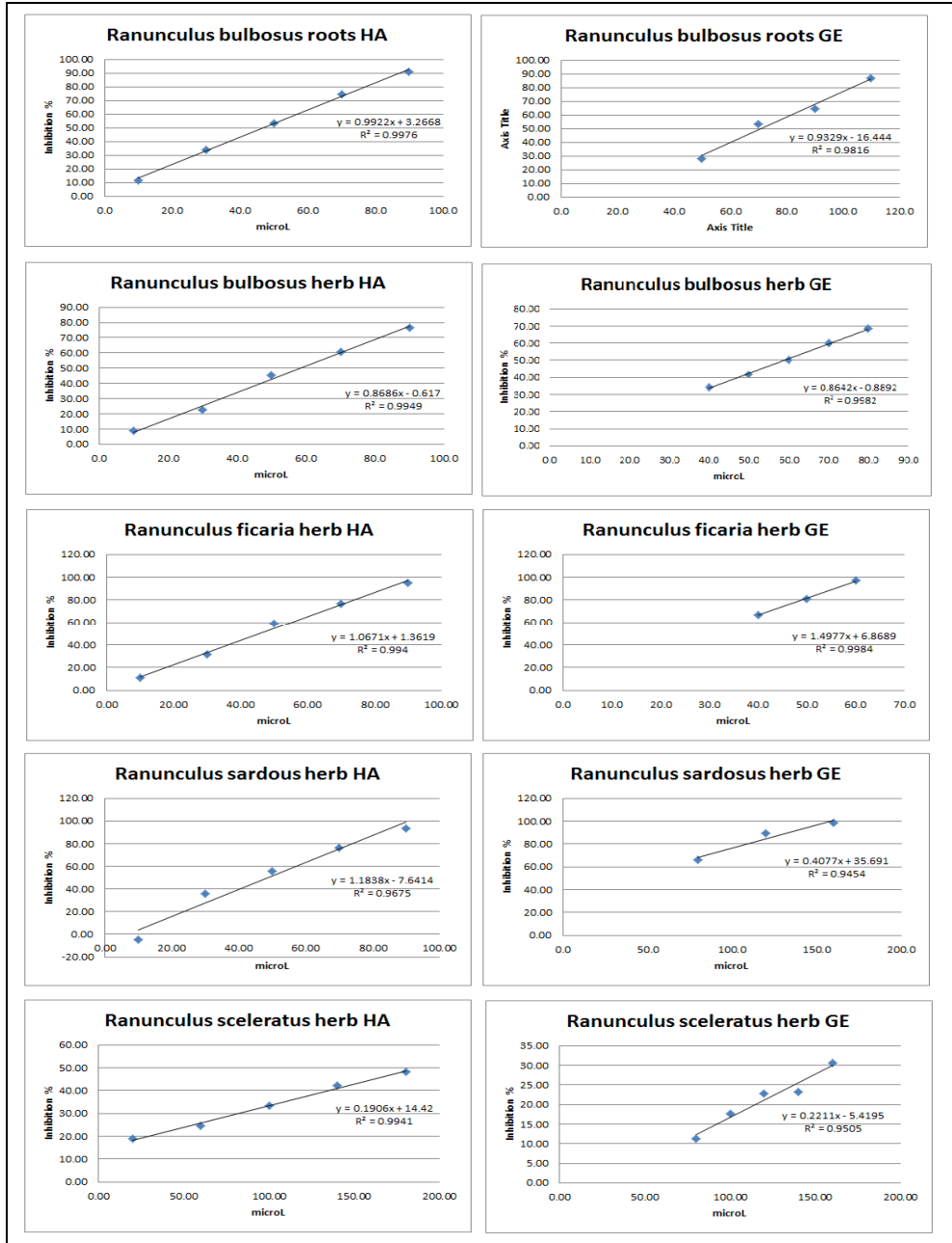


Figure 8. The inhibition curves of *Ranunculus* extracts obtained by TEAC method

It can be observed that all methods indicate as the *Ranunculus* species with less antioxidant activity the *R. sceleratus*, both extracts from this herb having very small trolox equivalent (TE) or high IC₅₀ values. The DPPH and TEAC methods indicates as the extracts with most important antioxidant activities the GE extracts from *R. ficaria* and *R. sardous*. According to FRAP, CUPRAC and SNP methods the extracts with most significant antioxidant activity are the GE herb extracts from *R. bulbosus* and *R. ficaria*, but also the *R. bulbosus* roots GE extract has important radical scavenging effect.

If we compare the *Ranunculus* extracts antioxidant effect with those of a standard antioxidant like trolox, we can observe that the *R. ficaria* herb GE (IC₅₀ = 28.8 µl) have almost similar antioxidant activity like the trolox (IC₅₀ = 17.4 µg) according the TEAC method and a more significant activity according DPPH method, where the extract has IC₅₀ = 1.9 µl and the trolox IC₅₀ = 50.4 g.

It can not be found a direct or linear correlation between the polyphenols (flavonoids and phenolic acids) content and the obtained antioxidant capacity, meaning that probably also other bioactive compounds classes will contribute to the *Ranunculus* species antioxidant effect.

CONCLUSIONS

In the bibliographic references cannot be found data about these *Ranunculus* species polyphenols or antioxidant activity, due by this fact these results seem to be the first regarding these bioactive compounds of these vegetal materials.

The study revealed that even if in GE extracts the flavonoids or phenolic acids content is mostly lower than in HA extracts the antioxidant activity is higher leading us to conclude that it is possible that these extracts to have a better therapeutic potential.

Despite the fact that the medicinal species from *Ranunculus* genus is *R. bulbosus* and the part of the plant used in therapy is the root, this study highlights that the herb of different *Ranunculus* species present a better antioxidant activity, mainly *R. ficaria* and *R. sardous* near *R. bulbosus*. The similar polyphenol profile of all studied *Ranunculus* species leads us to conclude that can be possible to use each of them to replace the other. To be sure about this must be made also an evaluation on anemonin and protoanemonin content, compounds that indicates these species toxicity.

EXPERIMENTAL SECTIONS

Extracts preparation

The plants were harvested from Arad county, Romania. There were prepared two types of extracts: hydroalcoholic (HA) and glycerol-ethanol (GE).

Mother tinctures were prepared from fresh plant by maceration with 70% vol. ethanol. It was kept at room temperature for 10 days, shaking 3-4 times a day. The extractive liquid was decanted and the residue pressed. The ratio of the mass of the plant product to the extraction solvent was 1:10 (m/m).

The glycerol-ethanol extracts were obtained by maceration the fresh vegetal material with a 1:1 mixture of 96% vol. ethanol and glycerol, using an extraction ratio of 1:20 (m/m) ratio. They were kept at room temperature for 20 days, after which they were filtered.

Antioxidant activity

DPPH method

DPPH method is based on the change in color of the 2,2-diphenyl-1-picrylhydrazyl free radical, which is violet, in presence of an antioxidant when the above-mentioned radical is reduced and the color is turn on yellow. This color change can be easily correlated with the antioxidant power by a spectrophotometric determination.

The antioxidant activity was performed at 517 nm. At 5 ml of 25 mM DPPH solution in methanol is added 5 ml of samples having different antioxidant quantities (60, 180, 240, 300, 360, 420, 480, 540, 600 and 660 μ l). All mixtures were incubated for 30 minutes at 40 C degrees. There was prepared in the same manner also a reference solution using 5 ml 25 mM DPPH solution and 5 ml methanol. As blank solution was used methanol. For each antioxidant quantity were determined the free DPPH radical inhibition percentage and from the curves built for each sample, quantity in function of inhibition percentage, were determined also the IC₅₀ values. There was used the following formula to determine the inhibition percentage: %I = $(A_r - A_s) \cdot 100 / A_r$ where A_r is the absorbance of reference solution and A_s is the absorbance of the solutions with samples [9, 10].

FRAP method

FRAP method is based on the change in color of a complex with iron of the TPTZ radical, 2,4,6-tripyridyl-s-triazine and on reduction of the ferric ion to the ferrous iron in this complex. The color of the complex is turn from

light yellowish-green to blue. This color change can be easily correlated with the antioxidant power by a spectrophotometric determination.

At 2.5 ml 10 mM TPTZ solution in 40 mM hydrochloric acid is added 2.5 ml 20 mM ferric chloride solution and 25 ml acetate buffer at pH = 3.6. This mixture is the FRAP reagent. At x ml sample solution were added water until 0.8 ml and 6 ml FRAP reagent (x = 0.02 ml for GE extracts and 0.01 ml for HA extracts). Blank solution was prepared using water in place of the samples. The spectrophotometric determination was performed at 593 nm. It was determined also the antioxidant capacity by calculate the μM Trolox equivalent/100 ml extract [10,11].

TEAC method

TEAC method is based on the change in color of the 2,2-azinobis(3-ethyl-benzothiazoline-6 sulfonic acid), named also ABTS, free cationic radical, which is blue, in presence of an antioxidant when the above mentioned radical is reduced and the color is turn on yellowish to colorless. The cationic radical is obtained with adding of potassium persulfate solution. This color change can be easily correlated with the antioxidant power by a spectrophotometric determination.

At 1 part of 7.5 mM ABTS solution in methanol is added 1 part of 2.6 mM potassium persulfate solution in water and left to stand 12 hours at dark. Than 1 ml of this mixture was mixed with 60 ml of methanol and used for determinations, as ABTS reagent solution. At x ml sample solution was added ABTS reagent solution until 6 ml and incubated at room temperature, at dark for 2 hours (x = 10, 20, 30, 40, 50, 60, 70, 80, 90, 100, 110, 120, 140, 160, 180 μl for each extract). There was prepared in the same manner also a reference solution using methanol in place of the samples. As blank solution was used methanol. The spectrophotometric determination was performed at 734 nm. For each antioxidant quantity were determined the free ABTS radical inhibition percentage and from the curves built for each sample, quantity in function of inhibition percentage, were determined also the IC₅₀ values. There was used the following formula to determine the inhibition percentage: %I = (Ar – As)*100/Ar where Ar is the absorbance of reference solution and As is the absorbance of the solutions with samples [10,12].

CUPRAC method

CUPRAC method is based on the change in color of a complex with copper of the Neocupreine, 2,9-dimethyl-1,10-phenantroline and on reduction of the copper ion (II) to the copper iron (I) in this complex. The

color of the complex is turn from light green to reddish-orange. This color change can be easily correlated with the antioxidant power by a spectrophotometric determination.

At 1 ml 7.5 mM neocupreine solution is added 1 ml 10 mM copper chloride solution and 1 ml ammonium acetate buffer at pH = 6.8. This mixture is the CUPRAC reagent. At x ml sample solution were added water until 1.1 ml and 3 ml CUPRAC reagent ($x = 0.03$ ml for HA extracts and 0.06 ml for GE extracts). The mixtures were incubated at room temperature for 30 minutes. There was prepared in the same manner also a blank solution using water in place of the samples. The spectrophotometric determination was performed at 450 nm. It was determined also the antioxidant capacity by calculate the μM Trolox equivalent/100 ml extract [13].

SNP method

The silver nanoparticles are obtained from silver nitrate at boiling and using as surface stabilizer the trisodium citrate. The method is based on reduction of the silver ion (colorless solution) to colloidal silver (pale yellow to brownish solution) with fine silver nanoparticles suspended in solution, reaction that is occur in presence of the antioxidants. This color change from pale yellow to brownish can be easily correlated with the antioxidant power by a spectrophotometric determination. At 2 ml of SNP reagent obtained from 10 mM silver nitrate solution and 1 % trisodium citrate solution at boiling is added x ml sample solution and water until 0.8 ml ($x = 0.025$ ml for HA extracts and 0.05 ml for GE extracts). The mixtures were incubated at room temperature for 30 minutes. There was prepared in the same manner also a blank solution using water in place of the samples. The spectrophotometric determination was performed at 423 nm. It was determined also the antioxidant capacity by calculate the μM Trolox equivalent/100 ml extract [14].

Total flavonoids assay

The total flavonoids expressed in rutoside were determined using aluminium chloride 2.5 % at 430 nm according to Romanian Pharmacopoeia [14]. 1 ml from each HA extract or 2 ml from each GE extract, excepting *R. sardous* extracts from that were taken 0.5 ml from each, was mixed with 5 ml of 10 % sodium acetate and 3 ml of 2.5 % aluminum chloride. These mixtures were filled with methanol until 25 ml. The same quantity from each extract was mixed with 8 ml of water and filled to 25 ml with methanol. These mixtures were used as blank solutions.

After 15 minutes the samples were read at 430 nm. There were made 3 determinations and at every determination were made 3 repeated readings. The results are the average of the 3 determinations. In the same conditions were built a calibration curve in rutoside, using solutions in methanol with a concentration of 4.08 to 20.4 µg/ml.

Total phenolic acids assay

The total phenolic acids expressed in caffeic acid were determined using phosphotungstenic reagent at 715 nm according to Romanian Pharmacopoeia [15]. 2 ml from each extract, excepting the *R. ficaria*, *R. sardous* and *R. sceleratus* HA respectively *R. sardous* GE extracts from that were picked up 1 ml, was mixed with 0,5 ml of phosphotungstenic reagent and filled with 15 % sodium carbonate until 25 ml. The same amount from each extract was filled to 25 ml with 15 % sodium carbonate and used as blank solutions. After 2 minutes the samples were read at 715 nm. There were made 3 determinations and at every determination were made 3 repeated readings. The results are the average of the 3 determinations. In the same conditions were built a calibration curve in caffeic acid, using solutions in methanol with a concentration of 4.20 to 21.0 µg/ml.

TLC conditions

The separations were performed on silicagel plates. As standards were used methanolic solutions of: rutoside, vitexine, quercetine, chlorogenic acid and caffeic acid, each of 1.00 mg/mL. On plates were applied 20 µL from tinctures and 30 µl from solution obtained after SPE separation of glycerol [16] from GE extract respectively 10 µL from each standard solution. The samples and standard solutions were applied as bands of 2 cm. The mobile phase was: ethyl acetate – ethyl-methyl ketone - formic acid (75:20:5, v/v) and development distance was 10 cm. After drying of plate the chromatograms were visualized at 254 nm.

REFERENCES

1. A. Ardelean, G.Mohan, "Medicinal Flora of Romania", Ed. ALL, Bucuresti, **2008**, 33.
2. L. Tongjian, X. Lingling, L. Liang, D. Huisheng, H. Xingjie, *Botanical Journal of the Linnean Society of London*, **2014**, 174 (2), 227.

3. W. C. Evans In: "Pharmacognosy", 14th Ed. WB Pourrat H., Texier O. and Regerat F. (1982), Use of an Saunders Company, Tronto- Sydney-Tokyo, **1996**.
4. J. Bruneton, „Pharmacognosie: Phytochimie, Plantes médicinales”, 2nd edition, Paris, **1993**, 55.
5. N. Hadaruga, *Chemistry Central Journal*, **2012**, 762.
6. S. Aslam, A. Bashir, M. Uzair, A. Subhan, *International Journal of Pharmacy and Pharmaceutical Sciences*, **2012**, 4(5),15.
7. I. Daraban, "Diversity, bio-economic potential and preservation of flora and halophile vegetation in Campia Aradului", PhD thesis abstract, **2013**.
8. H. Mei, S. Zuo, L. Ye, J. Wang S. Ma, *Journal of Medicinal Plants Research*, **2012**, 6(10), 1821.
9. M.N. Alam, N.J. Bristi, M. Rafiquzzaman, *Saudi Pharmaceutical Journal*, **2013**, 21, 143.
10. K. Thaipong, U. Boonprakob, K. Crosby, L. Cisneros-Zevallos, D. Hawkins Byrne, *Journal of Food Composition and Analysis*, **2006**, 19, 669.
11. I.F.F. Benzie, J.J Strain., *Analytical Biochemistry*, **1996**, 239, 70.
12. M.B Arnao., A.Cano, M Acosta, *Food chemistry*, **2001**, 73, 239.
13. M.Ozyurek, N. Gungor, S. Baki, K. Guclu, R. Apak, *Analytical Chemistry*, **2012**, 84(18), 8052.
14. "Romanian Pharmacopoeia", Xth ed., Medical Publishing House Bucharest, Romania, **1993**, 335.
15. "Romanian Pharmacopoeia", IXth ed., Medical Publishing House Bucharest, Romania, **1976**.
16. S. Cobzac, G. Cimpan, N. Olah, S. Gocan, *Journal of Planar Chromatography – Modern TLC*, **1999**, 12(1), 26.

In memory of prof. dr. Simion Gocan

INVESTIGATION ON IMAGE PROCESSING PARAMETERS FOR PLATE EVALUATION IN TLC ANALYSIS OF MYCOTOXINS

DORINA CASONI^a, MIHAELA BADEA^b, ILDIKO BROS^c,
SIMONA CODRUTA AURORA COBZAC^{a,*}

ABSTRACT. Based on advantages of available modern image processing techniques, thin-layer chromatography combined with image analysis becomes a promising alternative for the mycotoxins determinations in various foodstuffs. For this, the effect of digitizing channel selection and image processing parameters on aflatoxin B2 (AB2) and ochratoxin A (OTA) determination was evaluated and the obtained results were compared with those of classical photodensitometric analysis. The best exciting wavelength for OTA was found to be $\lambda_{\text{excitation}}=333\text{nm}$ while for AB2 $\lambda_{\text{excitation}}=365\text{nm}$. Low detection and quantification limits were determined ($\text{LOD}_{\text{OTA}}=0.310\text{ng/spot}$; $\text{LOQ}_{\text{OTA}}=0.616\text{ng/spot}$, $\text{LOD}_{\text{AB2}}=0.557\text{ng/spot}$, $\text{LOQ}_{\text{AB2}}=1.098\text{ng/spot}$). For image processing, the parameter with the highest influence upon the regression calibration curve was brightness and the best digitizing channel was found to be the green one. First-order calibration curve with a good determination coefficient ($R^2>0.99$) were obtained on the working range of 2.5-50ng/spot. Although image processing techniques do not provide higher LOD and LOQ values than classical photodensitometry, this method offers the advantage of simultaneous quantification of both mycotoxins.

Keywords: aflatoxin B1, ochratoxin A, TLC; densitometry, image processing

^a Babeş-Bolyai University, Faculty of Chemistry and Chemical Engineering, 11 Arany Janos Street, Cluj-Napoca, Romania

^b Transilvania University of Brasov, Faculty of Medicine, 56 N. Balcescu. Street, Brasov, Romania

^c National Institute for Research and Development of Isotopic and Molecular Technologies, 65–103 Donath Street, Cluj-Napoca, Romania

* Corresponding author: csimona@chem.ubbcluj.ro

INTRODUCTION

Mycotoxins are toxic secondary metabolite produced by moulds. One mould species can produce many different mycotoxins, and the same mycotoxin can be produced by several species. Mycotoxins may appear in the food chain as a result of fungal infection or improper storage conditions. Some mycotoxins are mutagenic and carcinogenic while other present specific organ toxicity. Mycotoxins are resistant against chemical decomposition, digestion or temperature treatments, such as cooking and freezing. The scientific literature offers a wide range of information on the occurrence of mycotoxins in food and feed [1, 2]. Due to their toxicity, aflatoxins and ochratoxins are the most studied mycotoxins.

Aflatoxins are produced by the *Aspergillus* species of fungi. The main source of mycotoxins is *Aspergillus flavus* that has in its composition four toxic compounds known as - aflatoxin B1, B2, G1 and G2. When aflatoxins B1 and B2 are ingested by lactating cows, a small proportion is converted to hydroxylated compounds (aflatoxins M1 and M2) which are excreted in milk. Structurally, aflatoxins are highly substituted coumarins (Fig.1). Under UV light, aflatoxins B present blue fluorescence, aflatoxins G present green fluorescence and aflatoxins M present violet fluorescence. Aflatoxins have teratogenic effects and can induce acute liver damage, liver cirrhosis and tumors development. Their toxicity decreases as follows: B1; M1; G1; B2; M2 and G2 [3].

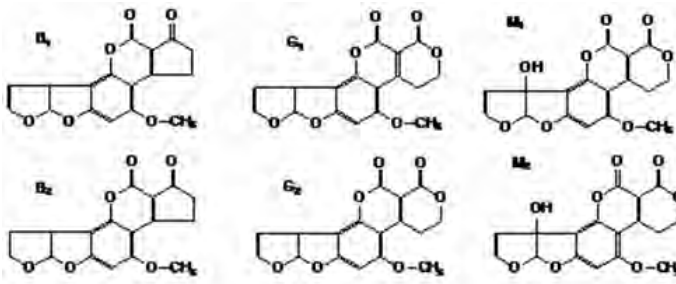


Figure 1. Aflatoxins structures

Ochratoxins are produced by *Aspergillus* and *Penicillium* species. There are at least seven structurally related compounds from which ochratoxins A (OTA), B (OTB) and C (OTC) are the most known (Fig.2). Like most other mycotoxins they are stable at high temperatures and under UV light present green (OTA) or blue fluorescence. OTA is more toxic than

OTB and OTC. Ochratoxins have immunotoxic, teratogenic and carcinogenic effects [4]. Human chronic OTA exposure is linked to increased incidences of nephropathy and urothelial tumors, especially in the Balkan region.

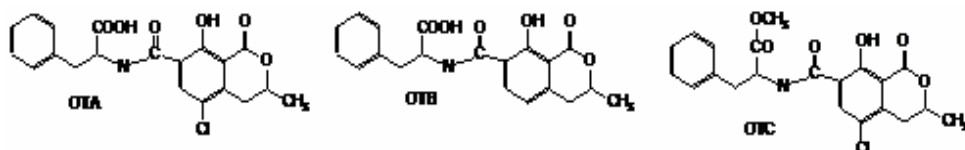


Figure 2. Ochratoxins structure

Grains, dried beans (cocoa, coffee and soy beans), barley, citrus, their products and wine can be contaminated when improper storage conditions are used. Ochratoxins can also be accumulated in meat and meat products.

Taking into account their high toxicity, regulatory limits have been established in many countries worldwide. The Commission of the European Communities [5] has set the maximum admitted levels for mycotoxins at $\mu\text{g}/\text{kg}$ in different foods.

From the viewpoint of the food production industry, raw materials should be analyzed to screen the presence of mycotoxins using fast techniques such as enzyme-linked immunosorbent assay (ELISA) or electrochemical methods using biosensor. Confirmatory methods rely on chromatographic techniques such as high performance liquid chromatography (HPLC), thin layer chromatography (TLC), gas chromatography (CG) and capillary electrophoresis (CE) [6]. Scientific literature presents many review articles regarding mycotoxins analysis [7-10]. By far, the most commonly used technique is RP-HPLC. Isocratic [9] as well gradient elution with organic solvent (methanol, acetonitril) and aqueous solution can be used [12, 13]. Detection is achieved by fluorimetric measurements [12] or by coupling with a mass spectrometer [15, 16].

TLC analysis for mycotoxins is still popular for both qualitative and quantitative determinations [17-24]. Silica gel layers seem to be the most common stationary phases used for such investigations. Different mobile phases combined with single, multiple, mono-dimensional or bi-dimensional development procedures [19, 23] were employed depending on the mycotoxins polarity and matrix complexity. Plate documentation was achieved either by measuring the fluorescence emission after UV light (364 nm) exposure or after spraying the plate with different reagents. Both scanning densitometry and image analysis techniques

were employed for spot area evaluation. While linear calibration curve is preferred in quantitative analyses, second-order polynomial dependence between spots area and concentration was often observed in the case of image processing techniques.

In the matter of TLC combined with image analysis method, even for linear signal/concentration dependence, the accuracy in spot area determination can be strongly influenced by variation of image processing parameters (as contrast and brightness) usually involved in such methodology. Moreover, the quantification of mycotoxins by TLC leads to an increased difficulty due to their native fluorescence property.

Taking into account the importance of detection and quantification of mycotoxins in various foodstuffs, the purpose of this study is to evaluate the effect of different image processing parameters on the thin-layer chromatographic determination of mycotoxins. For this, the effect of color channel, contrast and brightness selection on the mycotoxins (OTA, AB2) quantification will be evaluated based on linear dependence parameters (slope and coefficient of determination (R^2)) and method performance capacity (limit of detection (LOD) and limit of quantification (LOQ)).

RESULTS AND DISCUSSION

TLC analysis was carried out on Silica gel HPTLC plates using different solvent mixtures (Table 1) as mobile phase, the most efficient separation being achieved with ethyl acetate – toluene – formic acid (30:1.5:1, v/v). The chromatogram obtained in the conditions mentioned above is presented in Figure 3.

Table 1. Mobile phases used for OTA and AB2 separation on Silica gel plates

Nr. crt.	Mobile phase	R _f value	
		OTA	AB2
1	Toluene – Methanol – Acetic acid (6:3:1, v/v)	0.78	0.79
2	Ethyl acetate – Toluene – Formic acid – H ₂ O (30:1.5:4:3, v/v)	0.96	0.74
3	Ethyl acetate – Toluene – Formic acid – H ₂ O (30:1.5:2:1.5, v/v)	0.94	0.56
4	Ethyl acetate – Toluene – Formic acid (30:1.5:1, v/v)	0.78	0.30
5	Ethyl acetate – Toluene – Formic acid (30:2.5:0.5, v/v)	0.68	0.25

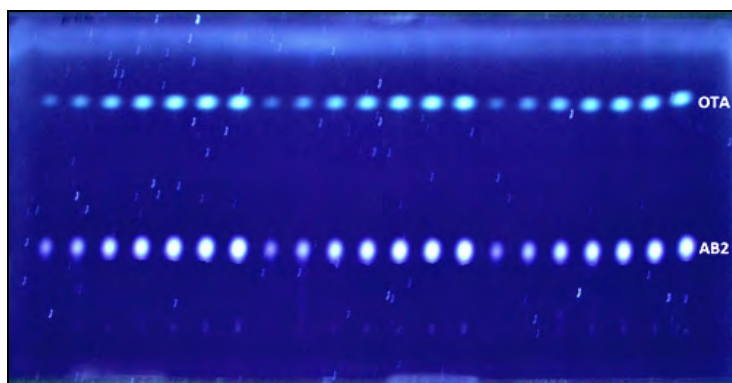


Figure 3. The chromatogram of separated mycotoxins using Silica gel HPTLC plates, mobile phase ethyl acetate – toluene – formic acid (30:1.5:1, v/v) and fluorescence mode ($\lambda_{\text{excitation}}=365$ nm)

For the determination of calibration curve equation, the plate was evaluated both by photodensitometry and by image processing. Photodensitometric measurements were carried out using two exciting wavelengths - 365nm and 333nm (Figure 4).

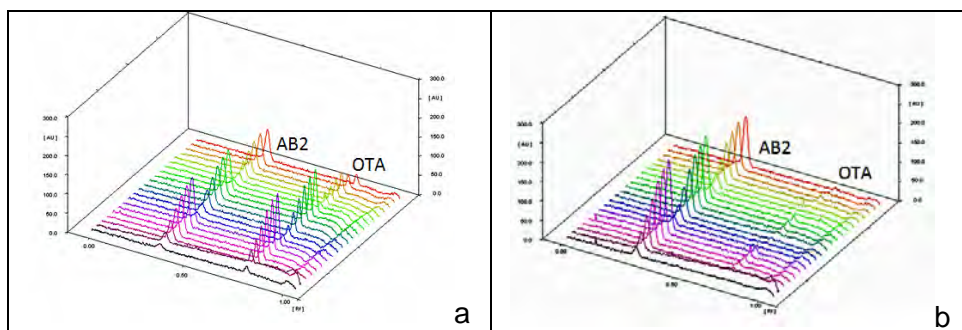


Figure 4. OTA and AB2 digitized chromatograms obtained using densitometric investigations at (a) $\lambda_{\text{excitation}} = 333$ nm and (b) $\lambda_{\text{excitation}} = 365$ nm

By plotting the emission signal vs. mycotoxins concentration (ng/spot), linear calibration curves were obtained in the working range of concentration 2.50 - 50ng/spot (Table 2). It has been noticed that incident radiation influences the size of the emission signal so that OTA can be determined only for $\lambda_{\text{excitation}} = 365$ nm. Moreover, AB2 can be determined at both wavelengths. Contrarily to OTA determination, the excitation radiation of 365nm offers the highest sensitivity for AB2 with show the lowest value of detection limit (LOD) in these conditions (Table 2).

Table 2. Calibration parameters for OTA and AB2 obtained based on densitometric evaluation of HPTLC plates

Compound	λ excitation (nm)	Linear regression parameters			LOD (ng)	LOQ (ng)
		Slope	Intercept	R ²		
OTA	333	88.764	268.19	0.9975	0.310	0.616
	365	---	---	---	---	---
AB2	333	118.04	205.83	0.9991	0.951	1.854
	365	171.62	248.78	0.9997	0.557	1.098

So far, image processing in TLC analysis has no established predefined rules. In principle, it is beneficial to use those combinations of processing parameters (contrast/brightness) that provide a white background, but do not lead to great loss of information. Moreover, when fluorescence visualization mode is used, an inversion operation is necessary in order to obtain positive values for spot area determination. Usually this procedure leads especially to background alteration and increases the difficulty of choosing the processing parameters. To have a deep insight of the problem, the image analysis was firstly performed without changing the contrast and brightness parameters. In this case a second-order calibration curve (spot area/concentration) was obtained for both investigated mycotoxins. Furthermore, if a linear dependence was taken into consideration, a significant decrease of the determination coefficient (R²) was observed (Table 3).

Table 3. Calibration curve equations for OTA and AB2 mycotoxins obtained by selecting different colour channels (grey (GY), green (GR) and blue (BL)) and without altering the contrast and brightness parameters

Channel	OTA calibration curve equation			
	$Y=ax^2+bx+c$	R ²	$Y=ax+b$	R ²
GY	$Y=-118.92x^2+17717x+84103$	0.9935	$Y=11219x+142585$	0.9752
GR	$Y=-209.85x^2+27300x+129347$	0.9945	$Y=15832x+232562$	0.9661
BL	$Y=-285.16x^2+14590x+382774$	0.9968	$Y=19358x+361196$	0.9847
	AB2 calibration curve equation			
GY	$Y=-318.15x^2+30849x+261575$	0.9794	$Y= 8654.9x+ 472759$	0.6717
GR	$Y=-383.39x^2+40284x+216681$	0.9861	$Y= 13539x + 471167$	0.7733
BL	$Y=-398.96x^2+39536x+186287$	0.9880	$Y= 11709x + 451072$	0.7092

By increasing the contrast and brightness with different percentages values the linear spot area/concentration dependence was observed. The calibration curve parameters and performance of detection and quantification obtained for different values of contrast (C1-C3) and brightness (B2-B4) are presented in Table 4.

The graphical representation of the slope according to the image processing parameters for each of the channel selected for chromatogram digitization highlights several aspects, namely: (i) the highest values of the slope are obtained for the grey and green channels; (ii) high slope values are obtained for low brightness selection (B2); (iii) the slope values decrease as the brightness increases (B3, B4); (iv) for the same brightness value, an increased contrast results in a slightly increased slope. To exemplify, only OTA graphical representation (Figure 5) is presented, but a similar trend has also been observed for AB2.

Table 4. Calibration parameters obtained by image processing at different contrast and brightness values on grey (GY), green (GR) and blue (BL) evaluation channels

Compound	Evaluation channel	Image processing parameters (contrast, brightness)	Linear regression parameters			LOD (ng/spot)	LOQ (ng/spot)
			Slope	Intercept	R ²		
OTA	GY	C1B2	1026.6	29657	0.9928	3.318	6.322
		C1B3	983.2	21829	0.9948	2.814	5.403
		C1B4	893.8	17489	0.9922	3.452	6.566
		C2B2	1096.4	28280	0.9945	2.894	5.549
		C2B3	1014.2	23077	0.9936	3.143	6.005
		C2B4	938.5	18968	0.9912	3.681	6.977
		C3B2	1091.6	28769	0.9942	2.971	5.691
		C3B3	1041.2	24648	0.9924	3.422	6.511
		C3B3	1003.0	20495	0.9913	3.649	6.920
	GR	C1B2	1520.6	29242	0.9940	3.038	5.814
		C1B3	1425.0	19666	0.9938	3.082	5.894
		C1B4	1358.2	12964	0.9910	3.721	7.048
		C2B2	1570.4	28420	0.9917	3.571	6.779
		C2B3	1514.3	20432	0.9912	3.679	6.974
	C2B4	1444.2	14359	0.9908	3.758	7.115	

Compound	Evaluation channel	Image processing parameters (contrast, brightness)	Linear regression parameters			LOD (ng/spot)	LOQ (ng/spot)	
			Slope	Intercept	R ²			
		C3B2	1586.9	28272	0.9901	3.895	7.359	
		C3B3	1577.9	21798	0.9895	4.027	7.594	
		C3B3	1543.4	16225	0.9896	3.999	7.543	
	BL	C1B2	1562.5	67058	0.9792	5.688	10.46	
		C1B3	1486.2	49282	0.9915	3.613	6.854	
		C1B4	1342.5	41267	0.9888	4.151	7.812	
		C2B2	1611.8	62241	0.9894	4.032	7.602	
		C2B3	1539.6	50885	0.9923	3.435	6.534	
		C2B4	1412.5	43639	0.9905	3.829	7.241	
		C3B2	1660.4	61335	0.9932	3.225	6.153	
		C3B3	1574.5	53787	0.9916	3.588	6.810	
		C3B3	1503.0	46513	0.9916	3.588	6.811	
		AB2	GY	C1B2	1722.3	60569	0.9944	2.930
	C1B3			1602.5	49886	0.9964	2.342	4.527
	C1B4			1509.1	41833	0.9933	3.194	6.097
	C2B2			1880.8	58338	0.9902	3.889	7.347
	C2B3			1741.7	50919	0.9889	4.145	7.801
	C2B4			1615.5	44102	0.9964	2.338	4.521
C3B2	1848.4			60266	0.9955	2.631	5.065	
C3B3	1786.0			53911	0.9966	2.263	4.381	
C3B3	1734.5			47183	0.9966	2.280	4.412	
GR	C1B2		2497.8	24195	0.9933	3.203	6.113	
	C1B3		2476.4	10208	0.9953	2.671	5.139	
	C1B4		2401.2	15640	0.9918	3.555	6.751	
	C2B2		2671.4	21222	0.9981	1.717	3.350	
	C2B3		2577.9	12436	0.9974	1.992	3.872	
	C2B4		2465.8	52389	0.9961	2.433	4.698	
		C3B2	2656.5	23156	0.9977	1.879	3.656	
		C3B3	2653.7	14404	0.9972	2.057	3.993	

Compound	Evaluation channel	Image processing parameters (contrast, brightness)	Linear regression parameters			LOD (ng/spot)	LOQ (ng/spot)
			Slope	Intercept	R ²		
		C3B3	2688.2	49674	0.9981	1.693	3.040
	BL	C1B2	2745.2	158106	0.9955	2.613	5.032
		C1B3	2596.8	135920	0.9842	4.948	9.201
		C1B4	2313.1	122101	0.9806	5.493	10.130
		C2B2	2915.3	159552	0.9966	2.293	4.437
		C2B3	2667.8	143588	0.9951	2.777	5.335
		C2B4	2419.3	130082	0.9956	2.593	4.994
		C3B2	2936.7	161544	0.9922	3.465	6.589
		C3B3	2847.9	148667	0.9865	4.570	8.546
		C3B3	2644.3	137618	0.9950	2.765	5.313

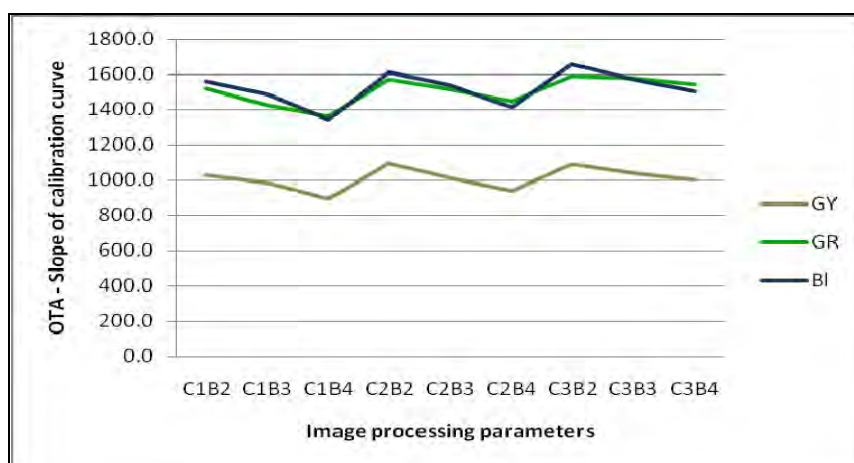


Figure 5. Slope variation according to image processing parameters (contrast (C1-C3) and brightness (B2-B4)) and selection of different colour channels (grey (GY), green (GR) and blue (BL)) for chromatogram digitization

For OTA, the determination coefficients (R^2) ranged from 0.9948 (GY) to 0.9901 (BL). The performance parameters LOD and LOQ show a variation in the range 2.814 (GY) - 4.151 (BL) ng/spot respectively 5.403 (GY) - 7.812 (BL) ng/spot. For AB2 quantification, the higher determination

coefficient ($R^2=0.9981$) and the lower value for detection and quantification (LOD=1.693 ng/spot, LOQ=3.040 ng/spot) were obtained by selecting the green channel for chromatograms evaluation.

The principal component analysis technique (PCA) was applied on data matrices consisting in numerical values of the slope, intercept and determination coefficient (as independent variables) corresponding to the investigated processing parameters (contrast (C1-C3) and brightness (B2-B4)) and colour channels (grey (GY), green (GR) and blue (BL)) used for chromatograms digitization. Based on the PCA investigations of OTA matrix, the most significant results are discussed as follows. The first principal component (PC1, representing 58% of the total variance in the data set) contains 34% information data regarding the slope, 39% regarding the intercept and 27% regarding the determination coefficient. The second PC (PC2, accounting 28% from the data variability) contains 67% information data regarding determination coefficient and 30% regarding the slope. The third PC (PC3, accounting 17.33% of data variability) is associated in a proportion of 58% to the intercept. The graphical representation of the PC3 vs. PC1 (Figure 6) shows that green channel (GR) selection for plate evaluation leads to a significant difference in method sensitivity (significantly higher values of PC3) compared to the grey (GY) and blue (BL) channels (that show no significant differences in PC3 values).

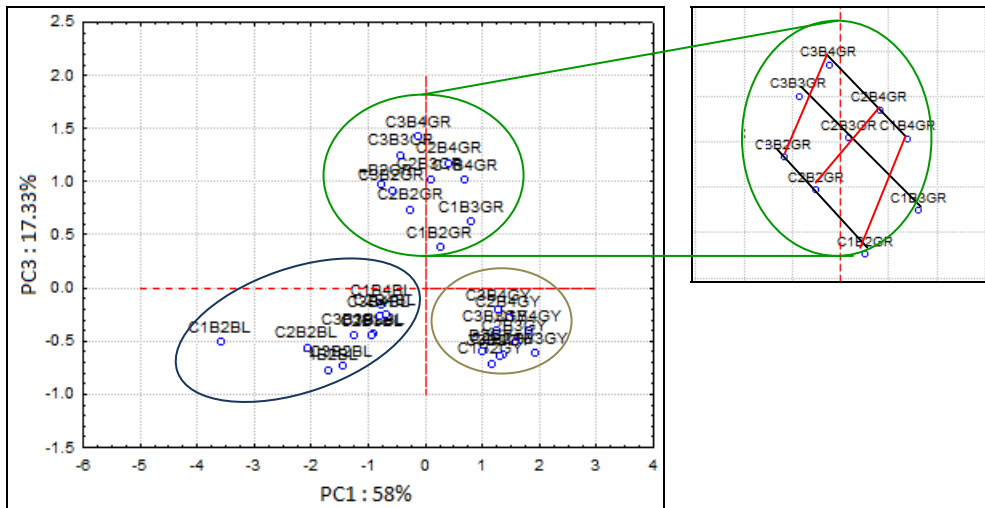


Figure 6. Projection of the cases (contrast, brightness, and digitizing channel) on the factor-plane (PC1 vs. PC3) obtained by PCA analysis on OTA regression parameters matrix

Moreover, for the green (GR) channel, it was observed a direct dependence of regression parameters (slope, intercept and determination coefficient) with brightness (black lines) and an inverse with contrast (red line) when processing parameters were increased with constant increments. The same behaviour was also observed in the case of AB2 investigations, but the direct relationships on the regression parameters based on the same brightness or contrast variations were not so evident.

CONCLUSIONS

The fluorescence photodensitometric investigation shows that both mycotoxins (AB2 and OTA) can be determined using 333nm as excitation wavelength, while 365nm leads to an increased sensitivity for AB2 determination. Moreover, better values for determination coefficient (R^2), and method performance parameters (LOD and LOQ) were obtained, compared to published data in scientific literature [24].

The image processing investigation revealed several aspects, namely: (i) linear calibration curve can be obtained by a proper image processing; (ii) the best digitizing channel for fluorescence evaluation mode is the green one; (iii) high slope values are obtained for low brightness selection; (iv) the slope values decrease as the brightness increases; (v) an increased contrast results in a slight slope increase; (vi) LOD and LOQ values obtained by image processing are comparable to those obtained by photodensitometric method.

Taking into account the above presented issues, it has been concluded that, besides the classical photodensitometric TLC evaluation technique, the modern technique of image processing can also be used with good results for mycotoxins analysis.

EXPERIMENTAL SECTION

Reagents and materials

Aflatoxin B2 (AB2) and ochratoxin A (OTA) were obtained from Fluka (Switzerland). Ethyl acetate, toluene and formic acid were from the Chemical Company (Iași, România). HPTLC Silica gel 60 plates (20 cm x10 cm) were acquired from Merck (Germany). Standard solution of OTA (2.5 μ g/mL) and AB2 (2.5 μ g/mL) was prepared in methanol.

Analytical equipment and Software

Linomat 5 TLC applicator (CAMAG, Muttenz, Switzerland) with an application rate of 80 nL s⁻¹ was used for standards application. A Nikon

CCD camera was used to capture the image of chromatographic plates and Camag TLC Scanner 3 (Camag, Switzerland) for densitometric evaluation of the chromatographic plates. ImageDecipher-TLC software version 2.0 (BioDit Technology, Co. www.biodit.com) was used for the digital processing of images and spot area integration. Limits of detection and quantification (LOD and LOQ) were calculated using statistical methods in analytical chemistry (SMAC) (Meier, 1993). Statistica 8.0 software package (www.statsoft.org) was used for statistical data treatment.

Thin Layer Chromatographic Analysis

The separation of the investigated mycotoxins was performed on high-performance silica gel 60 plates (20 cm × 10 cm, Merck, Darmstadt, Germany). Spots of 1-20 μ L of standard solutions were applied at 15 mm distance from the edges of plate. The plates were developed in a saturated chamber using different mixtures of solvents as the mobile phase. The evaluation of the plate was performed using the classical photodensitometry and modern image analysis technique respectively. Two excitation wavelengths, 365 nm and 333 nm, were used for fluorescence photodensitometry. The modern assessment technique involves digitizing of the chromatographic plate by capturing its image with a CCD camera and saving the obtained image as a bmp file. Image processing was performed with the help of the specialized ImageDecipher software, following several steps: (i) image reversal in order to obtain densitograms with positive peak; (ii) selecting the area of interest – the spot area; (iii) choosing values for contrast/brightness processing parameters; (iv) choosing the pure color channel (red, blue, green) or neutral-grey channel. The contrast and brightness image processing parameters were modified as follows: the contrast was increased by 10% (C1), 20% (C2), 30% (C3) and the brightness by 20% (B2), 30% (B3) and 40% (B4). Higher percentages of variation were not used as they were leading to information losses or major background changes.

In all cases, peak surface area determined from the digitized chromatograms was used for calibration curve plotting.

ACKNOWLEDGMENTS

This work has received partial funding from the European Community's Seventh Framework Programme (FP7/2007-2013) under grant agreement n° 245199. It has been carried out within the PlantLIBRA project (website: www.plantlibra.eu). This report does not necessarily reflect

the Commission views or its future policy on these areas. This paper is also partial supported by the Sectoral Operational Programme Human Resources Development (SOP HRD), financed from the European Social Fund and by the Romanian Government under the project number POSDRU/159/1.5/S/134378 and Bursa Universitatii Transilvania-2016. We hereby acknowledge the structural funds project "R&D Institute: High-tech products for sustainable development" (ID 123, SMIS 2637, ctr. no. 11/2009) for providing part of the infrastructure used in this research.

REFERENCES

1. J. M. Jay, M. J. Loessner, D. A. Golden, "Modern Food Microbiology", 7-th Edition, Springer, New York, **2005**.
2. J. I. Pitt, A. D. Hocking, "Fungi and Food spoilage", 2-nd Edition, Springer, New York, **2009**.
3. S. Z. Iqbal, M. R. Asi, A. Arino, "Aflatoxins" in "Brenner's Encyclopedia of Genetics", 2-nd Edition, Elsevier, London, **2013**.
4. R. C. Gupta, M. A. Lasher, I. R. Miller Mukherjee, A. Srovastava, R. Laal, "Aflatoxins, Ochratoxins, and Citrinin" in "Reproductive and Developmental Toxicology", 2-nd Edition, Elsevier, London, **2017**.
5. Commission Regulation (EC) No 1881/2006 of 19 December 2006, "Setting of maximum levels for certain contaminants in foodstuffs", <http://eur-lex.europa.eu/legal-content/EN/TXT/?uri=CELEX%3A32006H0576>
6. M. Miraglia, B. De Santis, S. Grossi, C. Brera, "Mycotoxins" in "Handbook of food analysis", 2-nd Edition, Marcel Dekker, New York, **2004**
7. N. W. Turner, S. Subrahmanyam, S. A. Piletsky, *Analytica Chimica Acta*, **2009**, 632, 168.
8. A. Rahmany, S. Jinap, F. Soleimany, *Chomprehensive review in food science and food safety*, **2009**, 8, 202.
9. A. Raiola, G. C. Tenore, L. Manyes, G. Meca, A. Ritieni, *Food and Chemical Toxicology*, **2015**, 84, 169.
10. N. W. Turner, H. Bramhmbhatt, M. Szabo-Vezse, A. Poma, R. Coker, S. A. Piletsky, *Analytica Chimica Acta*, **2015**, 901, 12.
11. L. Wang, Z. Wang, W. Gao, J. Chen, M. Yang, Y. Kuang, L. Huang, S. Chen, *Food Chemistry*, **2013**, 138, 1048.
12. Q. Liu, W. Kong, W. Guo, M. Yang, *Journal of Chromatography B*, **2015**, 988, 175.
13. D. Alkadri, J. Rubert, A. Prodi, A. Pisi, J. Manes, C. Soler, *Food Chemistry*, **2014**, 157, 111.
14. L. Wang, Z. Wang, C. Tessini, C. Mardones, D.von Baer, M. Vega, E. Herlitz, R. Saelzer, J. Silva, O. Torres, *Analytica Chimica Acta*, **2010**, 660, 119.
15. A. Prella, D. Spadaro, A. Garibaldi, M. L. Gullino, *Food Control*, **2014**, 39, 192.
16. N. Arroyo-Manzanares, J. F. Huertas-Perez, L. Gamiz-Gracia, A. M. García-Campana, *Talanta*, **2013**, 115, 61.

17. A. Kamkar, *Food Control*, **2006**, 17, 768.
18. A. A. Fallah, *Food Control*, **2010**, 21, 1478.
19. S. A. Bankole, A. A. Adenusi, O. S. Lawal, O. O. Adesanya, *Food Control*, **2010**, 21, .974.
20. I. Kamika, L. L. Takoy, *Food Control*, **2011**, 22, 1760.
21. M. Mulunda, D. Mike, *Food Control*, **2014**, 39, 92.
22. A. A. Fallah, M. Rahnama, T. Jafari, S. Siavash Saei-Dehkordi, *Food Control*, **2011**, 22, 1653.
23. I. Var, B. Kabak, F. Gok, *Food Control*, **2007**, 18, 59.
24. C. Braicu, C. Puia, E. Bodoki, C. Socaciu, *Journal of Food Quality*, **2008**, 31(1), 108.

In memory of prof. dr. Simion Gocan

NOVEL APPROACHES FOR THE DETERMINATION OF BIOGENIC AMINES IN FOOD SAMPLES

LUCA RIVOIRA^{a,*}, MOJCA ZORZ^b, MITJA MARTELANC^b, SARA BUDAL^b,
DAVIDE CARENA^{a,b}, MLADEN FRANKO^b, MARIA CONCETTA BRUZZONITI^a

ABSTRACT. Wine is a fermented beverage that could be affected by high concentrations of biogenic amines which alter organoleptic properties. In this work, new analytical approaches for determination of biogenic amines in wines were developed.

For the first time, we studied the derivatization of BAs in wines with naphthalene-2,3-dicarboxaldehyde (NDA) and with dabsyl chloride (DBS) and analysis of derivatized BAs by HPLC coupled to fluorescence (HPLC-NDA-FL) and thermal lens spectrometry (HPLC-DBS-TLS) detectors. The sensitivity of the two methods (LODs HPLC-NDA-FL in the range 27-73 µg/L; LODs HPLC-DBS-TLS in the range 3.4-11 µg/L) was higher than that of the official method for biogenic amines in wines, OIV-MA-AS315-18 (60-77 µg/L). For its best performances, the HPLC-DBS-TLS technique was applied to the analysis of putrescine, cadaverine, histamine and tyramine in two white wine samples. Additionally, exploiting the Berthelot reaction, the TLS fast screening of biogenic amines in wines, following the release of ammonia by transglutaminase, was also proposed. This approach allowed us to determine total biogenic amount content in concentrations below 0.1 mg/L, expressed as equivalents of histamine.

Keywords: *biogenic amines, NDA, liquid chromatography, TLS, fluorescence, wine.*

INTRODUCTION

Biogenic amines (BAs) are low molecular weight compounds which could be frequently found in food and beverage matrices [1-2]. They are

^a Department of Chemistry, University of Torino, via P. Giuria 5, 10125 Torino, Italy

* Corresponding author: luca.rivoira@unito.it

^b Laboratory for Environmental and Life Sciences, University of Nova Gorica, Vipavska 13, SI-5000 Nova Gorica, Slovenia

divided in three main classes, aliphatic (e.g. putrescine, cadaverine, spermine, spermidine), aromatic (e.g. tyramine, phenylethylamine) and heterocyclic (e.g. histamine, tryptamine). They mostly derive from four enzymatic reactions of bacteria (decarboxylation, transamination, reductive amination and degradation) performed on precursor amino compounds, such as amino acids.

Highest concentrations of biogenic amines are found in fermented food, where different species of bacteria, in particular lactic acid bacteria (LAB), are responsible for decarboxylase activity, in different degrees depending on the bacteria strain [3]. Lower concentrations are also found in non-fermented foods, as an endogenous origin [4].

Biogenic amines play essential roles in the development, metabolism and physiological functions of humans; however, several studies show that, biogenic amines at concentrations higher than 500 ppm can induce cancerogenic alteration of DNA [5-8]. At lower concentrations, BAs can cause many toxicological effects, such as headache and hypertension besides originating organoleptic alterations of the affected foods. Recently, several European Union Countries have set regulations for limits of histamine (one of the most active amine) in food matrices. As an example, EU Directive 1441/2007 regulates histamine in fish (the mean value must not exceed the value of 100 mg/kg) [9]. Local legislation of several countries regulates the concentration of histamine in wines also (i.e. France 8 mg/L, Germany 2 mg/L, Switzerland 10 mg/L).

Among the fermented beverages that could be affected by relevant concentrations of BAs, wines are intensively studied matrices. In fact, in these matrices, BAs are produced, along many stages of winemaking and ageing, by LAB bacteria, in concentrations which depend on regional variability, as well as on agricultural and production techniques [10-11]. Histamine, tyramine, putrescine, and cadaverine are among the biogenic amines mainly present in wines [3].

Various analytical methods have been developed for rapid and simultaneous determinations of biological amines in wine, such as liquid chromatography (LC), thin-layer chromatography (TLC) [12], gas chromatography (GC) [13] and capillary electrophoretic methods (CE) [14]. Among these, GC is not so often applied, whereas CE methods are not sensitive to low BA concentrations and have poor reproducibility [15]. Conversely, LC is the most applied technique for the determination of biogenic amines. MS detection is frequently reported, even if its routine application can be limited by the costs and by analyst's expertise required. More frequently, ion [16] and reversed-phase chromatography coupled with UV-Vis and fluorescence (FL) [17] detections are proposed for the analysis

of BAs. These approaches require a derivatization procedure. O-phthalaldehyde (OPA) [18], dansyl-chloride (DNS-Cl) [19], dabsyl-chloride (DBS-Cl)[20] and 6-aminoquinolyl-N-hydroxysuccinimidyl carbamate (AQC) [21] are some of the derivatizing agents used for fluorescence detection. Despite the good sensitivity achieved, the above mentioned derivatizing agents have peculiar disadvantages. More in detail, DNS-Cl is characterized by slow kinetics. OPA can derivatize primary amine groups also at low concentrations (ng/L) but at strictly controlled conditions of pH [22]. Recently [23], naphthalene-2,3-dicarboxaldehyde (NDA) was used to form derivatives of amines with fluorescent and electroactive properties. If compared with the products formed by derivatization with OPA, the NDA derivatives exhibit improved chemical stability, excitation maxima in the visible region (at 420 and 440 nm) and enhanced fluorescence quantum efficiency [24].

These properties, particularly absorption maxima in the visible range, open the possibility of applying novel techniques complementary to FL, such as highly sensitive thermal lens spectrometry (TLS). TLS is however based on radiationless de-excitation processes and is therefore hindered by higher fluorescence quantum yields [25-26]. For nonfluorescing analytes TLS offers detection of absorbances as low as 10^{-7} , and was shown to actually enable detection at single molecule level when performed in its microscopic configuration (Thermal lens microscopy – TLM) adapted for lab-on-chip detection [27]. Even though TLS enables sensitive detection also for fluorescing analytes such as cyanobacterial pigments [28], non-fluorescing derivatives such as dabsylated BAs, which have the primary absorbance maximum of BAs shifted into the visible spectral range, appear advantageous over the fluorescing derivatives. Besides an easier matching of absorbance maxima with the available laser emission lines, the longer wavelength further reduces the possibility of interference from other compounds. Due to high sensitivity, fast signal response and capability of probing sub- μ L volumes, TLS and TLM have recently found many applications also in vanguard analytical methods for fast screening of environmental and food samples. Such applications include determination of organophosphorous pesticides, microcystin [28], Cr(VI) [29], and ammonia [30]. As reported, ammonia is also produced from biogenic amines by the action of transglutaminase (TG), which hence can be used for determination of BAs [31].

In this work, for the first time, we compared NDA and dabsyl chloride as derivatizing agents for BAs determination in wines by HPLC coupled to fluorescence (HPLC-FL) and thermal lens spectrometry (HPLC-TLS) detectors. Additionally, exploiting the Berthelot reaction, leading to the

formation of indophenol, we propose for the first time the fast screening of BAs in wines by TLS, following the release of ammonia by TG.

In detail, after a preliminary optimization of chromatographic conditions, the effects of the main derivatization parameters on BA signals were assessed, so optimizing derivatization conditions.

The figures of merit for HPLC-NDA-FL and HPLC-DBS-TLS methods (linearity, limits of detection, limits of quantification) were evaluated and compared. Since the best performances were obtained by the HPLC-DBS-TLS method, this method was successfully applied for the determination of putrescine, cadaverine, histamine and tyramine in two white wine samples, comparing results with those obtained by using the official method for BAs determination in wines, which is based on the HPLC-OPA-FL procedure.

RESULTS AND DISCUSSION

DERIVATIZATION: OPTIMIZATION OF PARAMETERS

NDA derivatization

To optimize the derivatization of BAs in wine matrix, the effects of reaction time and initial NDA concentration on the derivatization performance were studied for ethanolamine, chosen as a model compound, in synthetic wine matrix.

Effect of reaction time.

A solution of 50 mg/L ethanolamine was derivatized with NDA at six reaction times ranging from 15 to 40 min and subsequently injected into the HPLC-FL system, measuring the peak area obtained for each trial. As shown in Figure 1, the response increases with reaction time up to 25 min, then reaching a plateau for increased reaction times. In the absence of other literature studies performed on wines, this reaction time was compared with other studies using NDA for BAs derivatization, observing that about 16 h are required to complete derivatization e.g. in human immunoglobulin samples [17]. This study, tests were performed at reaction times as long as 16 h, highlighted a 30% decrease of the responses, probably due to degradation of the derivatizing products. Further studies were performed for max. 40 min, choosing 25 min as optimal reaction time.

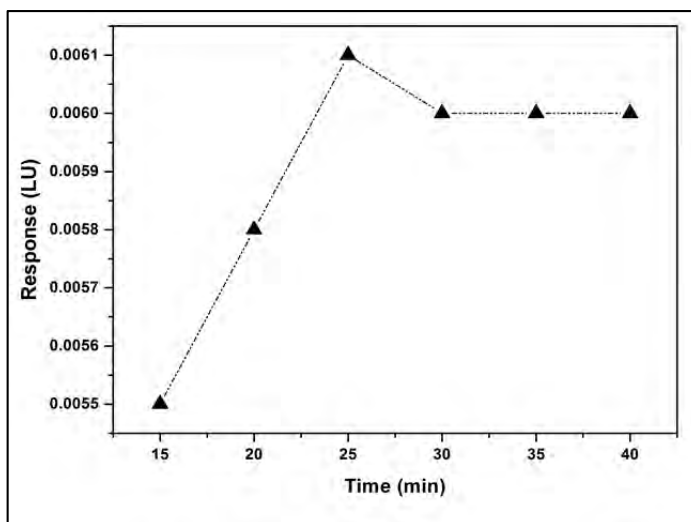


Figure 1. Effect of reaction time in the derivatization of 50 mg/L ethanolamine in synthetic wine. Response is referred to peak area in HPLC-FL analysis of derivatized amine.

Effect of initial NDA concentration.

Once identified the optimal reaction time, concentration of NDA necessary to obtain the highest derivatization yields (signal responses) was studied, applying the same detection procedure as detailed before. Studies involving BAs derivatization with NDA in biological human samples point out that concentration of $8 \cdot 10^{-5}$ M NDA was used to derivatize up to 0.15 mg/L (corresponding to $8 \cdot 10^{-7}$ M) histamine dihydrochloride [17]. Concentration of BAs in wines can achieve tens of mg/L. Our study was performed under precautionary conditions, considering concentrations of BAs in the range 50-500 mg/L in synthetic wine, which cause perceivable alterations of wine such as the reduction in overall wine aroma, observed with the formation of metallic, meaty or putrid aromas in wine. According to the BAs concentration levels studied, the tested NDA concentrations were 1.34 and 13.4 mM. Lower NDA concentrations are not advisable, especially for real samples, since derivatization of BAs could not be complete if more than one BA is present (see Figure 2).

Finally, the possibility to increase the derivatization efficiency of biogenic amines was investigated by evaluating the effect of the solvent in which NDA is dissolved. Previous published works reported that NDA could be dissolved both in acetonitrile or methanol, without detailing if a contribution of the solvent in the derivatizing reaction is present [17, 32].

Our study demonstrated that no statistically significant difference is observed when derivatizing with NDA dissolved in methanol or acetonitrile.

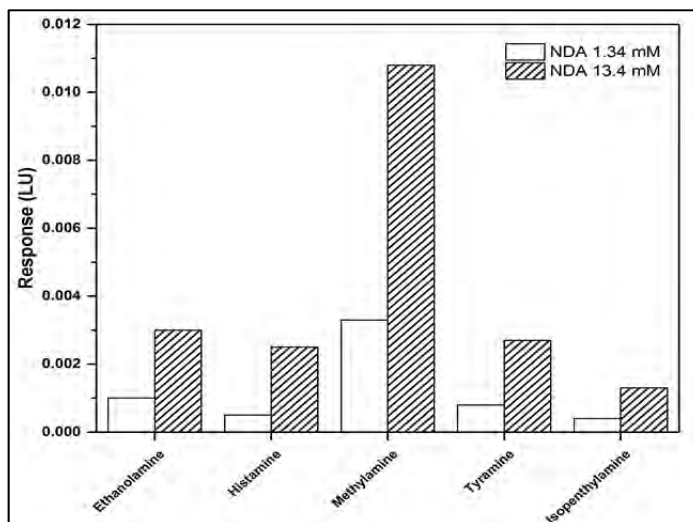


Figure 2. Response area for BAs in synthetic wine derivatized with two different concentration levels of NDA (1.34 and 13.4 mM). Analysis conditions are detailed in Experimental section.

Dabsyl derivatization

To optimize the derivatization of BAs, the effects of reaction time, temperature and DBS concentration on the derivatization performance were studied for 5.5 mg/L putrescine, as a model compound.

Effect of reaction temperature.

The DBS-putrescine peak area was monitored after heating for 21 min at temperatures ranging from 25 to 70 °C. It must be underlined that, at lower temperatures, dabsyl chloride remains undissolved. The highest reaction efficiency was obtained at 50 °C as shown in Table 1. Nevertheless, the response obtained at higher temperatures remains within the uncertainty of the experimental error. It should be remarked that at temperature of 50 °C, the efficiency of dabsylation decreases for concentrations of putrescine below 0.5 mg/L. For this reason, derivatization at 70 °C was chosen for further optimization steps.

Table 1. Effect of temperature on derivatization of putrescine with DBS.

<i>T [°C]</i>	<i>Response [peak area]</i>
25	290 ± 20
40	715 ± 50
50	830 ± 50
60	720 ± 50
70	760 ± 50

Effect of reaction time.

As shown in Table 2, the maximum efficiency for dabsylation reaction was achieved already after five minutes; longer derivatization times led to decreased efficiency (however within the limits of experimental error), which can be associated with degradation of the derivatization product.

Table 2. Effect of reaction time on derivatization of putrescine with DBS.

<i>time [min]</i>	<i>Response [peak area]</i>
5	970 ± 40
10	960 ± 40
21	900 ± 40

Effect of DBS concentration.

The effect of dabsyl chloride concentration on putrescine derivative peak area was studied for 400- and 3300-fold excess with respect to amine concentration, suggesting that higher excess of the reagent resulted in a 7.1-fold increase in dabsylation efficiency.

INDIRECT DETERMINATION OF BAs THROUGH ENZYMATIC RELEASE OF AMMONIA AND INDOPHENOL BLUE REACTION

During the TG enzymatic reaction with substrate N-carbobenzoxy-L-glutaminyglycine (CBZ-Gln-Gly) and biogenic amines, ammonia is released and detected by exploiting indophenol blue formation in the Berthelot reaction. Detection of structurally different biogenic amines (putrescine, cadaverine, histamine and tyramine) was investigated. Previously optimized Berthelot reaction [30] was used as colorimetric method for detection of biogenic amines based on indophenol blue formation.

Effect of buffers on TG reaction.

Optimum pH for TG is between 6 and 7, as specified by the producer. On the other side, recommended pH for indophenol formation is between 8-11.5 [33]. For this reason, a study on buffer influence on indophenol blue reaction in pH range 6-7 was necessary. Experiments were monitored at 650 nm by spectrophotometry, with phosphate- (pH 7), acetate- (pH 6) and Tris- (pH 7) buffers; results have shown that highest sensitivity of biogenic amine determination by TG and indophenol reaction is obtained in phosphate buffer at pH 7 (Figure 3). It should be remarked that TRIS buffer, usually suggested for TG enzymatic activity test protocols, was revealed incompatible with indophenol reaction.

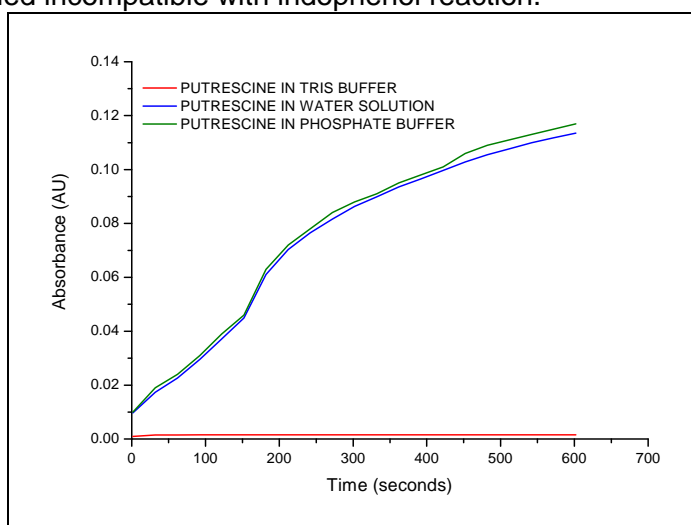


Figure 3. Effect of buffers on kinetics of indophenol formation using 2 mM putrescine as representative biogenic amine. Spectrophotometric detection was performed at 650 nm.

VALIDATION OF HPLC-NDA-FL AND HPLC-DBS-TLS METHODS AND COMPARISON WITH HPLC-NDA-FL AND HPLC-DBS-DAD

Validation of the novel methods was performed as suggested by European Union (EUR-FA Guide, Annex I) and IUPAC guidelines [34], evaluating the following performance parameters: linearity, limits of detection (LODs) and limits of quantification (LOQs) by analysing standard solutions of putrescine, cadaverine, histamine and tyramine in synthetic wine matrix. LODs and LOQs (see Table 3) were evaluated as $LOD = 3 \times SD_{xy}/b$ and $LOQ = 10 \times SD_{xy}/b$ (where SD_{xy} is the standard deviation of the response and b is the slope of the calibration curve) [35].

Table 3. Limits of Detections (LODs) and Limits of Quantitation (LOQs) for BAs obtained by HPLC-NDA-FL, HPLC-DBS-TLS and HPLC-DBS-DAD.

BAs	LOD ($\mu\text{g/L}$)			LOQ ($\mu\text{g/L}$)		
	NDA-FL	DBS-TLS	DBS-DAD	NDA-FL	DBS-TLS	DBS-DAD
PUT	73	3	15	219	11	50
CAD	55	4	23	165	14	77
HIS	27	11	85	81	40	282
TYR	66	10	86	198	34	288

The linearity of the methods was verified from LOQs to 1.2 mg/L, providing R^2 ranging from 0.985 to 0.997.

It is interesting to note that the detection limits obtained by the newly developed methods are about 10-fold (HPLC-NDA-FL) and 50-fold (HPLC-DBS-TLS) lower if compared with those obtained by CE with indirect UV detection [36] and almost equal (HPLC-NDA-FL) or lower (HPLC-DBS-TLS) to those obtained using direct analysis by CE coupled with mass spectrometric detection [37]. The LODs of the newly proposed methods were lower than those obtained by the official OIV method [38] based on OPA derivatization (i.e. LOD_{OPA} histamine= 60 $\mu\text{g/L}$; LOD_{OPA} tyramine= 77 $\mu\text{g/L}$).

VALIDATION OF ENZYMATIC METHOD

The performance of the enzymatic method coupled with TLS detection was initially verified by analyzing aqueous solutions with different concentrations levels of single biogenic amines. Results demonstrate acceptable recoveries (118-100 % for putrescine, 70 -133 % for cadaverine, 93-112 % for histamine, and 88-108 % for tyramine) and very low limits of detection. The linearity range is rather narrow (from LOQs to $2.5 \cdot 10^{-7}$ M) due to a TLS signal saturation effect observed for investigated solutions.

When compared to a previously reported method for BA determination by using TG [31], the LODs achieved in this work for standard solutions represent over 450-fold improvement. In addition to the TLS enhancement of sensitivity by 30 times for the 200 mW excitation power, such improvement in LOD is attributed also to 13.5-times higher extinction coefficient of indophenol at 650 nm compared to the extinction coefficient of NADH absorption maximum at 340 nm, which was related to concentration of BA in the method developed by Punakivi et al. [31]. However, matrix effects hinder the LODs in real samples, which were therefore found up to 3 times higher in the analyzed wines, as reported below (Table 4). Besides the significant improvement of the LODs, it should

be pointed out that for the previously reported TG method, two hours (reaction time) are required to achieve the indicated LODs, while the newly developed method here described requires just 10 min of reaction time, thus reducing the total time of analysis by 12 times.

Table 4. LODs and LOQs for batch mode determination of BAs in wine with TG and indophenol reaction on TLS detection unit.

BAs	LOD [$\mu\text{g/L}$]	LOQ [$\mu\text{g/L}$]
PUT	8	24
CAD	10	29
HIS	23	68
TYR	15	44

REAL SAMPLE ANALYSIS

Real samples (Slovenian white wines of Rebula variety) were analyzed to ascertain the presence of biogenic amines using HPLC-DBS-TLS since it resulted the best performing method developed according to what previously discussed. Samples were analyzed by applying the standard addition calibration, comparing the obtained concentrations with those obtained by the International method for analysis of biogenic amines in wine [29], i.e. OIV-MA-AS315-18, performed in our laboratory (Table 5). Typical chromatograms obtained for analysis of wine samples by HPLC-DBS-TLS are shown in Figure 4.

Table 5. Concentrations (mg/L) of BAs in wines determined by HPLC-DBS-TLS and HPLC-OPA-FL (official OIV method).

		PUT	CAD	HIS	TYR
Wine A	DBS-TLS	0.64 \pm 0.02	0.20 \pm 0.03	0.08 \pm 0.01	< LOD
	OPA-FL	0.59 \pm 0.13	0.20 \pm 0.11	< LOD	< LOD
Wine B	DBS-TLS	1.14 \pm 0.03	0.25 \pm 0.03	0.09 \pm 0.01	< LOD
	OPA-FL	1.10 \pm 0.23	0.15 \pm 0.08	< LOD	< LOD

For putrescine and cadaverine, the results obtained by the two HPLC approaches were in good accordance for both wine samples. Due to its higher sensitivity, the HPLC-DBS-TLS method enabled the determination of histamine as well, which could not be determined by the OIV method due to inadequate LODs.

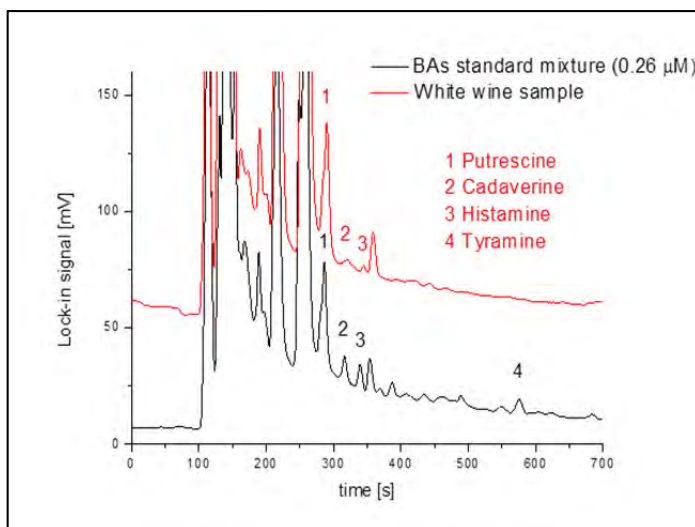


Figure 4. Typical chromatogram obtained for analysis of wine sample by HPLC-DBS-TLS

Rebula wines (one home made and one commercial) were additionally analyzed by the newly developed method based on indophenol reaction, through the standard addition procedure to confirm the applicability of the method. Synthetic wine was used as blank.

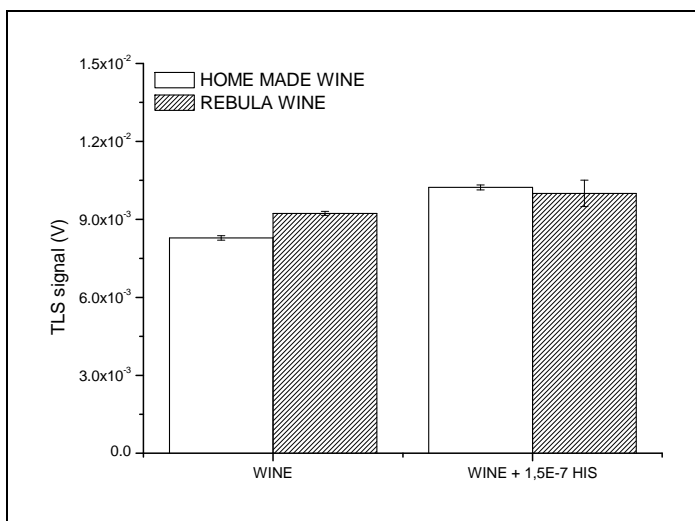


Figure 5. Signals of home made wine and Rebula wine with TLS detection unit.

Since the assay is not specific for identification of single biogenic amines, it allows the determination of the total biogenic amines present. As shown in Figure 5, the presence of BAs in samples can be confirmed. Higher signal in case of Rebula wine (commercial), is due to higher concentration of biogenic amines.

The quantity of biogenic amines present in wines was expressed as equivalents of histamine, the only BA for which the maximum contamination level in wine is regulated.

Based on the standard addition of histamine ($1.5 \cdot 10^{-7}$ M) and on the difference of TLS signals from spiked and original wine samples, a concentration of BAs corresponding to $(6.4 \pm 0.3) \cdot 10^{-7}$ M which corresponds to 0.069 ± 0.003 mg/L equivalents of histamine were estimated for home-made wine, and $(1.8 \pm 0.9) \cdot 10^{-6}$ M concentration which corresponds to 0.2 ± 0.1 mg/L equivalents of histamine for commercial Rebula wine. These results indicate that the concentrations of BAs are in good agreement with values found by HPLC-OPA-FL, and also comparable (on the lower range) to the previously reported values (recalculated as histamine equivalents) in Greek wines [33]. Due to the high sensitivity of TLS method, even concentrations below 0.1 mg/L can still be reliably detected.

CONCLUSIONS

In this work, naphthalene-2,3-dicarboxaldehyde (NDA) was tested for the first time for the analysis of BAs in wine samples by HPLC with fluorimetric detection. Optimal derivatizing and chromatographic conditions were successfully derived.

The method was validated in terms of linearity, limits of detection and quantification in a synthetic wine matrix. If compared to HPLC-OPA-FL method, the results showed that, despite slightly longer derivatization time (reaction time 25 min), the sensitivity of the NDA-FL method is greatly enhanced. It is worth to mention that the analysis time using NDA is about one fourth of the time needed with OPA.

The LODs were importantly decreased by HPLC-TLS using dabsyl chloride (DBS) as derivatizing non-fluorescing agent which provides up to 8.4-fold improvement compared to the HPLC-DAD applying the same chromatographic conditions. The newly developed method was tested on the analysis of BAs in white wine samples, finding good accordance with the results obtained by the standard OIV method for determination of BAs in wines. The newly developed HPLC-TLS method is therefore appropriate for determination of BAs in wine samples.

High sensitivity of TLS also enables fast detection of BAs by a novel vanguard screening method developed in this work, which is based on enzymatic transformation of BAs into ammonia and further to indophenol which can be sensitively detected by TLS. In real wine samples, BAs can be detected at concentration levels of 10^{-7} M with over 10 times improved sample throughput compared to previously reported enzymatic methods.

EXPERIMENTAL SECTION

Chemicals

Biogenic amine standards studied were: putrescine-2HCl (PUT), cadaverine (CAD), bought from Sigma Aldrich (Seelze, Germany), histamine (HIS), from Panreac Applichem (Darmstadt, Germany), and tyramine (TYR), from Alfa Aesar (Karlsruhe, Germany). Dabsyl-chloride was from Alfa Aesar. All other standards and reagents were bought from Sigma Aldrich and were of analytical grade.

High-purity water (18.2 M Ω -cm resistivity at 25 °C), produced by a Thermo Scientific Barnstead NANOpure Water Purification Systems (Barnstead, Germany) was used for standard solution and eluent preparation.

Microbial transglutaminase (TG) (E.C. 2.3.2.13, 1670 nkat/g) was purchased from Ajinomoto Co. INC., Japan (Europe Sales GMBH, Hamburg, Germany) and N-carbobenzoxy-L-glutaminyglycine (CBZ-Gln-Gly) was purchased from Sigma-Aldrich.

For the Berthelot reaction, sodium salicylate (99.5 %) purchased from Sigma-Aldrich, sodium hydroxide from Riedel-de-Haën (Seelze, Germany), solution of sodium hypochlorite (Pejo, Slovenia), potassium sodium tartrate tetrahydrate (99 %) and manganese sulfate monohydrate (98 %) from Fluka (Seelze, Germany) were used.

Preparation of solutions

Derivatizing solutions

3 mM o-phthalaldehyde (OPA) solution was prepared by dissolving 20 mg OPA in 50 mL methanol (the solution must be stored in dark conditions and should be prepared daily). 13.4 mM naphthalene-2,3-dicarboxaldehyde (NDA) solution was prepared by dissolving 12.3 g NDA in 5 mL acetonitrile. Both derivatization reactions should occur at controlled basic pH, therefore a 0.1 M borate buffer (pH 10.5) was used. In case of NDA, borate buffer contains 0.09M KCN. 1.3 mM NDA was prepared by 10-fold dilution of 13.4 mM solution in 0.1 M borate buffer.

The dabsyl chloride (DBS) solution was prepared by diluting 40 mg of dabsyl chloride in 10 mL of acetone, followed by 15 min ultrasonic treatment (Iskra PIO, Sonis GT, Slovenia), to obtain the final 12.4 mM concentration.

Solutions for enzymatic reaction

Standard solutions of BAs were prepared in water and stored in glass vials at 4° C. Donor substrate (2 mM) N-carbobenzoxy-L-glutaminyglycine (CBZ-Gln-Gly) was prepared in water. The TG enzyme was dissolved in cold water to obtain enzyme activity 16.7 nkat/mL (1 U/mL). Solutions for indophenol reaction. Two mixtures of reagents were used for indophenol blue reaction [39]. Mixture A: 10 mL of sodium salicylate (1.5 M), 10 mL of sodium potassium tartrate tetrahydrate (30 g/L) and 2 mL of manganese sulphate monohydrate (2.5×10^{-3} M). Mixture B: 10 mL of sodium hydroxide (0.5 M) and 10 mL of commercial bleach (source of hypochlorite). Each mixture was freshly prepared daily.

Synthetic wine (HPLC-NDA-FL)

This sample (1 L) was prepared by dissolving 3.5 g tartaric acid in 120 mL ethanol and acidifying with HCl to pH 3.5. Stock solutions of biogenic amines were prepared in synthetic wine for NDA derivatization; their concentrations were 50.6 mg/L (0.83 mM) ethanolamine, 487 mg/L (2.64 mM) histamine·2HCl, 114 mg/L (1.70 mM) methylamine·HCl, 158 mg/L (0.90 mM) tyramine·HCl, 150 mg/L (1.70 mM) isopentylamine, 118 mg/L (1.62 mM) butylamine.

BAs standards (HPLC-DBS-TLS)

Standards were prepared as 2.5 mM solutions by diluting the hydrochloride salts in 0.1 M HCl, containing 0.2 % (w/v) 3,3'-thiodipropionic acid (TDPA, Merck, Germany). An appropriate volume of the stock solution (or 1 mL of white wine) was afterwards transferred in a 10 mL-beaker and the pH was adjusted to 8.2 with Na₂CO₃ buffer.

Derivatizing reactions

OPA: the reaction was performed according to the indications reported within the Compendium of International Methods of Analysis [38]. Derivatization of BAs is performed according to a two-steps reaction. In detail, in a flask, 500 µL of OPA solution are mixed with 500 µL of borate

buffer and 150 μL of 2-mercaptoethanol. In another vial, 500 μL of the sample or synthetic wine solution containing biogenic amines at proper concentration are mixed with 500 μL of methanol; then 150 μL of this latter solution are spiked into solution in the first flask and, after a reaction time of 1 min, the solution is injected in the HPLC system.

NDA: 500 μL of the sample or synthetic wine solution containing biogenic amines are mixed with 200 μL of methanol, 50 μL of borate buffer containing potassium cyanide and 200 μL of NDA solution. The optimized reaction time was 20 min (see Results and Discussion section).

DBS-Cl: 500 μL of the BA (wine) buffer was transferred into an amber glass vial and 220 μL of the dabsyl chloride was added. The reaction mixture was heated in water bath at 70 $^{\circ}\text{C}$ for 5 min. Afterwards, 610 μL of the dilution solution, containing acetonitrile, eluent A and ethanol in the ratio 2:1:1 (v/v/v), was added to dissolve the remaining dabsyl chloride in the vial and heated at 70 $^{\circ}\text{C}$ for further ≈ 5 min.

HPLC mobile phases were prepared from the following solutions A: 0.05 M sodium acetate: tetrahydrofuran (96:4 v/v) and B: methanol, by gradient mixing as detailed in Table 6.

Table 6. Gradient conditions used for the separation of biogenic amines derivatized with NDA and OPA

NDA derivatization			OPA derivatization		
<i>Time [min]</i>	%A	%B	<i>Time [min]</i>	%A	%B
0	30	70	0	80	20
11	30	70	15	70	30
25	25	75	23	60	40
40	10	90	42	50	50
50	10	90	55	35	65
60	30	70	60	35	65
			70	80	20
			95	80	20

Experiments indicated that the presence of tetrahydrofuran (THF) in the mobile phase has two effects on the elution of BAs derivatized with NDA: it decreases the total time of the analysis and it increases the peak response (from 13 to 25% depending on BAs). The optimized total time of the elution for HPLC-NDA-FL is 25 min, about one fourth of the time needed to analyse BAs with OPA derivatization.

For dabsylation: The eluent was prepared as solvent A - solvent B composition of 35:65 % v/v. Solution A: $4.0 \cdot 10^{-2}$ M sodium acetate with 10 % (v/v) dimethylformamide and 0.23 % (v/v) triethylamine, adjusted to pH 5.0 with diluted acetic acid); solution B: acetonitrile, *t*-butylmethyl ether and water (87.5:10:2.5, v/v/v).

Enzymatic and Berthelot reaction

For determination of BAs, 1 mL of CBZ-Gln-Gly, 1 mL of enzyme solution and 1 mL of BA of interest were introduced into a 10 mL-flask. Afterwards, 1 mL of each mixture (A and B) was added to the enzymatic mixture and diluted with buffer and acetonitrile (total 25% v/v) to obtain the final volume of 10 mL. After 10 minutes, 2 mL of the solution was transferred into a quartz cuvette (batch mode measurement) and introduced in a TLS cuvette holder.

White wine samples were tested for the presence of studied BAs, all experiments were done with phosphate-diluted wine samples to reach basic pH.

Instrumentation

HPLC-FL system

An Agilent 1100 chromatograph (Agilent, Santa Clara, CA, USA) equipped with a Kinetex EVO (250 mm×4.6 mm I.D., 5 μ m particle size) with a 4 mm×3 mm I.D. guard column (Phenomenex), a 10 μ L-injection loop and a fluorescence detector was used. Eluent flow rate was set at 1.0 mL/min, while fluorescence detector was set at 356 nm (absorbance wavelength) and 445 nm (emission wavelength). Chromatographic data were handled by OriginPro 8.5 software, without any data correction or smoothing.

HPLC-TLS system

The dual-beam thermal lens spectrometer used in this work is schematically presented in Figure 6. It consists of a Krypton laser (Innova 300C, Coherent, USA) operating at 413 nm (35 mW–150 mW), which provides the pump beam, and a He-Ne probe laser (Model 1103P, Uniphase, USA) of 2 mW output power (632.8 nm). The pump beam was modulated with a mechanical chopper (300CD, Scitec Instruments, UK) at 28 Hz and focused onto the sample cell with a 100 mm focal length lens (L1). The probe beam was focused using two lenses with focal lengths of 100 mm (L2) and 60 mm (L3). To obtain a collinear propagation of pump

and probe beams, a dichroic mirror (T:633 nm, R: 410 nm) was used. Thermal lens signal was detected using an amplified photodiode detector (Thorlabs, USA) equipped with a 633 nm interference filter (Melles Griot, USA) and connected to a lock-in amplifier (SR830 DSP, Stanford Research, USA, 1 s time constant), which was further connected to a PC for data treatment and storage. The chromatographic system consisted of a HPLC pump (Smartline pump 1000, Knauer, Germany), a metal free manual injection valve (Knauer, Germany) for liquid chromatography equipped with 10 μ L injection loop. The column was the same as for HPLC-FL system. Detection was performed in an 8 μ L flow-through cell (Hellma, UK) with 10 mm optical path length.

TLS detection unit for indophenol blue measurements

The TLS detection unit was identical to the one described for HPLC-TLS system, with the only difference that the Kr-laser was operating at 647 nm (200mW) and the probe beam source was a He-Ne laser operating at 543.5 nm (5mW, MellesGriot, Carlsbad, California, USA). The dichroic mirror and the interference filter were replaced accordingly to enable transmission at 543.5 nm and reflection of the pump beam. The flow-through cell is replaced with a 10 mm quartz cuvette.

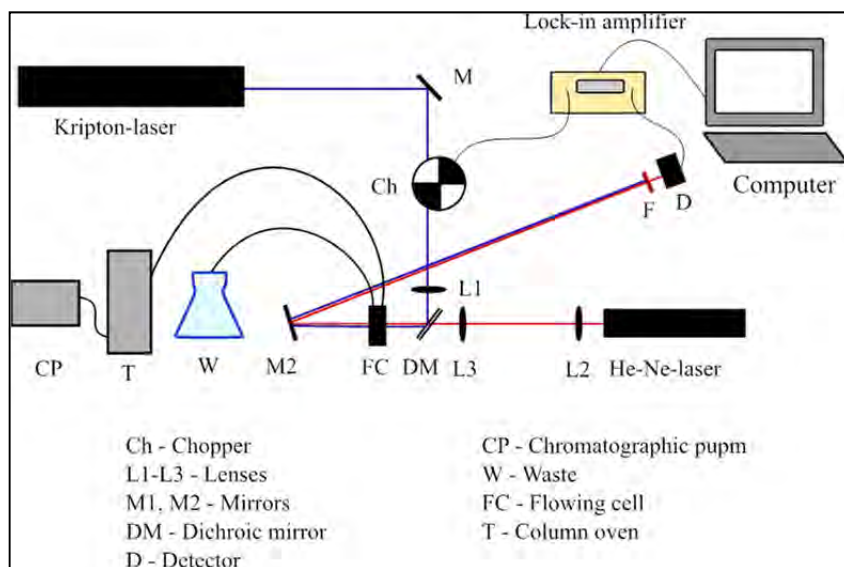


Figure 6. Schematic presentation of a HPLC-TLS system

Wine samples

Wine samples of Rebula variety were from producers in the Obalno-Kraška wine growing region in Slovenia. All wines were produced using the classic procedures of crushing, pressing, fermentation, filtration and bottling.

Samples were stored in 0.75 stoppered dark glass bottles, and kept at 4 deg. C until analysis. For the analysis, 2 mL of the sample was filtered through a 0.45 nylon syringe filter to remove suspended solids. 500 µL aliquot of the filtrate was then derivatized with OPA and DBS as described above, and injected for HPLC analysis.

ACKNOWLEDGEMENTS

Part of this work was performed under the bilateral scholarship Slovenia-Italy funded by the Centre of the Republic of Slovenia for Mobility and European Educational and Training Programmes (CMEPIUS). Financial support from Ministero dell'Istruzione, Università e Ricerca (MIUR, Italy) is gratefully acknowledged. On Slovenian side, this research was supported by the ARRS research program grant P1-0034 and young researcher grants to M.Ž. and S.B.

REFERENCES

1. M. H. S. Santos, *International Journal of Food Microbiology* **1996**, *29*, 213.
2. J. E. Stratton, R. W. Hutkins, S. L. Taylor, *Journal of Food Protection* **1991**, *54*, 460.
3. Y. Y. Guo, Y. P. Yang, Q. Peng, Y. Han, *International Journal of Food Science & Technology* **2015**, *50*, 1523.
4. A. Ōnal, *Food Chemistry* **2007**, *103*, 1475.
5. R. Tofalo, G. Perpetuini, M. Schirone, G. Suzzi, *Encyclopedia of Food and Health* **2016**, *1*, 424.
6. V. Ladero, M. Calles-Enruez, M. Fernandez, M. A Alvarez, *Current Nutrition & Food Science* **2010**, *6*, 145.
7. T. Komprda, R. Burdychov, V. Dohnal, O. Cwиков, P. Sldkov, H. Dvockov, *Food Microbiology* **2008**, *25*, 219.
8. A. Naila, S. Flint, G. Fletcher, P. Bremer, G. Meerdink, *Journal of Food Science* **2010**, *75*, R139.
9. E. Directive, *Official Journal of European Union* **2007**.
10. M. Garca-Marino, . Trigueros, T. Escribano-Bailn, *Journal of Food Composition and Analysis* **2010**, *23*, 455.

11. O. Martínez-Pinilla, Z. Guadalupe, Z. Hernández, B. Ayestarán, *European Food Research and Technology* **2013**, 237, 887.
12. A. Romano, H. Klebanowski, S. La Guerche, L. Beneduce, G. Spano, M.-L. Murat, P. Lucas, *Food Chemistry* **2012**, 135, 1392.
13. S. Cunha, M. Faria, J. Fernandes, *Journal of Agricultural and Food Chemistry* **2011**, 59, 8742.
14. D. Daniel, V. B. dos Santos, D. T. R. Vidal, C. L. do Lago, *Journal of Chromatography A* **2015**, 1416, 121.
15. P. Ginterová, J. Marák, A. Staňová, V. Maier, J. Ševčík, D. Kaniansky, *Journal of Chromatography B* **2012**, 904, 135.
16. R. Conca, M. C. Bruzzoniti, E. Mentasti, C. Sarzanini, P. Hajos, *Analytical Chimica Acta* **2001**, 439, 107.
17. J.-H. Kim, I. S. Shin, Y. K. Lee, H. J. Oh, S. J. Ban, *Osong Public Health and Research Perspectives* **2011**, 2, 127.
18. N. H. Kim, Y. Park, E. S. Jeong, C.-S. Kim, M. K. Jeoung, K. S. Kim, S.-H. Hong, J.-K. Son, J. T. Hong, I.-y. Park, *Archives of Pharmacal Research* **2007**, 30, 1350.
19. J. Hernández-Borges, G. D'Orazio, Z. Aturki, S. Fanali, *Journal of Chromatography A* **2007**, 1147, 192.
20. A. Bockhardt, I. Krause, H. Klostermeyer, *Zeitschrift für Lebensmitteluntersuchung und-Forschung A* **1996**, 203, 65.
21. P. Hernández-Orte, A. Peña-Gallego, M. J. Ibarz, J. Cacho, V. Ferreira, *Journal of Chromatography A* **2006**, 1129, 160.
22. R. E. Anlı, M. Bayram, *Food Reviews International* **2008**, 25, 86.
23. Q. Weng, W. Jin, *Electrophoresis* **2001**, 22, 2797.
24. P. De Montigny, J. F. Stobaugh, R. S. Givens, R. G. Carlson, K. Srinivasachar, L. A. Sternson, T. Higuchi, *Analytical Chemistry* **1987**, 59, 1096.
25. M. Franko, *Applied Spectroscopy Reviews* **2008**, 43, 358.
26. M. Franko, C. D. Tran, "Thermal Lens Spectroscopy". In *Encyclopedia of Analytical Chemistry*, John Wiley & Sons, Ltd: **2010**.
27. T. Kitamori, M. Tokeshi, A. Hibara, K. Sato, *Analytical Chemistry* **2004**, 76, 52 A.
28. M. Franko, M. Liu, A. Boškin, A. Delneri, M. A. Proskurnin, *Analytical Sciences* **2016**, 32, 23.
29. M. Liu, S. Malovrh, M. Franko, *Analytical Methods* **2016**, 8, 5053.
30. S. Budal, M. Martelanc, T. Radovanović, M. Franko, *International Journal of Environment and Health* **2014**, 7, 101.
31. K. Punakivi, M. Smolander, M.-L. Niku-Paavola, J. Mattinen, J. Buchert, *Talanta* **2006**, 68, 1040.
32. A. Zotou, M. Notou, *Analytical and Bioanalytical Chemistry* **2012**, 403, 1039.
33. C. Proestos, P. Loukatos, M. Komaitis, *Food Chemistry* **2008**, 106, 1218.
34. G. Simone, P. Robouch, "EURL-FA Guide: Protocol for verification studies of single laboratory/in-house validated methods. Working document v3. 00" European Commission, Directorate-General Joint Research Centre. [https://ec.europa.eu/jrc/sites/default/files/EURLFA-technical% 20guide% 20for% 20validation% 20and% 20verification% 20v: 2014](https://ec.europa.eu/jrc/sites/default/files/EURLFA-technical%20guide%20for%20validation%20and%20verification%20v:2014).

35. A. Shrivastava, V. B. Gupta, *Chronicles of Young Scientists* **2011**, 2, 21.
36. L. Arce, A. Ríos, M. Valcárcel, *Journal of Chromatography A* **1998**, 803, 249.
37. B. Santos, B. M. Simonet, A. Ríos, M. Valcárcel, *Electrophoresis* **2004**, 25, 3427.
38. OIV, *Compendium of International Methods of Wine and Must Analysis*, OIV Paris: **2013**.
39. T. Tsuboi, Y. Hirano, Y. Shibata, S. Motomizu, *Analytical Sciences* **2002**, 18, 1141.

In memory of prof. dr. Simion Gocan

BLAJ WHITE WINES CHARACTERIZATION

**RAMONA BLEIZIFFER^a, SONIA SUVAR^a, PAULA PODEA^{b *},
CORNELIA MESAROS^c, MONICA CULEA^a**

ABSTRACT Six white wines from Blaj vineyard obtained from clone and new created varieties of grapes, have been studied. Their volatile compounds, free amino acids, free fatty acids, content in polyphenols and flavonoid, antioxidant and antityrosinasic activity were compared. The results showed few differences among the analyzed wines. The volatile extracts of wines gave very similar compounds. The major compounds were phenylethyl alcohol. All the white wines of Blaj contained a large amounts of proline in comparison with the other amino acids and important essential amino acids. The fatty acids were found in very small quantities. Antioxidant activity and total content in polyphenols of wines showed that Muscat Ottonel have a very high antioxidant potential comparable with some red wines. The content in flavonoids is small in all white wines. Antityrosinasic activity of studied wine proved to be high to Blasius and Muscat Ottonel wine. The GC-MS method proved to be an excelent method for wine characterization.

Keywords: *essential amino acids, amino acids, fatty acids, antioxidant activity, GC/MS*

INTRODUCTION

Wine is an important beverage and it is consumed by human for thousands of years. Obtained from grapes, wine has a multitude of beneficial effect due to the chemical composition very related with fruits and herbs.

^a Babes-Bolyai University, Faculty of Physics, 1 Kogalniceanu st., Cluj-Napoca, Romania

^b Babes-Bolyai University, Faculty of Chemistry and Chemical Engineering, 11 Arany Janos st., Cluj-Napoca, Romania,

* Corresponding author: mpaula@chem.ubbcluj.ro

^c University of Medicine and Pharmacy, 38 Gh. Marinescu st., Târgu Mureş, Romania

Romania has a tradition in wine production, being on 12th place top of world wine production [1] and the sixth wine producer in the European Union. It is very important for appreciation the origin of wines, the consumers are using this attribute to evaluate the wine quality [2]. In Romania, there are some different recognized vineyards which offer high quality products. One of them is Tarnave-Jidvei Vineyard, which has four wineries: Jidvei, Blaj, Balcaciu and Tauni [3].

There are different elements which are influencing the composition, taste, aroma and properties of wines. Amino acids are importance to wine flavour and aroma because they constitute a source for yeast metabolism [4]. Most important are varieties of grapes, geographical origin, weather condition and human factor [5].

In literature, studies based on components characterization (phenolic compounds, amino acids, aroma compounds) are used for classification and comparison of wines [6-8].

The micronutrients in food are very important. Amino acids play an important role in human nutrition. In many foods, the level of essential amino acids dictates its nutritive value. Volatiles, amino acids, fatty acids influence wine taste. Antioxidant activity reflects the healthy value of wine.

Amino acids in wine have a considerable influence on wine quality and taste, being a source of nutrients for yeast fermentation [9].

Amino-acids profile in wine can be used to classify and differentiate wine on variety and geographical origin [5]. Volatiles profile in wines is connected with aroma, taste and varieties of wines [10]. The volatile composition depends also on the geographical origin, climate and viticulture proceeding, being an important indicator for wine characterization [11]. Fatty acids are minor components found in wines, but fatty acids composition can influence the wine aroma and taste [7]. Phenolic compounds are important constituents, natural antioxidants, found in wine, with a major influence in sensory assets, colour and taste [12]. Wine is a natural source of antioxidants and proves to have important healthy benefit in a balanced diet [13,14].

The aim of our study was to compare and characterize six white wines produced in 2014, from grapes cultivated in Blaj Vineyard, Tarnave area, Transylvania. The wines are obtained from clone and new created varieties of grapes obtained at Research Station of Viticulture and Enology Blaj [15].

RESULTS AND DISCUSSION

Six white wines from Blaj vineyard (Fetească regală, Blasius, Neuburger, Traminer roz, Muscat Ottonel, Selena) have been studied. Their physical-chemical characteristics, volatile compounds, free amino acids, free

fatty acids and content in polyphenols and flavonoid, antioxidant and antityrosinasic activity were compared.

Amino acids and fatty acids profiles were analyzed. The chemical composition of volatiles was determined and compared. Also, the content in polyphenols and flavonoid, antioxidant and antityrosinasic activity were compared.

Fatty acids were derivatized as fatty acid methyl esters (FAME) and in the case of amino acids as trifluoroacetic butyl esters derivatives to improve volatility and for better separation. The content in amino acids is influenced mainly by varieties of grapes, geographical origin and fermentation condition.

The dominant amino acids identified in the wines were proline (15.7mg/ml in Blasius), glutamic acid, aspartic acid, *gamma*-aminobutyric acid, alanine, glycine and lysine. Proline is the major amino acid in wine samples released in the fermentations and it is an intermediate product in the degradation of arginine [4]. The high concentrations of proline in wine is owed to the fact that yeast microorganisms do not consume this amino acid. Arginine was not found in wine because it is consumed during fermentation by yeast [16].

The total free amino acids were in the range 10.2mg/ml (Feteasca Regala Blaj) and 19.2mg/ml (Traminer Roz Blaj). Essential amino acids (EAA) had value ranged from 0.45mg/ml (Neuburger) to 1.44mg/ml (Traminer Roz).

The fatty acids present in wines were lower than 20µg/ml, stearic acid, palmitic acid and linoleic acid being dominant.

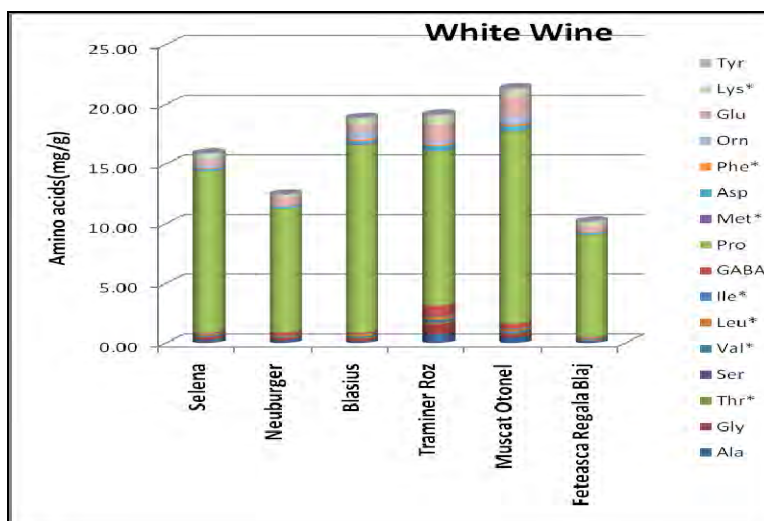


Figure 1. Free amino acids in Romanian wines

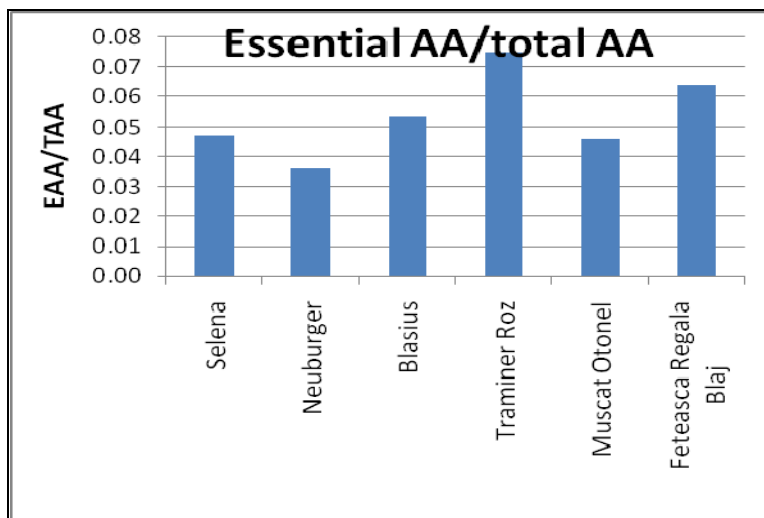


Figure 2. Ratio of essential amino acids and total amino acid

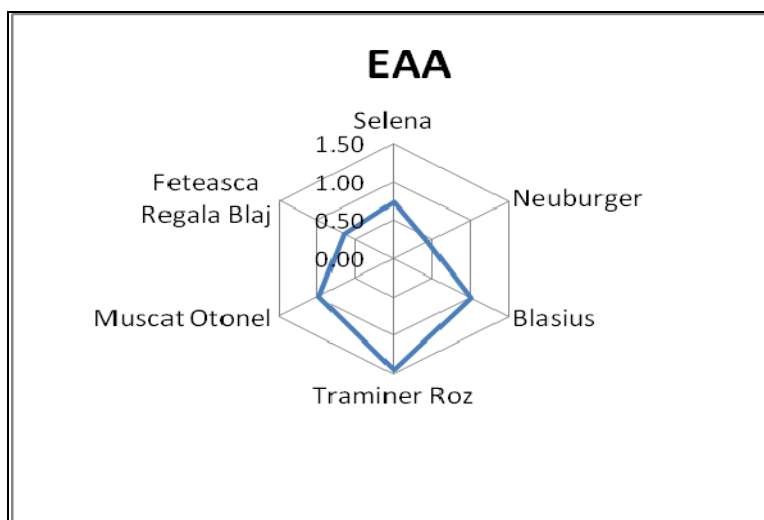


Figure 3. Comparison of essential amino acids (mg.g⁻¹)

The volatile extracts of wines gave very similar compounds. The major compounds were phenylethyl alcohol (21.5%-Muscat Otonel to 45.76%-Neuburger), succinic acid monoethyl ester (17.29%-Neuburger to 37.4%-Blasius) and 4-hydroxy-phenylethanol (6.7% in Muscat Otonel to 15.37% in Feteasca Regala). The high abundance of 2-phenylethanol was also detected in other wines. [11]

BLAJ WHITE WINES CHARACTERIZATION

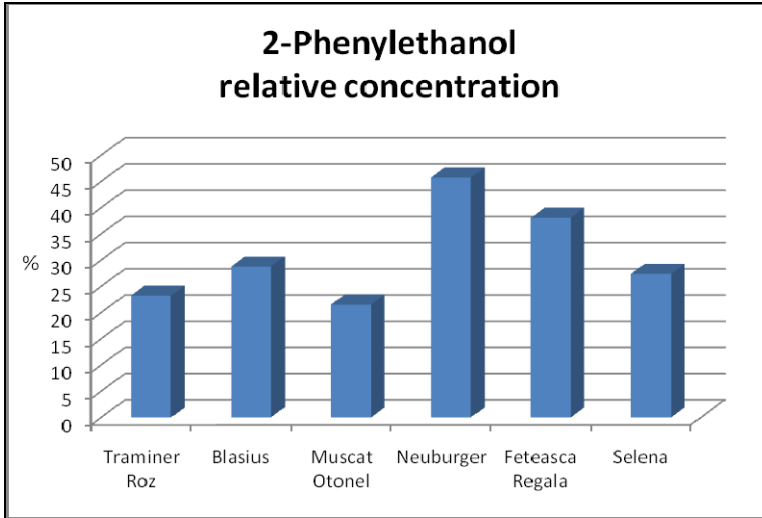


Figure 4. Relative concentration of phenethylalcohol in different wines from Blaj area

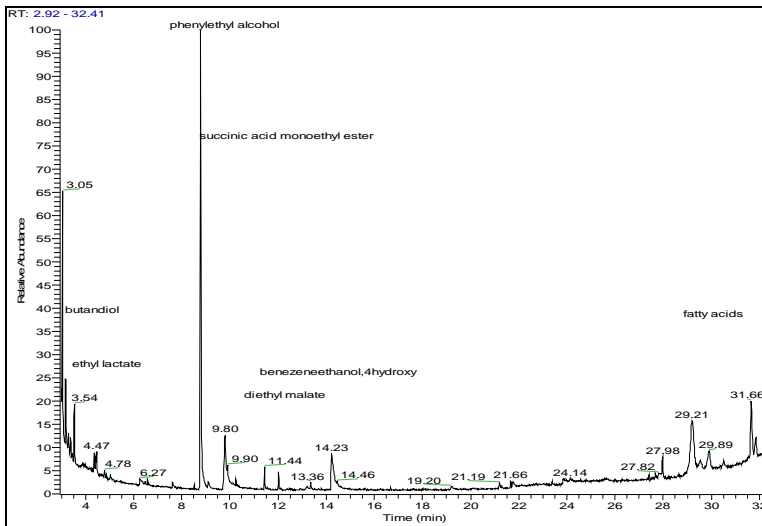


Figure 5. The GC chromatogram of volatiles identified in Neuburger wine

The antioxidant attributes of the selected wines were evaluated using DPPH (1,1-diphenyl-2-picrylhydrazyl), free radical scavenging antioxidant assays and TEAC (Trolox equivalent antioxidant capacity). Also the total polyphenolic content(TEPC) and content of flavonoids were determined.

White wines Muscat Ottonel and Feteasca Regala show a high antioxidant activity. A moderate antioxidant activity was observed in white wine Neuburger, Jidvei, Selena, Blasius. The antioxidant activity of wines was confirmed also by using TEAC assay. The content of polyphenols was indicated a higher quantity of polyphenols in Muscat Ottonel wine (1310 mg GAE/L), followed by Feteasca Regala wine (810 mg GAE/L), values comparable with the total polyphenols content in some red wines [17,18], but lower than other red wines [19]. A lower quantity of polyphenols was found in Blasius wine, but comparable with some others Romanian white wines [20]. It is known that flavonoids are found in skin of grapes, are very healthier, but are causing a bitterness effect on wines [21]. That's why producers of white wines are not using the skin of grapes not to alter the wine taste. The flavonoid content in white wines is not as high as in red wines also due to originally low quantity of flavonoids found in white grapes. All white wines studied have a low quantity on flavonoids, the highest quantity was found in Selena wine 8.96 mgQuE/L.

Table 1 Antioxidant capacity parameters obtained using several methods and total polyphenols content and total flavonoids content in studied wines. (Each value is the mean \pm SD of two independent measurements).

Wine	DPPH decolorization (%) (10 μ g/ml)	TEAC (mmolsTE/ml wine)	TPC (mg GAE/ml wine)	Flavonoids (μ gQuE/ml wine)
Blasius	19.3 \pm 0.62	4.97 \pm 0.01	0.22 \pm 0.02	7.21 \pm 0.14
Selena	22.5 \pm 0.45	6.04 \pm 0.13	0.29 \pm 0.01	8.96 \pm 0.17
Fetească regală	35.9 \pm 0.81	8.84 \pm 0.53	0.81 \pm 0.03	2.46 \pm 0.16
Muscat Ottonel	43.9 \pm 0.34	9.72 \pm 0.17	1.31 \pm 0.09	3.75 \pm 0.03
Neuburger	30.4 \pm 0.58	7.66 \pm 0.10	0.64 \pm 0.03	0.78 \pm 0.07
Traminer roz	24.5 \pm 0.72	7.15 \pm 0.22	0.31 \pm 0.01	1.00 \pm 0.06

Tyrosinase is an important enzyme involved in melanin biosynthesis [22]. Extracts and compounds which show anti-tyrosinasic inhibitory activity are useful whitening agents in cosmetics or additives in food industry to prevent fruits enzymatic browning phenomenon [23].

Anti-tyrosinase inhibitory activity of studied wines was evaluated. All wine prove to have a slightly inhibitory activity on tyrosinase enzyme, but Blasius and Muscat Ottonel wine proved to have a good inhibitory activity, lowering the reaction rate with 75%.

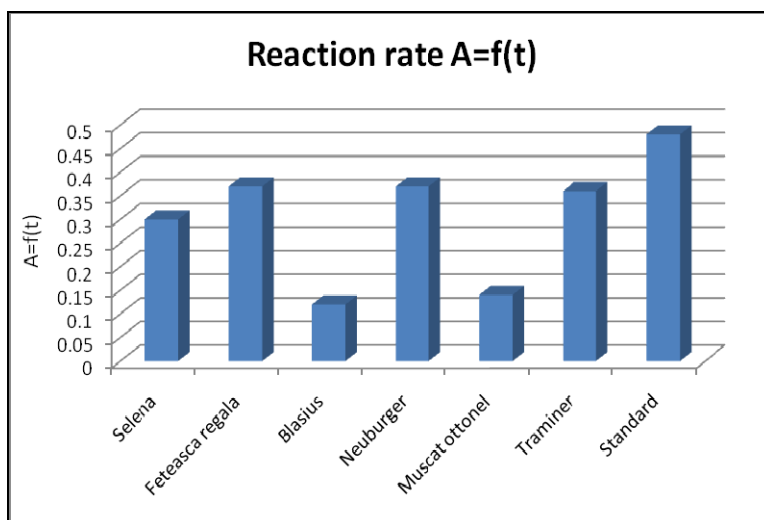


Figure 6. Comparison of reaction rates for tyrosinase enzyme inhibitory activity

CONCLUSIONS

The GC-MS method proved to be an excellent method for wine characterization. The volatile extracts of wines gave very similar compounds. The major compounds were phenylethyl alcohol. Amino acids are important to wine flavour and aroma because they constitute a source for yeast metabolism. All the white wines of Blaj contained large amounts of proline in comparison with the other amino acids and important essential amino acids. The fatty acids were found in very small quantities. Antioxidant activity and total content in polyphenols of wines showed that Muscat Ottonel have a very high antioxidant potential comparable with some red wines while the content in flavonoids is small in all white wines. Antityrosinase activity of studied wine proved to be high for Blasius and Muscat Ottonel wine.

EXPERIMENTAL SECTION

Material and methods

White wines produced in year 2014 (Fetească regală, Blasius, Neuburger, Traminer, Muscat Ottonel, Selenia) were procured from a vineyard from Blaj, Transylvania. All reactive and standards were purchased from Merck (Darmstadt, Germany).

GC–MS apparatus A Trace DSQ Thermo Finnigan quadrupole mass spectrometer coupled with a Trace GC was used. The Rtx-5MS capillary column, 30m x 0.25mm, 0.25µm film thickness was used in a temperature program from 50°C, 2 min, then 8°C /min to 250°C, with 30°C /min at 310°C (10 min) for fatty acids and volatile compounds separation. The amino acids were separated by using another program: from 50°C, 1 min, then increased with 6°C /min to 100°C, with 4°C /min to 200°C and 20°C /min to 300 ° for 3 min. The different extraction methods for volatile compounds, fatty acids and amino acids were described.

Extraction procedure for amino acids 100 ml of wine and 50 µg [¹⁵N]-glycine (internal standard) was passed through a Dowex 50W-W8 exchange resin, 4 x 40 mm column (activated). The collected solution was dried in a nitrogen flow at 60°C or by using a vacuum centrifuge at 60°C. The derivatization method included an esterification of the carboxylic function using 100 µl butanol: acetyl chloride (4:1 v/v), for 1 h at 110°C, followed by an acetylation of the amine function using 100 µl trifluoroacetic anhydride, for 20 min at 80°C.

Extraction procedure for fatty acids 100ml of wine was sonicated with 0.6 ml water/NaCl and 0.8 ml methanol for 1 min, then mixed with 0.8 ml chloroform and 3 min centrifuged (5800 rot/min); the lower layer was collected and extraction was repeated with 0.4 ml chloroform. The lower chloroform phase containing the extracted fatty acids was then dried in a nitrogen flow, at 60°C.

The lipids were converted to corresponding fames (fatty acids methyl esters) by esterification of the carboxylic functions with 100 µL methanol: acetyl chloride 4:1 (v:v), 20 min, 80°C. the derivatives were evaporated to dryness by a nitrogen stream, at 60°C, and then dissolved in 500 µl dichloromethane. 10 µg of C11:1 was added to each sample for GC-MS quantitation.

Extraction procedure for volatiles 5ml wine was mixed 1ml with a solvent (mixture of ethyl acetate: hexane: dichloromethane, 5/1/1) for 2 min and centrifuged (5800 rpm) 3 min. The supernatant was collected and 1µl was injected into the GC/MS.

Determination of antioxidant activity

DPPH antioxidant method For the determination of antioxidant activity, DPPH antioxidant assay was used. 10µL of each wine was used to decolorize an ethanolic solution of 40µM DPPH. The monitoring of DPPH

reduction was followed at 517nm. The percentage of DPPH scavenging activity is expressed using following formula: $\text{DPPH}_{\text{inhibition}}\% = [(A_i - A_t)/A_i] \times 100$.

Trolox equivalent antioxidant capacity assay (TEAC) For TEAC measurements a stock solution of ABTS (10mM) in sodium acetate buffer (5mM, pH=5) was activated with hydrogen peroxide (7 μ L, 30%), and 5 μ L met hemoglobine for 1h. After activation, the obtained ABTS+• solution was centrifuged to separate the protein. In 748 μ L water, 2 μ L each wine sample was added and 50 μ L solution of ABTS+•. The absorbance was measured at 735nm. Samples were done in duplicates and converted in Trolox equivalents by using of a calibration curve ($R^2 = 0.9987$) constructed with 0, 2, 4, 6, 8, 10 mg·L⁻¹ Trolox standards.

Determination of polyphenols and flavonoid content

Determination of polyphenolic content The total phenolic content (TPC) of wines was determined using the Folin-Ciocalteu method. Wines (5 μ L) was mixed with Folin-Ciocalteu reagent (50 μ L), distilled water (795 μ L) and 150 μ L solution of sodium carbonate (c= 20%). The samples were incubated in the dark for 30 min. The absorbance was measured at 760 nm. Experiments were done in duplicates. Gallic acid was used as standard for the calibration curve and was plotted at 2, 4, 6, 8, and 10 mg·L⁻¹, prepared in ethanol. TPC values were determined using an equation obtained from the calibration curve of gallic acid graph ($R^2 = 0.9990$). Results were expressed in mg of gallic acid/mL of wine.

Determination of flavonoid content For determination of flavonoid content a spectrophotometric aluminum chloride method was used⁴. Wine sample (200 μ L) was mixed with sodium acetate (200 μ L, 100 g·L⁻¹), aluminium chloride (120 μ L, 25 g·L⁻¹, and 480 μ L methanol. The absorbance was measured at 435 nm. Total flavonoids content values were determined using an equation obtained from calibration curve of the quercitine graph ($R^2 = 0.991$) obtained with 1, 2, 4, 6, 8, and 10 μ g·mL⁻¹ quercitine in methanol. Results were expressed in μ g of quercitine/mL of wine.

Determination of tyrosinase inhibition activity For determination of antyrosinasic activity of wines, a spectrophotometric method was used. To 897 μ L sodium phosphate buffer solution (20mM, pH= 6.8), 4 μ L tyrosine water solution (4mM) and 3 μ L phosphate buffer solution of tyrosinase (≥ 0.2 unit/mg solid in 1 μ L) 20 μ L wine sample was added. The enzymatic reaction was followed at 475nm for 15 minutes. The reaction rates were calculated from regression curve slope.

REFERENCES

1. R.D. Boc, A. Dobrei, *Journal of Horticulture, Forestry and Biotechnology*, **2015**, 19(2), 190.
2. T. Atkin, R. Johnson, *International Journal of Wine Business Research*, **2010**, 22(1), 42.
3. <http://www.crameromania.ro/en/en/wineries/jidvei-winery-mysterium-188.html>
4. S.H. Eom, W.J. Cheng, J.P. Hyoung, E.H. Kim, M.I. Chung, M.J. Kim, C.Y. Yu, D.H. Cho, *Korean Journal of Medicinal Crop Science*, **2007**, 15, 319.
5. Y. Bouzas-Cid, E. Falqué, I. Orriols, E. Trigo-Córdoba, E. Díaz-Losada, D. Fornos-Rivas, J.M. Mirás-Avalos, *Ciência e Técnica Vitivinícola*, **2015**, 30(2), 84
6. E. Soto Vazquez, S. Rio Segade, S. Cortes Dieguez, *International Journal of Food Science and Technology*, **2011**, 46(3), 542.
7. E. Bouloumpasi, E. H. Soufleros, C. Tsarchopoulos, C. G. Biliaderis, *Vitis*, **2002**, 41(4), 195.
8. L. Jaitz, K. Siegl, R. Eder et al., *Food Chemistry*, **2010**, 122(1), 366.
9. P. Hernandez-Orte, M. J. Ibarz, J. Cacho, V. Ferreira, *Chromatographia* **2003**, 58, 29.
10. Purificación Hernández-Orte, Juan F. Cacho, and Vicente Ferreira, *Journal of Agricultural Food Chemistry*, **2002**, 50 (10), 2891.
11. V. Avram, C. G. Floare, A. Hosu, C. Cimpoi, C. Măruțoiuc, Z. Moldovan, *Analytical Letters*, **2015**, 48 1099.
12. S. Y. Shu, J.G. Wen, Z. Yu Ping, *Food Chemistry*, **2011**, 127, 547.
13. K. W. Lee, H. J. Hur, H. J. Lee, C. Y. Lee, *Journal of Agricultural and Food Chemistry*, **2005**, 53, 1990.
14. K. M. Yoo, M. Al-Farsi, H. Lee, H. Yoon, C. Y. Lee, *Food Chemistry*, **2010**, 123, 734.
15. <http://www.scvblaj.ro/scdvv-blaj-en/>
16. B. Zoecklin, K. Fugelsang, B. Gump, F. Nury, „Wine Analysis and Production” Chapman & Hall New York, **1995**.
17. M. Seruga, I. Novak, L. Jakobek, *Food Chemistry*, **2011**, 124, 1208.
18. A. Hosu, V. M. Cristea, C. Cimpoi, *Food Chemistry*, **2014**, 150, 113.
19. I. Garaguso, M. Nardini, *Food Chemistry*, **2015**, 179, 336.
20. A. Hosu, V. Floare-Avram, D. A. Magdas, I. Feher, M. Inceu, C. Cimpoi, *Journal of Analytical Methods in Chemistry*, 2016, 4, 1-10.
21. D. Komes, D. Ulrich, K. Kovacevic Ganic, T. Lovric, *Vitis*, **2007**, 46(2), 77.
22. S.Y Seo, V. K. Sharma, N. Sharma, *Journal of Agricultural Food Chemistry* **2003**, 51, 2837.
23. M. R. Loizzo, R. Tundis, F. Menichini, *Comprehensive Reviews in Food Science and Food Safety*, **2012**, 11, 378.

In memory of prof. dr. Simion Gocan

SIMULTANEOUS DETERMINATION OF Zn, Cd, Pb AND Cu IN MUSHROOMS BY DIFFERENTIAL PULSE ANODIC STRIPPING VOLTAMMETRY

ENIKÓ COVACI^{a,*}, EUGEN DARVASI^a, MICHAELA PONTA^a

ABSTRACT. The present work presents the optimization of differential pulse anodic stripping voltammetry with hanging mercury drop electrode for the determination of Zn, Cu, Cd and Pb in mushrooms. The optimized method was characterized in terms of limits of detection and quantification, accuracy and precision and applied for the analysis of 4 food supplements (Chaga and Shiitake powders; Reishi tablets and capsules containing a Mixture of mushroom extracts) and a fresh mushroom (King bolete (*Boletus Edulis*)). The concentrations of Zn and Cu as essential elements were discussed in relation with the recommended daily allowance, while Cd and Pb compared with maximum acceptable levels of toxic elements set in the European legislation. It has been found that fresh mushroom King bolete (100 g serving per day) represents a more significant source of Cu and Zn than food supplements, namely up to 24% and 10% from the recommended daily allowance. The concentration of Cd (0.09-0.69 $\mu\text{g g}^{-1}$) and Pb (1.83-3.60 $\mu\text{g g}^{-1}$) in the edible King bolete fungus and food supplements revealed no human health risk, since they were below 1.5 mg provisional tolerable monthly intake (Cd) and 72 mg/day (Pb) for 60 kg body weight.

Keywords: *Differential pulse anodic stripping voltammetry, Zn, Cd, Pb, Cu, mushroom*

INTRODUCTION

Mushrooms and mushroom supplements are being consumed worldwide in a continuously increasing rate due to their countless therapeutic

^a Babeş-Bolyai University, Faculty of Chemistry and Chemical Engineering, 11 Arany Janos str., RO-400028, Cluj-Napoca, Romania.

* Corresponding author: kkeenniikkoo@yahoo.com

effects, such as anticancer, antioxidant, immunostimulator and antihypercholesterolemic effects [1-8], although it has to be mentioned that so far no scientific evidence exists that proves these claims [9]. The most used medicinal mushrooms, like Reishi, Shiitake, Turkey tail, Chaga and Lion's mane, originate from China and Japan, where they have been used for centuries to treat many diseases [9]. Mushrooms, medicinal or edible, are known to be able to accumulate essential elements (e.g. Zn, Cu) and toxic heavy metals (e.g. Cd, Pb) [10], depending on species and environmental factors (soil composition, pollution) [11]. Some food supplements have had to be recalled because of noncompliance related to heavy metal content [12].

The importance of Cu and Zn determination is due to the fact that they are essential for the human organism as part of many essential proteins and enzymes with key roles in metabolic processes [13, 14]. The recommended values for daily allowance for adults set in Commission Regulation 2008/100/EC are 10 mg Zn and 1 mg Cu [15].

Cd and Pb determination are even more important because of their high toxicity and easy intake route, namely ingestion with contaminated foods. Cd negative effects include impaired immune and kidney functions [16], while Pb toxic effects cause damage of the central and peripheral nervous system, renal functions and vascular system [17].

Anodic stripping voltammetry is an attractive method for the determination of both essential and toxic metals in mushrooms with several advantages, such as the ability for simultaneous determination with good sensitivity, selectivity, precision and accuracy, possibility of element speciation and non-expensive instrumentation compared to other techniques such as graphite furnace atomic absorption spectrometry (GFAAS) [2,11] and inductively coupled plasma optical emission spectrometry (ICP-OES) [10,18,19]. Several researchers found differential pulse anodic stripping voltammetry (DPASV) with hanging mercury drop electrode (HMDE) suitable for the determination of Zn, Cd, Pb and Cu in a large variety of samples [20-27].

The aim of this study was quantification of Zn, Cd, Pb and Cu in mushrooms by DPASV with HMDE using the standard addition method. Prior determinations an optimization study was conducted regarding working conditions (deposition time, mercury drop size and concentration/volume of the solution used for standard additions) to achieve the best analytical performances. The method was characterized in terms of limit of detection, limit of quantification, precision and accuracy and applied for the analysis of mushroom food supplements (Reishi, Chaga, Shiitake and a Mixture of mushrooms extracts), and fresh mushroom (King bolete). The concentrations of Zn and Cu as essential elements found in samples were discussed in relation with the recommended daily allowance set in Commission Directive 2008/100/EC [15]. Cadmium and Pb were examined

in relation with maximum acceptable levels of toxic elements in mushrooms and mushroom supplements, set in Commission Regulation No 1881/2006 [28] and 629/2008 [29]. The risk of intoxication *via* ingestion of analyzed samples was examined in light of Joint FAO/WHO Expert Committee on Food Additives (JECFA) recommendations [30].

RESULTS AND DISCUSSION

Method optimization

Prior to simultaneous determination of Zn, Cd, Pb and Cu by DPASV, several parameters such as volume/metal concentrations of the spiking solution, drop size and deposition time were optimized in order to achieve the best figures of merit for the method.

Multi-element standard solution

Optimization of the multi-element standard solution used in the standard addition calibration was considered necessary because of the uncertainty in precision of measurements when adding smaller volumes of higher concentration vs. higher volumes of lower concentration. For this, five multi-element standard solutions with variable metal concentrations were prepared, and four spikes were added to supporting electrolyte in each case (Table 1). The added amounts were adjusted to keep constant the final metal concentration in the electrolytic cell ($59.8 \mu\text{g L}^{-1}$ Zn, $3.74 \mu\text{g L}^{-1}$ Cd, $3.12 \mu\text{g L}^{-1}$ Pb and $12.5 \mu\text{g L}^{-1}$ Cu). These metal concentrations were found to be appropriate to result in an increase of 2-3 times of the analytic signal in the standard addition method.

Table 1. Metal concentrations in the multi-standard solution and spike amounts for the optimization study

	Added volume (mL)	Metal concentration in the multi-element standard solution (mg L^{-1})			
		Zn	Cd	Pb	Cu
Standard solution 1	0.025	24.0	1.50	1.25	5.00
Standard solution 2	0.050	12.0	0.752	0.626	2.51
Standard solution 3	0.100	6.04	0.378	0.315	1.26
Standard solution 4	0.200	3.05	0.191	0.159	0.636
Standard solution 5	0.500	1.26	0.079	0.066	0.262

For each multi-element standard solution, the signal was plotted versus the metal ion concentration resulted in the electrolyte following successive spikes. The coefficients of determination (R^2) as statistical measure of linear relationship were calculated and plotted versus the added volumes (Fig. 1).

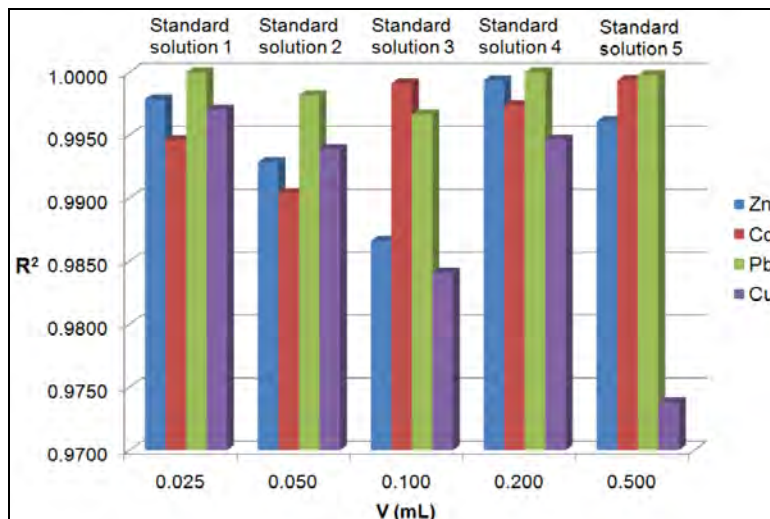


Figure 1. Effect of the volume/concentration of multi-element standard solution (Table 1) on the determination coefficient in standard addition in DPASV.

The spike volume of 0.200 ml (standard solution 4, Table 1) provided good coefficients of determination for all four metals (0.9993 for Zn, 0.9974 for Cd, 0.9999 for Pb and 0.9946 for Cu) and was selected as optimal for subsequent measurements. For few samples it was however necessary to adjust the concentration of the multi-element standard in order to keep constant the added volume of 0.2 mL.

Drop size

Mercury drop size needs to be optimized as it should provide suitable surface for an efficient deposition of metal ions. The optimal value was determined by varying the drop size, expressed in arbitrary units (a.u.) between 4-8 and recording the corresponding voltammograms (measuring conditions in Table 4) of a solution containing 10 mL supporting electrolyte and 0.2 mL multi-element standard solution 4. The signals for different drop sizes of HMDE (Fig. 2) indicated as optimal the drop size 6 (a.u.) as it provided the highest signals. All further experiments were carried out using this HMDE size.

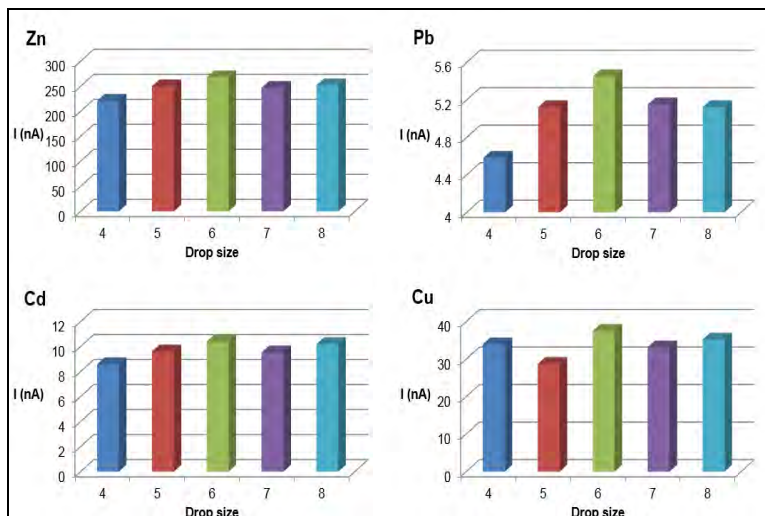


Figure 2. Effect of mercury drop size on peak height. Experimental conditions: 10 mL electrolyte + 0.2 mL multi-element standard solution 4 containing (mg L^{-1}): 3.05 Zn, 0.191 Cd, 0.159 Pb and 0.636 Cu.

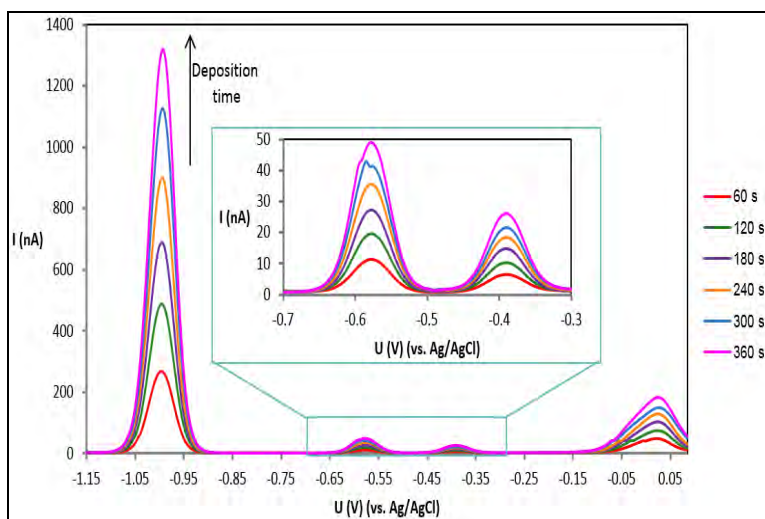


Figure 3. Effect of deposition time on peak height. Experimental conditions: 10 mL electrolyte + 0.2 mL multi-element standard solution 4 containing (mg L^{-1}): 3.05 Zn, 0.191 Cd, 0.159 Pb and 0.636 Cu.

Deposition time

The deposition time was optimized by recording the voltammogram of the multi-element standard solution using increasing deposition times in the range of 60-360 s with 60 s increments under the conditions given in the Experimental section (Table 5). For all four metals the peak height increased linearly with deposition time as a consequence of gradual metal concentration on the mercury drop (Fig. 3), however the use of long accumulation times renders analysis slow and impractical.

A deposition time of 60 s was found to be a good compromise between sensitivity and speed of analysis.

Method performances

Limits of detection and quantification

The DPASV method for the determination of Zn, Cd, Pb and Cu in mushrooms was characterized in terms of limit of detection (LoD) and limit of quantification (LoQ) in solution and dry mass under the optimized conditions. The LoD was calculated as $3s_{y/x}/b$, and LoQ as 3LoD , where $s_{y/x}$ is the residual standard deviation and b is the slope of the standard addition curve [31]. LoD and LoQ in solid samples were expressed taking into account the sample preparation protocol (Table 2).

Table 2. Limits of detection and quantification of Zn, Cd, Pb and Cu in mushrooms by DPASV

Metal	LoD ^a ($\mu\text{g L}^{-1}$)	LoQ ^b ($\mu\text{g L}^{-1}$)	LoD ^c ($\mu\text{g g}^{-1}$ dry mass)	LoQ ^c ($\mu\text{g g}^{-1}$ dry mass)
Zn	19.1	57.4	0.95	2.84
Cd	0.24	0.72	0.012	0.035
Pb	3.17	9.52	0.16	0.47
Cu	14.0	42.1	0.70	2.09

^a calculated as $3s_{y/x}/b$.

^b calculated as 3LoD .

^c calculated for 1 g solid sample digested and diluted to 50 mL and 0.5 mL solution taken for analysis.

According to Table 2, lower LoDs were obtained for Cd ($0.24 \mu\text{g L}^{-1}$) and Pb ($3.17 \mu\text{g L}^{-1}$), and higher for Zn ($19.1 \mu\text{g L}^{-1}$) and Cu ($14.0 \mu\text{g L}^{-1}$). Compared to LoDs obtained in other reports for DPASV ($0.26\text{-}0.69 \mu\text{g L}^{-1}$ Zn, $0.05\text{-}1.00 \mu\text{g L}^{-1}$ Cd, $0.5\text{-}0.8 \mu\text{g L}^{-1}$ Pb and $0.24\text{-}2.00 \mu\text{g L}^{-1}$ Cu) [22,25,32], our LoD for Cd in sample solution was similar, while for Cu, Pb and Zn poorer. The difference is explained by the fact that our LoDs were calculated from the parameters of the standard addition curve, while the

literature values refer to synthetic solutions. In comparison with other widely used spectrometric techniques (ICP-OES, GFAAS), our LoDs were comparable for Cd and Pb ($0.2\text{-}1\ \mu\text{g L}^{-1}$ (Cd), $1\text{-}5\ \mu\text{g L}^{-1}$ (Pb) [33]) and poorer for Zn and Cu ($0.09\text{-}1\ \mu\text{g L}^{-1}$ (Zn), $0.2\text{-}2\ \mu\text{g L}^{-1}$ (Cu) [33]). The optimized DPASV method makes possible determination of Cd and Pb as toxic elements in mushrooms/food supplements, since LOQ found by us provide quantification starting from $0.04\ \mu\text{g g}^{-1}$ Cd and $0.5\ \mu\text{g g}^{-1}$ Pb, which are much lower than the maximum allowed concentration in mushroom supplements ($1\ \mu\text{g g}^{-1}$ Cd and $3\ \mu\text{g g}^{-1}$ Pb) [29]. The use of DPASV method, on the other hand, provides the advantage of simultaneous multi-element determination compared to AAS and low analysis costs.

Accuracy

Method accuracy was assessed through a spike recovery test ($n=3$ spikes). A good agreement between found and theoretical amounts was obtained for 95% confidence level. Mean recoveries were (%): 104 ± 6 Cu, 102 ± 4 Cd, 100 ± 7 Pb and 102 ± 5 Cu and included in all cases the 100% value.

Analysis of mushroom samples

Results obtained for metal concentration in mushroom food supplements and mushroom expressed in dry weight are summarized in Table 3.

Table 3. Metal concentrations in the analyzed mushroom and mushroom supplements

Mushrooms	Mean \pm C.I. ^a ($\mu\text{g g}^{-1}$ dry weight)			
	Zn	Cd	Pb	Cu
<i>Food supplements</i>				
Reishi	32.7 ± 1.2	0.06 ± 0.01	2.63 ± 0.34	1.44 ± 0.12
Chaga	49.0 ± 2.0	0.40 ± 0.06	3.60 ± 0.12	4.00 ± 0.72
Shiitake	10.4 ± 0.5	0.57 ± 0.16	2.34 ± 0.18	6.62 ± 4.90
Mixture	46.4 ± 7.2	0.09 ± 0.01	3.27 ± 0.16	21.5 ± 5.8
<i>Fresh mushroom</i>				
King bolete	102 ± 4	0.69 ± 0.02	1.83 ± 0.05	24.1 ± 1.4
RSD ^b (%)	1.5-7.4	1.4-11.6	1.1-5.2	2.4-10.9

^a C.I. is the confidence interval for 95% confidence level ($n=3$ successive measurements).

^b RSD (%) is the relative standard deviation.

RSD for all four metals varied between 1.1 and 11.6 %, thus proving precision better than 10% for Zn and Pb and up to 11% for Cd and Cu, fulfilling the recommendation of AOAC in terms of precision [34].

The most abundant metal was found to be Zn ($10.4\text{-}102\ \mu\text{g g}^{-1}$), in agreement with the characteristic of mushrooms to accumulate Zn [2,35-

37], while Cu was found in lower concentrations (1.44-24.1 $\mu\text{g g}^{-1}$). The high concentration of Zn is beneficial as human organism has greater need for Zn than Cu [29]. Among the analyzed samples, the highest amounts of both Zn and Cu were found in King bolete mushroom (102 $\mu\text{g g}^{-1}$ Zn and 24.1 $\mu\text{g g}^{-1}$ Cu), followed by the mixture of medicinal mushroom capsules (46.4 $\mu\text{g g}^{-1}$ Zn and 21.5 $\mu\text{g g}^{-1}$ Cu).

Cadmium in the edible mushroom (0.69 $\mu\text{g g}^{-1}$) was found to be only slightly higher than in supplements (0.06-0.57 $\mu\text{g g}^{-1}$).

Lead was in the range 1.83-3.60 $\mu\text{g g}^{-1}$. Thus, the benefit of high concentration of essential elements is limited to some extent.

The comparison of results obtained for the edible King bolete with dietary supplements revealed no evident discrepancy in terms of Cd, Pb and Cu, unlike Zn, for which the content was approximately twofold higher, namely 102 $\mu\text{g g}^{-1}$ for the King bolete, versus 10.4-49.0 $\mu\text{g g}^{-1}$ in dietary supplements. Much higher concentrations of Zn, Cd and Pb were reported in other studies for the same mushroom species (55.5-283.9 $\mu\text{g g}^{-1}$ Zn, 0.66-283.9 $\mu\text{g g}^{-1}$ Cd and 0.14-86 $\mu\text{g g}^{-1}$ Pb), while similar concentrations were found for Cu (13.7-55.7 $\mu\text{g g}^{-1}$) [1-2,10,18,37].

Assessment of Cu, Pb, Zn and Cd intake via mushroom and mushroom supplements consumption

The maximum allowed concentrations of Cd and Pb in mushroom supplements are 1.0 $\mu\text{g g}^{-1}$ and 3.0 $\mu\text{g g}^{-1}$ dry weight according to Commission Regulation (EC) No 629/2008 [29], and 0.2 $\mu\text{g g}^{-1}$ and 0.3 $\mu\text{g g}^{-1}$ wet weight respectively in cultivated fungi set in Commission Regulation (EC) No 1881/2006 [28]. Assuming 90 % moisture content in fresh mushrooms, the maximum acceptable levels expressed in dry mass become 2 $\mu\text{g g}^{-1}$ Cd and 3 $\mu\text{g g}^{-1}$ Pb in King bolete mushroom. As show data in Table 3, Cd concentrations in all samples were below the set values, while Pb limit was exceeded in the case of Chaga and Mixture supplement by up to 20%.

Table 4 presents the intake of Zn and Cu as essential elements, and Cd and Pb as toxic heavy metals from mushroom supplements *via* the maximum dose recommended by the manufacturer (5.4 g day⁻¹ Reishi, 2 g day⁻¹ Chaga, 4 g day⁻¹ Shiitake and 2.46 g day⁻¹ mushroom Mixture) and a serving of 100 g mushroom per day, respectively. Values for Cd were compared to the provisional tolerable monthly intake (PTMI) of 0.025 mg Cd/kg body weight (1.5 mg for 60 kg body weight) set by the Joint FAO/WHO Expert Committee on Food Additives (JECFA) [30]. According to data in Table 4 the limit was not exceeded in none of the cases.

For the evaluation of Pb intoxication *via* contaminated food, JECFA advises a dose-response analysis, separately for adults and children (1-4

years old) [30]. Accordingly, for a 60 kg adult the exposure to 0.02 $\mu\text{g Pb/kg}$ body weight per day (1.2 $\mu\text{g/day}$) represents a negligible health risks, 1.2 $\mu\text{g Pb/kg}$ body weight per day (72 $\mu\text{g/day}$) is associated with an increase of systolic blood pressure and 3 $\mu\text{g Pb/kg}$ body weight per day (180 $\mu\text{g/day}$) is proven to cause systolic blood pressure increase associated with increase in the risks of ischemic heart disease and cerebrovascular stroke. The comparison of these values with Pb concentrations found in our samples emphasized a non-existing/low health risk (5.36-18.3 $\mu\text{g/day}$) even for samples in which Pb slightly exceeded the maximum acceptable levels.

Table 4. Metals intake^a and recommended daily allowances

Mushrooms	Zn		Cu		Cd	Pb
	mg day^{-1}	RDA^{b} (%)	mg day^{-1}	RDA (%)	$\text{mg month}^{-1\text{c}}$	$\mu\text{g day}^{-1}$
<i>Food supplements</i>						
Reishi	0.18	1.8	0.01	1	0.01	14.2
Chaga	0.10	1.0	0.01	1	0.02	7.20
Shiitake	0.04	0.4	0.03	3	0.07	5.36
Mixture	0.11	1.1	0.05	5	0.01	8.04
<i>Fresh mushroom</i>						
King bolete	1.02	10.2	0.24	24	0.21	18.3

^a Consumption of 100 g fresh King bolete (90% moisture)/day, 5.4 g/day Reishi, 2 g/day Chaga, 4 g/day Shiitake and 2.46 g/day Mixture.

^b RDA is the Recommended Daily Allowance (10 mg/day Zn and 1 mg/day Cu [15]).

^c Calculated for a 60 kg adult and month consisting of 30 days.

Zn intake through supplements expressed as Recommended Daily Allowance (%RDA) was in the range 0.4 (Shiitake)-1.8 (Reishi) and much higher in the case of the King bolete (10.2%). The situation was very similar in the case of Cu, with higher %RDA for the fresh mushrooms (24%) than in supplements (1% for Reishi and Chaga - 5% for the Mixture).

CONCLUSIONS

Anodic stripping voltammetry with hanging mercury drop electrode was optimized for the determination of Zn, Cd, Pb and Cu in mushroom food supplements and fresh mushroom in terms of multi-element standard solution used in the standard addition method, Hg drop size and deposition time. Performances of the methods were assessed regarding LoD, LoQ, accuracy and precision and were found to be satisfactory for the analyses of mushroom samples after mineralization.

The comparison of metal concentration in food supplements and the edible King bolete fungus revealed no difference in terms of Cd, Pb and Cu content, while Zn was more abundant in the fresh mushroom. It has been found that King bolete represents a significant source of Cu and Zn compared to the recommended daily allowance, while Cd and Pb pose no health risk for both food supplements and fresh mushroom.

EXPERIMENTAL SECTION

Reagents, stock solutions and samples

Nitric acid 69%, perchloric acid 70%, hydrochloric acid fuming 37% and stock solutions of Zn, Cd, Pb and Cu (1000 mg L^{-1}) were purchased from Merck (Darmstadt, Germany); acetic acid $\geq 99.5\%$ and sodium hydroxide $\geq 99\%$ were purchased from Sigma-Aldrich (Hamburg, Germany). All dilutions throughout this study were made using doubly distilled water obtained with Fistream Cyclon Double (Bi-) Distiller (United Kingdom).

The analyzed samples were mushroom supplements: Reishi (*Ganoderma lucidum*) as tablets, Chaga (*Inonotus obliquus*), Shiitake (*Lentinula edodes*) as dried powders and a Mixture of medicinal mushroom extracts as capsules recommended for their benefit associated to overall good health, balance in the organism, memory, respiratory function and resistance to the aging process, as well as a fresh mushroom, King bolete (*Boletus edulis*), from local market.

Instrumentation

Voltammetric measurements were carried out using the 797 VA Computrace, Metrohm AG (Switzerland) instrument. The voltammetric analyzer was controlled by computer, using the VA Computrace software Metrohm. Operating conditions are given in Table 5.

Table 5. Working conditions for DPASV measurements

Electrode	HMDE - Hanging mercury drop electrode
Drop size	4-8, optimal 6
Stirring rate	2000 rpm
Initial Ar purging	180 s
Deposition potential	-1.2 V
Deposition time	60-360 s, optimal 60 s
Equilibration time	5 s
Start potential	-1.2 V
End potential	0.08 V
Pulse amplitude	0.05 V
Pulse time	0.04 s
Voltage step	0.005 V
Voltage step time	0.3 s
Scan rate	0.0168 V s^{-1}
Quantification	Peak height
Oxidation potentials (vs. Ag/AgCl)	
Zn	(-0.90)-(-1.00) V
Cd	(-0.56)-(-0.58) V
Pb	(-0.38)-(-0.41) V
Cu	(-0.03)-(+0.01) V
Supporting electrolyte	1 mL acetate buffer (pH 4.6, ionic strength 0.1) and 9 mL H ₂ O

Sample preparation

All samples were dried to constant weight, ground in a mortar (if necessary) and sieved to $\leq 63 \mu\text{m}$. The King bolete analytical sample was constituted of whole mushroom (stem and cap). An amount of 1 g sample was digested with 20 mL HNO_3 and 5 mL HClO_4 , by heating on a sand bath. The digest was filtered and diluted to 50 mL in volumetric flasks.

Sample measurement

Quantitative analyses were realized using 0.5 mL aliquots from the digested sample added to 10 mL supporting solution (9 mL H_2O and 1 mL acetate buffer). Steps of DPASV: deaeration of electrolyte by Ar purging for 180 s; analyte deposition at HMDE at -1.2 V under stirring, equilibration for 5s; anodic stripping and voltammogram recording in the range (-1.2) - (0.08) V. Simultaneous determination of Zn, Cd, Pb and Cu was performed using the standard addition method ($n=4$ spikes) under the optimized conditions given in Table 5.

REFERENCES

1. S. W. Chiu, Z. M. Wang, T. M. Leung, D. Moore, *Food and Chemical Toxicology*, **2000**, 38, 173.
2. C. Wang, Y. Hou, *Biological Trace Element Research*, **2011**, 142, 843.
3. K. K. W. Chu, S. S. S. Ho, A. H. L. Chow, *Journal of Clinical Pharmacology*, **2002**, 42, 976.
4. N. Caglarirmak, *Food Chemistry*, **2007**, 105, 1188.
5. M. G. Shashidhar, P. Giridhar, K. Udaya Sankar, B. Manohar, *Journal of Functional Foods*, **2013**, 5, 1013.
6. J. Glamoclija, A. Ciric, M. Nikolic, A. Fernandes, L. Barros, R. C. Calhelha, I. C. F. R. Ferreira, M. Soković, L. J. L. D. van Griensven, *Journal of Ethnopharmacology*, **2015**, 162, 323.
7. <http://plants.alaska.gov/pdf/Conks.pdf> (Accessed: 14 April 2017).
8. <http://www.medicalmushrooms.net/fomes-fomentarius/> (Accessed: 14 April 2017).
9. N.P. Money, *Fungal Biology*, **2016**, 120, 449.
10. P. L. George, T. D. Ranatunga, S. S. Reddy, G. C. Sharma, *American Journal of Food Technology*, **2014**, 9, 360.
11. D. Zhang, T. Gao, P. Ma, Y. Luo, P. Su, *Wuhan University Journal for Natural Sciences*, **2008**, 13, 267
12. <https://www.fda.gov/ForConsumers/ConsumerUpdates/ucm050803.htm>
13. <http://www.rcsb.org/pdb/home/home.do> (Accessed: 02 February 2017)
14. J. Osredkar, N. Sustar, *J. Clinic. Toxicol.*, **2011**, S3:001. doi: 10.4172/2161-0495.S3-001.
15. Commission Directive 2008/100/EC amending Council Directive 90/496/EEC on nutrition labeling for foodstuffs as regards recommended daily allowances, energy conversion factors and definitions, *Official Journal of the European Union*, 28 October **2008**, L 285/9.

16. R.A. Bernhoff, *The Scientific World Journal*, **2013**, 2013, Article ID 394652, 7 pages. Available at: <http://dx.doi.org/10.1155/2013/394652> (Accessed: 10 March 2017).
17. L. Patrick, *Alternative medicine review*, **2006**, 11, 2.
18. G. Giannaccini, L. Betti, L. Palego, G. Mascia, L. Schmid, M. Lanza, A. Mela, L. Fabbri, L. Biondi, A. Lucacchini, *Environmental Monitoring and Assessment*, **2012**, 184, 7579.
19. E. Kuldo, G. Jarzynska, M. Gučia, J. Falandysz, *Chemical Papers*, **2014**, 68, 484.
20. J. Raj, A.R. Mohineesh, T.D. Dogra, *E3S Web of conferences*, **2013**, 1, 09009. <http://dx.doi.org/10.1051/e3sconf/20130109009> (Accessed: 15 March 2017).
21. S. Kucukkolbasi, O. Temur, H. Kara, A. R. Khaskheli, *Food Analytical Methods*, **2014**, 7, 872.
22. P. Suwannasom, C. Ruangviriyachai, *International Food Research Journal*, **2011**, 18, 803.
23. J. A. Rodrigues, C. M. Rodrigues, P. J. Almeida, I. M. Valente, L. M. Goncalves, R. G. Compton, A. A. Barros, *Analytica Chimica Acta*, **2011**, 701, 152.
24. W. Opoka, M. Jakubowska, B. Bas, M. Sowa-Kucma, *Biological Trace Element Research*, **2011**, 142, 671.
25. S.A. Mahesar, S.T.H. Sherazi, A. Niaz, M.I. Bhangar, S.A. Rauf, *Food and Chemical Toxicology*, **2010**, 48, 2357.
26. F.R. Bento, M.T. Grassi, A. Sales, L.H. Mascaro, *International Journal of Electrochemical Journal*, **2008**, 3, 1523.
27. A.F. Al-Hossainy, A.E. Mohamed, F.S.M. Hassan, M.M.A. Allah, *Arabian Journal of Chemistry*, **2017**, 10, S347.
28. Commission Regulation (EC) No 1881/2006 setting maximum levels for certain contaminants in foodstuffs. *Official Journal of the European Union*, **2006**, L 364/5.
29. Commission Regulation (EC) No 629/2008 amending Regulation (EC) No 1881/2006 setting maximum levels for certain contaminants in foodstuffs. *Official Journal of the European Union*, **2008**, L 173/6.
30. Joint FAO/WHO Expert Committee on Food Additives (JECFA), Seventy-third meeting, 8-17 June **2010**, Summary and Conclusions, Geneva (JECFA/73/SC). Available at: <http://www.fao.org/3/a-at862e.pdf> (Accessed: 06 May 2017).
31. J. Mocak, A. M. Bond, S. Mitchell, G. Scollary, *Pure and Applied Chemistry*, **1997**, 69, 297.
32. M.H. Barcelo-Quintal, J.A. Manzanilla-Cano, E.O. Reyes-Salas, J. Flores-Rodrigues, *Analytical Letters*, **2001**, 34, 2349.
33. X. Hou, B.T. Jones, Inductively Coupled Plasma – Optical Emission Spectrometry. *Encyclopedia of Analytical Chemistry*, **2008**.
34. AOAC. (2002). Guidelines for Single Laboratory Validation of Chemical Methods for Dietary Supplements and Botanicals. Available at: https://www.aoac.org/aoac_prod_imis/AOAC_Docs/StandardsDevelopment/S_LV_Guidelines_Dietary_Supplements.pdf. (Accessed: 15.02.2017)
35. Z.Bano, K. Nagaraja, S. Vibhakar, O.P. Kapur, *Mushroom Newslett. Trop.*, **1981**, 2, 3.
36. P. Kalac, L. Svoboda, *Food. Chem.*, **2000**, 69, 273.
37. O. Isildak, I. Turkekul, M. Elmastas, M. Tuzen, *Turkey Food Chemistry*, **2004**, 86, 547.

In memory of prof. dr. Simion Gocan

ELECTROCHEMICAL SENSORS FOR MALACHITE GREEN BASED ON CARBONACEOUS NANOMATERIALS

ANA-MARIA SĂCARĂ^a, LIANA MARIA MUREȘAN^{a*}

ABSTRACT Synthetic dyes are widely used in many fields, such as textile industry, plastics, cosmetics, paper industry and many others. Due to their toxicity, they should be removed from wastes before discharging in the environment. In order to determine the efficiency of the removal process, different methods are used to detect traces of dyes in wastewaters. The most used are spectrophotometry and FIA, however the expensive equipment and complicated testing process make these methods difficult to use. On the contrary, electrochemical sensors have multiple advantages such as short response time, low price and easiness to use. In this context, several electrochemical sensors based on new carbonaceous materials were developed and characterized. Carbon nanotubes, graphene and activated carbon from *Abies nordmanniana* cones together with Nafion were used to modify the surface of a glassy carbon electrode by drop casting. The resulting modified electrodes were tested by SWASV and amperometry for Malachite Green detection in aqueous solutions, having low detection limits in the order of μM .

Keywords: *Malachite Green; electrochemical detection; activated carbon; carbon nanotubes; reduced graphene oxide; modified electrodes.*

INTRODUCTION

The textile industry is one of the most important contributors to water pollution by discharging up to 200,000 tons of wastewaters every year as effluents [1]. Dyes are a large and varied class of compounds with coloring abilities that usually show affinity for the substrate they are applied on, generally in aqueous solution, with or without the use of a mordant for improved fastness [2]. They are widely used in many fields, such as the

^a Babeș-Bolyai University, Faculty of Chemistry and Chemical Engineering, Department of Chemical Engineering, 11 Arany Janos str., RO-400028, Cluj-Napoca, Romania.
^{*} Corresponding author: limur@chem.ubbcluj.ro

textile industry, plastics, cosmetics, paper industry and many others [3]. Unfortunately, they are usually persistent in the environment [4] and can easily be assimilated in living organisms [5-7]. The dye selected for this study, Malachite Green (MG), exhibits these common characteristics being a potential threat to aquatic life because of its cytotoxic [8], biocidal [9] and bioaccumulation properties [5-7].

Classic detection methods such as HPLC used to detect MG need expensive equipment and a complicated testing process [10]. This is why this study intends to develop new electrochemical sensors designed to accurately and easily determine the concentration of MG from an aqueous solution in a fast and inexpensive way. A new activated carbon (AC) produced from fir (*Abies nordmanniana*) cones has been utilized for modification of a glassy carbon electrode in order to obtain a very sensitive and selective sensor for MG. The results were compared with those obtained with other nanomaterials such as single-walled carbon nanotubes (SWCNTs) and reduced graphene oxide (RGO) and with those reported in literature [11-14].

The glassy carbon electrodes modified with carbonaceous materials and Nafion presented in this paper were prepared by drop casting and characterized by using square wave anodic stripping voltammetry (SWASV), batch amperometry and electrochemical impedance spectroscopy (EIS).

RESULTS AND DISCUSSION

Characterization of the carbonaceous materials

SWCNTs and RGO were commercial products of analytical grade, characterized by the manufacturer.

The artisanal activated carbon prepared in various conditions was characterized by TEM analysis, (Figure 1).

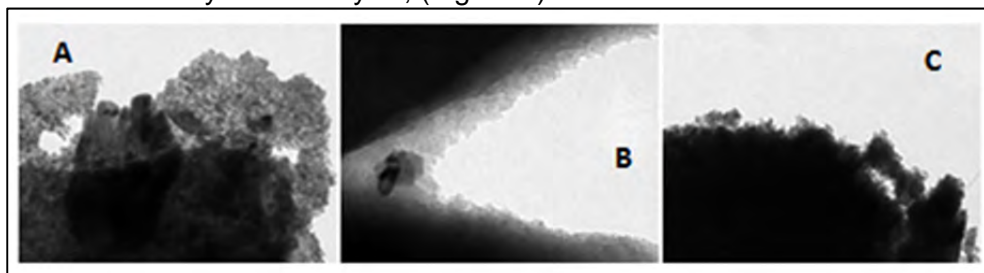


Figure 1. TEM analysis of activated carbon (AC) types, with different concentrations of NaOH used for chemical activation: A – NaOH 5%, B – NaOH 10% and C – NaOH 20%.

It is observed that the size of the particles can be obviously correlated with the concentration of NaOH solution in an inverse proportion. The porosity of the material seems to be also affected by NaOH concentration.

Square wave anodic stripping voltammetry (SWASV)

Influence of activated carbon (AC) activation conditions and concentration

Before conducting further experiments with the AC, the best nanomaterial had to be chosen among three varieties resulted from various levels of chemical activation with NaOH solutions of different concentrations. For this purpose, SWASV measurements in MG containing solutions were used at electrodes prepared with the three types of AC.

The anodic oxidation of MG was previously reported and described [14] as taking place with the ejection of an integral unit of the central carbon attached to a phenyl group, intramolecular coupling of two phenyl fragments succeeding this phase, leading to the formation of the oxidized form of N,N,N',N'-tetramethylbenzidine (TMB), that is 1,1'-biphenyl-4,4'-diamine (TMB_{ox}). Thus, the oxidation of MG in acidic aqueous solutions was shown to proceed *via* an electrochemically irreversible, diffusion controlled, two electron transfer process [15,16].

This process is visible in SWASV measurements where two oxidation peaks occur at approx. 0.4 V and 0.85 V vs. Ag/AgCl/KCl_{sat} (Figures 2A, 4A and 5A). The height of the peaks is proportional to MG concentration, therefore calibration curves were obtained by plotting I as function of MG molar concentration (Figs. 2B, 4B and 5B, for peak II)

In Figure 2 the SWASV curves are illustrated for the variety of AC that gave best results (activated with NaOH 5 %).

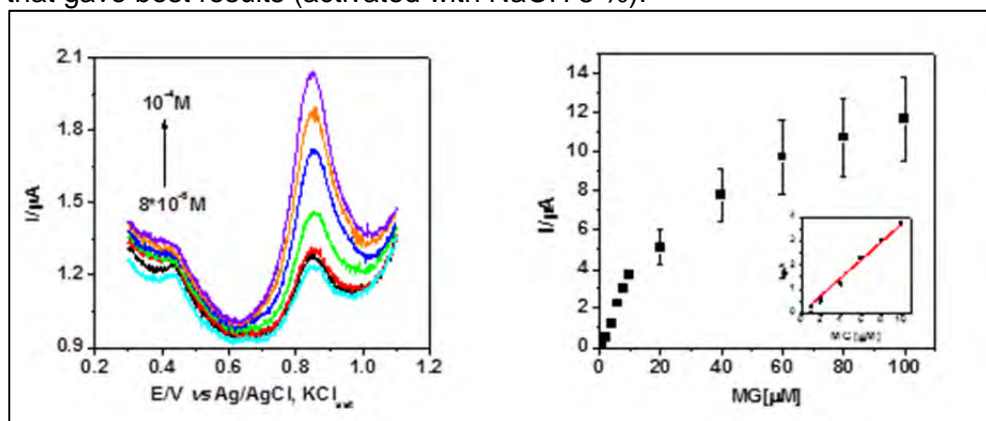


Figure 2. SWASV and calibration curves for **GC/AC/Nafion** electrodes prepared with AC activated with NaOH 5 %. Experimental conditions: PB 0.1M, pH 3; 10^{-6} – 10^{-4} M MG; frequency, 25 Hz; amplitude, 0.01 V; deposition time, 300s; start potential, 0.3 V vs. Ag/AgCl, KCl_{sat}.

Further, the calibration curves for the three tested AC varieties plotted for peak II were compared (Fig 3A). All preliminary experiments were carried

out in the presence of Nafion coating, for a better stability of the electrodes. Nafion keeps and protects the carbonaceous material on the electrode's surface. Moreover, the possibility of a favorable ionic association between negatively charged Nafion ionomer and cationic MG also exists. These interactions were put in evidence by FT-IR spectra in a previous study [17].

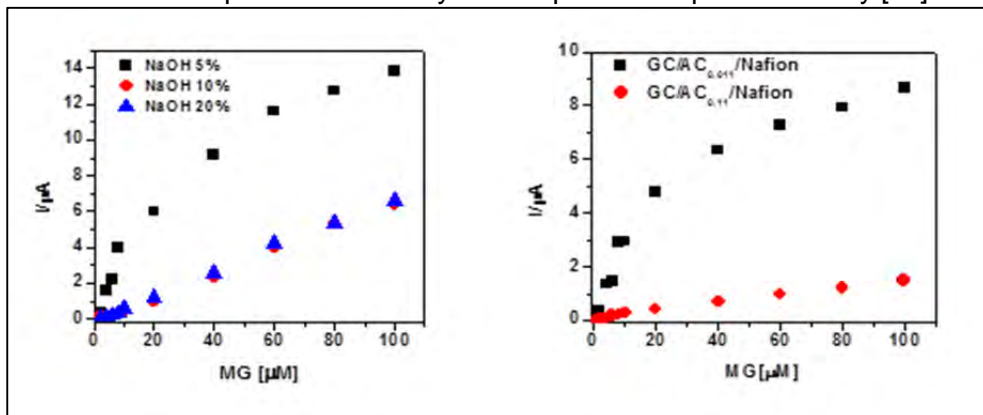


Figure 3. SWASV calibration curves for **GC/AC/Nafion** electrodes; influence of NaOH solutions concentration (A) and of AC concentration (B) Experimental conditions: see Fig.2.

As it can be seen from Fig. 3A, the best response corresponds to the variety of AC obtained after chemical activation in 5% NaOH solution; the others, activated more aggressively, had lower performances. It is possible that the porosity of the materials was affected by an aggressive treatment with concentrated NaOH. Consequently, the variety activated with NaOH 5% was the one chosen for further experiments and comparisons.

As a second important parameter, the concentration of the AC containing suspension used for electrode surface modification was taken into consideration. Two different concentrations were considered: 0.011 mg/mL, used for SWCNT concentration in other studies [18] and a tenfold higher concentration of 0.11 mg/mL. The concentration corresponding to the best electrochemical answer (0.011mg/mL) (Figure 3B) was kept to prepare **GC/AC/Nafion** electrodes used in further experiments.

CG electrodes modified with SWCNTs and RGO

Aiming to select the most effective carbonaceous nanomaterial for the preparation of the modified GC electrodes, SWCNT and RGO were also used and their electrochemical response was recorded (Figs 4A and 5 A). Based on the SWAS voltammograms, calibration curves were plotted (Figs 4B and 5 B)

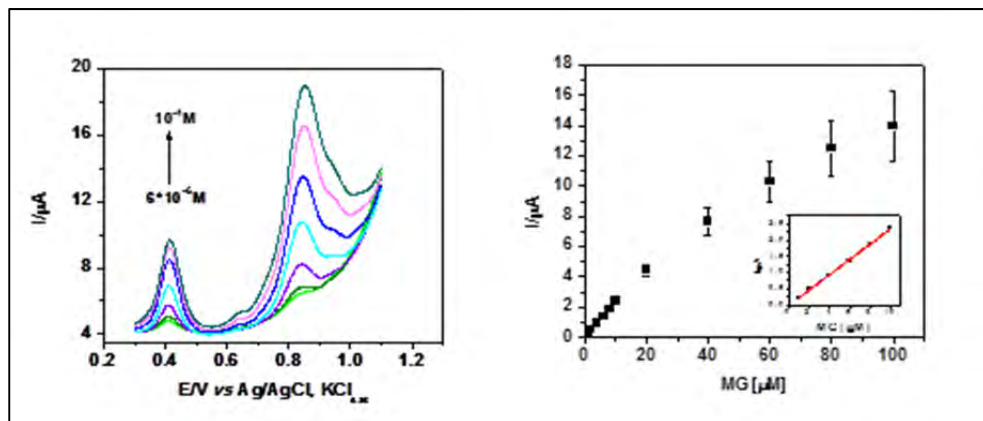


Figure 4. SWASV (A) and calibration curves (B) for **GC/SWCNTs/Nafion** electrode with linear part (inset in Fig 4B)). Experimental conditions: see Fig 2.

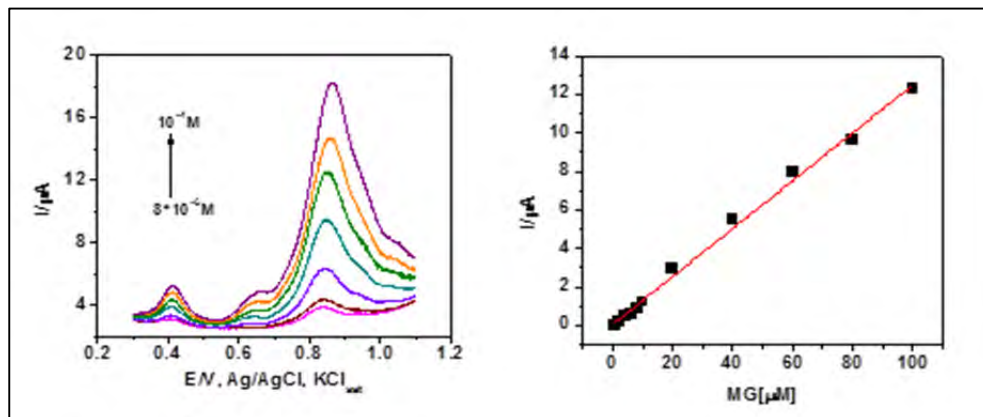


Figure 5. SWASV and calibration curves for **GC/RGO/Nafion** electrodes. Experimental conditions: see Fig. 2.

The electrochemical parameters of the electrodes prepared with different carbonaceous materials (E_{peak} and I_{peak}) are given in Table 1. The values were taken from SWASV peak currents rendered for MG 10 μM .

Table 1. Electrochemical parameters of electrodes modified with carbonaceous materials. MG concentration, 10 μM .

Electrode	E_{peak} (V)	I_{peak} (μA)
GC	0.86	1.46
GC/Nafion	0.89	1.10
GC/SWCNTs/Nafion	0.84	2.37
GC/RGO/Nafion	0.84	1.21
GC/AC/Nafion	0.85	3.71

It can be observed that both **GC/SWCNTs/Nafion** and **GC/RGO/Nafion** electrodes exhibit excellent catalytic activity toward MG oxidation, put in evidence by the increase of the peak current and a slight shift of the oxidation peak potentials toward more negative values. A direct comparison between the three carbonaceous materials is presented in Figure 6, by means of the corresponding calibration curves.

The electroanalytical parameters presented in Table 2 point out to the fact that the electrodes prepared with SWCNT and AC exhibit best sensitivities and lowest detection limits. This suggests that these nanomaterials ensure best conductivity and active surface area to the modified electrodes.

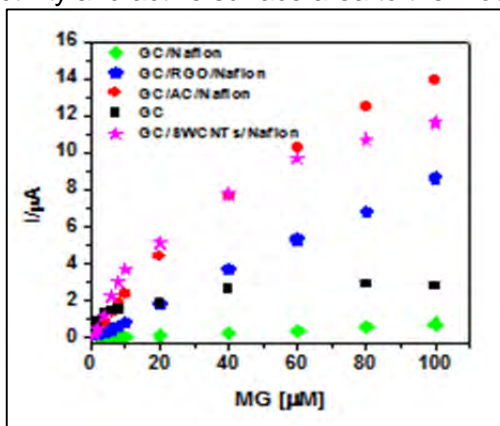


Figure 6. Calibration curves obtained for **GC**, **GC/SWCNTs**, **GC/RGO** and **GC/AC** electrodes, with Nafion coating, in SWASV.

Table 2. Electroanalytical parameters obtained for **GC/Nafion**, **GC/SWCNTs/Nafion**, **GC/RGO/Nafion** and **GC/AC/Nafion** electrodes' from SWASV calibration curves

	GC/Nafion	GC/SWCNTs/ Nafion	GC/RGO/ Nafion	GC/AC/ Nafion
Sensitivity (A/M)	0.008±0.001	0.236±0.003	0.087±0.011	0.403±0.013
Linear domain (μM)	2 – 100	1 – 10	1 – 90	1 – 10
DL* (μM)	7.880	0.3308	3.9372	0.7763
R²/n	0.9945/10	0.999/6	0.9986/10	0.9945/6

* detection limit is calculated by formula $DL=3*SD/ \text{slope}$.

Amperometry

Amperometric analysis (Fig.7) was also carried out at **GC/Nafion**, **GC/SWCNTs/Nafion**, **GC/RGO/Nafion** and **GC/AC/Nafion** electrodes. The differences between the amperometric (Table 3) and SWASV results could

be due to the absence of the accumulation step (300 s) used in SWASV measurements, which lead to lower detection limits in this method.

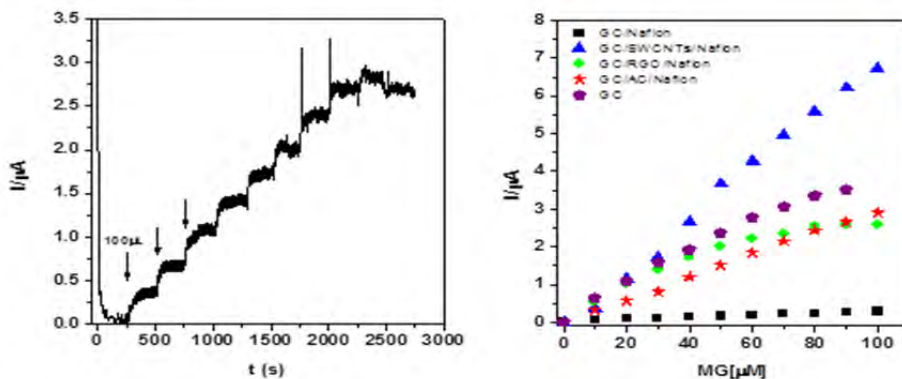


Figure 7. Amperometric measurements at **GC/AC/Nafion** electrode (A) and calibration curves obtained for **GC**, **GC/Nafion**, **GC/SWCNTs/Nafion**, **GC/RGO/Nafion** and **GC/AC/Nafion** electrodes (B). Experimental conditions: PB solution, pH 3, working potential 0.85 V vs. Ag/AgCl/KCl_{sat}.

As expected, the analytical parameters extracted from the amperometric calibration curves (Table 3) show the best performances of the electrodes modified with SWCNTs, but **GC/AC/Nafion** has also convenient characteristics. For all tested electrodes, the DL values are lower than those stipulated in the European legislation, (maximum allowed concentration of dyes in wastewater is 3.2×10^{-5} M) [19]

Table 3. Electroanalytical parameters obtained for **GC/SWCNTs/Nafion**, **GC/RGO/Nafion** and **GC/AC/Nafion** electrodes

	GC/Nafion	GC/SWCNT/ Nafion	GC/RGO/ Nafion	GC/AC/ Nafion
Sensitivity (A/M)	0.0026±0.0001	0.069±0.001	0.046±0.001	0.0233±0.0006
Linear domain (µM)	0 – 100	0 – 100	0 – 40 µM	0 – 100 µM
DL* (µM)	13.355	3.724	5.655	8.838
R²/n	0.9841/11	0.9978/11	0.9953/5	0.9929/1

* detection limit is calculated by formula $DL=3 \cdot SD / \text{slope}$.

Electrochemical impedance spectroscopy

To assess the activity of **GC/SWCNTs/Nafion**, **GC/RGO/Nafion** and **GC/AC/Nafion** modified electrodes, the $[\text{Fe}(\text{CN})_6]^{4-/3-}$ couple (10^{-3} M in 0.1 M KCl solution) was employed as a redox probe in electrochemical impedance

spectroscopy measurements. Fig. 8 shows the Nyquist plots corresponding to different modification of the GC electrode surface. It can be seen that the investigated electrodes exhibit a capacitive behavior at all frequencies.

The **GC/Nafion** electrode has the highest impedance when compared to the other electrodes, suggesting a more difficult electron transfer due to the polymeric coating that acts as a physical barrier. On the other hand, the negatively charged Nafion layer deposited on GC surface increases the bare electrode impedance by electrostatic rejection of the negative $[\text{Fe}(\text{CN})_6]^{4-}/^{3-}$ couple.

As expected, when carbonaceous materials are embedded in Nafion, the impedance decreases visibly due to the enhanced conductivity of the modified surface. The smallest impedance corresponds to the **GC/SWCNTs/Nafion** electrode, which exhibit also the largest surface area. The EIS results are thus in agreement with SWASV measurements.

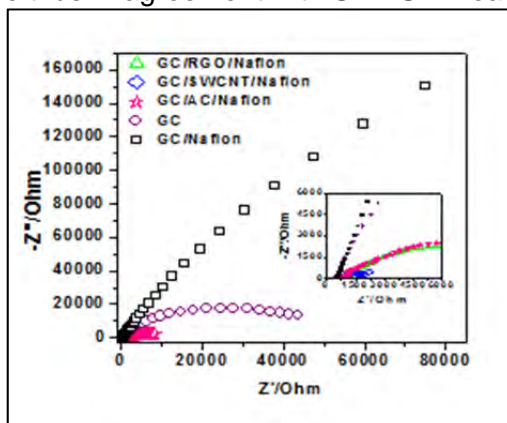


Figure 8. Electrochemical impedance spectroscopy at **GC**, **GC/Nafion**, **GC/SWCNTs/Nafion**, **GC/RGO/Nafion** and **GC/AC/Nafion** electrodes.

Repeatability and stability

Electrodes' stability was determined by cyclic voltammetry in MG solution simulating operational conditions. The modified electrodes were tested for 50 cycles in the working potential range (0.3 – 1.1V), at 50mV/s scan rate, in 100 μ M MG. The peak current decreased visibly for the first 10 cycles until a proper stabilization was established, being followed by steady currents further on. This behavior was similar for all tested electrodes. The stability after 50 cycles, taking cycle 10 as reference, was found to be $96.21 \pm 0.07\%$ for **GC/SWCNTs/Nafion** and $91.23 \pm 0.37\%$ for **GC/RGO/Nafion**. The working stability for **GC/AC/Nafion** was a bit lower, $85.78 \pm 0.07\%$, but the stability in buffer was comparable, 90.71%.

Repeatability of the measurements was calculated from peak current values obtained in SWASV for two or three different electrodes of each type, at a concentration of MG corresponding to the middle of the linear range of the calibration curves for each electrode. The values obtained for **GC/SWCNTs/Nafion** were RSD = 3.99% with a mean of 1.372 μA at 6 μM MG for 3 measurements; for **GC/RGO/Nafion** RSD = 5.80% with a mean of 1.913 μA at 10 μM MG (and 1.42% with a mean of 1.549 μA at 6 μM MG) for 2 measurements; and for **GC/AC/Nafion** RSD = 0.44% with a mean of 2.24 μA at 6 μM MG for 2 measurements.

CONCLUSIONS

- A simple and sensitive electrochemical method was developed for the determination of MG in aqueous solutions.
- The MG oxidation peak current in SWASV is proportional to its concentration over a large range at all tested electrodes.
- All carbonaceous materials have a beneficial effect on the GC electrode, making it more sensitive and decreasing the detection limit due to the enhanced active surface and conductivity.
- SWCNTs have proven to be an excellent material for developing sensitive sensors, rendering the best results in SWASV and amperometry, with low detection limits.
- New artisanal AC has not reached the performances of SWCNTs, however it is comparable to commercial RGO, but much more cost-effective.
- Carbonaceous nanomaterials have demonstrated their ability to be good auxiliary materials for modified electrodes in detecting large organic molecules like dyes.

EXPERIMENTAL SECTION

CHEMICALS

All the chemicals used were analytical grade, used as received, without further purification. Phosphate buffer solution was made from $\text{NaH}_2\text{PO}_4 \cdot \text{H}_2\text{O}$ and Na_2HPO_4 salts and pH corrected with $\text{o-H}_3\text{PO}_4$ acid from Merck, Germany. Malachite Green oxalate salt was purchased from Penta, Czech Republic. MG solutions were made in phosphate buffer 0.1M. Sodium dodecyl sulphate (SDS) was acquired from Sigma, Switzerland. Nafion (perflourinated 5% alcoholic solution from Aldrich, Belgium) was diluted using pure ethanol to obtain lower concentrations.

Single-walled carbon nanotubes (SWCNTs) were obtained from Aldrich, USA and reduced graphene oxide (RGO) from Graphenea, Spain.

PREPARATION OF ACTIVATED CARBON

The activated carbon was obtained from *Abies nordmanniana* fir cone biomass [20] by chemical and physical activation. The fraction size chosen for treatment was (0.2-0.4 mm). Firstly, the fir cone biomass was mixed with a NaOH solution and left 72h for activation. Three different concentrations (5%, 10%, 20%) were tried to find an optimum. Thorough washing was needed to reach a neutral pH. Subsequently, physical activation in Ar at 750°C for 2 h took place, resulting in a finely granulated activated carbon.

PREPARATION OF THE MODIFIED ELECTRODE

First and foremost, the GC electrode was cleaned thoroughly by polishing on felt with alumina slurry until mirror-like shine was obtained. Further cleaning was realized in acetone and distilled water in an ultrasound bath to remove any traces of MG or impurities.

The working electrode was modified with single-walled carbon nanotubes (SWCNT), reduced graphene oxide (RGO) or activated carbon (AC). Suspensions in 1% sodium dodecyl sulphate (SDS) were made with all three materials in the same concentration of 0.011 mg/mL, which were applied by drop-casting and dried. A Nafion protective membrane was formed by evaporating 5 μ L 0.5% Nafion alcoholic solution.

ELECTROCHEMICAL MEASUREMENTS

All electrochemical experiments were performed on a Metrohm Autolab PGSTAT 302N, electrochemical workstation (Eco Chemie, Netherlands). A three-electrode system was used, equipped with a Ag/AgCl, KCl_{sat} electrode as reference, a platinum wire as counter-electrode and a bare (or modified) glassy carbon (GC) electrode as the working electrode. The electrolyte solution was 0.1M phosphate buffer, pH 3 adjusted with phosphoric acid. All experiments were performed at an ambient temperature of 25°C.

Square wave anodic stripping voltammetry (SWASV)

Square wave anodic stripping voltammetry experiments were performed in phosphate buffer solutions with various concentrations of MG. The potential was varied from 0.3V to 1.1V, at a frequency of 25Hz. Deposition time was established to be optimal at 300s, in open circuit, with 5s equilibration time before each measurement.

Amperometry

Batch amperometry was employed as a second method for measuring MG concentrations in aqueous solutions. Additions of 100 μ L MG stock

solution were made every precise number of seconds, under agitation at 200 rpm in a 10mL cell. The working potential was fixed at 0.85 V vs. Ag/AgCl/KCl_{sat}, value where MG peaks are very well contoured in SWASV voltammograms.

Electrochemical Impedance Spectroscopy

EIS experiments were performed in 0.1mol/L⁻¹ KCl solution containing 1mM Fe(CN)³⁻/Fe(CN)⁴⁻ at open circuit potential (OCP), in a frequency domain of 10⁻² – 10⁵ Hz.

ACKNOWLEDGMENTS

This work was supported by European Social Fund under the Human Resource Development Sectorial Operational Program 2007-2013, according to the 1st Priority axes, project title “Quality, excellence and mobility in transnational doctoral research” POSDRU/187/1.5/S/155383.

The authors thank Dr. Gabriel Katona from the Faculty of Chemistry and Chemical Engineering for TEM analysis.

REFERENCES

1. F. Chequer, G. Rodrigues de Oliveira, E. Ferraz, J. Cardoso, M. Zanoni, D. Palma de Oliveira, “Eco-Friendly Textile Dyeing and Finishing”, **2013**, InTech.
2. G. Booth, “Dyes, General Survey”, **2000**, Wiley-VCH.
3. M.T. Yagub, T.K. Sen, S. Afroze, H.M. Ang, *Advances in Colloid and Interface Science*, **2014**, 209: 172-184.
4. A. Hazrat, *Water, Air, & Soil Pollution*, **2010**, 213(1), 251.
5. P. Saravanan, P. Sivakumar, T. Suganya, N Nagendra, S. Renganathan, *Indian Journal of Environmental Protection*, **2012**, 32(3): 249.
6. Y. Sun, Y. Yin, J. Zhang, H. Yu, X. Wang, *Environmental Toxicology*, **2006**, 21(12): 256.
7. E. Daneshvar, M. Kousha, N. Koutahzadeh, M. Sohrabi, A. Bhatnagar, *Environmental Progress & Sustainable Energy*, **2013**, 32(2), 285.
8. A. Panandiker, C. Fernandes, K.Rao, *Cancer Letters*, **1992**, 67, 93.
9. S. Srivastava, R. Sinha, D. Roy, *Aquatic Toxicology*, **2004**, 66, 319.
10. G. Crini, *Bioresource Technology*, **2006**, 97(9), 1061-86.
11. F.H. Wu, G.C. Zhao, X.W. Wei, *Electrochemistry Communications*, **2002**, 4, 690.
12. L.M. Ochiai, D. Agustini, L. Figueiredo-Filho, C.E. Banks, L.H. Marcolino-Junior, M.F. Bergamini, *Sensors and Actuators B*, **2017**, 241: 978.
13. M. Zhou, Y. Zhai, S. Dong, *Analytical Chemistry*, **2009**, 81, 5603.

14. H. Liu, K. Guo, C. Duan, X. Dong, J. Gao, *Biosensors and Bioelectronics*, **2017**, 87, 473.
15. M. Mijanur-Rahman, M. Mollah, M. Muhibur-Rahman, A. Hasan-Susan, *Hindawi Publishing Corporation*, **2013**, Article ID 839498; doi.org/10.1155/2013/839498.
16. Z. Galus, R. N. Adams, *Journal of the American Chemical Society*, **1964**, 86, 1666.
17. A.M. Sacara, C. Cristea, L.M. Muresan, *Journal of Electroanalytical Chemistry*, **2017**, 792, 23.
18. G.I. Turdean, G. Szabo, *Food Chemistry*, **2015**, 179, 325.
19. ec.europa.eu/DocsRoom/documents/19163/attachments/1/.../pdf viewed in June, 2017
20. A.M. Săcară, C. Indolean, L.M. Mureșan, *Studia UBB Chemia*, **2016**, 61 (3),183.

In memory of prof. dr. Simion Gocan

THE ANALYSIS OF CONSTITUENT MATERIALS OF THE NAOS DOORS BELONGING TO THE WOODEN CHURCH FROM PETRINDU, SALAJ COUNTY

IOAN BRATU^a*, CONSTANTIN MARUTOIU^b*, DANA POSTOLACHE^c,
CLAUDIU TANASELIA^d, OLIVIA FLORENA NEMEȘ^b

ABSTRACT In order to preserve and restore the door that separate the Naos and Pronaos belonging to the wooden church of Petrindu, Salaj County, the scientific expertise (with FTIR, XRF spectroscopy and restoring) of the wooden stage and of the painting materials (ground, pigments) was performed. FTIR spectroscopy offers information about the wooden stage whereas XRF and FTIR spectroscopic methods were employed for structural painting materials characterization. These structural data can be correlated with the artistic, theological and historical analysis of this religious patrimony object. After obtaining information about wooden stage and the painting materials, the door was restored.

Keywords: *wooden church, painting materials, XRF and FTIR spectroscopy*

INTRODUCTION

The forested landscape of Salaj County contained various types of wood species. This made possible for the people to settle in those areas and to acquire the materials to build their homes and churches. The first

^a National Institute for R&D of Isotopic and Molecular Technologies, Cluj-Napoca, Romania

* Corresponding author ibratu@itim-cj.ro

^b Babeș-Bolyai University, Faculty of Orthodox Theology, Cluj-Napoca, Romania

^c University of Craiova, Faculty of Orthodox Theology, Romania

^d INCDO-INOE 2000 Research Institute for Analytical Instrumentation, Cluj-Napoca, Romania

documentary attestation of these localities dates from 1219 [1]. The Tartar and Ottoman invasions resulted in the disappearance of many wooden churches. More were destroyed by Christians like General Bucow (1760 – 1762) or by natural calamities. These adversities did not discourage the inhabitants who raised new churches replacing the destroyed ones. This is also the story of the Petrindu wooden church, Salaj County. The church was built in the Eighteenth century, and in 1965 was moved to the “Romulus Vuia” National Ethnographic Park from Cluj-Napoca [2, 3].

The identification of pigments, binders, varnishes or other materials employed in manuscripts, ceramics and other artefacts were recognized for long time as important in understanding our cultural heritage. The topic is an art-science border subject, being studied intensively by art historians, art curators and scientists involved in preservation and restoration belonging to those museums. Many techniques were employed for this purpose, among them several are specific for the chemical elements present in pigments, for the molecular groups. One speaks on the electronic microscopy (SEM), X-ray fluorescence (XRF), gas and liquid chromatography coupled with mass-spectrometry, Raman and IR spectroscopy, etc. [4, 5]. Petrindu wooden church has a door separating the narthex and nave (Fig.1). This is a less common occurrence in the wooden church architecture [3, 6].

Several Imperial Gates from various wooden churches and other religious objects were already investigated [7-10]. The aim of the paper is the scientific investigation of the painting materials and of the conservation state of the wooden backing (stand) of the gates that separate the Naos from Pronaos and belonging to the wooden church from Petrindu.



Figure 1. The door that separate the Naos and Pronaos belonging to the wooden church from Petrindu: a) before restoration b) after restoration

RESULTS AND DISCUSSION

XRF spectroscopic results

Based on the XRF data analysis presented in Table 1, one can propose the following composition of the painting materials employed: red door-Pb, Hg, As; yellow-As, Cu; red cloths-Fe, As; black-Fe, As; red frame-Pb=Hg> As; green- Cu, As; aura-As; green Dimitrie clothes-As, Fe.

Table 1. XRF data for the investigated gates Set II (2 segment doors)

Sample (door)	Fe mg/kg	Cu mg/kg	Zn mg/kg	As mg/kg	Hg mg/kg	Pb mg/kg
Red door Nave-Narthex (Left)	357	<LOD ^a	68	4104	16871	16871
Green (Left)	1324	19583	789	11865	227	227
Yellow clothing (Left)	1226	<LOD ^a	63	11041	<LOD ^a	<LOD ^a
White face (Left)	253	<LOD ^a	84	112	170	170
Red clothing (Left)	5852	76	97	9273	192	192
Black (Left)	1165	<LOD ^a	289	4689	76	76
Red casing (Left)	1420	<LOD ^a	1394	13603	73689	73689
Green (Right)	1571	21379	<LOD ^a	13709	201	201
Red (Right)	739	<LOD ^a	85	6963	31255	31255
White (Right)	504	<LOD ^a	<LOD ^a	137	302	302
Black (Right)	1389	32	<LOD ^a	232	343	343
Aura (Right)	976	<LOD ^a	<LOD ^a	5099	25	25
Red Saint George (Right)	1215	<LOD ^a	72	4560	21668	21668
Green clothing Dimitrie (Right)	1813	<LOD ^a	<LOD ^a	9417	23	23
Red casing (Right)	1023	<LOD ^a	75	5033	22678	22678

^a LOD limit of detection <20%

FTIR spectroscopy results

FTIR data obtained for the painting and of the wooden materials are presented in the Figures 2-3.

The significance of the painting materials is given in Table 1.

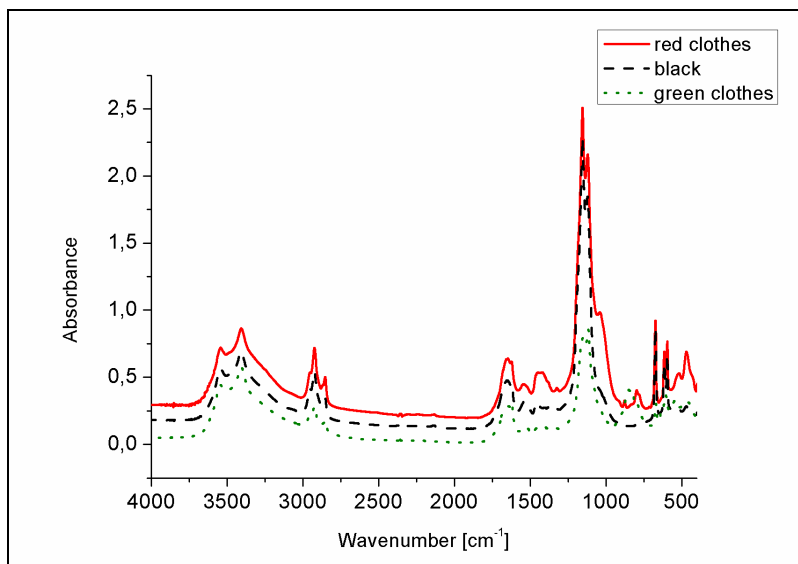


Figure 2. FTIR spectra of the painting materials, 4000-400 cm^{-1} spectral domain

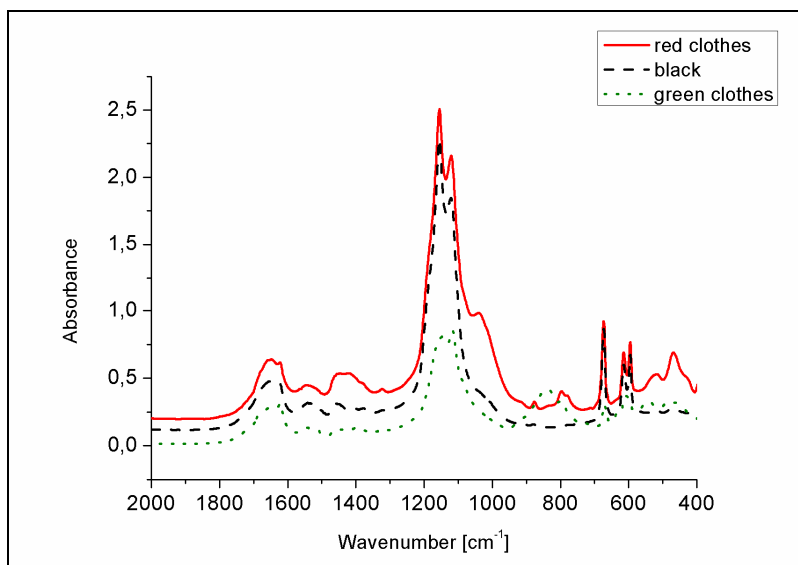


Figure 3. FTIR spectra of the painting materials, 2000-400 cm^{-1} spectral domain

Composition, deduced from FTIR spectra analysis: red lead (470 and 517 cm^{-1}), gypsum (3543 , 3406 , 1623 , 1422 , 1155 , 1120 , 644 and 595 cm^{-1}), traces of carbonate (~ 1422 and 877 cm^{-1}), aliphatics (2953 cm^{-1} -methyl, 2924 and 2854 cm^{-1} -methylene), proteins (1648 , 1541 , 1323 cm^{-1}), carbon black. Fig. 4 presents FTIR spectra of different wooden stages.

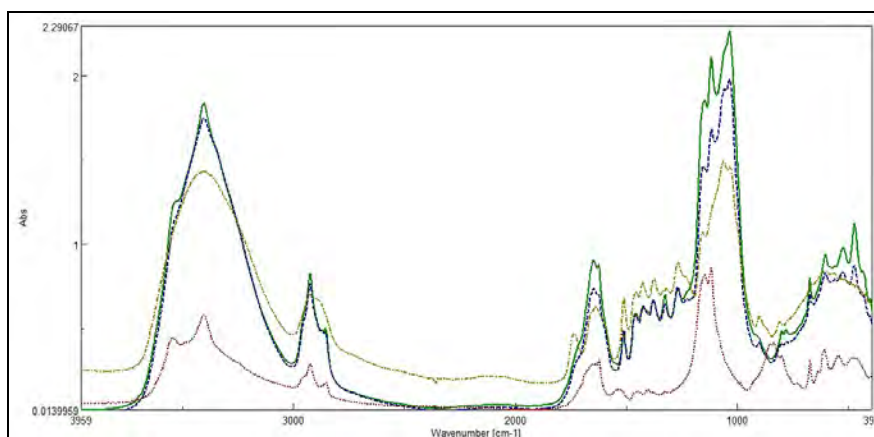


Figure 4. FTIR spectra of door's wood (continuous line), of back wood (dash line), of green St George cloth (dot line) and of fir wood (dash-dot line)

One can conclude that fir wood was employed for these doors. A report of the wood conservation state is presented in Table 2.

Table 2. Wood conservation state

Sample	l_{cr}^1	TCI	$(L/C)_1$	$(L/C)_3$
Nave / narthex wood	0.83	0.81	1.53	1.11
Back side wood	0.99	0.87	1.80	1.19
Modern fir wood	1.03	1.32	1.47	1.19

The crystallinity decreases for historical wood as compared to modern one (see for example the l_{cr}^1 and TCI factors in Table 2). The

cellulose content decreased in time as compared to lignin one if we compare the $(L/C)_1$ si $(L/C)_3$ ratios. If we see the background wood, its crystallinity decreased more rapidly in time (see the l^{1cr} and TCI ratios), whereas the $(L/C)_1$ increased in time due to a more rapid cellulose consumption than the lignin one.

The wooden assembly after restoration

The wooden assembly after restoration is presented in **Figure 1b**. The methodological approach was established and implemented in conformity with the scientific conservation-restoration principles, original technique, and state of conservation and the results of preliminary research, which was constituted by a set of interventions: gap filling of the support, consolidation of the paintings' layers, removal of dirt deposits, chromatic integration and final coating.

CONCLUSIONS

N-P doors are made from fir wood and the following painting materials were employed: red-red lead, Cinnabar, iron red and red arsenic; yellow-orpiment; black-iron arsenic; green-copper, calcium carbonate, gypsum, proteins.

The conservation-restoration methodology rendered the aesthetic unity of the painted wooden doors; the interventions were based on the minimum intervention principle as well as the interventions on the interior mural paintings (*distemper paint*) of the wooden church. By consolidation interventions, the cohesion of the painting layers with all its qualities were recovered, respectively the elasticity and flatness parameters. The original aesthetic imagery was recovered by the interventions of dirt deposits removal and the image disruptions caused by the extended lacunae and erosions were altered by means of chromatic retouching of the erosions.

EXPERIMENTAL SECTION

The door that separated the two chambers is made from two wooden pieces anchored by the wall using hinges (Fig. 2). The doors are painted by Dimitri Ispas from Gilau and each door is divided in two scenes, each portraying a saint. The door to the right measures 146 by 41.5 cm and portrays Saint George and Saint Dimitrie. The door to the left measures 146 by 40 cm and portrays Saint Martyr Nestor and Saint Martyr Lup. The painting was executed in Tempera on wood.

X-ray fluorescence measurements were performed *in situ* using an INNOV-X Alpha-6500 portable instrument (35 kV voltage, 15 μ A intensity, 3 mm filter, Be window, 2 square mm spot size and PIN Si detector). Integration time was set to 60 seconds, in two consecutive runs of 30 seconds each. FTIR measurements were done with a JASCO 6100 spectrometer in the 4000 to 400 cm^{-1} spectral range with a resolution of 4 cm^{-1} employing the KBr pellet technique-

Wood preservation status

In order to determine the preservation status of the Imperial Gates' wood, several indexes are defined [11]: $I_{cr}^1 = A_{1377}/A_{669}$, or as TCI = A_{1378}/A_{2925} (Total Crystallinity Index) and LOI = A_{1426}/A_{895} (Lateral Order Index), A being the absorbance at maximum for each absorption band. The lignin/cellulose ratios, defined as [12] $(L/C)_1 = A_{1506}/A_{1738}$ and $(L/C)_3 = A_{1506}/A_{895}$ were calculated for wooden samples in agreement to these definitions. They can be used only as a measure of their evolution in time.

For an optimal methodological approach of the restoration of the wooden painted doors, consolidation and cleaning preliminary tests were done. Consequently, the consolidation of the painted layer was done using the aqueous solution of fish glue, in a very poor concentration, which rendered best the cohesion of the painting layers. The removal of dirt deposits was done by the use of tested solvent mixtures and mechanically with a surgical scalpel, both on the verso and recto of the doors. Chromatic attenuation of the erosions and lacunae was done using *rittocco* and *velatura techniques* with water-based colours. In the end, the whole painted surface was coated by a protective thin layer, which also has an important aesthetic role in controlling the glossiness of the painting.

DISCLOSURE

I. Bratu and C. Marutoiu are co-first authors

ACKNOWLEDGMENTS

Thanks are due to UEFISCDI for financial supporting on PN II-PT-PCCA-2013-4-1882 project

REFERENCES

1. Nicolae Iorga, *Istoria bisericii românești și a vieții religioase a românilor*, vol. I, cap. III, „Cele d'întaiu biserici romanesti”, Tipografia „Neamul Românesc”, Vălenii-de-Munte, **1908**.
2. Ioana Cristache-Panait, „Bisericile de lemn din Sălaj”. *Buletinul Monumentelor Istorice* **1971**, 1, 31.
3. Leontin Ghergariu, „Meșterii construcțiilor monumentale de lemn din Sălaj”. *Anuarul Muzeului Etnografic al Transilvaniei*, editia **1971-1973**: 255-273, Cluj.
4. L. Burgio, R.J.H. Clark, L. Sheldon, G.D. Smith, *Analytical Chemistry* **2005**, 77, 1261.
5. Andreotti, L. Bonaduce, M.P. Colombini, G. Gautier, F. Modugno, E. Ribechini, *Analytical Chemistry*, **2006**, 78, 4490.
6. Ioan Godea, Ioana Cristache-Panait, Monumente istorice bisericesti din Eparhia Oradei, judetele Bihor, Salaj si Satu-Mare. Bisericile de lemn, Ed. Episcopiei Ortodoxe Romane a Oradei, Oradea, **1978**
7. Măruțoiu, I. Bratu, L. Troșan, C. Neamtu, V.C. Măruțoiu, D. Pop, C. Tănăselia, S. Garabagiu, *Spectrochim Acta A, Molecular and Biomolecular Spectroscopy*, **2016**, 152, 311.
8. Măruțoiu, I. Bratu, A.M. Budu, Gh. Șanta, O. F. Măruțoiu, C. Neamțu, C. Tănăselia, I. Kacso, I. C. A. Sandu, *Revista de Chimie*, **2015**, 66 (7) 992.
9. Măruțoiu, L. Troșan, V-D. Toader, Z. Moldovan, Al. I. Turza, C. Tănăselia and I. Bratu, *Studia UBB Chemia.*, **2013**, 58 (4), 161.
10. Hernanz, I. Bratu, O.F. Măruțoiu, C. Măruțoiu, J. M. Gavira-Vallejo, H.C.M. Edwards, *Analytical and Bioanalytical Chemistry*, **2008**, 392, 1-2. 263.
11. M. Popescu, Y. Sakara, M. C. Popescu, A. Osaka and C. Vasile, *e-Preservation Science*, **2005**, 2, 19.
12. C.M., Popescu, M.C Popescu, C Vasile, *International Journal of Biological Macromolecules*, **2011**, 48(4), p.667.

In memory of prof. dr. Simion Gocan

INFLUENCE OF THE COBALT NITRATE:ETHYLENE GLYCOL MOLAR RATIO ON THE FORMATION OF CARBOXYLATE PRECURSORS AND COBALT OXIDES

THOMAS DIPPONG^a, FIRUTA GOGA^{b*}, ALEXANDRA AVRAM^b

ABSTRACT This paper focuses on the obtaining of carboxylate precursors through the redox reaction of cobalt nitrate and ethylene glycol, in different stoichiometric ratios, as well as the decomposition of precursors into cobalt oxides. The influence of the $\text{NO}_3^-:\text{C}_2\text{H}_6\text{O}_2$ stoichiometric ratio on the formation of the precursors is studied through thermal analysis, FTIR spectroscopy and acido-basic analysis (conductometric/potentiometric titrimetry). Phase analysis by XRD and FTIR of the powders obtained at the decomposition of the precursors at 400°C has evidenced the formation of CoO for a high $\text{NO}_3^-:\text{C}_2\text{H}_6\text{O}_2$ synthesis ratio and of Co_3O_4 for a low $\text{NO}_3^-:\text{C}_2\text{H}_6\text{O}_2$ ratio. The Scherrer equation and scanning electron microscopy (SEM) were used to determine the dimensions of the nanoparticles obtained.

Keywords: *carboxylate precursors, cobalt oxide, acido-basic titration*

INTRODUCTION

Nanomaterials have been the subject of intense research due to their many fascinating properties that are not attainable by bulk materials. Due to their exceptional attributes and reduced dimensions, they can be exploited in a large range of fields [1].

^a Technical University of Cluj-Napoca, Faculty of Sciences North University Center at Baia Mare, 76 Victoriei Street, 430122 Baia Mare, Romania.

^b Babeş-Bolyai University, Faculty of Chemistry and Chemical Engineering, 11 Arany Janos Street, RO-400028, Cluj-Napoca, Romania.

* Corresponding author: firutagoga@yahoo.com

Cobalt oxides are important materials with a wide array of applications, such as, catalysts [2, 3, 4, 5, 6], different kind of sensors [7, 2, 4, 5], lithium ion batteries [8,7, 5], optoelectronic devices [9,10], combustion of hydrocarbons at gas purification [11], supercapacitors [12,13], Fisher-Tropsh syntheses [14] and biomedical sciences [1,7,12]. Cobalt oxides obtained as nanoparticles present a particular interest due to their different properties compared to the bulk material. Obtaining methods for the cobalt oxid nanoparticles Co_xO_y are mentioned in scientific literature: the pyrolytic process [15], the combustion method [16, 17, 18, 4], the mechanico-chemical method [19], the hydrothermal method [4], pyrolytic spraying technique [20, 6], photochemical synthesis [21], sonochemical synthesis [13] etc.

In this paper we are following to obtain cobalt oxide nanoparticles through the decomposition of some carboxylate type complex combinations resulted in the redox reaction between $\text{Co}(\text{NO}_3)_2 \cdot 6\text{H}_2\text{O}$ and $\text{C}_2\text{H}_6\text{O}_2$. The influence of the $\text{NO}_3^- : \text{C}_2\text{H}_6\text{O}_2$ molar ratio on the formation of the oxidation products, precursors of cobalt oxides, and on the composition of the oxide system Co_xO_y obtained by thermal decomposition of the precursors has been studied. For the characterization of the precursors thermal analysis, FTIR spectrometry, XRD, SEM and acidic-basic titrations were employed.

RESULTS AND DISCUSSION

This paper studies the redox reaction between $\text{Co}(\text{NO}_3)_2$ and ethylene glycol, at different $\text{NO}_3^- : \text{C}_2\text{H}_6\text{O}_2$ molar ratios: 4:1 (sample D₁), 2:1 (sample D₂), 1.33:1 (sample D₃) and 1:1 (sample D₄).

The progress of the $\text{NO}_3^- - \text{C}_2\text{H}_6\text{O}_2$ redox reaction in all cases (D₁ – D₄) was followed with a thermal analysis. The cobalt nitrate – ethylene glycol solutions were submitted to a thin layer deposition on platinum trays and heated in air up to 500°C. Figure 1 presents the TG and DTA curves obtained for samples: D₁, D₂, D₃ and D₄. TG curves register two distinct mass loss steps, the first one, going up to 120 °C, is attributed to the decomposition of $\text{Co}(\text{NO}_3)_2$ and the volatilization of crystallization water. The second step, in between 200 and 260 °C, is attributed to the oxidative decomposition of the formed complex combination. This decomposition develops with a high speed in a short amount of time, generating a *in situ* reductive atmosphere that induces the reduction of Co(II) to metallic Co. Metallic Co further reoxidates to a weak crystallized oxide with increased reactivity [22].

The TG curve shows that the glyoxylate forming stoichiometric sample presents the lowest mass loss, whereas the glycolate forming stoichiometric sample presents the highest mass loss.

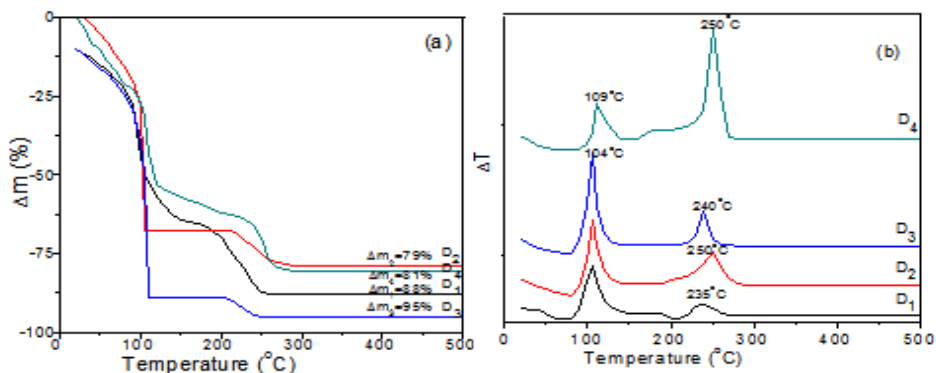


Figure 1. Thermogravimetric curves for D₁÷D₄ (a) TG and (b) DTA

From the evolution of the DTA curves it can be observed that in all cases, regardless of the $\text{Co}(\text{NO}_3)_2 - \text{C}_2\text{H}_6\text{O}_2$ molar ratio, two exothermic effects are registered, corresponding to mass losses on the TG curve. The first such effect, with a maximum between 104-110°C corresponds to the $\text{NO}_3^- - \text{C}_2\text{H}_6\text{O}_2$ redox reaction, with the formation of compounds (Co (II) combinations with ethyleneoxide oxidation products). The second effect, with a maximum between 235-250°C, corresponds to the oxidative decomposition of the formed compounds. Following the thermal analysis data, it was established that the optimal synthesis temperature of these compounds is 130°C.

The purified products were analysed by FTIR spectrometry. Figure 2 presents the FTIR spectra for samples D₁÷D₄, obtained at 140°C and 300°C. The FTIR spectrum for D₁ obtained at 140°C presents bands that are characteristic to $(\text{NO}_3)^-$ vibrations (1384 cm^{-1}), showing that for this sample, the carboxylate precursor was not completely formed. The FTIR study of the precursors has evidenced the presence, in all four cases, of the characteristic vibrations of carboxylate groups: $\nu_{\text{as}}(\text{COO}^-)$ at $1646\text{-}1588 \text{ cm}^{-1}$ and $\nu_{\text{s}}(\text{OCO})$ at $1316\text{-}1352 \text{ cm}^{-1}$ [23]. The OH bonds in the carboxylate precursors are associated with the $3380\text{-}3410 \text{ cm}^{-1}$ and $881\text{-}790 \text{ cm}^{-1}$ wavelenght numbers [23] respectively. The vibrations of the C-O bonds are also identified at $1063\text{-}1065 \text{ cm}^{-1}$ [10]. For samples D₁ and D₂ bands corresponding the Co-O bond can be observed at 490 cm^{-1} [10]. The FTIR spectra for samples D₃ and D₄, thermally treated at 300°C, do not show any bands characteristic to cobalt carboxylates. Samples D₁ and D₂ show traces of these bands at 1360 cm^{-1} , attributed to the thermal decomposition and the formation of the metallic oxide. All samples evidentiare intense bands at 663 cm^{-1} and 570 cm^{-1} , corresponding to the vibration of the Co-O bond.

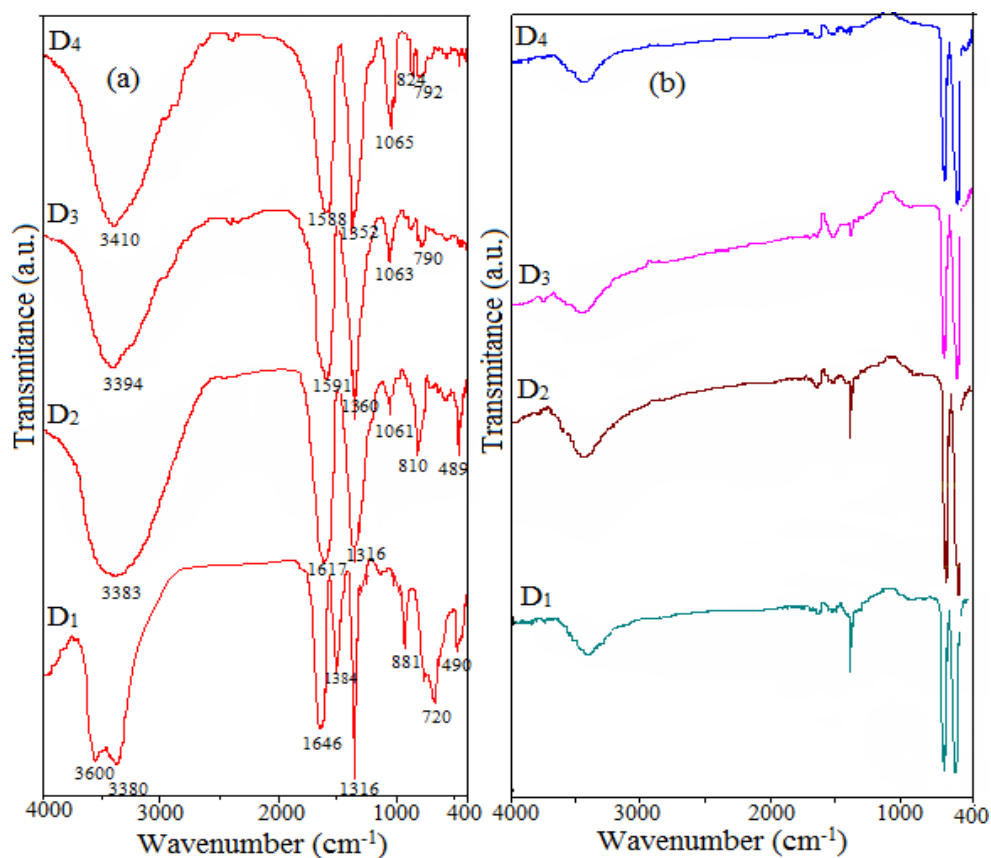


Figure 2. FTIR spectra of samples D1÷D4 at a)140°C and b) 300°C

Factoring in the reactants' ratio and the reaction conditions, the ethylene glycol oxidation can produce cobalt oxalate (CoC_2O_4), cobalt glyoxylate ($\text{Co}(\text{CHOHCOO})_2$), or a mixture of the both (the acido-oxalate form is excluded). The cobalt (II) may occur in neutral form Co^{2+} , hydrolyzed (CoOH^+), as a hydroxide $\text{Co}(\text{OH})_2$, or as a mixture.

For the study of the acido-basic properties, the 4 compounds, D₁-D₄, were treated with a 0,1M HCl solution. It was observed that they have different solubilities. Samples D₃ and D₄ solubilize completely, whereas samples D₁ and D₂ solubilize partially. The insoluble phase was filtered, washed, and submitted to a FTIR analysis. The FTIR spectra (Figure 3) of samples D₁ and D₂ evidences vibration bands typical to cobalt oxalate (1620 cm^{-1} , 1360 cm^{-1} , 1320 cm^{-1} , 820 cm^{-1} , 480 cm^{-1}) [17].

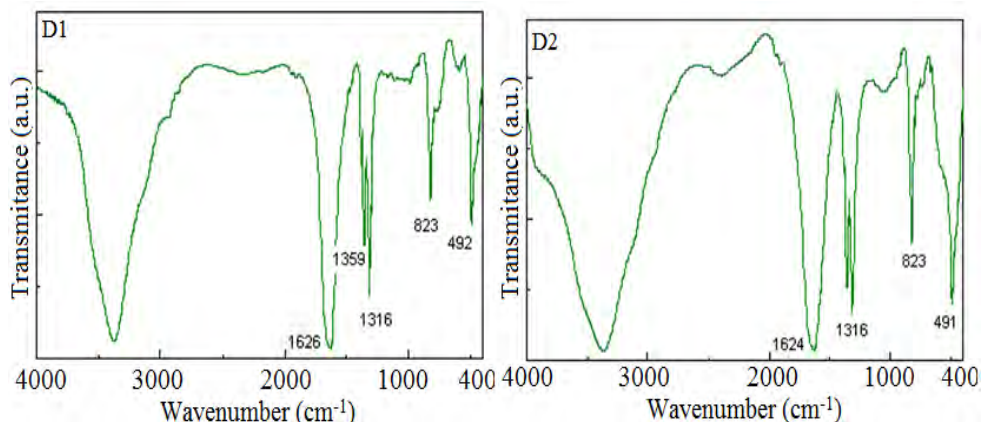
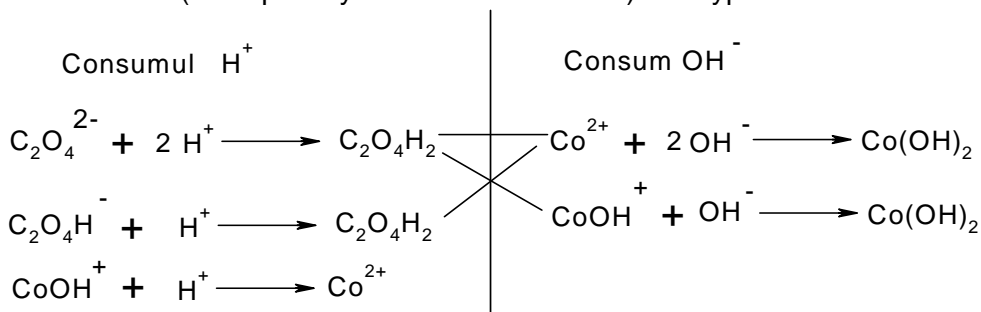


Figure 3. FTIR spectra of the HCl insoluble components of precursors D₁ and D₂

Furthering the supposition that samples D₁ and D₂ produce oxalates, the acido-basic properties of these compounds were focussed on. These can be determined by the ratio of HCl mols consumed while dissolving and protonation of the precursors and the NaOH mols consumed for the Co(OH)₂ precipitation. The following reactions, establishing the H⁺/HO⁻ ratios (acid quantity and consumed base) are hypothesized:



Scheme 1. The processes which may occur when the precursor was treated with HCl (left) and NaOH (right)

From the presented reactions one can calculate the theoretical ratio $r = \text{moles of HCl} / \text{moles of NaOH}$ for the different possible species: CoC₂O₄ ($r = 1/1$), [Co(OH)]₂C₂O₄ ($r = 2/1$) or Co(HC₂O₄)₂ ($r = 1/2$).

Figure 4 presents the conductometric curves for D1-D4.

On the titration curves in Figure 4, two sets of data can be observed, the first corresponding to the 'standard' titration, HCl with NaOH, formed by 2 lines with a single equivalence volume at ~ 10 cm³. The second set corresponds to the (sample + HCl) NaOH titration, the

conductometric, curve being formed by 3 lines with 2 equivalence volumes. The lines were evidenced between the mean conductance points, corrected with the dilution volume (100 cm³). Each graph contains a titration curve of the analyzed compound and a titration reference for the 2 reactants (acid/base). There are 2 equivalence points for the sample, namely V_{e1}, V_{e2}, and one for the reference, V_{eR}.

On the pH metric curves (Figure 5), 2 sets of data are also observed. The first set corresponds to the HCl-NaOH reference, with a single saltation with the equivalence volume around 10 cm³. The second set corresponds to the (sample + HCl) NaOH titration, presenting 2 pH saltations consistent with the 2 equivalence volumes.

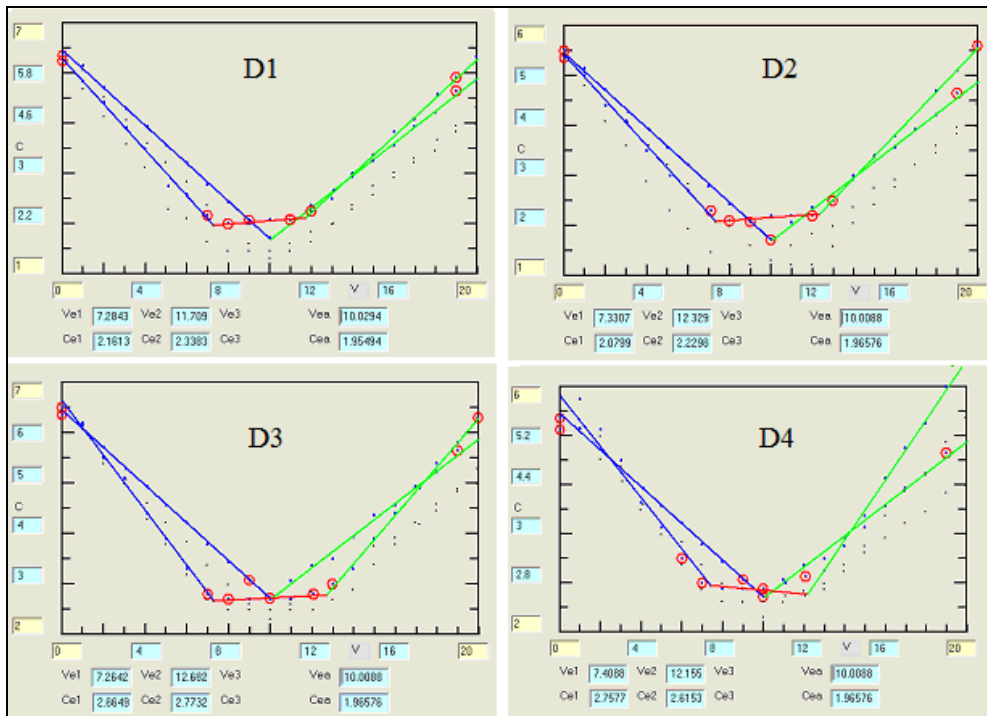


Figure 4. The conductometric titration curves for the HCl titration with NaOH and the titration of samples D₁-D₄ with NaOH in HCl

The 3 sets of data from the conductometric titration were statistically processed. For calculating the acid/ base consumption, the $R \pm sR = (VeR \pm sVeR) - (Ve1 \pm sVe1) / (Ve2 \pm sVe2) - (VeR \pm sVeR)$ formula is applied. Table 1 presents the acid/ base consumption ratios that resulted from the acido-basic titrations, for all 4 analysed samples.

The ratio of the acid consumption/ base consumption for sample D₁ differs from the rest of the samples. This corresponds to the fact that a mixture of basic oxalate and neutral oxalate is obtained. The formation of these 2 cobalt oxalates is explained by the existence of the metal ion MeOH^+ in equilibrium. At a certain pH level, hydrolysed metal ions appear in equilibrium, and if the solubility of the 2 oxalates are approximately the same, both oxalates will precipitate.

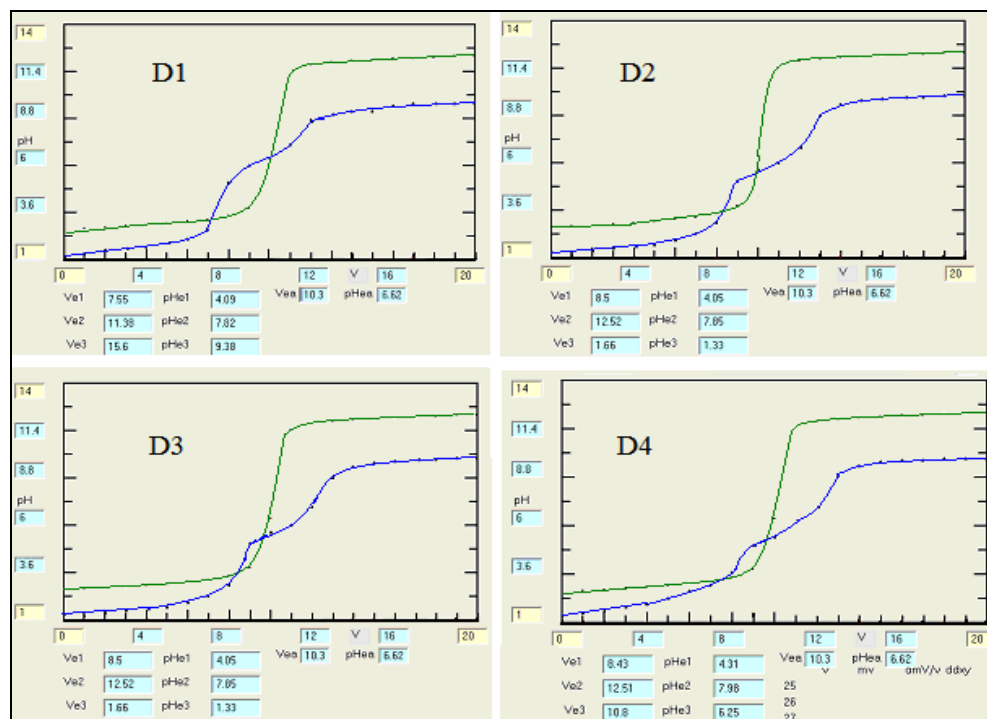


Figure 5. Potentiometric titration curves for the HCl – NaOH titration (green), and the NaOH titration of D₁-D₄ samples in HCl (blue)

Table 1. The acido-basic species formed during the conductometric and pH metric titrations

Sample	Conductometry ratio formed species	pH-metry ratio formed species
D1	1,8± 0.3 oxalate basic oxalate	1,6± 0.3 oxalate basic oxalate
D2	1,1± 0.3 oxalate	1,1± 0.3 oxalate
D3	1,0± 0.1 glyoxylate	1,0± 0.3glyoxylate
D4	1,2± 0.2 glyoxylate	1,0± 0.3 glyoxylate

The mixture of the 2 oxalates will lead to a ratio between 1-2. The basic oxalate forms through the the partial hydrolization of the metal ion resulted from the oxidation process, leading to more acid being consumed than base. In the case of sample D₂, considering that the acid/ base ratio is close to 1:1, only neutral oxalate is formed. At Co(NO₃)₂/C₂O₂H₆ ratios that differ from 4/3, mixtures of neutral oxalate salts and cobalt glyoxylate will result, in different ratios. At an excess of diol, only cobalt glyoxylate will result.

The acido-basic properties of the synthetised compounds correspond to the thermal analysis and FTIR spectra, confirming that carboxylate and hidro-carboxylate precursors are formed in the redox reaction, coordinating Co(II) ions in different acidic or basic compounds.

After the clarification of the precursor's nature, of the decomposition and thermal treatment conditions, the ways in which CoO and Co₃O₄ can be obtained as single phases are being followed.

D₁-D₂ precursors were thermally treated in air at 300°C for 2h, obtaining single oxide phases (CoO, Co₃O₄) or a mixture comprised of the two. Figure 6 presents the XRD spectra for samples D₂ and D₄, thermally treated at 300, 400 și 700°C for 3h. Following the decomposition (20°C/min) and the thermal treatment of D₂ at 300 și 400°C, CoO is obtained as a single, crystalline phase (JCPDS chart 75-0393 [24,25]). If the thermal treatment goes to 700°C, it is observed that CoO oxidises to Co₃O₄ (Figure 6a). For precursor D₄, following the same heating pattern, it is evidenced that, at 300°C, a mixture of CoO și Co₃O₄ is formed, a mixture that at 400 și 700°C oxidizes into a single Co₃O₄ phase(JCPDS chart 42-1467 [24]).

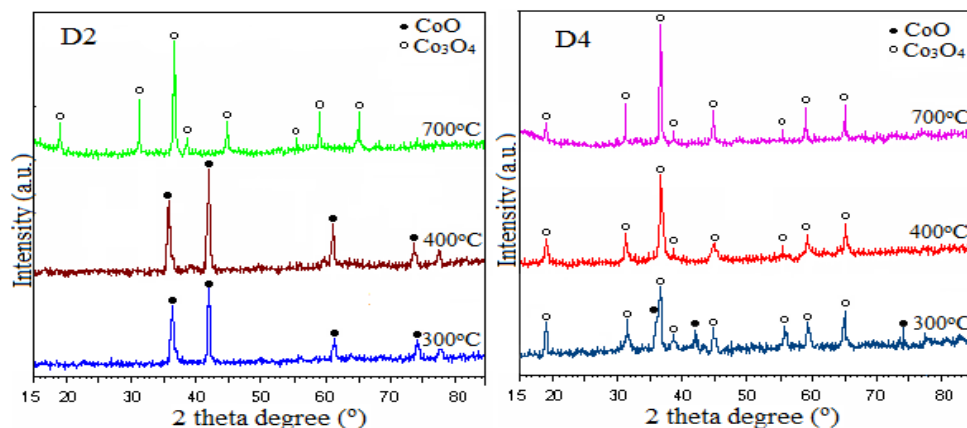


Figure 6. XRD spectra for samples D₂ and D₄ calcined at 300, 400 and 700°C for 3h

If the $\text{Co}(\text{NO}_3)_2 - \text{C}_2\text{H}_6\text{O}_2$ solutions are directly heated to a high temperature, a strongly exothermic redox reaction occurs, leading to the formation of a complex combination with an abundant release of nitrogen oxides. A thermal decomposition of this complex combination (auto combustion, reductive atmosphere) then follows. The obtained residue contains CoO as a single phase, regardless of the utilised precursor [22]. The median diameter of the crystallites were calculated from the XRD data for the samples calcined at 400 și 700°C using the Scherrer equation [26].

The average crystallite size was calculated from the XRD data using Debye-Scherrer formula [26]:

$$D_{XRD} = \frac{C \lambda}{\beta_{1/2} \cos \theta} \quad (1)$$

where D is the average crystallite size, $\beta_{1/2}$ is the broadening of full width at half maximum intensity (FWHM) of the main intense peak (311) in radian, $C=0.9$ for spherical particles θ is the Bragg angle, λ is the X-ray wavelength. At 400°C, the cobalt oxide crystallite diameter is 18,4 nm pentru D_2 și 19,1 nm pentru D_4 , whereas at 700°C, it is 27,7 nm for sample D_2 and 28,1 nm for D_4 . The cobalt oxide nanocrystallite diameter grows with a rise in temperature.

The SEM images for precursor D_4 , thermally treated at 400 and 700°C (Figure 7), show an agglomeration of nanoparticles into micrometric aggregates.

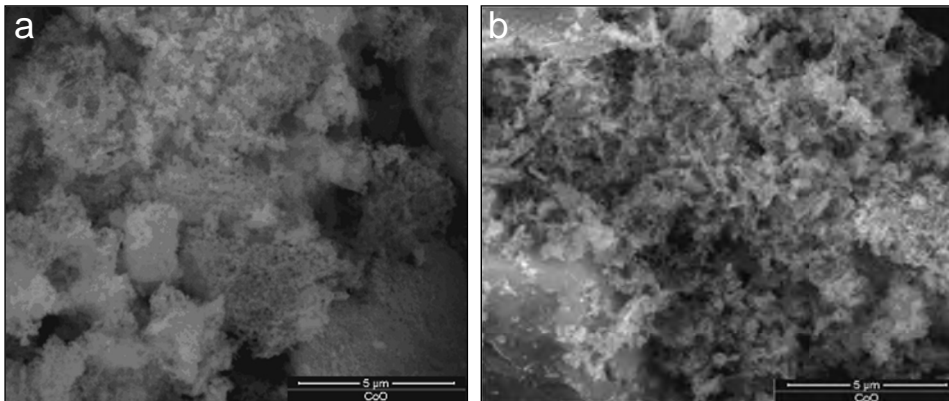


Figure 7. SEM images for precursor D_4 thermally treated at: (a) 400°C and (b) 700°C

CONCLUSIONS

This study highlights the formation of some carboxylate or hydro carboxylate complexes, through the redox reaction between $\text{Co}(\text{NO}_3)_2$ and diol. According to the utilized NO_3^- : ethyleneglycol molar ratio and the nature of the diol, single compounds or compound mixtures were obtained. The metal-organic precursor thermal decomposition method has the advantage of working at a low temperature, a temperature at which the precursors are thermally decomposed, leading to low crystallization oxide compounds. These compounds are highly reactive, being able to lead to the formation of crystallized CoO systems following further thermal treatments. FTIR analysis and the acido-basic studies have confirmed the formation of carboxylate and hydrocarboxylate compounds, single phased or in a combination. Electrometric titrations have also the advantage of automation, increasing the analysis throughput and securing the consistent quality of the results. Regardless of the nature of the precursor, the decomposition occurs up to 300°C , generating a reductive atmosphere according to the nature of the precursor. During the thermal decomposition of the precursors, the reductive atmosphere leads to redox processes $\text{Co}(\text{II}) \rightarrow \text{Co}(0) \rightarrow \text{CoO}$ or Co_3O_4 , which stabilize into a single phase. The XRD diffraction spectra showed that CoO, Co_3O_4 are obtained in either a single phase or a combination, according to the thermal treatment and nature of the precursor. The CoO and Co_3O_4 crystallite median diameter calculation shows that, with the synthesis conditions and thermal treatment, cobalt oxide nanoparticles up to 30 nm in diameter are obtained.

EXPERIMENTAL SECTION

The reagents used in synthesis were: $\text{Co}(\text{NO}_3)_2 \cdot 6\text{H}_2\text{O}$ and ethylene glycol ($\text{EG} = \text{C}_2\text{H}_6\text{O}_2$) of purity p.a. (Merk). In the redox reaction between ethylene glycol and metallic nitrates, ethylene glycol ($\text{C}_2\text{H}_6\text{O}_2$) may be oxidized by NO_3^- ions to carboxylate anions (oxalate, glyoxylate, glycolate), according to the equations (1) ÷ (3), with the corresponding NO_3^- : $\text{C}_2\text{H}_6\text{O}_2$ molar ratios:

- 1) $3\text{C}_2\text{H}_4(\text{OH})_2 + 8\text{NO}_3^- + 2\text{H}^+ \rightarrow 3\text{C}_2\text{O}_4^{2-} + 8\text{NO} + 10\text{H}_2\text{O} \rightarrow \text{EG} : \text{NO}_3^- = 1 : 2,67$
oxalate anion
- 2) $\text{C}_2\text{H}_4(\text{OH})_2 + 2\text{NO}_3^- + \text{H}^+ \rightarrow \text{C}_2\text{H}_3\text{O}_4^- + 2\text{NO} + 2\text{H}_2\text{O} \rightarrow \text{EG} : \text{NO}_3^- = 1 : 2$
glyoxylate anion
- 3) $3\text{C}_2\text{H}_4(\text{OH})_2 + 4\text{NO}_3^- + \text{H}^+ \rightarrow 3\text{C}_2\text{H}_3\text{O}_3^- + 4\text{NO} + 5\text{H}_2\text{O} \rightarrow \text{EG} : \text{NO}_3^- = 1 : 1.33$
glycolate anion

There were prepared 4 samples with different molar ratios (NO_3^- : EG), as presented in Table 2.

Table 2. Sample preparation correlated to the NO_3^- :EG molar ratio and 1-3 equations

Sample	Mol no. NO_3^-	Mol no. EG	Correlated to reaction 1	Correlated to reaction 2	Correlated to reaction 3
D ₁	4	1	exces NO_3^- :1.33	Exces NO_3^- :2.0	exces NO_3^- :2.67
D ₂	2	1	exces EG:0.25	stoichiometric	exces NO_3^- :0.67
D ₃	1.33	1	exces EG:0.50	exces EG:0.34	stoichiometric
D ₄	1	1	exces EG:0.62	exces EG:0.5	exces EG:0.25

The synthesis method consists in dissolving cobalt nitrate in the corresponding EG amount followed by controlled heating at temperatures higher than 100°C. At these temperatures, the redox reaction starts accompanied by nitrogen oxid emission (brown-reddish gas).

The redox reaction initiation temperature is around 140°C, the reaction being energetic, an important actor being the catalytic role of cobalt. According to the molar ratio (NO_3^- : EG), the reaction can be more or less controlled, leading to a reaction product that is hard to isolate (it presents a high combustion tendency) . The reaction compounds were maintained at a 140°C temperature until the cessation in the release of brown gas (NO_x) (end of the reaction).

The obtained powders were milled and washed in acetone to remove any reactant excess. The obtained products were characterised through thermal analysis, FTIR spectrometry and acido-basic titrations (conductometric and pH-metric).

For the conductometric and potentiometric titrations, 0,2 mmols of Co(II) were used, with and addition of 10,0 cm³ HCl 0.1M. The conductometric and potentiometric titrations were carried out with NaOH 0.1M.

The obtained nanocomposites were analyzed by thermogravimetry (TG), derivative thermogravimetry (DTG) and differential thermal analysis (DTA) using a SDT Q600 type instrument. The analysis was carried out in air, up to 1000°C at 10 °C min⁻¹ using alumina standards.

The FTIR spectra were recorded on 1% KBr pellets using a Spectrum BX II spectrometer.

The XRD patterns were recorded using a high resolution Bruker D8 Advance diffractometer with Cu K α 1 ($\lambda_{\text{CuK}\alpha 1}$ =1,54056 Å) radiation.

The nanoparticle size was determined by transmission electron microscopy (TEM) using a Jeol JEM1010 with a resolution of 0.35 nm, equipped with a digital image recording system, a photographic film image recording system and a high resolution scanner.

The acido-basic properties of the precursors were studied through acido-basic titrations, conductometric and pH-metric, using a Crison MM41 multimeter.

REFERENCES

1. S.M. Ansari, R.D. Bhor, K.R. Pai, D. Sen, S. Mazumder, K. Ghosh, Y.D. Kolekar, *Applied Surface Science*, **2017**, 414, 171.
2. B.M. Mogudi, P. Ncube, R. Meijboom, *Applied Catalysis B: Environmental*, **2016**, 198, 74.
3. M.M. Durano, A.H. Tamboli, H. Kim, *Colloids and Surfaces A: Physicochemical and Engineering Aspects*, **2017**, 520, 355.
4. S. Harish, K. Silambarasan, G. Kalaiyarasan, A.V.N. Kumar, J. Joseph, *Material Letters*, **2016**, 165, 115.
5. J.M. Xu, J. Zhang, B.B. Wang, F. Liu, *Journal of Alloys and Compounds*, **2015**, 619, 361.
6. R.F. Klein Gunnewiek, C. Floriano Mendes, R.H. Goldschmidt Aliaga Kiminami, *Advanced Powder Technology*, **2016**, 27, 1056.
7. A. Ashok, A. Kumar, R.R. Bhosale, M.A.H. Saleh, U.K. Ghosh, M. Al-Marri, F.A. Almomani, M.M. Khader, *Ceramics International*, **2016**, 42, 12771.
8. S. Sun, X. Zhao, M. Yang, L. Ma, X. Shen, *Nanomaterials*, **2015**, 5, 2335-2347.
9. H.K. Lin.,H.C Chiu,H.C.Tsai,S.H.Chien,C.B. Wang, *Catalysis Letters* **2003**, 88, 3.
10. R.V. Narayan, V. Kanniah A. Dhathathreyan, *Journal of Chemical Sciences*, **2006**, 118:2, 179.
11. A.M. Garrido Pedrosa, M.J.B. Souza, D.M.A. Melo, A.S. Araujo, L.B. Zinner, J.D.G. Fernandes, A.E. Martinelli, *Solid State Sciences*, **2003**, 5, 725.
12. M. Pang, G. Long, S. Jiang, Y. Li, W. Han, B. Wang, X. Liu, Y. Xi, D. Wang, F. Xu, *Chemical Engineering Journal*, **2015**, 280, 377.
13. M. Montazerozohori, A. Masoudiasl, S. Farokhiyani, S. Joohari, P. McArdle, *Ultrasonic Sonochemistry*, **2017**, 38, 134.
14. F. Grillo, M.M. Natile, A. Glisenti, *Applied Catalysis B: Environmental*, **2004**, 48, 267.
15. Y. Zhan, C. Yin, W. Wang, G. Wang, *Materials Letters*, **2003**, 57, 3402.
16. L. Zhang, D. Xue, C. Gao, *Journal of Magnetism and Magnetic Materials*, **2003**, 267, 111.
17. J. Jiu, Y. Ge, X. Li, L. Nie, *Materials Letters*, **2002**, 54, 260.
18. K. Vojisavljevic, S. Wicker, I. Can, A. Bencan, N. Barsan, B. Malic, *Advanced Powder Technology*, **2017**, 28, 1118.
19. H. Yang, Y. Hu, X. Zhang, G. Qiu, *Materials Letters*, **2004**, 58, 387.
20. Z.W. Yhao, Z.P. Guo, H.K.Liu, *Journal of Power Sources*, **2005**, 147, 264.
21. C.Y. Su, W.J. Lan, C.Y. Chu, X.J. Liu, W.Y. Kao, C.H. Chen, *Electrochimica Acta*, **2016**, 190, 588.
22. M. Stefanescu, T. Dippong, M. Stoia, O. Stefanescu, *Journal of Thermal Analysis and Calorimetry*, 2008, 94:2, 389.
23. K. Shalini, A.U. Mane, S.A. Shivashankar, M.Rajeswari, S.Choopun, *Journal of Crystal Growth*, 2001, 231, 242.
24. Joint Committee on Powder Diffraction Standards. International Center for Diffraction Data, 1999.
25. . E. Lima Jr., E.L. Winkler, D. Tobia, H.E. Troiani, R.D. Zysler, E. Agostinelli, D. Fiorani, *Chemistry of Materials*, **2012**, 24:3, 512.
26. L. Wang, M. Lu, Y. Liu, J. Li, M. Liu, H. Li, *Ceramic International*, **2015** 41, 4176.

In memory of prof. dr. Simion Gocan

ELECTROCHEMICAL RECYCLING OF WASTE PRINTED CIRCUIT BOARDS IN BROMIDE MEDIA. PART I: PRELIMINARY LEACHING AND DISMANTLING TESTS

SORIN-AUREL DORNEANU^{a*}

ABSTRACT. In the context of the large and increasing interest for an efficient and ecological recycling of the Waste Electrical and Electronic Equipments (WEEEs), we decide to evaluate the feasibility of an electrochemical recycling process for waste printed circuit boards (WPCBs) based on bromine-bromide leaching system. For this preliminary study, a perforated rotating drum chemical reactor (RDCR), interconnected with a divided electrochemical reactor (DER) in a closed hydraulic loop, was successfully used to dismantle consecutively three computer motherboards (CMB) after a minimal mechanical pre-treatment. Essentially, the base metals were leached at the RDCR level and the bromine-bromide system was regenerated at the DER level, simultaneously with the partial electrodeposition of dissolved metals. Even if the operating parameters were not optimized, each CMB was completely dismantled in around 18 h, with cathodic and anodic mean current efficiencies of 43.6% and 58.4%, respectively. Notably, grace to the proposed process, the remaining undissolved parts (fiberglass reinforced epoxy boards, electronic components, plastics, etc.) preserve their original shape and structure, allowing an easier consequent separation-classification and a more efficient and profitable recycling.

Keywords: *Waste printed circuit boards, metals recovery, electrochemical recycling, bromine-bromide leaching system, environmentally friendly process*

^a *Babes-Bolyai University, Faculty of Chemistry and Chemical Engineering, 11 Arany Janos str., RO-400028, Cluj-Napoca, Romania*

* *Corresponding author: dorneanu@chem.ubbcluj.ro*

INTRODUCTION

At this hour, the quantity of generated WEEEs exceeds 45 Mt/year and tends to increase with 4% each year [1]. Moreover, the traditional linear production philosophy (“take-make-dispose”) increases resource scarcity, causes great environmental costs and endangers human health. As a solution, the concept of circular economy has been introduced and generally accepted, maximizing the utility and value of components and materials [2]. In this context, for the recycling of WEEEs and, especially, of WPCBs, many researchers have studied and proposed various processes, e.g. physico-mechanical [3], hydrometallurgical [4], pyrometallurgical [5], pyrolytic [6] biometallurgical [7] or by combination of thereof as presented in several reviews [8 - 12]. In spite of an intense research activity, proved by the increased number of published papers [13], many of the proposed technologies present serious disadvantages, e.g. extremely low speed for the bioleaching processes and, for the other mentioned processes, high energy and materials consumption, leak of selectivity and generation of toxic or unusable supplementary waste fluxes. The electrochemical recycling of metals from WPCBs represents a feasible alternative and allows the minimization of the drawbacks mentioned before. Several regenerable leaching systems were proposed and tested, e.g. electro-generated Cl_2 in HCl solution [14], $\text{FeSO}_4/\text{H}_2\text{SO}_4$ [15], $\text{Fe}_2(\text{SO}_4)_3/\text{H}_2\text{SO}_4$ [16], FeCl_3/HCl [17 - 19], SnCl_4/HCl (for solder stripping) [20]. Unfortunately, the electrochemical regeneration of chloride based leaching agents presents the risk of chlorine evolution, requiring well sealed equipments. Also, the presence of sulfate induces a low rate of the solder alloy dissolution if large amounts of Pb are present. The Br_2 based lixivants can be also used, but some authors suggest that these are unattractive due to the high vapor pressure of Br_2 (ex. 28 kPa at 35 °C) [21]. Contrarily, other researchers indicate that the use of the adequate complexing agents like bromide or organic ammonium perchalides can resolve this problem [22].

In this context, during the present work, we test the ability of the aqueous Br_2/KBr leaching system to remove all exposed metallic parts from different models of computer motherboards (CMB), simultaneous with the electrochemical lixivants regeneration and the partial electrodeposition of the dissolved metals. The experimental setup has included a perforated rotating drum chemical reactor (RDCR) and a divided electrochemical reactor (DER), connected in an electrolyte closed loop. The resulting setup was successfully used for the consecutive dismantling of three different CMB after a minimal mechanical pre-treatment. Even if the operating parameters were not optimized, each CMB was completely dismantled in around 18 h, with cathodic and anodic mean current efficiencies of 43.6% and 58.4%, respectively, and a cumulated specific electric energy consumption of 0.65 kWh/kg of treated WPCB. Finally, it is worth to note that, after the leaching tests, the remaining

undissolved parts (fiberglass boards, electronic components, plastics, etc.) preserve their original shape and structure, allowing an easier consequent separation/classification and a more efficient recycling.

RESULTS AND DISCUSSION

Before the leaching experiments, several components were manually removed from the used CMB: the Li batteries, aluminium heat sinks, Cr/Ni plated bronze screws from the peripheral interfaces (RS232, WGA, LPT1, etc.) and the cylindrical aluminium electrolytic capacitors. This minimal mechanical pre-treatment, which lasted less than 2 min. for each CMB, was compulsorily in order to avoid few unwanted problems:

- risk of explosion when the extremely reactive inner of the Li batteries cams in contact with the leaching solution;
- risk of leaching solution contamination with extremely toxic polychloride-biphenyls presented in some cylindrical aluminium electrolytic capacitors;
- increased total time of leaching due to the high thickness of the mentioned screws;
- significant and unjustified consumption of leaching agent for the Al dissolution due to the small commercial value of Al and the difficulty of Al recovery from the resulting solution. Moreover, the reaction between Al and the aqueous solutions of bromine generates high amount of gaseous hydrogen and is extremely vigorous and exothermic, increasing the risk of explosion.

After the mechanical pre-treatment of the CMB, the resulted components were weighted separately and each board was broken in few pieces in order to full fit the dimension of the rotating drum from the RDCR. Subsequently, the fragments of the first CMB (model PIII-GA-60XT, designed as CMB1) were introduced in the rotating drum, the RDCR and DER were interconnected and filed with 3.4 L of KBr 2 M. Only before the first test (designed as Test1), 38 mL of liquid bromine and 350 mL of HCl (32%) were added to the leaching solution, resulting concentrations of around 0.25 M and 1 M for bromine and HCl, respectively. In order to allow the reaction between the initial added bromine and the metals from the CMB1, the drum was rotated for 1 h without the DER energising and the solution was circulated between reactors at a flow rate of 250 mL/min. During this period, the solution colour change from intense orange to light green, indicating the complete consumption of the initial bromine.

After this preliminary step, we started effectively the Test1, that was divided in 10 successive short experiments, completed at different combinations of current (I_{WE}) and electrolyte flow rate (V_F) values, presented in

Table 1, where t_{START} , t_{STOP} and t_{NET} represent the experiment starting, ending and net time, respectively, and S_{CAT} stands for the cathode surface. During the measurements, the values of the voltage at the DER terminals (U_{CELL}), working electrode potential (U_{WE}), counter-electrode potential (U_{CE}) and I_{WE} were recorded, the corresponding concatenated data being presented in Figure 1.

Table 1. Experimental parameters used during Test1

Parameter	t_{START} [min]	t_{STOP} [min]	t_{NET} [min]	I_{WE} [A]	V_{F} [mL/min]	S_{CAT} [cm ²]
Test1-Exp.1	0	50	50	-2.0	100	298
Test1-Exp.2	50	200	150	-2.0	250	298
Test1-Exp.3	200	339	139	-3.5	150	192
Test1-Exp.4	339	403	64	-3.5	150	192
Test1-Exp.5	403	439	36	-3.5	150	192
Test1-Exp.6	439	477	38	-3.5	150	192
Test1-Exp.7	477	601	124	-4.0	100	192
Test1-Exp.8	601	746	145	-4.5	50	192
Test1-Exp.9	746	847	101	-4.0	100	192
Test1-Exp.10	847	1103	256	-4.0	25	192

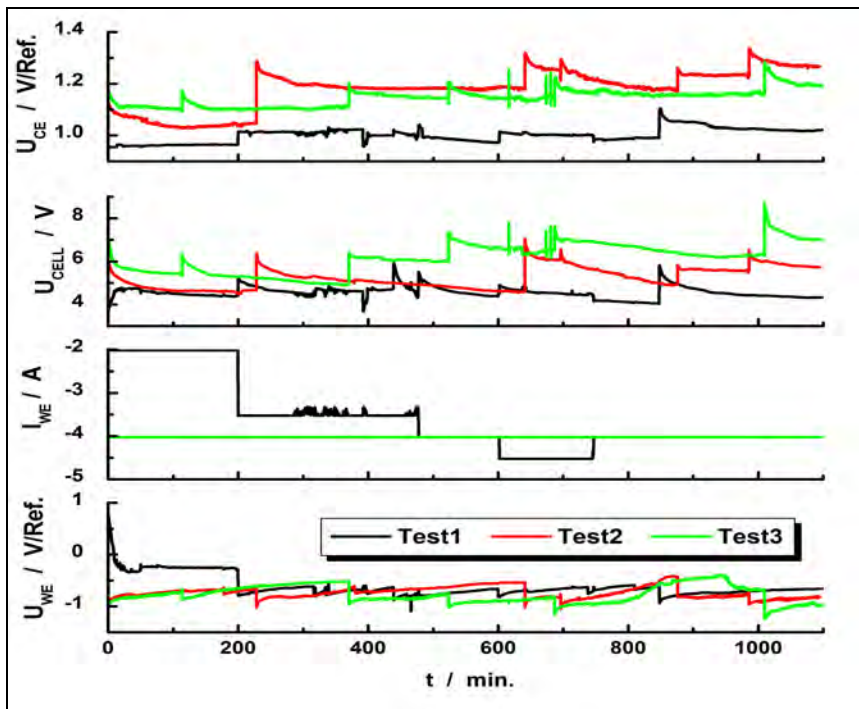


Figure 1. Evolution of the electric parameters recorded at the DER level during the three successive tests of metal leaching using the bromine-bromide system

Correlating the data from Table 1 and Figure 1 with the visual observation concerning the quality and quantity of the obtained deposits, we conclude that the combination of $I_{WE} = 4$ A and $V_F = 100$ mL/min represents an acceptable compromise in respect to the electric energy consumption, leaching rate and quantity of the electrodeposited metal. It is worth to note that for all the tested experimental parameters combinations, pulverulent deposits, consisting mainly of Cu, were obtained. After each short experiment, the content of the rotating drum was inspected, revealing that all the accessible thin metallic parts (thickness less than 0.5 mm, e.g. pins, foils, chip terminals, solder points and balls, etc.), were completely dissolved after around 18 hours. The undissolved metallic parts resulted from the CMB1 include only 6 surface mounted MOS-FET power transistors and few pieces of thick enameled copper wires ($\phi > 0.5$ mm).

At the end of Test1, the content of the rotating drum was discarded, washed with distilled water, dried, manually sorted and weighted. Also, the pulverulent metal deposit was collected by suction from the DER cathodic compartment, decanted, filtered, washed with distilled water and acetone, fast dried and weighted. In order to evaluate the metallic composition of the obtained deposit, samples of 1-2 g were re-dissolved in aqua regia and analyzed by flame atomic adsorption spectroscopy (FAAS). The final concentrations of the dissolved metals in the leaching solution were also evaluated by FAAS.

Following the protocol described before, other two CMB (both of AMD-DURON - Socket 462 type) were mechanically pre-treated and successively leached using the same electrolyte solution. For Test2 and Test3, identical experimental parameters ($I_{WE} = 4$ A and $V_F = 100$ mL/min) were used, the recorded data being also presented in Figure 1.

As can be seen in Figure 1, during the Test2 and Test3, the recorded electrical parameters are similar with those of Test1, with a small increase of the U_{CELL} and U_{CE} . A more accurate comparison can be made base on the calculated mean values, presented in Table 2, where the total consumed electric charge (Q_T) and power (W_T) values are also included.

Table 2. The averaged values of the electrical parameters recorded during the three successive CMB leaching tests (Standard deviation)

Parameter	Test1	Test2	Test3
$U_{WE, MEAN}$ [V]	-0.62 ± 0.21	-0.74 ± 0.11	-0.78 ± 0.17
$I_{WE, MEAN}$ [A]	-3.59 ± 0.81	-4.02 ± 10^{-3}	-4.02 ± 10^{-3}
$U_{CELL, MEAN}$ [V]	4.56 ± 0.26	5.26 ± 0.49	6.17 ± 0.69
$U_{CE, MEAN}$ [V]	1.01 ± 0.03	1.18 ± 0.08	1.15 ± 0.03
Q_T [A*s]	$238 \cdot 10^3$	$264 \cdot 10^3$	$267 \cdot 10^3$
W_T [W*s]	$1.09 \cdot 10^6$	$1.38 \cdot 10^6$	$1.65 \cdot 10^6$

The data from in Table 2 indicate small differences between the averaged values of the electrical parameters recorded during the three successive tests, excepting W_T that increase constantly. This fact suggests that the same solution can be used for repetitive leaching processes.

Based on FAAS analyses, we evaluated, for all three tests, the amount of the electrodeposited (m_{DEP}) and dissolved (m_{DIS}) base metals and the current efficiency for the cathodic ($r_{f, CAT}$) and anodic ($r_{f, ANOD}$) processes, the corresponding data being presented in Table 3.

Table 3. Amount (in g) of the electrodeposited and dissolved base metals and the current efficiencies (in %) for the three successive CMB leaching tests

Metal / Efficiency		Test1		Test2		Test3	
		m_{DEP}	m_{DIS}	m_{DEP}	m_{DIS}	m_{DEP}	m_{DIS}
Cu		52.62	62.31	53.44	50.60	52.90	54.60
Ni		0.14	4.70	0.32	3.00	0.63	2.80
Zn		0.05	14.10	0.08	15.50	0.67	9.50
Sn		12.63	17.16	19.20	16.20	22.75	22.00
Pb		2.10	8.34	7.20	7.20	10.73	8.10
Fe		0.04	16.33	0.12	8.30	0.06	6.50
$r_{f, CAT}$	$r_{f, ANOD}$	43.36	42.73	45.75	73.52	41.78	59.03

The data presented in Table 3 reveal very important information:

- The great dispersion of the measured m_{DIS} values indicate large differences between the compositions of the leached CMBs.
- For all three tests, the major component of the deposits is Cu (around 53%) and its amount remains quasi-constant, suggesting that this metal can be efficiently recovered by electrodeposition if the operational parameters are optimized.
- The amount of electrodeposited Sn and Pb increase constantly, indicating their accumulation in the leaching solution and the necessity of their constant extraction from the electrolyte.
- The quantities of Ni, Zn and Fe are extremely small (less than 1%), suggesting that, using optimal operational parameters, their capture in the Cu deposits can be eliminated.
- The simple recirculation of the leaching solution on the route RDCR - cathodic - anodic induces very low values of the current efficiency, for both $r_{f, CAT}$ and $r_{f, ANOD}$. This fact can be explained by the electrochemical short-circuit due to the presence of the Cu^+/Cu^{2+} , Fe^{2+}/Fe^{3+} and Br_2/Br^- reversible redox couples on all three compartments. To overcome this drawback, the setup must be re-designed in order to separate the anodic and cathodic fluxes.

Based on the cumulated m_{DEP} , m_{DIS} values and amounts of parts separated mechanically for all three tests, we elaborated the mass balance and the flowchart of the global process, presented in Figure 2.

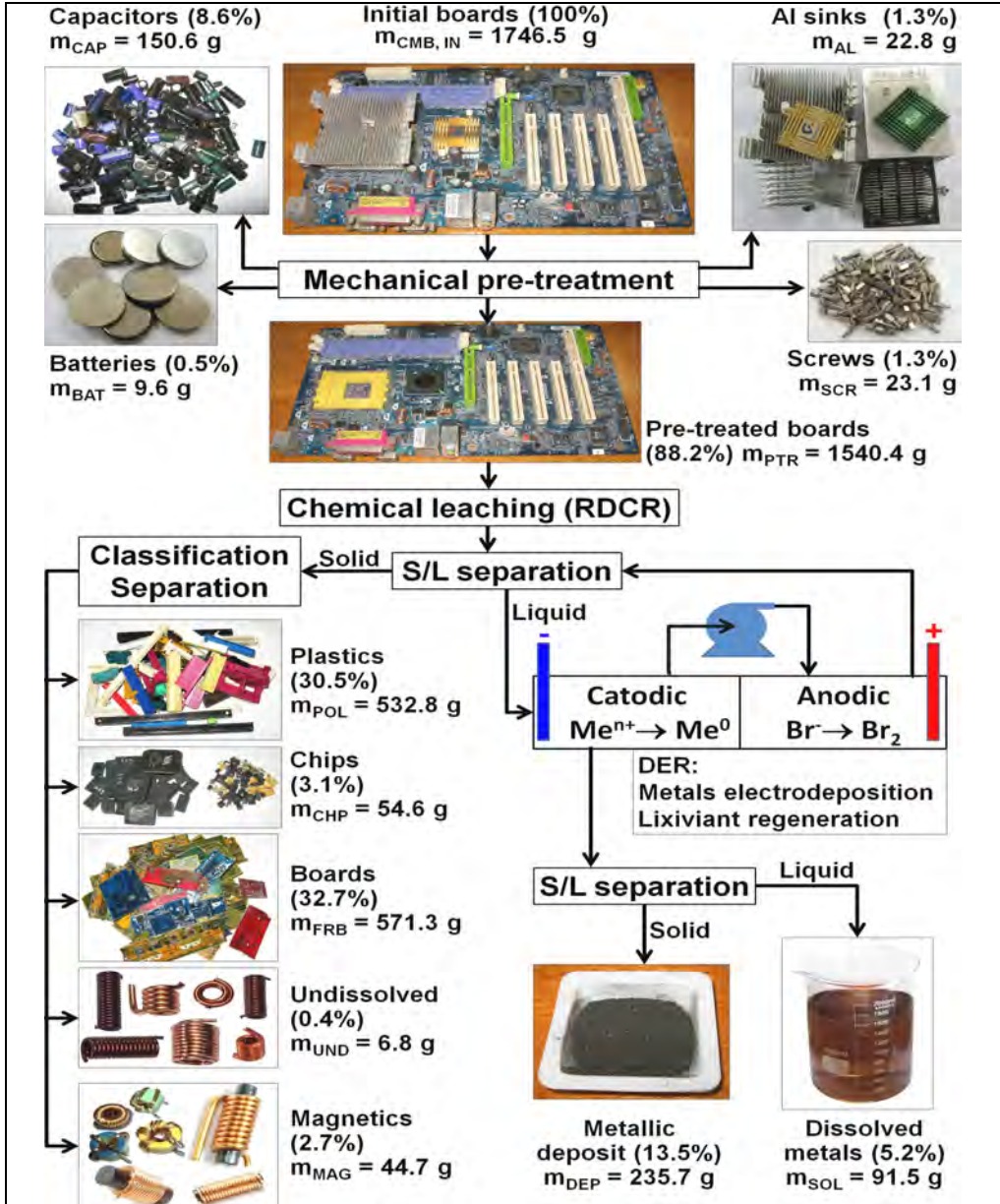


Figure 2. Mass balance and flowchart of the global dismantling process

For Figure 2, the designed names, corresponding weight symbols and compositions of the resulted fractions after the mechanical pre-treatment and leaching steps are summarized in Table 4.

Table 4. Designed names, weight symbols and compositions of separated fractions from CMB by mechanical pre-treatment and leaching

Fractions designed names	Weight symbol	Composition of the fractions
Initial boards	$m_{\text{CMB, IN}}$	Untreated boards with all components
Batteries	m_{BAT}	Button cell Li-batteries for CMBs clock
Al sinks	m_{AL}	Aluminium heat sinks
Capacitors	m_{CAP}	Al based cylindrical electrolytic capacitors
Screws	m_{SCR}	Ni/Cr plated screws from peripheral connectors
Pre-treated boards	m_{PTR}	Mechanically pre-treated CMBs
Boards	m_{FRB}	Fiberglass reinforced epoxy boards
Magnetics	m_{MAG}	Ferrite or iron coil cores, CPU locking levers
Plastics	m_{POL}	Polymer based extruded/injected parts
Chips	m_{CHP}	Electronic chips and small surface mounting devices (SMD), all without terminals
Undissolved	m_{UND}	Undissolved metallic parts like high power SMD-MOS-FETs and thick enameled cooper wires
Dissolved metals	m_{SOL}	Dissolved metals remained in lixiviant

The mass balance presented in Figure 2 indicate that the direct leachable metals represents 18.7% from the total weight of CMBs and, for the used operational parameters, at least 72% from the dissolved base metals can be recovered by electrodeposition in one stage.

Finally, based on the cumulated values of W_T , m_{DIS} and $m_{\text{CMB, IN}}$ (see Table 2 and Figure 2), the global specific electricity consumptions were calculated, values of 0.65 and 3.5 kWh/kg being obtained in respect to the mass of treated CMBs and recoverable metals, respectively. Taking into account the market value of the leached base metals, the composition of the deposits and the price of electric energy, we conclude that the expenses for the consumed electricity during the leaching process can be covered by the value of the recovered base metals. In this conditions, the high value of the precious metals presented on the CMB, neglected during this study, can increase significantly the process profitability.

CONCLUSIONS

The main conclusion of the present study consists in the certitude that the electrochemical regenerable Br_2/Br^- leaching system can be successfully

used for the dismantling of WPCBs and the recovery of the base metals from wasted CMBs. The proposed process requires only a minimal mechanical pre-treatment, and its profitability can be increased significantly by recovering and valorising the precious metals from the WPCBs.

Finally, it is very important to note that the proposed and tested process allows to preserve the original shape and structure of the remaining undissolved parts (fiberglass boards, electronic components, plastics, etc.), facilitating a more easier and profitable classification, separation and recycling of these secondary waste fluxes.

EXPERIMENTAL SECTION

The leaching tests were performed in a RDCR made from HD-PP, the volume of the drum and reactor being of 1.5 and 3 L, respectively. The DER, of rectangular shape, was constructed also from HD-PP, divided in two chambers by a ceramic porous membrane. A peristaltic pump (model TC, Medorex, Germany) was used to transfer the electrolyte from the cathodic to the anodic compartment of DER. Both DER compartments were connected with RDCR following the principle of communicating vessels, assuring an uniform circulation of the electrolyte in the whole system. The anode was a rectangular graphite block ($H*W*D = 80*70*20 \text{ cm}^3$), immersed 6.5 cm in solution. The "brush" shape cathode consisted in 30 or 20 cylindrical bares of spectral graphite ($\phi = 0.5 \text{ cm}$, $H = 10 \text{ cm}$), immersed 6 cm in solution. The U_{WE} and U_{CE} were measured and reported in respect to two reference electrode of Ag/AgCl/KCl_{SAT} type ($\varepsilon = +0.197 \text{ V/SHE}$).

Before the Test1, the reactors were filled with 3.5 L of solution containing 2 M KB, 0.25 M Br₂ and 0.2 M HCl that was reused during Test2 and Test3. A computer controlled P/G-stat (model DXC236, Datronix Computers, Romania) was used to impose the current through DER and measure the resulting potentials. A data acquisition board (model PCI-6221M, National Instruments, USA) and dedicated LabView 2015 (National Instruments, USA) applications were used to control the P/G-stat operation and acquire data. The FAAS analyses were performed using an AVANTA-PM spectrometer (GBS, Australia) in air/acetylene flame mode. The weights of the initial CMBs and all the other separated fraction were measured using a laboratory electronic balance (model PLJ-510-3m, KERN&SOHN GmbH, Germany).

ACKNOWLEDGMENTS

The author would like to acknowledge to Florica Imre-Lucaci and Vasile Coman for their help concerning the FAAS analyses and mass balance evaluation, respectively.

REFERENCES

1. B. Tansel, *Environment International*, **2017**, 98, 35.
2. L. Cong, F. Zhao, J. W. Sutherland, *Journal of Cleaner Production*, **2017**, 149, 378.
3. M. Kaya, "Recovery of Metals and Nonmetals from Waste Printed Circuit Boards (PCBs) by Physical Recycling Techniques" in *Energy Technology 2017, The Minerals, Metals & Materials Series*, Springer, Chambrige, **2017**, 433-451.
4. E. M. Iannicelli-Zubiani, M. I. Giani, F. Recanati, G. Dotelli, S. Puricelli, C. Cristiani, *Journal of Cleaner Production*, **2017**, 140, 1204.
5. M. Ghodrat, M. A. Rhamdhani, A. Khaliq, G. Brooks, B. Samali, *Journal of Material Cycles and Waste Management*, **2017**, 1.
6. C. Zhao, X. Zhang, L. Shi, *Waste Management*, **2017**, 61, 354.
7. A. Priya S. Hait, *Environmental Science and Pollution Research*, **2017**, 24(8), 6989.
8. A. Chatterjee, J. Abraham, *International Journal of Environmental Science and Technology*, **2017**, 14(1), 211.
9. A. Kumar, M. Holuszko, D. C. R. Espinosa, *Resources, Conservation and Recycling*, **2017**, 122, 32.
10. F. Tesfaye, D. Lindberg, J. Hamuyuni, P. Taskinen, L. Hupa, *Minerals Engineering*, **2017**, 111, 209.
11. M. Wang, Q. Tan, J. F. Chiang, *Frontiers of Environmental Science & Engineering*, **2017**, 11(5), 1.
12. T. Oki, T. Suzuki, "The Advanced Recycling Technology for Realizing Urban Mines Contributing to Climate Change Mitigation" in *Handbook of Climate Change Mitigation and Adaptation*, Springer International Publishing Switzerland, **2017**, 1007-1035.
13. G. Cecere, A. Martinelli, *Research Policy*, **2017**, vol. 46(5), 925,.
14. E. Y. Kim, M. S. Kim, J. C. Lee, J. Jeong, B. D. Pandey, *Hydrometallurgy*, **2011**, 107(3-4), 124.
15. T. E. Lister, P. Wang, A. Anderko, *Hydrometallurgy*, **2014**, 149, 228.
16. L. A. Diaz, T. E. Lister, J. A. Parkman, G. G. Clark, *Journal of Cleaner Production*, **2016**, 125, 236.
17. S. Fogarasi, F. Imre-Lucaci, P. Ilea, Á. Imre-Lucaci, *Journal of Cleaner Production*, **2013**, 54, 264.
18. S. Fogarasi, F. Imre-Lucaci, Á. Imre-Lucaci, P. Ilea, *Journal of Hazardous Materials*, **2014**, 273, 215.
19. S. Fogarasi, F. Imre-Lucaci, A. Egedy, Á. Imre-Lucaci, P. Ilea, *Waste Management*, **2015**, 40, 136.
20. Y. Jian-guang, L. Jie, P. Si-yao, L. Yuan-lu, *Journal of Hazardous Materials*, **2016**, 304, 409.
21. Y. Zhang, S. Liu, H. Xie, X. Zeng, J. Li, *Procedia Environmental Sciences*, vol. **2012**, 16, 560.
22. C. N. Mpinga, J. J. Eksteen, C. Aldrich, L. Dyer, *Minerals Engineering*, **2015**, 78, 93.

In memory of prof. dr. Simion Gocan

ENHANCEMENT OF PHYSICAL PROPERTIES IN ZrO_2/Ga_2O_3 CO-SUBSTITUTED INDIUM OXIDE

LILIANA BIZO^{a*}, ADRIANA VULPOI^b, FIRUȚA GOGA^a

ABSTRACT. The effect of coupled substitution of Zr^{4+}/Ga^{3+} for In^{3+} in In_2O_3 upon the structural, electrical and optical properties has been studied. The $In_{2-2x}Ga_xZr_xO_3$ solid solution with bixbyite structure has been synthesized for $0 \leq x < 0.15$. A decrease in resistivity for the composition $x = 0.025$ ($\rho_{RT} = 5.5 \times 10^{-3} \Omega \cdot cm$) by approximately one order of magnitude if compared to In_2O_3 ($\rho_{RT} = 2.2 \times 10^{-2} \Omega \cdot cm$) was obtained. The maximum percent reflectance around 500 nm is lowered by 15% with respect to pure In_2O_3 . These novel oxides show their potential as transparent conductors.

Keywords: *transparent conducting oxides, solid state reaction, electrical conductivity, optical properties.*

INTRODUCTION

The simultaneous presence of optical transparency and electronic conductivity in metal oxides produces a special class of materials, transparent conducting oxides (TCOs). These materials are suitable for a wide range of applications, such as sensors, solar cells, smart windows, and many other scientific, commercial and consumer products (see for example reference [1] and references therein). In the last years, numerous investigations were carried out to discover new potential n- or p-type TCOs, due to the increasing interest in this class of materials. Most of the TCOs that are suitable for

^a Babeş-Bolyai University, Faculty of Chemistry and Chemical Engineering, 11 Arany Janos str., RO-400028, Cluj-Napoca, Romania.

* Corresponding author: lbizo@chem.ubbcluj

^b Babeş-Bolyai University, Institute for Interdisciplinary Research on Bio-Nano-Sciences, 42 Treboniu Laurian str., RO-400271 Cluj-Napoca, Romania

practical use are still n-type semiconductors, due to the ease of forming cation interstitials or oxygen vacancies [2]. The important TCO semiconductors are impurity-doped ZnO, In₂O₃, and SnO₂ as well as multicomponent oxides consisting of combinations of these oxides including some ternary compounds existing in their systems. The In₂O₃ with its bixbyite structure and more generally oxygen deficient fluorite type oxides, involving d¹⁰ cations seem to play a prominent role in the discovery of transparent conductors. Beside the well-known ITO (indium tin oxide), considered the best material for optoelectronic applications, other types of doping or substitutions in indium oxide were intensely studied in the last years [3-13]. Indium and its compounds are considered critical raw materials (CRM) and many efforts are focused on investigating CRM substitution alternatives [14]. However, substitution of flat panel displays containing ITO, either by an ITO alternative or a different display technology, is currently not possible without a loss of performance or the use of another indium containing component.

In this context, reducing the amount of highly expensive and scarce indium oxide by substitutions in indium oxide has to be investigated intensively. For this reason, we decided to check the ability for the substitution of the (Ga/Zr) couple for indium in In₂O₃. We hereafter report the results of such an investigation in terms of In_{2-2x}Ga_xZr_xO₃ solid solutions, which previously has not been reported. X-ray powder diffraction (XRPD), Scanning Electron Microscopy (SEM) and Energy Dispersive X-ray Spectroscopy (EDS), UV-VIS spectroscopy and electrical resistivity measurements were used to analyze the effect of coupled substitution of Zr⁴⁺/Ga³⁺ for In³⁺ in In₂O₃ on the structural and physical properties.

RESULTS AND DISCUSSION

According to the above reported experimental procedure, a new series of compositions belonging to In_{2-2x}Ga_xZr_xO₃ solid solution (0 ≤ x < 0.15) were experimented. The X-ray powder diffraction (XRPD) spectra of six compositions were shown in Figure 1(a). All samples have good crystallinity and all of the major reflections could be well indexed to bixbyite-type cubic lattice structure. The extent of the homogeneity range of this solid solution was deduced from the variation of the parameter of their cubic unit cell obtained from the refinement of XRPD data using the bixbyite-based structural model, S.G. Ia $\bar{3}$ (206), with two sets of cationic positions 8(b): $\frac{1}{4}, \frac{1}{4}, \frac{1}{4}, 24(d): x, 0, \frac{1}{4}$, and one set of oxygen position 48(e): x, y, z [16]. In Figure 1(b) we give as an example the results of the Rietveld refinement of XRPD pattern for a sample with nominal composition In_{1.9}Ga_{0.05}Zr_{0.05}O₃. The calculated parameter values are listed in Table 1. As expected from the smaller cationic mean size resulting from the double substitution reaction 2 In³⁺ (0.80 Å) → Ga³⁺ (0.62 Å) + Zr⁴⁺ (0.72 Å), the value of the a parameter decreases with increasing x, which

indicate solubility up to $x = 0.15$ (Figure 2). Hence, the substitution of $\text{Zr}^{4+}/\text{Ga}^{3+}$ for In^{3+} in In_2O_3 is evident. The lattice parameter no longer changes as the doping level is increased beyond $x = 0.15$, confirming that the solubility limit is around 7.5 at%. The solubility limits of Ga and Zr in indium oxide are in good agreement with results reported by Edwards et al. and Sasaki et al. [17, 18]. Above this composition ($x = 0.15$) the a parameter remain practically constant and impurity phases identified to both tetragonal and monoclinic ZrO_2 starts to appear. It is known that ZrO_2 has three polymorphs: monoclinic (m-phase, below 1170 °C), tetragonal (t-phase, between 1170 and 2370 °C) and cubic (c-phase, above 2370 °C) [19, 20].

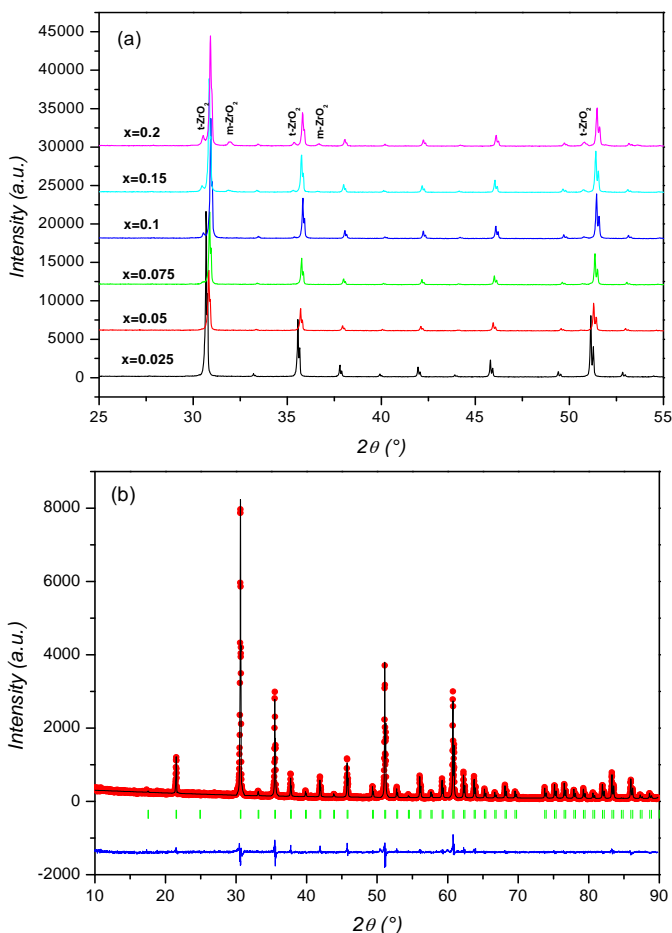


Figure 1. (a) XRPD pattern of six compositions belonging to $\text{In}_{2-2x}\text{Ga}_x\text{Zr}_x\text{O}_3$ system and (b) observed (dots), calculated (lines) and difference XRPD pattern of $x = 0.05$ composition (after heating at 1400 °C).

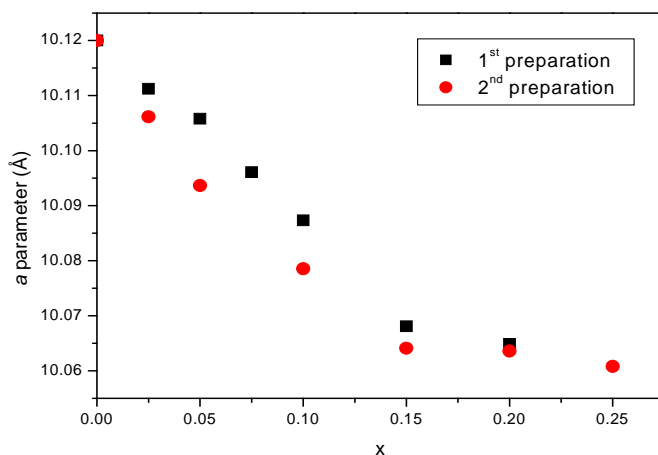


Figure 2. Variation of a parameter (Å) versus composition x of the cubic unit cell in the $\text{In}_{2-2x}\text{Ga}_x\text{Zr}_x\text{O}_3$ system.

In order to check the reproducibility of the synthesis procedure, two sets of samples were prepared, using the same preparative method, namely 1st and 2nd preparation, respectively. As observed from Table 1, no major difference of the cell parameters values occurred.

Table 1. Values of a parameter obtained from Rietveld refinement of XRPD data for two different preparations of the same composition belonging to $\text{In}_{2-2x}\text{Ga}_x\text{Zr}_x\text{O}_3$ system.

Composition	a [Å]	
	1 st preparation	2 nd preparation
x = 0.025	10.11123(11)	10.106140(10)
x = 0.05	10.10579(17)	10.093659(10)
x = 0.075	10.09609(16)	-
x = 0.1	10.08734(17)	10.078545(15)
x = 0.15	10.0681(2)	10.0641(2)
x = 0.2	10.0649(3)	10.0636(6)
x = 0.25	-	10.0608(5)

The surface morphology of x = 0.05 and x = 0.1 compositions appear homogenous and consist of small grains as shown in Figure 3. The grain size ranges from approximately 5 to 15 μm . The results of EDS analysis corresponding to the same nominal cationic compositions highlight the simultaneous presence of the In, Ga and Zr elements and no others was systematically detected. The results for x = 0.05 sample are less definitive as the Ga and Zr content is very small.

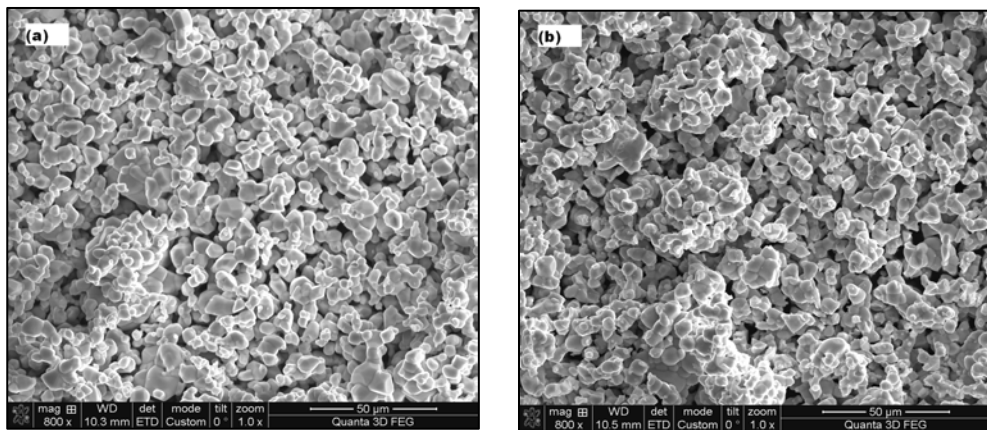


Figure 3. SEM images of $x = 0.05$ (a) and $x = 0.1$ (b) compositions at 800x magnification.

The color of the samples prepared at 1400 °C is medium green. Their measured diffuse reflectance spectra (DRS) are displayed in Figure 4(a) together with the corresponding spectra of an undoped indium oxide ceramic sample annealed at the same temperature. In any case, a systematic decrease of the maximum percent reflectance around 550 nm, if compare to pure indium oxide, was observed. This decrease is more pronounced in the $x = 0.075$ composition, by approximately 15% with respect to undoped indium oxide. A slight increase of bandgap due to the substitution of In^{3+} ions with Zr^{4+} and Ga^{3+} was observed. This increase of bandgap with doping is well known as a result of the Burstein-Moss effect that occurs in degenerate doped semiconductors [21].

Regarding the influence of firing temperature on optical properties, DRS spectra for $x = 0.05$ sample were recorded after three heating treatments, 1200 °C, 1300 °C and 1400 °C, respectively. As visible from Figure 4(b), the maximum percent reflectance is lowered by 18 % at increasing temperature from 1200 °C to 1400 °C. It is clear that bandgap increases with increasing annealing temperature and its maximum value of 3.306 eV is obtained at a temperature of 1400 °C. The increase in optical bandgap may be related to the improvement of sample crystallinity. On the other hand, the optical band gap broadening with increasing firing temperature can be described in terms of Burstein-Moss model. Moreover, in the case of degenerated semiconductors the optical bandgap is influenced by changes in the carrier concentration, which blocks the lowest states of the bottom of the conduction band, resulting in the Burstein–Moss shift. As the firing temperature increases, the absorption edge shifts to longer wavelengths.

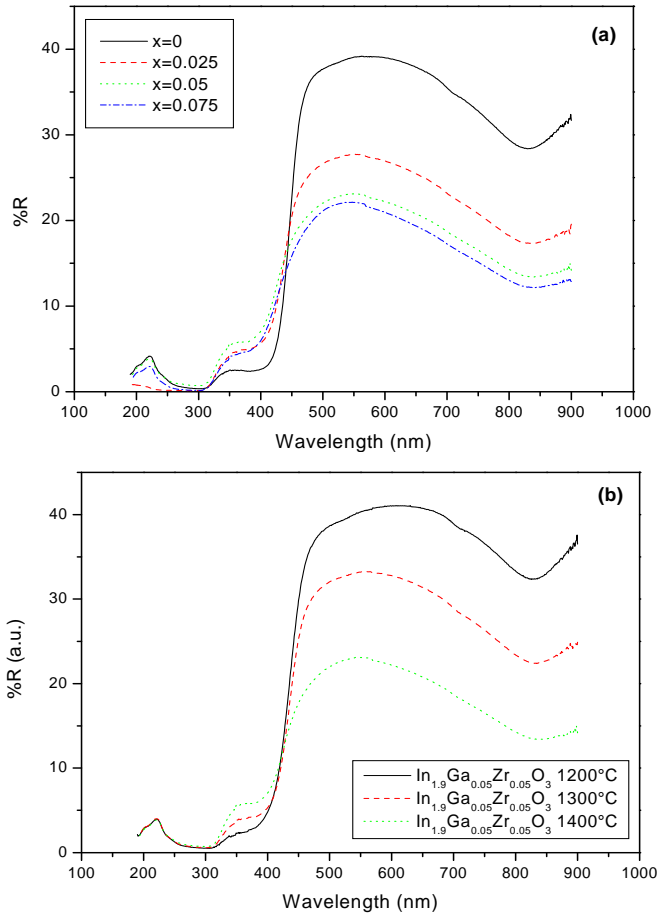


Figure 4. DRS spectra for $x = 0.025$, $x = 0.05$, $x = 0.075$ compositions and In_2O_3 ($x = 0$) for comparison (a) and $x = 0.05$ composition treated at three different temperatures (b).

The temperature dependence of the electrical resistivity of the three compositions of $\text{In}_{2-2x}\text{Ga}_x\text{Zr}_x\text{O}_3$ solid solution ($x = 0.025$, $x = 0.05$ and $x = 0.075$) and indium oxide for comparison is displayed in Figure 5. Within the whole temperature range 5-320 K a semi-metallic behavior of the (Ga/Zr) compositions is observed. In any case, the introduction of the cationic couples (Ga/Zr) in In_2O_3 triggers systematically a decrease of the resistivity if compare to In_2O_3 . The best value of resistivity obtained for the $x = 0.025$ compositions, $\rho_{\text{RT}} = 5 \times 10^{-3} \Omega\cdot\text{cm}$, is lowered by almost one order of magnitude compared to bulk In_2O_3 . It should be emphasized that this resistivity value is comparable to that of an ITO ceramic sample (3% Sn) prepared at the same temperature (1400 °C), in air ($\rho_{\text{RT}} = 0.5 \times 10^{-3} \Omega\cdot\text{cm}$) [22].

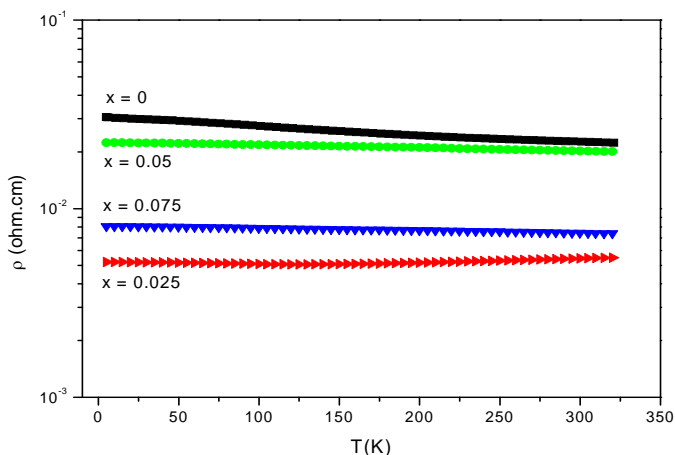


Figure 5. Electrical resistivity (ohm.cm) versus temperature (K) for $x = 0.025$, $x = 0.05$ and $x = 0.075$ compositions and compared with In_2O_3 ($x = 0$).

CONCLUSIONS

Different compositions belonging to the $\text{In}_{2-2x}\text{Ga}_x\text{Zr}_x\text{O}_3$ system have been successfully synthesized by the solid-state reaction method. X-ray powder diffraction (XRPD) technique used for phase analysis and structure calculation verified that all samples exhibited a single bixbyite structure up to $x = 0.15$. The homogeneity of the substitution procedure $2\text{In}^{3+} \rightarrow \text{Zr}^{4+} + \text{Ga}^{3+}$ was confirmed. The maximum percent reflectance around 500 nm is lowered by 15% with respect to pure In_2O_3 . The optical bandgap is somewhat shifted towards the lower wavelengths, i.e. the larger energies. A decrease of room temperature resistivity for the composition $x = 0.025$ ($\rho_{\text{RT}} = 5.5 \times 10^{-3} \text{ } \Omega \cdot \text{cm}$) was observed, which is approximately one order of magnitude less than undoped In_2O_3 ($\rho_{\text{RT}} = 2.2 \times 10^{-2} \text{ } \Omega \cdot \text{cm}$). The coupled substitution of the (Ga/Zr) for In promotes a good level of conductivity of the bulk materials together with a satisfying optical transparency as compared to pure indium oxide prepared under the same conditions. We can conclude that these novel oxides are promising candidates as transparent conducting oxides for optoelectronic applications.

EXPERIMENTAL SECTION

Samples preparation

The different compositions of $\text{In}_2\text{O}_3:(\text{Zr}, \text{Ga})$ oxides were prepared by solid state reaction in air. The raw materials were pure oxides of In_2O_3

(Alfa Aesar 99.995%), ZrO_2 (Alfa Aesar 99%) and Ga_2O_3 (Alfa Aesar 99.999%). The oxide mixture was milled using an agate mortar and then heated in an alumina crucible using a high-temperature Nabertherm LHT 04/16 furnace. Successive 12h heating temperature, from 600 °C up to 1400 °C, followed by air quenching and regrinding were performed. The samples preparation was repeated (1st and 2nd preparation). Multiple samples were prepared at the $x = 0.025$, $x = 0.05$, $x = 0.075$, $x = 0.1$, $x = 0.15$ and $x = 0.2$ compositions in order to test the reproducibility of the preparation procedure (Table 1).

Characterization methods

X-ray powder diffraction (XRPD) was used for phase analysis and further for structure calculations. The diffractograms were recorded on a Panalitcal X'Pert diffractometer (CuK α 1 radiation), equipped with an X'Celerator detector, in the angular range $2\theta = 6-120^\circ$. A Rietveld analysis (Fullprof code [15]) of the diffractograms was systematically performed.

UV–VIS diffuse reflectance spectra (DRS) of the as-prepared compositions were determined by a double beam spectrophotometer (Cary Varian 100 Scan), in the range 190-900 nm with a 600 nm/min scan rate.

The electrical resistivity of pellets sintered at 1400 °C in the air was measured by the four-probe method in the range of 5-320 K, using a PPMS (Physical Properties Measurements System) device.

The samples morphology was investigated using an FEI Quanta 3D FEG dual beam microscope in scanning electron microscopy (SEM) mode. Chemical analysis of local area was carried out by energy dispersive X-ray spectroscopy (EDS) measurements performed on the same microscope.

REFERENCES

1. D. S. Ginley, H. Hosono, D. C. Paine, "Handbook of Transparent Conductors", Springer, Berlin, **2010**.
2. S. Lany, A. Zunger, Dopability, *Physical Reviews Letters*, **2007**, 98, 0455011.
3. L. Bizo J. Choynet, R. Retoux, B. Raveau, *Solid State Communications*, **2005**, 136, 163.
4. L. Bizo, J. Choynet, B. Raveau, *Materials Research Bulletin*, **2006**, 41, 2232.
5. J. Choynet, L. Bizo, R. Retoux, B. Raveau, *Solid State Science*, **2004**, 6, 1121.
6. D. Berardan, E. Guilmeau, A. Maignan, B. Raveau, *Solid State Communications*, **2008**, 146, 97.

7. F. Nanni, F. R. Lamastra, F. Franceschetti, F. Biccari, I. Cacciotti, *Ceramics International*, **2014**, *40*, 1851.
8. T. Asikainen, M. Ritala, M. Leskela, *Thin Solid Films*, **2003**, *440*, 152.
9. H. K. Kim, C. C. Li, G. Nykolak, P.C. Becker, *Journal of Applied Physics*, **1994**, *76*, 8209.
10. T. Koida, M. Kondo, *Applied Physics Letters*, **2006**, *89*, 0821041.
11. Y.-C. Liang, Y.-C. Liang, *Applied Physics A-Material Science*, **2009**, *97*, 249.
12. H. J. Chun, Y. S. Choi, S. Y. Bae, H. C. Choi, J. Park, *Applied Physics Letters*, **2004**, *85*, 461-464.
13. J.-H. Lim, E.-J. Yang, D.-K. Hwang, J.-Ho Yang, J.-Y. Oh, S.-J. Park, *Appl. Phys. Lett.*, **2005**, *87*, 0421091.
14. European Commission, Report on Critical Raw Materials for the EU, **2014**.
15. J. Rodriguez-Carvajal, T. Roisnel, Proc. 8-th European Powder Diffraction Conference (EPDIC) 8, Uppsala, Sweden, Ed. Y. Andersson, E. J. Mittemeijer, U. Welze, Trans Tech Publications Ltd, Switzerland, **2004**, 123.
16. N. Nanaud, N. Lequeux, M. Nanot, *Journal of Solid State Chemistry*, **1998**, *135*, 140.
17. D. D. Edwards. P. E. Folkins, T. O. Mason, *Journal of American Ceramic Society*, **1997**, *80*, 253.
18. T. O. Mason G. B. González, J.-H. Hwang, D. R. Kammler, *Physical Chemistry Chemical Physics*, **2003**, *5*, 2183.
19. T. Chraska, A. H. King, C. C. Berndt, *Materials Science and Engineering: A*, **2000**, *286*, 169.
20. T. Y. Luo, T. X Liang, C. S. Li, *Materials Science and Engineering: A*, **2004**, *366*, 206.
21. E. Burstein, *Physical Reviews*, **1954**, *93*, 632.
22. Ambrosini, A. Duarte, K. R. Poeppelmeier, M. Lane, K. N. Kannewurf, T. O. Mason, *Journal of Solid State Chemistry*, **2000**, *153*, 41.

In memory of prof. dr. Simion Gocan

DIMENSIONALITY OF BIG DATA SETS EXPLORED BY CLUJ DESCRIPTORS

CLAUDIU LUNGU^a, SARA ERSALI^a, BEATA SZEFLER^b,
ATENA PÎRVAN-MOLDOVAN^a, SUBHASH BASAK^c, MIRCEA V. DIUDEA^{a*}

ABSTRACT. Dimensionality of a relatively big data set (95 compounds) observed for toxicity (mutagenicity) was explored in order to compute QSAR models. Distinct molecular descriptors were used. Dimensionality of data, using PCA, correlation plots and clustering, was evaluated. Analyzing data dimensionality allowed model optimization. Docking studies and PCA were used in order to expand data dimensionality. Pearson correlation coefficient (r^2) values, obtained for both perceptive and predictive models, were satisfactory.

Keywords: *topological descriptor, QSAR, data dimensionality, mutagenicity, principal component analysis (PCA), Ames test.*

INTRODUCTION

In a data case, involving big data, one faces the curse of dimensionality, reflected by the minimum number of variables necessary to represent the data without any loss of information. A dataset in R_p is said to have Intrinsic Dimensionality (ID) equal to m if its elements lie entirely within an m -dimensional subspace of R_p (where $m < p$). In a multivariate statistical scenario, using methods like principal components analysis¹ (PCA), first few selected principal

^a Babes-Bolyai University, Faculty of Chemistry and Chemical Engineering, 400028 Cluj, Romania

^b Nicolaus Copernicus University, Faculty of Pharmacy, Department of Physical Chemistry, Collegium Medicum, 85-096 Bydgoszcz, Poland

^c University of Minnesota Duluth Natural Resources Research Institute and Department of Chemistry and Biochemistry, 5013 Miller Trunk Highway, Duluth, MN 55811, USA

* Corresponding author: diudea@chem.ubbcluj.ro

¹ Jolliffe I.T. Principal Component Analysis, Series: Springer Series in Statistics, 2nd ed., Springer, NY, , XXIX, 487 p. 28 . ISBN 978-0-387-95442-4, 2002.

components (PCs) explaining a reasonably high (90-95%) fraction of the variance in the original variables may be taken as an approximate measure of m . The abundance of data (big data) poses a challenge in many fields of chemometrics². In toxicological research, strategies are manifold: grouping and classifying of data, searching of patterns and searching of correlations to biological activity, related to particular toxic endpoints³. One can use a perceptive model to evaluate a phenomenon occurrence. If occurrence is confirmed, a predictive model is used to find a best prediction⁴.

RESULTS AND DISCUSSION

First a perceptive model was built using commercial descriptors, generated using 2D, 3D and ADME descriptors (which simulate the behavior of compounds in culture medias – used for toxicity). A selection algorithm led to the results shown in Table 1: the best model was obtained with 15 descriptors. The toxicity model equation is: $y = -0.0196617 + 0.9002748x$; $r^2 = 0.900$; $p = 0.946501$; $q^2 = 0.900$; $RMSD = 0.604$; it is plotted in Figure 1.

Table 1. Descriptors in the toxicity r^2 model (ordered in non-increasing Pearson r^2);
(..) = no. descriptors

r^2 (..)	DESCRIPTOR
0.900 (15)	E_nb; E_stb; Gcut_Peoe_2; Gcut_SlogP_0; SlogP_VSA9; vsurf_HL1; vsurf_IW6; SMR_VSA6; logS; opr_nring; opr_nrot; opr_violation; radius; vsurf_CW5; vsurf_DD13.
0.892 (14)	E_nb; E_stb; Gcut_Peoe_2; Gcut_SlogP_0; SMR_VSA6; logS; radius; vsurf_HL1; vsurf_DD13; vsurf_IW6; SlogP_VSA9; opr_nring; opr_nrot; opr_violation.
0.887 (13)	E_nb; E_stb; Gcut_Peoe_2; SMR_VSA6; SlogP_VSA9; logS; opr_nring; opr_nrot; opr_violation; vsurf_DD13; vsurf_HL1; vsurf_IW6; radius.
0.880 (12)	E_stb; Gcut_Peoe_2; SMR_VSA6; SlogP_VSA9; logS; opr_nring; opr_nrot; opr_violation; radius; vsurf_DD13; vsurf_HL1; vsurf_IW6.
0.759 (4)	E_stb; logS; opr_nring; opr_nrot.
0.743 (3)	E_stb; logS; opr_nring
0.723 (2)	logS; opr_nring
0.690 (1)	opr_nring

² Hair, J. F. Jr., Anderson, R. E., Tatham, R. L. & Black, W. C. *Multivariate Data Analysis* (3rd ed). New York: Macmillan, **1995**.

³ Wallace A.D. *Progress in Molecular Biology and Translational Sciences*, **2012**, 112, 89.

⁴ Basak, S.C.; Vračko, M.; Witzmann, F.A. *Current Computer Aided Drug Design*, **2016**, 12(4), 259.

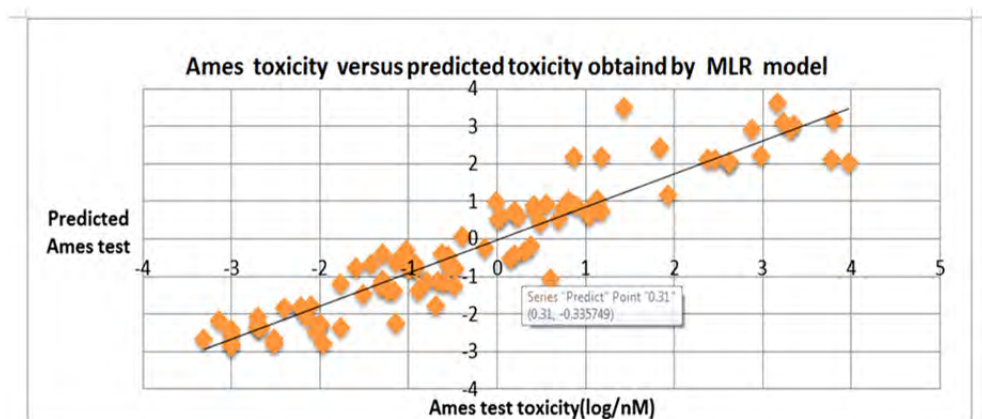


Figure 1. Correlation between observed Ames test values and predicted values.

Note that the descriptor `opr_nring` alone explains 69 % of the toxicity variance; thereby the aromatic nature of the compounds was further investigated, mainly in a docking study (see below). As expected, this descriptor correlates with all other 14 descriptors, having a very low tolerance and increased inflation VIF values. Indeed, statistical insignificant values have all descriptors that describe aromatic properties: `logS`, `opr_nring`, `vsurf_CW5` and `vsurf_HL1`. (Table 2, bolded values).

Table 2. Tolerance and VIF value calculated for the variables used in the model.

Descriptor	r^2 for each variable	Tolerance ($1-r^2$) (0.20 min. value)	VIF 1/Tolerance (4-20 max value)
E_nb	0.1756	0.824	1.213
E_stb	0.5473	0.452	2.212
Gcut_Peoe_2	0.7116	0.288	3.372
Gcut_SlogP_0	0.3399	0.660	1.515
logS	0.8998	0.100	10.000
opr_nring	0.8967	0.103	9.708
opr_nrot	0.7543	0.247	4.048
opr_violation	0.3205	0.679	1.472
Radius	0.7516	0.243	4.115
SlogP_VSA9	0.7427	0.257	3.891
SMR_VSA6	0.1871	0.812	1.231
vsurf_CW5	0.9698	0.032	31.250
vsurf_DD13	0.4878	0.512	1.950
vsurf_HL1	0.9628	0.037	27.027
vsurf_IW6	0.6796	0.320	3.125

Note that, in Figure 1, a “region” between 1 and 3 units where the Ames values are dispersed. It was assumed that relatively low value of r^2 is due to the insufficient description of the phenomena involved in toxicity.

As anticipated in the Methods section, a docking study, performed on a presumable target, transferase DNA fragment 3KHH, retrieved the results shown in Figure 2 . It is observed that the compound #53 has the favorable energy; its complex with 3KHH is represented in Figure 3.

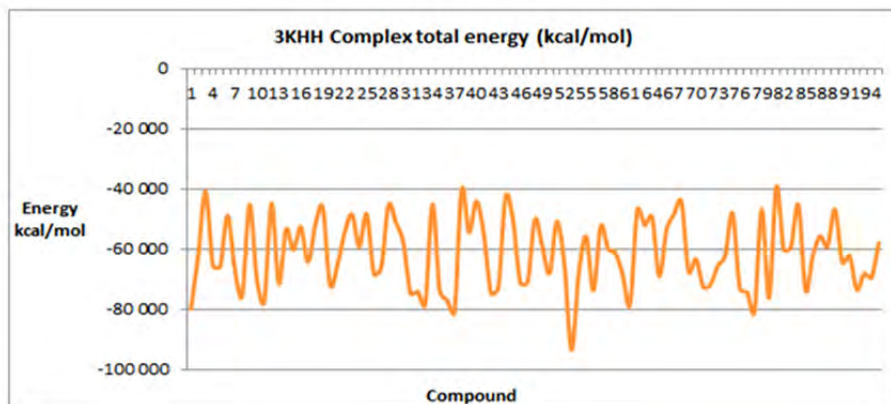


Figure 2. Docking energy data: the smooth lines represent total energy of the complex of amine compounds with the transferase DNA fragment (3KHH).

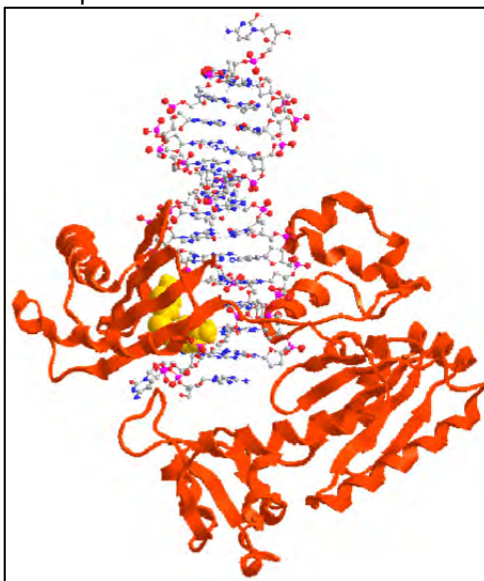


Figure 3. Ligand #53(space filling –yellow) in the complex with its presumable target 3KHH.

A linear model using Cluj topological descriptors and including docking data was computed. Docking data were explained 2% by the Cluj descriptors (in single variable), totally unsatisfactory. These descriptors better describe log P (in ligand aligned/oriented approach):

$y = 1.01 + SD_{\log P}(\text{fragmental mass})$; $n = 92$, $r^2 = 0.77$ (three molecules were found as outliers).

To further increase the correlation value, a new set of Cluj topological descriptors (considering the heteroatoms) was computed; then, different types of models were generated. The models using only Cluj topological descriptors provided unsatisfactory results, irrespective what technique was used (e.g., MLR, NNR, SVM); among these, the best values, $r^2 = 0.583$, $p = 0.506$, $q^2 = 0.334$ were given by the NNR model.

In ligand orientated approach⁵, a cluster correlation mapping⁶ of the entire Cluj topological descriptors was performed. Correlations and disturbance in data dimensionality were observed (boded continuous red regions – Figure 4). These regions suggest that there is yet information that needs to be explored (eventually by using other descriptors). Receptor aligned/oriented approach is not appropriate manly because the real target and consecutively mutagenicity mechanism is not known.

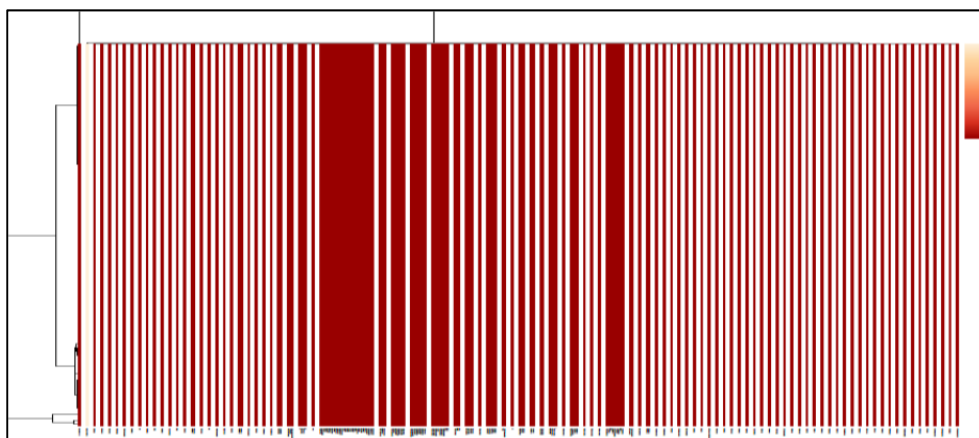


Figure 4. Cluj topological descriptors cluster correlation space. Confluent lines suggest correlation

⁵ Deng Z, Chuaqui C, Singh J, *Journal of Medicinal Chemistry*. **2004**, 47 (2), 337.

⁶ Campbell M.K., Grimshaw J.M., Elbourne D.R., *BMC Medical Research Methodology*, **2004**, 4, 9.

In order to prove that data dimensionality can be improved by new descriptors, a predictive model, based on interactions between descriptors was developed. PCA was calculated for all 95 compounds TopoCluj descriptors set. A further selection algorithm was used to choose the independent variables; the number of descriptors used was 19. The descriptors are: C[Sh[CjMin]]; IP[CjMin]; PC10; PC11; PC12; PC13; PC16; PC17; PC2; PC22; PC3; PC4; PC5; PC6; PC7; PC8; PC9; X[LM[Electronegativity]]; X[LM[Mass]]. Model was computed using MLR: $\text{RMSE}=0.000337$, $q^2=0.99$, $r^2=0.99$ and plotted in Figure 5.

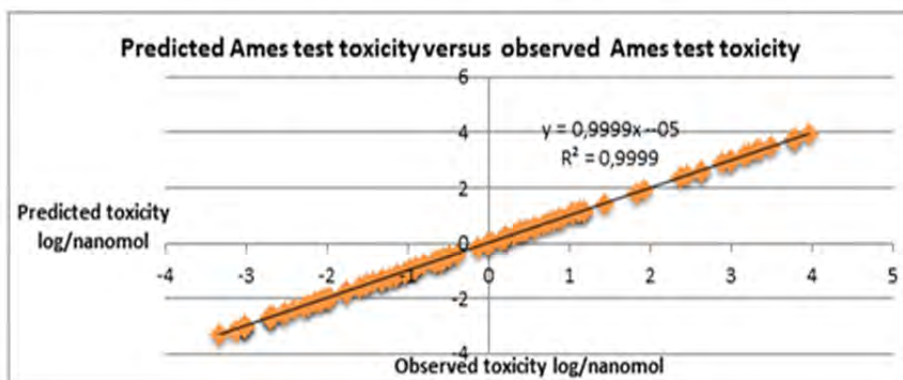


Figure 5. Plot of Observed toxicity vs predicted toxicity (mutagenicity), with 19 descriptors.

CONCLUSION

Data dimensionality can be explored using PCA. Models based on descriptors interactions include information of all descriptors of the chemical space. Models built using descriptors based on culture media simulations are superior in predicting occurrence of toxicity compared with the models developed on the basis of Cluj topological descriptors.

EXPERIMENTAL

In order to explore data dimensionality, a set of 95 amine compounds with observed Ames mutagenicity test ($\log C$; nM) were used. QSAR methodology with related regression models was implemented for exploring data dimensionality. Two type of models were consider: (i) discriminant (perceptive) models, where collinearity and

multicollinearity are avoided by using statistical tests applied to descriptors (like variability, tolerance and value of inflation (VIF)); (ii) predictive models, where collinearity and multicollinearity were not taken into account, the target being the r^2 value, which in this case is not influenced by descriptors dimensionality. Correlation between observed and predicted data was studied.

Descriptors used for characterizing the data set were topological descriptors based on adjacency, connectivity and distance matrix and Cluj matrices, respectively. Using this methodology, 185 topological descriptors were computed for each compound using TopoCluj software. A future selection algorithm was used to select topological descriptors with relevant information regarding mutagenicity explored by Ames test.

Regression models were built using distinct methodologies: multiple linear regression (MLR), partial least square regression (PLS), support vector regression (SVR) and neural network regression (NNR). Models were validated internally, using the leave-one-out technique, and externally, by evaluating the test set. Compounds were randomly divided into a training and a test set. For the predictive model, interactions between descriptors were computed providing multiplicative cross-terms and principal component analysis (PCA).

Docking studies were performed on a hypothetical complex (DNA-protein-ligand) binding site located on DNA strings. Strings were retrieved from literature and from PDB data: 3KHH. Complex total energy (kcal/mol) was chosen to generate a new QSAR model in order to obtain a better r^2 using combined docking energy and Cluj topological descriptors. To explore deeper in data dimensionality a set of commercially available descriptors was computed and a regression model was compiled. Models from both descriptor type were compared.

ACKNOWLEDGEMENT

This work was supported by a grant of the Romanian National Authority for Scientific Research and Innovation, CCCDI – UEFISCDI, project number 8/2015, acronym GEMNS (under the frame of the ERA-NET EuroNanoMed II European Innovative Research and Technological Development Projects in Nanomedicine).

REFERENCES

1. Jolliffe I.T. Principal Component Analysis, Series: Springer Series in Statistics, 2nd ed., Springer, NY, , XXIX, 487 p. 28 . ISBN 978-0-387-95442-4, **2002**.
2. Hair, J. F. Jr., Anderson, R. E., Tatham, R. L. & Black, W. C. Multivariate Data Analysis (3rd ed). New York: Macmillan, **1995**.
3. Wallace A.D. *Progress in Molecular Biology and Translational Sciences*, **2012**, 112, 89.
4. Basak, S.C.; Vračko, M.; Witzmann, F.A. *Current Computer Aided Drug Design*, **2016**, 12(4), 259.
5. Deng Z, Chuaqui C, Singh J, *Journal of Medicinal Chemistry*. **2004**, 47 (2), 337.
6. Campbell M.K., Grimshaw J.M., Elbourne D.R., *BMC Medical Research Methodology*, **2004**, 4, 9.
7. Norman R. Draper, Smith H., Applied Regression Analysis. Wiley, New York, **1998**.
8. Wold, S; Sjöström, M.; Eriksson,L., *Chemometrics and Intelligent Laboratory Systems* **2001**, 58, 109.
9. Fisher, R.A., *Annals of Eugenics* **1936**, 7, 179.
10. Fernández, S., Graves, A., Schmidhuber, J., *In Proc. 20th Int. Joint Conf. on Artificial Intelligence, Ijcai: 2007*, 774.
11. Kohavi, R., Mateo, C.A., Morgan K., *Proceedings of the Fourteenth International Joint Conference on Artificial Intelligence. San. 1995*, 2 (12), 1137.
12. San-Martin A1, Donoso V, Leiva S, Bacho M, Nunez S, Gutierrez M, Roviroza J, Bailon-Moscoso N, Camacho SC, Aviles OM, Cazar ME, *Current Topics Medicinal Chemistry*, **2015**, 15(17), 1743.
13. Gramatica P. *QSAR & Combinatorial Science* **2007**

In memory of prof. dr. Simion Gocan

THE OCCURRENCE AND SOURCE EVALUATION OF POLYCYCLIC AROMATIC HYDROCARBONS IN URBAN ATMOSPHERE USING MOSS AS BIOMONITOR AND GC-MS ANALYSIS

ANDREEA ROTARU^a, EDINA REIZER^a, VLAD PĂNESCU^a, SORIN POP^a,
MIHAIL SIMION BELDEAN-GALEA^{a*}

ABSTRACT: Polycyclic aromatic hydrocarbons (PAHs) make part of the persistent organic pollutants (POPs) class. The most harmful PAHs are generated during the incomplete combustion of organic material. European legislation has recommended the use of bioindicators to estimate the impact of PAHs on the ecosystem. The aim of this work was to investigate the occurrence of atmospheric PAHs in 14 urban areas in Romania, using moss as bioindicator. The pollution emission sources, applying diagnostic ratios, were also evaluated. The PAHs were analyzed by gas chromatography-mass spectrometry (GS-MS). This study showed the presence of PAHs in moss samples in concentrations which are dependent on the sampling zone, ranging from 2.7 to 394 ng g⁻¹. The cities with the highest amounts of total PAHs were found within the Carpathian arch, while the cities situated in the western part of the country had the lowest amounts. The FLA/(FLA+PYR) and FL/(FL+PYR) ratios indicate both the diesel emission source, fossil fuels combustion source and wood or coal combustion source which may come either from traffic, industrial activities, centralized heating systems, or from other type of industry.

Keywords: *Polycyclic aromatic hydrocarbons, urban atmosphere, bioindicators, moss, GC-MS*

^a Babeş-Bolyai University, Faculty of Environmental Science and Engineering, 30 Fântânele street, RO-400294, Cluj-Napoca, Romania
^{*} Corresponding author simion.beldean@yahoo.com

1. INTRODUCTION

Polycyclic aromatic hydrocarbons (PAHs) make part of the persistent organic pollutants (POPs) class, having a structure composed of multiple aromatic rings. In 1976, the U. S. Environmental Protection Agency (U.S. EPA) reduced the group of hundreds of PAHs to only 16 relevant compounds [1-2], issuing a list with "16 priority PAHs" to be representative for all. Furthermore the 16 EPA PAHs became crucial subjects for environmental examinations.

The most harmful PAHs are generated during the incomplete combustion of organic material, predominantly due to anthropogenic activities [3]. In highly populated and heavily urbanized or industrialized areas, the most significant emission sources are residential heating, coal gasification, asphalt production, and motor vehicle exhaust [4]. In order to identify and assess the source of PAHs, numerous studies have been published most of them based on different diagnostic ratios [5-8].

Environmental assessment of PAHs in ambient air is essential, because many of them exhibit carcinogenic and mutagenic properties [9]. PAHs are omnipresent in two phases in the lower atmosphere with different concentration levels: in vaporous phase and in solid phase as sorbet onto aerosols [10]. After their atmospheric transportation and dry or wet deposition, processes that are strongly dependent on the relationship between vapor pressure and molecular weight [11], PAHs tend to accumulate in vegetation. Biomonitoring of PAHs on plants gained popularity in the last four decades [12-15]. The application of moss as passive accumulator for PAHs is widespread in so-called air quality assessment studies, because of (i) their strong presence at the local scale, (ii) their relative cost-effective methodology (compared to physical-chemical approach) [15], (iii) their morphological and physiological properties [16-17].

In addition, European legislation has recommended the use of bioindicators to estimate the impact of PAHs on the ecosystem [18]. Directive 2004/107/EC of the European Parliament granted the Member State the employment of any other sampling methods to assess spatial deposition of PAHs, with which they can demonstrate that the results are equivalent to those obtained with reference methods, such as: ISO standard 12884:2000.

The aim of this work was to investigate the occurrence of atmospheric PAHs in 14 urban areas in Romania, using moss as bioindicator and to establish the pollution emission sources, applying different diagnostic ratios.

2. RESULTS AND DISCUSSION

2.1. Analytical performance of the analysis method

Precision, linearity, limit of detection (LOD) and limit of quantification (LOQ) (Table 1) were the variables taken into account to study the performance of the GC-MS method used for the analysis of PAHs in moss samples.

Table 1. Analytical performances of GC-MS method

Compound	Linear curve equation (range 0.04-2 $\mu\text{g mL}^{-1}$)	R ²	Slope	SD	LOD ($\mu\text{g mL}^{-1}$)	LOQ ($\mu\text{g mL}^{-1}$)	RSD %
Naphthalene	y= 104860236x + 14714750	0.994	104860236	208708	0.006	0.020	3.26
Acenaphthylene	y= 86128700x + 12316361	0.992	86128700	213042	0.007	0.025	4.35
Acenaphthene	y= 29620687x + 4318189	0.992	29620687	76969	0.008	0.026	4.07
Fluorene	y= 53467933x + 7941405	0.991	53467933	90371	0.005	0.017	2.93
Phenanthrene	y= 57418106x + 8784001	0.992	57418106	164470	0.009	0.029	3.49
Anthracene	y= 65827841x + 11237350	0.981	65827841	146115	0.007	0.022	3.54
Fluoranthene	y= 52675476x + 9097934	0.985	52675476	114724	0.007	0.022	3.31
Pyrene	y= 52161938x + 9634681	0.982	52161938	105882	0.006	0.020	3.00
Benz[a]anthracene	y= 30467866x + 5076543	0.976	30467866	48552	0.005	0.016	2.36
Chrysene	y= 30795452x + 7611809	0.957	30795452	59244	0.006	0.019	2.37
Benzo[b]fluoranthene	y= 22969230x + 3977709	0.973	22969230	61071	0.008	0.027	3.43
Benzo[k]fluoranthene	y= 23772068x + 5908712	0.951	23772068	41801	0.005	0.018	2.11
Benzo[a]pyrene	y= 21785791x + 4918591	0.954	21785791	33623	0.005	0.015	1.84
Indeno(1.2.3 cd)pyrene	y= 14855868x + 3799708	0.946	14855868	71739	0.014	0.048	5.06
Dibenz[a,h]anthracene	y= 18949082x + 6355776	0.929	18949082	152213	0.024	0.080	6.62
Benzo[ghi]perylene	y= 16697664x + 5366355	0.928	16697664	79739	0.014	0.048	4.12

R² - coefficient of determination; SD - standard deviation; LOD - limit of detection, LOQ - limit of quantification, RSD - relative standard deviation for (n = 6);

Intra-day precision (repeatability) was expressed by means of six replicates ($n=6$) of a 16 PAHs standard mixture in concentration of $0.04 \mu\text{g mL}^{-1}$. The obtained results were situated under 15%, ranging between 1.84% and 6.62%, which prove a good repeatability of the method.

Calibration curve method was used to quantify the target compounds in real samples. In Table 1 one may observe a good linearity for all target PAHs, R^2 values ranging from 0.928 to 0.994. LOD and LOQ of each of the PAHs were determined using the standard deviation and the slope of each calibration curve. LODs and LOQs were situated in the range of 0.005 and $0.024 \mu\text{g mL}^{-1}$, and between 0.016 and $0.08 \mu\text{g mL}^{-1}$, respectively.

2.2. Analysis of moss samples

The presence of multiple PAHs in moss samples collected from various central parks from some of Romania's largest cities is demonstrated in all analyzed samples. In Figure 1 it is shown an integrated chromatogram of an extract of mosses collected from Copou Park, Iași city, where the presence of PAHs can be observed.

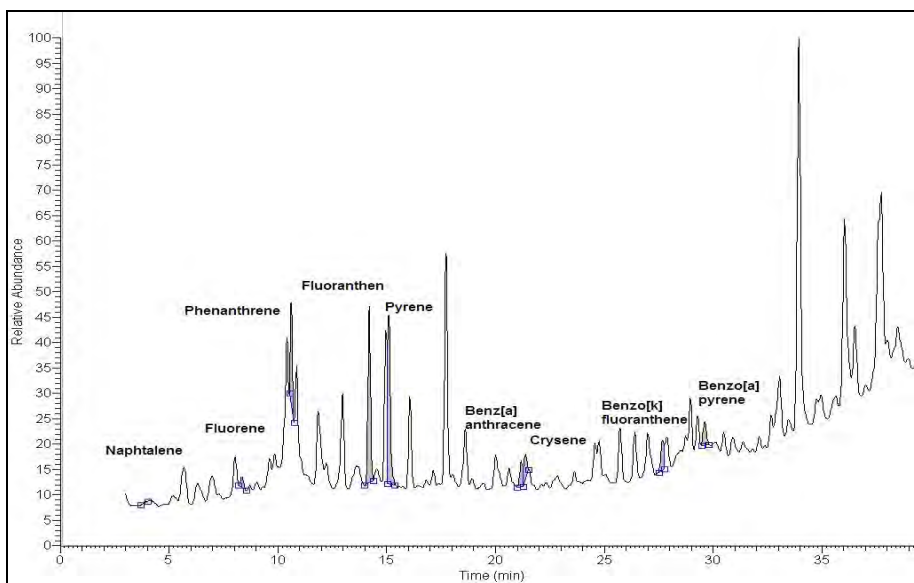


Figure 1. SIM Chromatogram of tested PAHs in moss sample (Iași city)

The content of PAHs in the analyzed moss samples collected from the selected sampling areas is shown in Table 3.

Table 3. The occurrence of PAHs in analyzed moss samples

Compound	Abb.	Sample code/Concentration (ng g ⁻¹)													
		S1	S2	S3	S4	S5	S6	S7	S8	S9	S10	S11	S12	S13	S14
Naphthalene	NP	0.87	nd	0.06	16.42	nd	3.9	1.95	nd	0.76	2.44	0	0	nd	nd
Acenaphthylene	ACY	1.38	nd	nd	97.43	8.85	nd	3.59	2.28	3.5	1.81	4.12	4.62	nd	2.79
Acenaphthene	ACE	nd	nd	nd	34.24	2.71	nd	1.92	nd	1.54	nd	nd	nd	nd	2.35
Fluorene	FL	1.1	2.36	1.26	5.95	5.31	nd	nd	nd	8.81	nd	nd	10.09	nd	2.68
Phenanthrene	PHE	1.57	0.98	6.69	12.84	21.15	17.17	9.33	1.79	2.54	4.92	4.14	1.87	nd	10.14
Anthracene	ANT	nd	nd	nd	nd	nd	nd	nd	nd	nd	nd	nd	nd	1.59	50.46
Fluoranthene	FLA	2.73	1.39	19.41	33.47	28.74	16.26	13.27	8.47	5.98	8.28	2.66	6.38	nd	3.15
Pyrene	PYR	0.91	nd	18.83	nd	14.6	11.06	11.57	4.85	4.74	11.02	2.62	5.22	1.13	5.78
Benz[a]anthracene	BaA	0.67	0.18	7.2	5.7	1.33	0.3	0.84	15.85	1.08	0.44	0.68	0.54	nd	0.98
Chrysene	CHR	nd	0.02	5.11	nd	nd	nd	nd	nd						
Benzo[b]fluoranthene	BbF	nd	nd	nd	4.93	nd	nd	nd	nd	nd	nd	1.81	nd	nd	nd
Benzo[k]fluoranthene	BkF	nd	nd	12.89	23.75	nd	nd	nd	nd	nd	nd	nd	nd	nd	88.01
Benzo[a]pyrene	BaP	2.4	6.56	10.81	8.65	54.77	10.39	9.76	8.43	15.73	4.04	8.14	5.71	nd	2.53
Indeno(1,2,3-cd)pyrene	lcdP	344.9	156.8	nd	nd	nd	nd	206.3							
Dibenz[a,h]anthracene	DahA	nd	4.94	nd	nd	nd	nd	16							
Benzo[ghi]perylene	BghiP	2.49	nd	nd	nd	nd	nd	nd	3.59	nd	nd	nd	nd	nd	2.81
Total PAHs		359	173.3	82.3	243.4	137.5	59.1	52.2	45.3	44.7	33	24.2	34.4	2.7	394

nd- not detected

The results of the analyzed moss samples showed that, the cities with highest amounts of Σ PAHs were found within the Carpathian arch. The highest amount of Σ PAHs, 394 ng g⁻¹ was found in Cluj-Napoca city (S14), followed by Alba Iulia city (S1), with 359 ng g⁻¹ and Braşov city (S4), with 243 ng g⁻¹, Sibiu city (S2), with 173.3 ng g⁻¹, Bistriţa city (S5), with 137.5 ng g⁻¹, and Târgu Mureş city with 45.3 ng g⁻¹

The cities situated in the western part of the country had the lowest amounts, below 40 ng g^{-1} , top of which, with 2.7 ng g^{-1} was Timișoara city (S13), followed by Arad city (S11), with 24.2 ng g^{-1} , and Oradea city (S12), with 34.4 ng g^{-1} , although Ploiești city, situated in the southern part of Romania had a slighter smaller amount, of 33 ng g^{-1} .

The cities situated in the eastern part of the country have slightly higher concentrations of PAHs in moss samples than those situated in the southern part, with 52.2 ng g^{-1} in Bacău city (S7) and 82.7 ng g^{-1} in Iași city (S3). The south of the country had values between 33 ng g^{-1} in Ploiești city (S10), 59 ng g^{-1} in Pitești city (S6) and 44.7 ng g^{-1} in Bucharest (S9), the country's capital.

2.3. PAHs sources identification using isomeric ratios

To establish the source of the analyzed PAHs, several isomeric ratios were used such as: Σ sum of Low Molecular Weight PAHs (two-three ring PAHs) and Σ sum of High Molecular Weight PAHs (four-six rings PAHs) ratio ($\Sigma_{\text{LMW}}/\Sigma_{\text{HMW}}$); sum of PAH resulted from combustion (FLA, PYR, BaA, CHR, BkF, BbF, BaP, IcdP and BghiP) and sum of total PAHs ($\Sigma_{\text{COMB}}/\Sigma_{\text{PAHS}}$), the FL/(FL+PYR) and FLA/(FLA+PYR) ratios [19]. As one may observe in Table 3, the $\Sigma_{\text{LMW}}/\Sigma_{\text{HMW}}$ ratio indicates that there is a pyrogenic source in all the samples, except Brașov city (S4) the obtained values being situated under 1 value. The $\Sigma_{\text{COMB}}/\Sigma_{\text{PAHS}}$ ratio indicates a combustion source (~ 1) in most of the cities, except Brașov city (S4), Oradea city (S12) and Timișoara city (S13) of which the values are far away from 1. The FL/(FL+PYR) ratio indicates a petrol emission in Alba Iulia city (S1), București city (S9) and Oradea city (S12) (values under 0.5), and a diesel emission in Iași city (S3), Bistrița city (S5) and Cluj-Napoca city (S14) (values over 0.5). Finally, the FLA/(FLA+PYR) ratio, indicates petrogenic source in Cluj-Napoca city (S14) (value under 0.4), fossil fuel combustion source in Ploiești city (S10) (value between 0.4 and 0.5), and grass, wood or coal combustion source (value over 0.5) in all the other cities that could have this ratio calculated.

Table 3. Available PAH diagnostic ratios according to sampling locations

	S1	S2	S3	S4	S5	S6	S7	S8	S9	S10	S11	S12	S13	S14
$\Sigma_{\text{LMW}}/\Sigma_{\text{HMW}}$	0.01	0.01	0.02	1.72	0.14	0.07	0.17	0.05	0.49	0.15	0.21	0.75	NA	0.02
$\Sigma_{\text{COMB}}/\Sigma_{\text{PAHS}}$	0.99	0.95	0.9	0.31	0.72	0.64	0.68	0.91	0.62	0.72	0.66	0.52	0.42	0.79
FL/(FL+PYR)	0.55	NA	0.06	NA	0.27	NA	NA	NA	0.65	NA	NA	0.66	NA	0.32
FLA/(FLA+PYR)	0.75	NA	0.51	NA	0.66	0.6	0.53	0.64	0.56	0.43	0.5	0.55	NA	0.35

NA- not available

If the sources according to the FLA/(FLA+PYR) and FL/(FL+PYR) ratios are cross-examined (Figure 2), one may observe that mixed sources of

PAH are present in all studied areas. Thus, in Cluj-Napoca (S14) there is a petrogenic and petrol emission source, which is probably due to vehicle emissions. In Alba Iulia city (S1), București city (S9) and Oradea city (S12) the sources are both from diesel emission and from wood or coal combustion. These ratios indicate both heavy traffic (the diesel emission source) and industrial activities (wood or coal combustion source – either from the centralized heating systems or from other type of industries). In Iași city (S3) and Bistrița city (S5) the sources are both from petrol and from wood or coal combustion. Bistrița city seems to be more inclined towards industry, while Iași city tends to have a more likely fossil fuels combustion source.

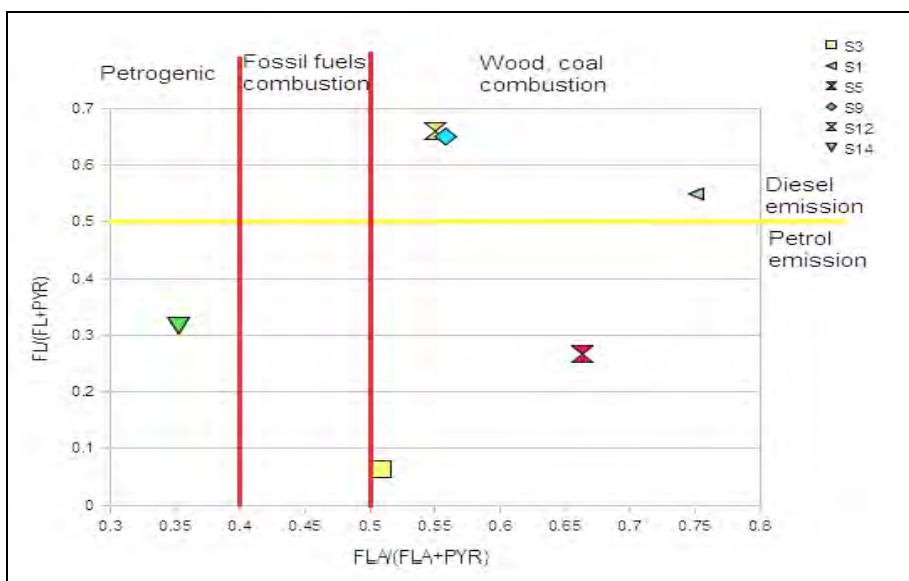


Figure 2. Cross examination of the FLA/ (FLA+PYR) against FL/ (FL+PYR) ratios in the selected locations

3. CONCLUSIONS

This study showed the presence of PAHs in moss samples in concentrations which are dependent on the sampling zone.

The cities with the highest amounts of Σ PAHs were found within the Carpathian arch, while the cities situated in the western part of the country had the lowest amounts. The cities located in the eastern part of the country have slightly higher concentrations of PAHs in moss samples than those situated in the southern part.

The \sum_{LMW}/\sum_{HMW} ratio indicates that there is a pyrogenic source in all the samples, and the \sum_{COMB}/\sum_{PAHS} ratio confirms the combustion source (~1) in most of the cities.

The FLA/(FLA+PYR) and FL/(FL+PYR) ratios indicate both heavy traffic (the diesel emission source and fossil fuels combustion source) and industrial activities (wood or coal combustion source), which may come either from the centralized heating systems, or from other type of industries.

4. EXPERIMENTAL SECTION

4.1. Reagents and solutions

For the qualitative and quantitative analysis an EPA PAH standard mixture containing 16 compounds in concentration of $2 \mu\text{g mL}^{-1}$ of each compound purchased by Supelco was used. The PAHs determined were: naphthalene, acenaphthene, acenaphthylene, fluorene, phenanthrene, anthracene, fluoranthene, pyrene, benz[a]anthracene, chrysene, benzo[b]fluoranthene, benzo[k]fluoranthene, benzo[a]pyrene, indeno(1,2,3-cd)pyrene, dibenz[ah]anthracene and benzo[ghi]perylene. Dichloromethane and n-hexane in purity of 99.99% were purchase from Merck, Germany and helium in purity of 99.9999% from Linde Gas, Romania.

4.2. Instrumentation and chromatographic conditions

The PAHs were analyzed by gas chromatography-mass spectrometry using a gas chromatograph model Thermo Electron Corporation (Focus GC) equipped with a DSQII mas spectrometer and a TriPlus Autosampler. The separation of target compounds was performed on DB-5 MS column ($25 \text{ m} \times 0.25 \text{ mm} \times 0.25 \mu\text{m}$) using helium as carrier gas at a constant flow of $1,2 \text{ mL min}^{-1}$. The MS ion source was heated at 200°C , and the detection of the target compounds was made on selected ion monitoring (SIM) mode.

The separation of the PAHs was performed with two gradient of temperature as follows: from 120°C , up to 220°C with $10^\circ\text{C min}^{-1}$, and from 220°C to 300°C with 3°C min^{-1} . Injection volume was $1 \mu\text{L}$ in splitless mode.

The quantification of the target compounds in real samples was made by the calibration curve method. For this purpose five standard solutions in concentration of 0.04, 0.05, 0.07, 0.1 and $0.2 \mu\text{g mL}^{-1}$ were prepared by dilution of the standard mixture ($2 \mu\text{g mL}^{-1}$). The calibration curves were built using the chromatographic peak area and the concentration of each of the PAHs.

4.3 Ultrasound assisted extraction procedure

From each sample, 3 g of milled moss were weighed in a Berzelius beaker then added thirty milliliter of a mixture of n-hexane:dichloromethane (1:1 v/v). The samples were placed in ultrasonic bath for 15 minutes and then the solvent was decanted and filtered through a PVDF sample filter with pore size of 0.45 μm (Merck Milipore). The resulted extract was evaporated to dryness with a rota-evaporator and the residue was dissolved with 2 milliliter of n-hexane:dichloromethane (1:1 v/v) mixture and kept in the freezer until the analysis.

4.4 Sampling points

The study was carried out in 14 of the largest cities in Romania (Figure 3). All of the samples were collected at distances of more than 5 m from roads and houses, from 1 - 2 meters high. The samples were all collected from central parks areas.

The moss samples were collected with a stainless steel scissors in sterilized polyethylene bags and kept at 8°C until analysis.



Figure 3. The map of moss sampling points (Alba Iulia city (S1), Sibiu city (S2), Iași city (S3), Brașov city (S4), Bistrița city (S5), Pitești city (S6), Bacău city (S7), Târgu Mureș city (S8), Bucharest (S9), Ploiești city (S10), Arad city (S11), Oradea city (S12), Timișoara city (S13), Cluj-Napoca city (S14))

ACKNOWLEDGEMENTS

This study was performed in the frame of a performance scholarship funded by Babeş-Bolyai University.

REFERENCES

1. ATSDR, *Toxicology profile for polyaromatic hydrocarbons*. ATSDR's Toxicological Profiles on CD-ROM, CRC Press, Boca Raton, FL, **2005**.
2. L. Keith, Polycyclic Aromatic Compounds., **2014**, 35, 147.
3. J.H. Rodriguez, E.D. Wannaz, M.J. Salazar, M.L. Pignata, A. Fangmeier, J. Franzaring, *Journal of Atmospheric Environment*, **2012**, 55, 35.
4. H.I. Abdel-Shafy, M.S.M. Mansour, *Egyptian Journal of Petroleum*, **2016**, 25, 107.
5. Katsoyiannis, E. Terzi, Q.-Y. Cai, *Chemosphere*, **2007**, 69, 1337.
6. Oliveira, N. Martins, J. Tavares, C. Pio, M. Cerqueira, M. Matos, H. Silva, C. Oliveira, F. Camões, *Chemosphere*, **2011**, 83, 1588.
7. W. Zhang, S. Zhang, C. Wan, D. Yue, Y. Ye, X. Wang, *Environmental Pollution*, **2008**, 153, 594.
8. M.B. Yunker, R.W. Macdonald, R. Vingarzan, R.H. Mitchell, D. Goyette, S. Sylvestre, *Organic Geochemistry*, **2002**, 33, 489.
9. IARC, *Chemical, Environmental and Experimental Data*, Part 1, **1983**, vol. 32.
10. K. Ravindra, R. Sokhi, R.V. Grieken, *Journal of Atmospheric Environment*, **2008**, 42, 2895.
11. EPRI (Electric Power Research Institute). Literature review of background polycyclic aromatic hydrocarbons. Final report; March **2000**.
12. W. Thomas, *Journal of Ecotoxicology and Environmental Safety*, **1986**, 11, 339.
13. E.-L. Viskari, R. Rekilä, S. Roy, O. Lehto, J. Ruuskanen, L. Kärenlampi, *Journal of Environmental Pollution*, **1997**, 97, 153.
14. H.G. Zechmeister, S. Dullinger, D. Hohenwallner, A. Riss, A. Hanus-Ilmar, S. Scharf, *Environmental Science and Pollution Research*, **2006**, 13, 398.
15. F. Capozzi, S. Giordano, A. Di Palma, V. Spagnuolo, F. De Nicola, P. Adamo, *Chemosphere*, **2016**, 149, 211.
16. L. Foan, V. Simon, *Journal of Chromatography A*, **2012**, 1256, 22.
17. H. Harmens, L. Foan, V. Simon, G. Mills, *Environmental Pollution*, **2013**, 173, 245.
18. European Union, 2004. Directive 2004/107/EC of the European Parliament and of the Council of 15 December 2004 relating to arsenic, cadmium, mercury, nickel and polycyclic aromatic hydrocarbons in ambient air. Official Journal 23, 3–16.
19. M. Tobiszewski, J. Namiejnik, *Environmental Pollution*, **2012**, 162, 110.

OPTICAL PROPERTIES AND MICROSTRUCTURAL CHANGES OF HARD DENTAL TISSUES IN GASTRO-ESOPHAGEAL REFLUX DISEASE PATIENTS

OLGA HILDA ORASAN^a, ANDREA MARIA CHISNOIU^{b *},
MONICA LAURA DASCĂLU (RUSU)^c, OVIDIU PĂSTRAV^d,
MIHAELA PĂSTRAV^e, MARIOARA MOLDOVAN^f, RADU CHISNOIU^d

ABSTRACT. Dental erosion is a frequent complication of patients with gastro-esophageal reflux disease. Loss of superficial enamel can be observed by a color change towards yellow and increased translucency of the teeth. The aim of our study was to analyze salivary parameters and dental erosion status in patients with gastro-esophageal reflux disease, and to evaluate optical properties (color parameters variation) and microstructural modifications (using atomic force microscopy) of eroded compared to healthy dental structures. The association of dental erosion and gastro-esophageal reflux disease was significant. Variations of ΔE are higher than general average variations of ΔL in these patients.

Keywords: *gastro-esophageal reflux disease, dental erosion, color parameters variation, atomic force microscopy*

^a 4th Medical Department, Faculty of Medicine, University of Medicine and Pharmacy "Iuliu Hațieganu", 18 Republicii Street, 400015, Cluj-Napoca, Romania.

^b Department of Prosthetic Dentistry, Faculty of Dental Medicine, University of Medicine and Pharmacy "Iuliu Hațieganu", 32 Clinicilor Street, 400006, Cluj-Napoca, Romania.

* Corresponding author: ANDREA CHISNOIU, e-mail: dr.chisnoiu@yahoo.com

^c Department of Preventive Dentistry, Faculty of Dental Medicine, University of Medicine and Pharmacy "Iuliu Hațieganu", 32 Clinicilor Street, 400006, Cluj-Napoca, Romania.

^d Department of Odontology and Oral Pathology, Faculty of Dental Medicine, University of Medicine and Pharmacy "Iuliu Hațieganu", 33 Motilor Street, 400001, Cluj-Napoca, Romania.

^e Department of Orthodontics and Orofacial Orthopaedics, Faculty of Dental Medicine, University of Medicine and Pharmacy "Iuliu Hațieganu", 33 Motilor Street, 400001, Cluj-Napoca, Romania.

^f "Babes Bolyai" University - "Raluca Ripan" Chemistry Research Institute, 30 Fântânele Street, 400294, Cluj-Napoca, Romania.

INTRODUCTION

Gastro-esophageal reflux disease (GERD) is the most frequent esophageal pathology, a chronic disease with high morbidity risk and potential mortality by its complications [1].

A positive correlation has been identified between excessive acid exposure and chemical dissolution of dental structures, assessed by esophageal pH monitoring [2-4]. The enamel dissolution is a fast process that produces the extensive diffusion of protons layer in solution [5,6].

Hydrochloric acid from the gastric contents is responsible for the demineralization of dental hard tissues and release of matrix metalloproteinase from the dentin. The clinical effect, produced by the opening of dentinal tubules, is the apparition of cervical dentinal sensitivity, as a result of dynamic changes of dentinal fluids and dental tissues loss [7,8].

Tooth wear is usually assessed using visual scoring systems. These methods lack criteria for distinguishing stages of erosion limited to the enamel. Thus, erosion is mostly diagnosed at a severe stage and is difficult to monitor [9,10,11]. Currently two quantitative assessment methods have been described: profilometry and ultrasound. Loss of superficial enamel can be observed by a color change of the teeth towards yellow. Reducing enamel thickness will increase translucency, making the underlying dentin more visible [12-14]. We hypothesized that a useful tool for detecting and monitoring dental erosion might be represented by this color change.

Most data from research about color in dentistry are obtained under the CIEL*a*b* (CIE: Commission Internationale de l'Eclairage; International Commission on Illumination) system, and these are reported by corresponding symbols L* (luminosity), a* (green-red color coordinate), b* (blue-yellow color coordinate), C* (shade), h (saturation) and ΔE_{ab} (global color difference). The formula for ΔE_{ab} is:

$$\Delta E_{ab} = [(\Delta L^*)^2 + (\Delta a^*)^2 + (\Delta b^*)^2]^{1/2},$$

where ΔL*, Δa*, Δb* represent the difference between two values of the same parameter. The values of color difference ΔE_{ab} can offer a clear image of the "matching" degree between two samples or teeth [15, 16].

SEM microscopy performs qualitative analysis of the enamel surfaces changes under erosive processes. SEM microscopy determines the extension of the affected enamel surfaces regarding the alteration degree of enamel prisms accordingly to SEM images [17].

This study aimed to analyze salivary parameters (pH and buffering capacity) and dental erosion status in patients with GERD symptoms. The research was also focused on the evaluation of optical properties (color parameters variation) and microstructural changes (using atomic force microscopy- AFM) of eroded compared to healthy dental structures.

RESULTS AND DISCUSSION

The degree of erosion in patients with GERD (group 1) was higher than in controls. Most of the patients in the non-GERD group (89.5%, n=43) presented a BEWE score lower than 9. In the GERD group, 63.6% (n=14) of patients presented a BEWE score higher than 9 (Fig. 1).

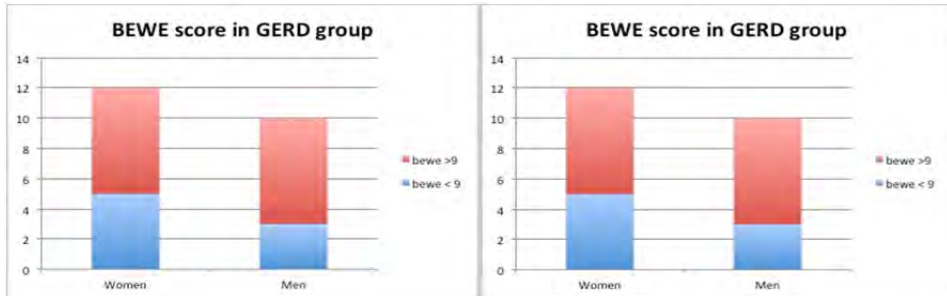


Figure 1. BEWE score in the GERD group vs the non-GERD group (BEWE: Basic Erosive Wear Examination; GERD: gastro-esophageal reflux disease)

The risk for developing dental erosion was mostly absent or low among non-GERD patients. Patients in the GERD group more frequently presented a medium or high risk for dental erosion ($p=0.032$) (Fig. 2).

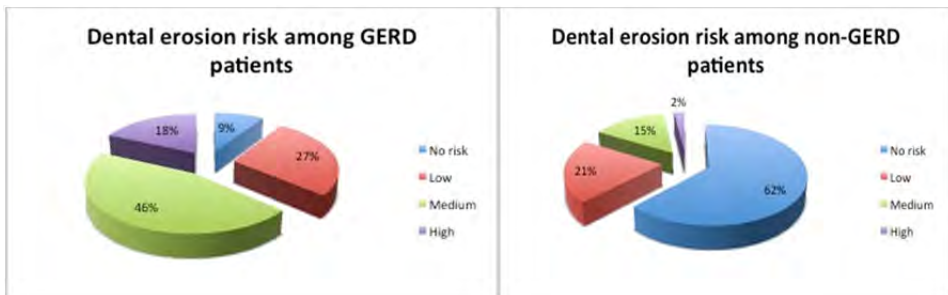


Figure 2. Dental erosion risk in the GERD group vs the non-GERD group (GERD: gastro-esophageal reflux disease)

There were no pH differences between the 2 groups ($p=0.36$). Salivary buffering capacity in patients with GERD showed lower values than in controls ($p=0.048$). The mean buffering capacity in the GERD group was 8. A significant direct correlation was identified between the BEWE score and buffering capacity ($p=0.003$). For each type of substrate taken into study, the 2 groups of teeth, respectively, the average values of ΔE and

ΔL were calculated. The results and the statistical analysis for measuring color parameters using the Vita Easyshade spectrophotometer are presented in Tables 1 and 2. The calculation of the two parameters tracked by us was made according to the above formulas, and statistical calculation was performed based on samples taken into work.

Table 1. Calculated ΔE and ΔL values in the extracted teeth samples from healthy (non-GERD) patients and GERD patients

Samples	ΔE	ΔL
	1.70	1.30
Non-GERD	0.70	-0.70
	1.89	-1.60
	3.01	2.90
	2.92	2.70
	10.87	0.70
GERD	14.81	-5.80
	10.04	2.90
	9.57	1.00
	11.07	8.20

ΔE : color differences; ΔL : luminosity differences; GERD: gastro-esophageal reflux disease

Table 2. t-Test for the GERD group

t-Test: Paired Two Sample for Means		
GERD	ΔE	ΔL
Mean	2.04270652	0.92
Variance	0.90918759	4.052
Observations	5	5
Pearson Correlation	0.486657501	0.083285954
Hypothesized Mean Difference	0	0
Df	4	4
t Stat	-3.858925877	-2.248726175
P (T<=t) one-tail	0.009081931	0.043884463
t Critical one-tail	2.131846786	2.131846786
P (T<=t) two-tail	0.018163862	0.087768926
t Critical two-tail	2.776445105	2.776445105

ΔE : color differences; ΔL : luminosity differences; GERD: gastro-esophageal reflux disease

Statistics applied to color parameters (ΔE) in the healthy (non-GERD) and GERD groups showed significant changes for eroded dental structures on the analyzed surfaces. The results registered for the morphology and topography of dental enamel on teeth extracted from healthy patients show the surface of enamel with uniform projections of smaller sizes, without a specific alignment (Figure 3) .

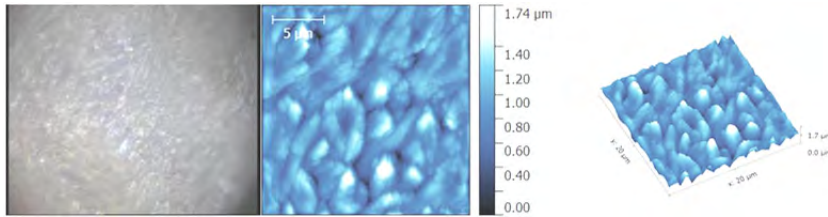


Figure 3. Enamel aspect from a healthy patient: a-optical image, b- two-dimensional AFM image; c- three-dimensional AFM image. Scan parameters: scanned area $20 \times 20 \mu\text{m}^2$, 256×256 pts, scanning frequency 1 Hz, FB 1, scanning speed $97.85 \mu\text{m/s}$, set point

AFM images registered on teeth from patients with GERD, have revealed irregular surfaces of higher sizes, with deep porosities between dimples (Figure 4).

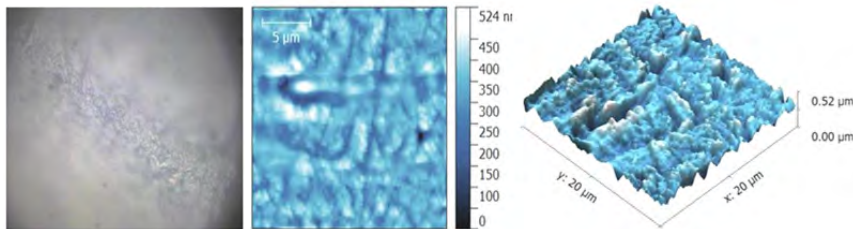


Figure 4. Enamel aspect from GERD patients: a-optical image, b- two-dimensional AFM image; c- three-dimensional AFM image. Scan parameters: scanned area $20 \times 20 \mu\text{m}^2$, 326×326 pts, scanning frequency 1 Hz, FB 1, scanning speed $97.85 \mu\text{m/s}$, set point

The association of dental erosion and GERD in our study is significant. Similar results were obtained by Fatemeh Farahmand et al. [19], who found that 53 of 54 (98.1%) GERD patients and 11 of 58 (19.0%) controls had dental erosions ($p < 0.0001$). Jarvinen et al. [20] examined 109 patients with upper gastrointestinal symptoms and found only 6.4% to have erosion, while Meurman et al. [21] found 26.2% out of 107 patients diagnosed with gastro-esophageal reflux to have dental erosion. For Pace

F et al. [22], the median prevalence of dental erosion in GERD patients was 24%, with a large range (5–48%), and the median prevalence of GERD in adult patients with dental erosion was 32.5% (range 21–83%), while in pediatric patients it was 17% (range 14–87%).

Lower pH values in GERD patients according to other studies (19–21) confirm the higher risk of dental erosion in this condition.

There are many factors that may contribute to the variation in the reported CIELab values in different studies. Of course, there may be a considerable variation in the actual tooth colors of the subjects or extracted teeth studied. In addition, the measurement technique and circumstances may introduce differences [23]. Spectrophotometers are extremely sensitive devices that can detect minimal color changes which are not really observable clinically. For these reasons, it was decided to use spectrophotometric analysis in the current study for evaluation and determination of color changes in the teeth by using the parameters CIE L * a * b * and delta E and also, the closest shades using the intraoral Vita Easyshade spectrophotometer [24–25]. Regarding the results of our study on the extracted teeth, we found the following: ΔE variations are higher than general average ΔL variations in the case of GERD patients.

AFM evaluation of hard dental structures has proven the presence of increased enamel micro-porosities in GERD patients. Hydrochloric acid from gastric juice can affect not only the surface but also the internal structure of enamel [26].

CONCLUSIONS

It was concluded that the high degree of dental erosion must be a consequence of acid attack and reduced salivary buffering capacity in patients with GERD symptoms. Tooth color variations might represent a useful tool for monitoring dental erosion in GERD patients.

EXPERIMENTAL SECTION

The research was divided into two parts: the first section included a clinical evaluation of dental structures and salivary parameters in patients with and without GERD symptoms. The second section focused on the evaluation of optical properties of eroded compared to healthy dental structures.

The first part of the study consisted of the evaluation of 70 patients (mean age 45 ± 15 years) attending an internal medicine service in Cluj-Napoca, of which 48 were healthy subjects (group 1) and 22 presented GERD symptoms (group 2). GERD symptoms were evaluated based on a

valid questionnaire. For dental erosion, BEWE (Basic Erosion Wear Examination) was used. Oral clinical examinations were performed and DE was evaluated using the BEWE (Basic Erosive Wear Examination) Index [17]. The buccal (B), palatal (P)/lingual (L) and occlusal (O)/ incisal (I) surfaces of all teeth were examined, and the highest score in each sextant was noted. The final score was obtained by summing up the values of all sextants; it was used to assess the risk for DE development in each patient. Dental examination was conducted by trained investigators.

The BEWE score quantifies the DE risk as follows: < 3: no risk; 3-8: low risk; 9-13: medium risk; ≥ 14 : high risk.

Analysis of pH (5-5.8 highly acid, 6-6.6 moderately acid, 6.8-7.8 healthy saliva) and buffer capacity (0-5 very low, 6-9 low, 10-12 normal) of the saliva was also performed and was recorded using specific salivary tests (GC Saliva Tests).

The second part of the study was conducted using 32 decay-free human teeth, extracted for periodontal reasons. The study was conducted on two groups as follows:

Group 1 – 16 teeth were obtained from patients with GERD. The teeth were free of decay or other dental disorders and had indications for dental extraction due to periodontal disease.

Group 2 – 16 teeth were collected from healthy patients, free from GERD. The procedures for extraction and preservation of the teeth were carried out after patients signed an informed consent.

All teeth used for study were washed right after extraction, professionally sanitized by scaling and brushing of crown and root surfaces, and kept in artificial saliva until use. For their better handling, they were embedded in self-curing acrylic resin (Duracryl Plus, Spofa Dental, Czechia; shade 0). Subsequent to incorporation, the crown and the cervical third of the root (non-embedded portion) were indented with a high consistency silicone material, in order to obtain the patterns necessary to achieve some polyethylene caps. The latter were made by thermoforming, with the closest adaptation to the coronal surface. Making the caps had a double role – to allow the registration of color parameters, with the Vita Easyshade spectrophotometer, as well as to allow a more precise adjustment of the spectrophotometer loop to the dental surface. As such, for each tooth, on the vestibular and oral surface of the cap, holes were made with a diameter equivalent to the diameter of the loop of the Vita Easyshade spectrophotometer (Vita-Zahnfabrik).

For measuring the color parameters we used a Vita Easyshade (Vita-Zahnfabrik) spectrophotometer consisting of three essential elements: a source of light, a means of directing the light reflected by the object, and

a spectrophotometer designed to determine the intensity of the received light depending on wave length. A major advantage of this device is to determine dental color regardless of lighting conditions, thanks to its own source of light.

The measurements were performed globally, initially immediately after extraction and after 5 days of immersion in artificial saliva, and aimed at determining the parameters of color in absence of the oral environment. The measurements were made on the vestibular and oral surfaces of each tooth, and for each area four measurements were made. The arithmetic average of measurements was used for calculating the difference in color using the formula [1]. Average values of luminosity differences ΔL^* , chromatic parameters Δa^* and Δb^* , color differences ΔE^* for each tested substance were statistically analyzed using the ANOVA test and t test for the comparison of two groups.

The retrieval protocol of color parameters with the spectrophotometer was the following: for the extracted teeth: the reading end of the spectrophotometer was applied perpendicular to and centered mesio-distally on the vestibular surface, with its margin 1 mm from the cervical line.

The AFM images were taken over with a commercial microscope Ntegra Spectra (NT-MDT, Russia), at room temperature, in the air, in intermittent contact mode (semi contact), with rectangular cantilever of silicon with reflective surface of Au (NSG30-A, NT-MDT), normal spring constant $k = 40$ N/m, resonant frequency 240-440 kHz, peak radius < 10 nm. After acquisition, the images were processed using the Nova v1.1.0.1837 (NT-MDT) program.

STATISTICS

All data were analyzed using SPSS Statistics version 21 software. Statistical comparisons were performed using Student's t-test. The values were expressed as mean \pm standard deviation (SD). A P value < 0.05 was considered statistically significant.

ACKNOWLEDGMENTS

This work was funded by the Romanian Ministry of Education and Research, National project 142PED/2017.

REFERENCES

1. N. Vakil, S.V. van Zanten, P. Kahrilas, J. Dent, R. Jones, *American Journal of Gastroenterology*, **2006**, *101*, 1900.
2. E. Ness-Jensen, A. Lindam, J. Lagergren, K. Hveem, *Gut*, **2012**, *61*, 1390.
3. S. Bruley Des Varannes, L. Marek, B. Humeau, M. Lecasble, R. Colin, *Gastroenterology Clinical Biology*, **2006**, *30*, 364.
4. R.C. Orlando. *American Journal of Medical Science*, **2003**, *326*, 274.
5. D.W. Bartlett, D.F. Evans, B.G. Smith, *Journal of Oral Rehabilitation*, **1996**, *23*, 289.
6. D. Bartlett, C. Ganss, A. Lussi, *Clinical Oral Investigations*, **2008**, *12*, 65.
7. B.G. Smith, J.K. Knight, *British Dental Journal*, **1984**, *156*, 435.
8. G.K. Johnson, J.E. Sivers, *Clinical Preventive Dentistry*, 1987, *9*, 12.
9. N. Schlueter, C. Ganss, S. De Sanctis, J. Klimek, *European Journal of Oral Science*, **2005**, *113*, 505.
10. M.C. Huysmans, J.M. Thijssen, *Journal of Dentistry*, **2000**, *28*, 187.
11. M. Moldovan, L.S. Dumitrescu, C. Prejmerean, D. Dudea, V. Popescu, *Materiale Plastice*, **2010**, *47*, 421.
12. C. Louwse, M. Kjaeldgaard, M.C. Huysmans, *Journal of Dentistry*, **2004**, *32*, 83.
13. J.J. Ten Bosch, J.C. Coops, *Journal of Dental Research*, **1995**, *74*, 374.
14. R.D. Douglas, *Journal of Prosthetic Dentistry*, **1997**, *77*, 464.
15. R.D. Paravina, G. Majkic, F. Imai, J. Powers, *Journal of Prosthodontics*, **2007**, *16*, 269.
16. A. Baltzer, V. Kaufmann-Jinoian, *Quintessenz Zahntechnik*, **2004**, *30*, 726.
17. J. Field, P. Waterhouse, M. German, *Journal of Dentistry*, **2010**, *38*, 182.
18. A. Lussi, T. Jaeggi. "L'erosion dentaire. Diagnostic, évaluation du risque, prévention, traitement." Paris, Berlin, Chicagio: Quintessence International DL, 132, 2012
19. F. Farahmand, M. Sabbaghian, S. Ghodousi, N. Seddighorae, M. Abbasi, *Gut Liver*, **2013**, *7*, 278.
20. V. Jarvinen, J.H. Meurman, H. Hyvarinen, I. Rytomaa, H. Murtomaa, *Oral Surgery Oral Medicine Oral Pathology*, **1988**, *65*, 298.
21. J.H. Meurman, J. Toskala, P. Nuutinen, E. Klemetti, *Oral Surgery Oral Medicine Oral Pathology*, **1994**, *78*, 583.
22. F. Pace, S. Pallotta, M. Tonini, N. Vakil, G. Bianchi Porro. *Aliment Pharmacology Therapeutics*, **2008**, *27*, 1179.
23. A. Dozic, C.J. Kleverlaan, I.H. Aartman, A.J. Feilzer, *Dental Materials*, **2005**, *21*, 187.
24. R.R. Seghi, W.M. Johnston, W.J. O'Brien, *Journal of Dental Research*, **1989**, *68*, 1755.
25. D. Dudea, M. Moldovan, L. Silaghi Dumitrescu, H. Colosi, A. Botos, A. Irimie, C. Alb, *Studia UBB Chemia*, **2010**, *1*, 65.
26. A.M. Bargan, G. Ciobanu, C. Luca, E. Horoba, *Studia UBB Chemia*, **2013**, *58*, 137.

CHROMIUM REMOVAL FROM POLLUTED WATER AND ITS INFLUENCE ON BIOCHEMICAL AND PHYSIOLOGICAL PARAMETERS IN ALGAL CELLS USED FOR PHYTOREMEDIATION

SEBASTIAN RADU CRISTIAN PLUGARU^a, TUDOR RUSU^a,
KATALIN MOLNAR^b, LASZLO FODORPATAKI^{c,*}

ABSTRACT. The aim of the study is to evaluate the suitability of a local strain of the microalga *Scenedesmus opoliensis* in remediation of water pollution with different amounts of chromium(VI), and also to identify new biochemical and physiological markers for a more reliable indication of sustainability and efficiency of bioextraction and phytoaccumulation processes. Quantitative analysis of photosynthetic pigments reveals that the chlorophylls to carotenoids ratio is a sensitive marker of chromium toxicity and of algal metal tolerance on which the remediative capacity relies. From among the chlorophyll fluorescence parameters, the Fv/Fm ratio, related to potential quantum yield of photochemical reactions, indicates that alkaline pH of the medium (8.65-9.15) favors algal vitality as compared to acidic conditions with pH values around 5. The highest extraction rate (91%) is achieved upon exposure of algae for one week to lower chromium concentrations (5 μ M) in alkaline water environment, and a longer exposure time does not increase bioaccumulation. These results may directly contribute to optimization of remediation technology for chromium-polluted water, providing new markers and a new algal strain to be introduced in wastewater treatment.

Keywords: bioaccumulation, chromium, microalgae, photosynthetic pigments

^a Technical University of Cluj-Napoca, Faculty of Materials and Environmental Engineering, 103-105 Muncii Bd., RO-400641, Cluj-Napoca, Romania.

^b Sapientia Hungarian University of Transylvania, Department of Horticulture, 1C Sighișoarei Rd., RO-540485, Târgu Mureș, Romania.

^c Babeș-Bolyai University, Faculty of Biology and Geology, 1 M. Kogălniceanu St., RO-400084, Cluj-Napoca, Romania.

* Corresponding author: lfodorp@gmail.com

INTRODUCTION

Use of plants and micro-organisms may be a cost-effective, environmental friendly and applicable on large scale in remediation of polluted waters, if the proper species and developmental conditions are selected, and the adequate indicator and efficiency parameters are established [1]. Microalgae exhibit advantageous characteristics of both plants and micro-organisms for an effective bioremediation of aquatic environments anthropically affected by the spill of various organic and inorganic xenobiotics. Due to their wide metabolic plasticity based on autotrophy characteristic to plants, and to their high reproductive rate and pronounced adaptability specific to micro-organisms, microalgae possess a well-defined biosorption, bioaccumulation and biotransformation capacity, which make them advantageous candidates for rehabilitation of domestic, agricultural and industrial wastewaters [2].

Because heavy metals are not degradable, bioremediation of waters polluted with these very toxic chemicals may be achieved by: a) bio-extraction followed by sequestration in internal cell compartments or by adsorption to structural components of the cell wall and related extracellular spaces, b) stabilization by reduction of mobility of heavy metals, e. g. through decreasing the redox potential (aqueous solution becoming more reducing), increasing pH (heavy metals are less water-soluble under less acidic conditions), or chelating with organic acids and sulfur-containing molecules, c) volatilization by transformation into methylated derivatives which leave the aqueous phase (possible only in the case of certain metals and metalloids, such as mercury, bismuth, antimony, arsenic) [3, 5, 6, 11]. Use of metal-accumulating plants for removal of metals from contaminated waters may generate recyclable metal-rich plant residues, causes only minimal environmental disturbance and has a general public acceptance, so optimization of bioremediation technologies represents a priority for applied environmental sciences [13, 25, 27, 33].

Chromium is abundantly found in the earth's crust, but as a polluting agent it reaches in aquatic habitats mainly through human activities, such as leather tanning, stainless steel production, metal finishing, manufacture of pigments and of refractory brick [14, 20]. In very small amounts it stimulates enzymatic activity of phosphoglucomutase enzyme with benefic influence on carbohydrate metabolism, but at micromolar concentrations it may be highly toxic to different metabolic and developmental processes, causing: a) membrane damage by lipid peroxidation, b) excessive catabolic processes by increased protease activity, c) reduction in dry matter production by a decline in carbon dioxide assimilation, and finally d) causing a

generalized oxidative stress by enhanced generation of hydroxyl radicals. Its most characteristic indirect effect is iron, manganese, sulfur and phosphorus deficiency due to competition with these inorganic ions for transmembrane transporters. Because it interacts with DNA, chromium exhibits genotoxicity, causing mitotic irregularities, chromosome fragmentation and hypermethylation of pyrimidines [14, 15, 28, 29]. Inside the plant cells, hexavalent chromium is reduced to the less soluble form of trivalent chromium, than it is immobilized by chelation with metallothioneins and phytochelatins which accumulate under heavy metal stress and sequester chromium ions in vacuoles. Several aquatic plants, including unicellular microalgae, green, red and brown macroalgae (seaweeds), as well as macrophytes (e. g. water hyacinth, duckweed), have been assayed for bioremediation of waters polluted with heavy metals, and the efficiency of remediation process varied greatly depending on plant species, growth conditions, exposure time, pH values, competitive and cooperative interactions with other inorganic and organic pollutants etc. [7, 18, 19, 21, 22, 23, 26, 32]. This is the main reason why selection of most suitable plant species based on sensitive biochemical and physiological markers, as well as optimization of growth conditions during phytoextraction are key factors for a cost-effective cleaning of wastewaters with reduced negative impact on the environment.

The aim of the present study is to evaluate the bioremediative capacity of a local strain of the globally occurring freshwater microalga *Scenedesmus opoliensis*, and also to identify biochemical and physiological markers that enable a rapid and reliable indication of algal vitality and tolerance on which the efficiency of chromium bioaccumulation relies. Results are expected to be directly applicable in clearance of waters polluted with chromium(VI).

RESULTS AND DISCUSSION

Biochemical markers related to vitality and tolerance of living organisms exposed to different degrees of environmental stresses are valuable indicators of water pollution and of its effects on plants which contribute crucially to the biogeochemical cycles of essential elements. From among the many biochemical parameters of metabolic processes, it is hard to find those which vary in correlation with disturbing external factors and may be interpreted in terms of significance for evaluating the efficiency of biosorption and bioaccumulation of polluting agents. In this context, the photosynthetic pigments are directly responsible for harvesting light energy and for primary photochemical reactions that enable plants to

use this energy source for primary production of new organic compounds. Some of these pigments (certain carotenoids, especially xanthophylls) also have an indispensable role in the antioxidative defense against reactive oxygen species generated during photosynthesis if photon flux is too high and assimilation is limited by low concentration of available inorganic carbon source. Because high concentrations of heavy metals disturb biosynthesis and decomposition of chlorophylls and carotenoids, and many of them induce oxidative damage to photosynthesizing membranes and to enzymes of the carbon assimilation pathway, it is expected that water pollution with chromium(VI) will have an impact on the dynamics of photosynthetic pigments in algae, with a direct consequence on energy supply for primary production of new organic compounds.

Our experimental results reveal that after one week of exposure to 5 μM of chromium(VI), the chlorophyll content of algal cells increases moderately in alkaline aqueous solution (pH value of 9), but becomes significantly lower under acidic conditions (pH = 5), while carotenoid pigment content increases in both acidic and alkaline media. In the presence of higher Cr(VI) concentrations (50 μM and 500 μM) the algae exhibit a decreased chlorophyll content irrespective of the pH value, but carotenoid content becomes higher in the acidic medium and lower in the alkaline one. After two weeks of exposure, the amount of both chlorophylls and carotenoids decreases progressively with the elevation of chromium(VI) concentration, but this decrement is more moderate in the case of carotenoids and in the alkaline media (data not shown). Because the two types of photosynthetic pigments vary in different degrees under similar conditions, the most suitable parameter to indicate integrate influence of chromium(VI) on their overall dynamics proved to be the ratio between chlorophylls and carotenoids. In the acidic medium this ratio decreases after one week of exposure to all chromium(VI) concentrations, and this decrease is more pronounced as chromium content increases. After one more week, lowered value of this ratio persists only in the aqueous solution polluted with 500 μM chromium(VI), while in the presence of 50 μM Cr(VI) it registers a significant increment (Fig. 1).

In the alkaline medium the chlorophylls to carotenoids ratio in the algal cells varies differently during the first week of exposure, according to the different chromium(VI) concentrations: it decreases at 5 μM , it increases at 50 μM , and it does not change significantly at 500 μM . After two weeks of exposure, a moderate, but statistically significant increment is registered under the influence of 50 μM chromium(VI), while 500 μM causes a pronounced lowering of this ratio. This means that the chlorophylls to carotenoids ratio is a very good marker of chromium exposure of the alga,

because it exhibits differential changes related to exposure time, chromium(VI) concentration and acidic or alkaline pH of the water. Previously published experiments revealed only a decrease in chlorophyll content of plant cells under chromium toxicity or found no relevant changes in photosynthetic pigment content upon exposure to hexavalent chromium ions [14, 16], but we did not find any report about specific changes in the chlorophylls to carotenoids ratio in the context of biochemical reactions to water pollution with chromium(VI). Further interpretation of the results reveals that, if one takes into account that chlorophylls are the major light-harvesting pigments, while carotenoids have a primary role in the photoprotective processes, it can be stated that water pollution with chromium(VI) exerts the most pronounced negative influence on the primary processes of photosynthetic light energy utilization after two weeks of exposure to chromium(VI) concentrations higher than 50 μM , in acidic aqueous solutions.

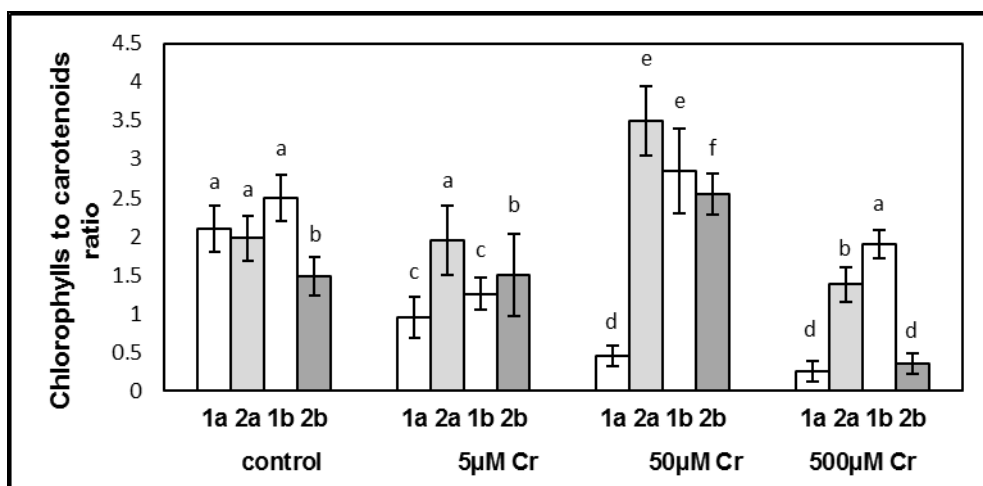


Figure 1. Chlorophyll to carotenoid pigment ratio in the green alga *Scenedesmus opoliensis* exposed for one week to different concentrations of hexavalent chromium, in acidic and alkaline aqueous solutions. 1a – after one week at acidic pH, 2a – after two weeks at acidic pH, 1b – after one week at alkaline pH, 2b – after two weeks at alkaline pH (vertical bars represent \pm SE from means, n = 4, different letters show significant differences at P < 0.05)

From among the several chlorophyll fluorescence parameters, the ratio between the variable and the maximal fluorescence yield (F_v/F_m , F_v being the difference between the maximal fluorescence F_m and the ground

fluorescence F_o) was found to be the mostly suitable marker of functional changes caused by chromium in the light reactions of photosynthesis. The value of this ratio shows a strong positive correlation with the potential quantum yield of photosynthesis, meaning that it reflects the capability of photosystems to convert the absorbed light energy into chemical energy stored in newly synthesized organic compounds resulting from carbon assimilation through the Calvin cycle. Under optimal conditions, when no disturbing factors limit photosynthesis, the value of the F_v/F_m ratio is between 0.9-0.8. Whenever photochemical processes in the chloroplasts are impaired and stress conditions occur, the F_v/F_m value drops below 0.7. In our experiments the maximal chlorophyll fluorescence decreased already at 5 μM chromium(VI) during the first week of exposure under acidic conditions, reflecting that photochemical reactions on the acceptor side of photosystem II are very sensitive to the presence of chromium in chloroplasts. After two weeks, the F_o decreased even more than F_m , indicating that upon longer exposure the functional organization of the light-harvesting pigment antenna and its light energy transfer capacity becomes inhibited by chromium. In the alkaline medium F_o and F_m decrease abruptly only at 500 μM chromium(VI), irrespective of the exposure time, but lower Cr concentrations do not significantly influence the above-mentioned chlorophyll fluorescence parameters. Integrating these results into changes in the F_v/F_m ratio, it can be noticed that in the acidic media its value decreases significantly at all of the applied chromium(VI) concentrations and after both exposure times, while in the alkaline aqueous solutions the potential quantum yield exhibited in the first week only a moderate decrease and only at chromium(VI) concentrations as high as 500 μM , after two weeks it became slightly lower at 50 μM and much lower at 500 μM of chromium(VI) in the aqueous medium of the algae (Fig. 2). These results suggest on one hand that decrease in F_v/F_m may be used for a sensitive indication of functional damage to photochemical processes in algal photosynthesis, on the other hand they show that chromium causes more severe damages to the photosynthetic apparatus if algae are grown in acidic waters (with pH values around 5).

These results may have a direct practical applicability in assessing impact of chromium on algal productivity, because F_v/F_m values may be determined *in vivo* and *in situ*, without affecting algal populations, and offer early and reliable indication on changes in photosynthetic efficiency on which algal vitality, heavy metal tolerance and defensive capacity rely. Even though potential quantum efficiency is frequently used in plant stress physiological investigations, no conclusive reports exist in the literature concerning its relevance in the context of water pollution with

different concentrations of chromium(VI) under acidic and alkaline pH conditions [8, 17].

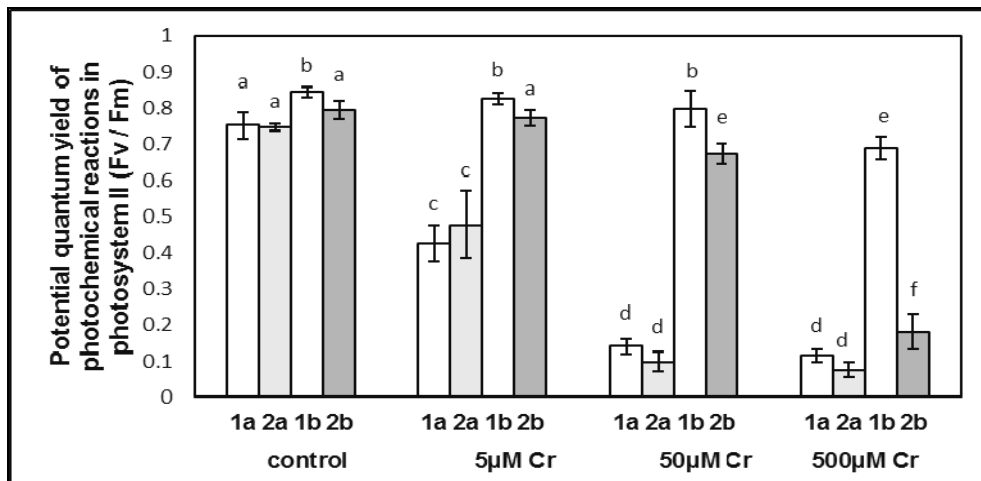


Figure 2. Potential quantum yield of photochemical reactions in photosystem II, expressed as the ratio between the variable and maximal chlorophyll fluorescence (Fv/Fm) in dark-adapted cells of the green alga *Scenedesmus opoliensis* exposed for one week and for two weeks to different concentrations of hexavalent chromium, in acidic and alkaline aqueous solutions. 1a – after one week at acidic pH, 2a – after two weeks at acidic pH, 1b – after one week at alkaline pH, 2b – after two weeks at alkaline pH (vertical bars represent \pm SE from means, $n = 4$, different letters show significant differences at $P < 0.05$)

The spread of algal individuals in the entire water body is a prerequisite for an efficient and uniform bioextraction of polluting agents, this is why the rate of algal reproduction through cell divisions is an important parameter in the evaluation of bioremediation efficiency, as well as in the examination of developmental status of the algal populations exposed to adverse environmental factors. Investigation of the dynamics of cell density in the algal populations exposed to different chromium(VI) concentrations at two different pH values (5 and 9) revealed that the decrease in cell division rate is proportional with the chromium concentration in the medium at a given pH value, suggesting that cell density of algal populations is a good indicator of the degree of water pollution with chromium(VI) and of its effects on algal growth. One can also notice that at chromium(VI) concentrations which do not exceed 50 μ M, the alkaline aqueous solution is more favorable to algal reproduction as

compared with the acidic conditions, and after two weeks of exposure the differences in algal cell number per unit of water volume are more obvious than after one week (Fig. 3).

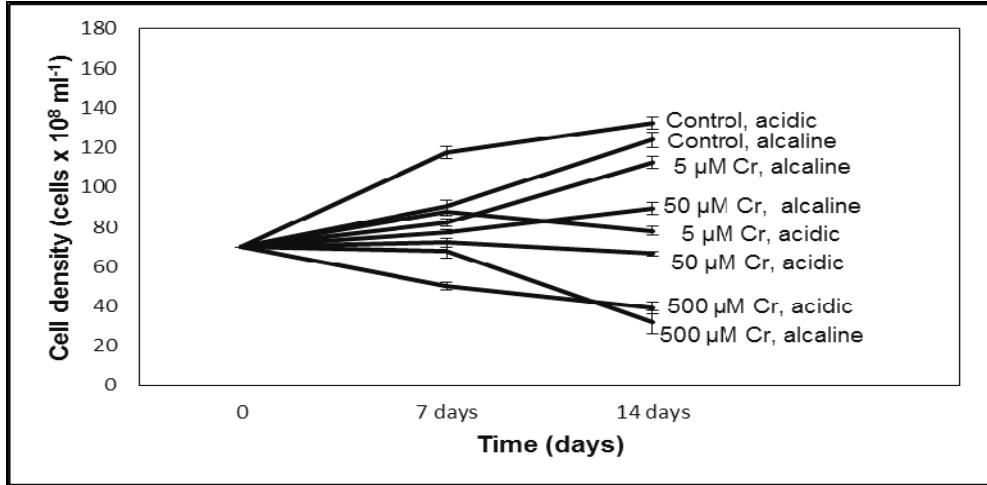


Figure 3. Influence of different concentrations of hexavalent chromium on the dynamics of cell density in populations of the green alga *Scenedesmus opoliensis*, in acidic and alkaline aqueous solutions (vertical bars represent \pm SE from means, $n = 4$, different letters show significant differences at $P < 0.05$)

Variations of the cell density of algal populations were monitored in several experiments concerning the influence of different heavy metals on several microalgal species, and it was found that dynamics of cell multiplication correlates with the intensity of impact exerted by these various chemical stress factors present in polluted aquatic environments [12, 16, 18, 24].

Because pH values of the aqueous medium have a significant impact on solubility of chromium in water, on which its bioavailability depends (generally, heavy metals are more soluble in aqueous solutions under acidic conditions, and metal-polluted waters often have a low pH), and because algal growth is also influenced by the pH of the medium (freshwater algae are adapted to the slight alkalinity of their natural aquatic environment, but they can properly take up mineral nutrients also from moderately acidic aqueous solutions), it is worth mentioning that the presence of different chromium(VI) concentrations did not cause relevant changes in the pH values of the aqueous media after two weeks of

exposure, but they slightly decreased the initial pH value in both the acidic and the alkaline solutions (with the initial pH values set to 5 and to 9, respectively). As compared with the control, this decrement did not exceed 0.48 units in the presence of 5 μM Cr, 0.63 units in the media with 50 μM Cr, and 1.14 units when 500 μM Cr was added to the water solution in which the algae grew. pH of the control cultures moderately increased during two weeks from 5.00 to 5.24 ± 0.17 , and from 9.00 to 9.33 ± 0.21 .

Determination of the chromium concentration in the aqueous medium of algal cultures after one and two weeks of exposure to different initial Cr(VI) concentrations in acidic and alkaline solutions revealed that low amounts of chromium(VI) (5 μM) can be extracted by this alga in a proportion of $87 \pm 3\%$ in one week and $89 \pm 2\%$ in two weeks under alkaline conditions, while in the acidic medium this percentage is slightly lower after one week and considerably lower after two weeks of exposure (Table 1).

Table 1. Degree of chromium extraction from the aquatic environment by the planktonic microalga *Scenedesmus opoliensis*, after one week and two week of exposure to different initial Cr(VI) concentrations in acidic (initial pH = 5) and alkaline (initial pH = 9) media (n = 4)

Initial Cr(IV) concentration in the water solution	Percentage of removal after 1 week at acidic pH	Percentage of removal after 2 weeks at acidic pH	Percentage of removal after 1 week at alkaline pH	Percentage of removal after 2 weeks at alkaline pH
5 μM	$81 \pm 3\%$	$69 \pm 2\%$	$87 \pm 3\%$	$89 \pm 2\%$
50 μM	$62 \pm 2\%$	$54 \pm 1\%$	$68 \pm 1\%$	$51 \pm 4\%$
500 μM	$22 \pm 4\%$	$17 \pm 2\%$	$51 \pm 3\%$	$34 \pm 5\%$

More than half of the initial chromium amount is bioextracted and accumulated by the algal cells if the initial Cr(VI) concentration in the polluted water is 50 μM (irrespective of acidic or alkaline conditions), while chromium(VI) quantities as high as 500 μM are extracted only in smaller degree, the best performance being registered in the alkaline aqueous solution after one week of exposure. In most cases, two weeks of algal development in chromium-polluted aquatic environments did not result in enhanced bioaccumulation capacity in comparison with one week of exposure. On the contrary, the chromium(VI) content of water increased in the second week, probably because due to prolonged exposure more algal cells have died than those which still could divide, and the destroyed cells lost the selectivity of their membrane permeability and liberated back in the medium a part of the formerly accumulated chromium ions. These results

suggest that a shorter exposure time, which does not exceed one week, and an elevated, alkaline pH (e.g. around 9) of the aqueous medium favor a more efficient bioextraction of the chromium(VI) from polluted waters, and are in agreement with experimental data existing for phytoextraction of several other heavy metals from polluted waters and soils [13, 19, 21, 22, 34].

CONCLUSIONS

The algal strain used in the experiments proved to be useful for an effective bioremediation of water polluted with moderate amounts of chromium(VI). The highest biosorption efficiency (91% of 5 μM initial Cr concentration in the aqueous solution) was achieved at an alkaline pH value in the range of 8.65-9.15. The major part of Cr ions is bioaccumulated during the first week of exposure, and an increase in the exposure time does not result in significant further absorption, but may lead to a decreased degree of accumulation because a part of the formerly uptaken chromium(VI) ions reenter in the aquatic environment upon decay of senescent algal cells. Chlorophyll to carotenoid pigment ratio varies specifically with different exposure times, chromium(VI) concentrations and pH of the aqueous medium, being a sensitive molecular marker of changes in physiological status of algae. Potential photosynthetic light use efficiency of algal cells, reflected by the Fv/Fm ratio of induced chlorophyll fluorescence parameters, is a useful indicator of algal vitality indispensable for a sustained bioaccumulation of water-polluting chromium(VI) ions, its decrease being proportional with the decrease in yield of photochemical reactions which follow photon absorption and precede carbon assimilation into new organic metabolites. Dynamics of cell density of the algal populations grown in aquatic environments polluted with chromium(VI) shows a proportional inhibition of cell divisions with chromium(VI) concentration, and it also indicates that algal development enables a suitable bioextraction only at chromium(VI) concentrations lower than 500 μM , and an alkaline pH is more favorable to algal growth in polluted water than the acidic nature of the aqueous solution. These results may directly contribute to an enhanced efficiency of bioremediation of freshwater ponds anthropically polluted with chromium(VI), bringing new information concerning biochemical and functional markers that can be used successfully in an early indication of water pollution status, as well as in implementation of improved environmental-friendly technologies for purifying wastewaters contaminated with chromium(VI).

EXPERIMENTAL SECTION

Microbiologically sterile monoalgal cultures of the freshwater green microalga *Scenedesmus opoliensis* P. Richter, strain AICB 141 (collected from the Stiucilor Lake, Cluj county) were grown in Bold's basal nutrient medium, at a constant temperature of 22 °C, the light intensity being set to a photon flux density of $130 \mu\text{M m}^{-2}\text{s}^{-1}$ for 14 hours per day [8, 17]. Identical amounts of a homogenous static cell culture, being in the exponential growth stage of its algal population, were inoculated in growth vessels containing aqueous nutrient solution supplemented with different concentrations of potassium dichromate (as source of water-soluble chromium(VI) ions) at two different pH values of the media. The initial chromium ion concentration of the algal cultures was set to 5 μM , 50 μM and 500 μM , respectively, while the control cultures were grown in the same nutrient medium, but without chromium source. All the variants were set up in media with the pH adjusted (with aliquots of concentrated solutions of sulfuric acid and potassium hydroxide) to the values of 5 and 9, respectively, in order to observe the influence of acidic and alkaline aquatic environment on the uptake and bioaccumulation of chromium. Every experimental variant was set in four repetitions, and every culture was grown under the above-mentioned conditions for two weeks.

Cell density of algal cultures, reflecting the reproductive capacity under the given developmental conditions, was determined every three days cytometrically, using Bürker's cell counter slide to establish by microscopic investigation the number of viable algal cells in a given volume of homogenized suspension. Dry biomass production of one and two weeks old algal cultures was measured after filtration and dehydration of cells at 85 °C for three days, until a constant weight was reached [16].

Photosynthetic pigment content (i.e. chlorophyll-a, chlorophyll-b and carotenoids amount) of algal cells was determined spectrophotometrically, by measuring the absorbance at 450 nm, 646.8 nm and 663.8 nm, after extraction of pigments performed in darkness at room temperature from 0.1 g dry algal biomass in 5 ml of dimethylformamide [10]. Induced chlorophyll fluorescence parameters, related to efficiency of photochemical conversion of the absorbed light energy into chemical energy stored in new organic compounds, were determined in dark-adapted algal cell suspensions with a photosynthetic efficiency analyzer (FMS2 fluorometer, Hansatech, UK). A very weak ($0.1 \mu\text{M photons m}^{-2}\text{s}^{-1}$) red flash (of 650 nm) was applied for 1 μs to measure the ground fluorescence (F_0), while the maximal temporary chlorophyll-a fluorescence yield (F_m) was determined with application of a saturating ($10000 \mu\text{M photons m}^{-2}\text{s}^{-1}$) red flash applied for 0.5 s. Variable

fluorescence (Fv) was calculated as the difference between the maximal and the ground fluorescence values, and was used to determine the potential quantum efficiency of photosynthetic light energy use, reflected by the ratio Fv/Fm [9, 10, 24].

The remaining chromium content of the aqueous medium, which was not extracted by algal cells after one and two weeks of exposure at different initial chromium concentrations and under different pH values, was determined by atomic absorption spectrometry (with a Shimadzu AA-6800 spectrometer). Calibration was performed with a series of standard solutions containing known concentrations of chromium in the range of 0.4-40.0 mg L⁻¹ [4, 31]. The algal cells were removed from the aqueous media by centrifugation at 3000 g and 4 °C for 20 min.

All experimental setups had four replicas, and every measurement was repeated three times. Statistical analysis of experimental data was performed in the R environment (R Developmental Core Team 2014), using the Shapiro-Wilk test for normality, Bartlett's test for homogeneity of variances, the one-way ANOVA and the post-hoc Tukey HSD test for the significance of differences between treatments. Differences were considered statistically significant at $P < .05$.

ACKNOWLEDGMENTS

The authors thank dr. Ioana Monica Sur from the Department of Environmental Engineering and Sustainable Development Entrepreneurship at the Technical University of Cluj-Napoca for her technical support in determining chromium concentrations in water samples, and Mr. Szabolcs Barna (former M. Sc. student in Aquatic and terrestrial ecology at the "Babeş-Bolyai" University) for his expertise in experimental data analysis and statistical evaluation.

REFERENCES

1. N. Ahalya, T. V. Ramachandra, R. D. Kanamadi, *Research Journal of Chemistry and Environment*, **2003**, 7(4), 4544.
2. I. Aharchaou, M. Rosabal, F. Liu, E. Battaglia, D. A. L. Vignati, C. Fortin, *Aquatic Toxicology*, **2017**, 182, 49.
3. R. J. Bartlett, *Environmental Health Perspectives*, **1991**, 92, 17.
4. I. M. Berar Sur, V. Micle, S. Avram, S. Marin, V. Oros, *Environmental Engineering and Management Journal*, **2012**, 11(8), 1389.

5. S. Clemens, *Biochemistry*, **2006**, *188*, 1707.
6. N. Das, R. Vimala, P. Karthika, *Indian Journal of Biotechnology*, **2008**, *7*, 159.
7. F. R. Espinoza-Quinones, N. Martin, G. Stutz, G. Tirao, S. M. Palacio, M. A. Rizzutto, A. N. Modenes, F. G. Silva, N. Szymanski, A. D. Kroumov, *Water Research*, **2009**, *43*, 4159.
8. L. Fodorpataki, J. Papp, *Contribuții Botanice*, **2002**, *37*, 221.
9. L. Fodorpataki, I. Z. Vass, *Studia UBB, Seria Biologia*, **2005**, *50(1)*, 17.
10. L. Fodorpataki, J. Papp, Cs. Bartha, Zs. Gy. Keresztes, "Laboratory Experiments in Plant Physiology and Ecophysiology" (in Hungarian), Cluj University Press, Cluj-Napoca, **2010**, chapter 2.
11. M. Fomina, G. M. Gadd, *Bioresource Technology*, **2014**, *160*, 3.
12. E. Fosso-Kankeu, A. F. Mulaba-Bafubiandi, *Physics and Chemistry of Earth*, **2014**, *67*, 242.
13. C. Garbisu, I. Alkorta, *Bioresource Technology*, **2001**, *77*, 229.
14. P. S. Gonzalez, M. A. Talano, A. L. W. Oller, S. G. Ibanez, M. I. Medina, E. Agostini, Update on mechanisms involved in arsenic and chromium accumulation, translocation and homeostasis in plants. In: D. K. Gupta, S. Chatterjee (eds.), "Heavy Metal Remediation", Nova Science Publishers, New York, **2014**, chapter 3.
15. S. S. Hayat, G. Khalique, M. Ifram, A. S. Wani, B. N. Tripathi, A. Ahmad, *Protoplasma*, **2012**, *249*, 599.
16. T. Zs. Hörcsik, R. Láposi, I. Mészáros, L. Simon, Á. Balogh, Gy. Lakatos, *Acta Biologica Szegediensis*, **2006**, *50*, 19.
17. H. Hu, Y. Deng, Y. Fan, P. Zhang, H. Sun, Z. Gan, H. Zhu, Y. Yao, *Chemosphere*, **2016**, *150*, 285.
18. S. Khan, I. Shamshad, M. Waqas, J. Nawab, L. Ming, *Ecological Engineering*, **2017**, *102*, 536.
19. Y. C. Lee, S. P. Chang, *Bioresource Technology*, **2011**, *102*, 5297.
20. M. E. Losi, C. Amrhein, W. T. Frankenberger, *Reviews in Environmental Contamination and Toxicology*, **1994**, *136*, 91.
21. P. C. Mane, A. B. Bhosle, *International Journal of Environmental Research*, **2012**, *6*, 571.
22. V. Murphy, H. Hughes, P. McLoughlin, *Chemosphere*, **2008**, *70*, 1128.
23. L. B. Paiva, J. G. Oliveira, R. A. Azevedo, D. R. Ribeiro, M. G. Silva, A. P. Vitoria, *Environmental and Experimental Botany*, **2009**, *65*, 403.
24. U. N. Rai, R. D. Tripathi, N. Kumar, *Chemosphere*, **1992**, *25*, 1721.
25. I. Raskin, B. D. Ensley, "Phytoremediation of Toxic Metals: Using Plants to Clean Up the Environment", John Wiley and Sons, Inc., New York, **2000**.
26. A. Ruiz-Marin, G. Leopoldo, M. Mendoza-Espinosa, T. Stephenson, *Bioresource Technology*, **2010**, *101*, 58.
27. H. Seidel, C. Lser, A. Zehnsdorf, P. Hoffmann, R. Schmerold, *Environmental Science and Technology*, **2004**, *38(5)*, 1582.
28. H. P. Singh, P. Mahajan, S. Kaur, D. R. Batish, R. K. Kohli, *Environmental Chemistry Letters*, **2013**, *11*, 229.
29. S. Sinha, R. Saxena, S. Singh, *Chemosphere*, **2015**, *58*, 595.

30. I. M. Sur, V. Micle, T. Gabor, *Studia UBB Chemia*, **2016**, 61(3), 355.
31. Y. Uysal, *Journal of Hazardous Materials*, **2013**, 263, 486.
32. J. Wang, C. Chen, *Biotechnology Advances*, **2009**, 27, 195.
33. M. Zabochnicka-Swiatek, M. Krzywonos, *Polish Journal of Environmental Studies*, **2014**, 23(2), 551.

COMPARATIVE STUDY ON GROWTH AND PHOTOSYNTHETIC PIGMENT DYNAMICS OF TWO MICROALGAE UNDER THE INFLUENCE OF WATER POLLUTION WITH THE HERBICIDE GLUFOSINATE

SEBASTIAN RADU CRISTIAN PLUGARU^a*, LASZLO FODORPATAKI^b,
MIHAELA ORBAN^a, ANCA SARB^c, BERNAT TOMPA^b, BALAZS KOVACS^b

ABSTRACT. The aim of the study is to compare biochemical and physiological reactions of two related species of green microalgae (*Scenedesmus acuminatus* and *Scenedesmus opoliensis*), both considered suitable for bioindication and remediation of aquatic environments polluted with herbicides. Monoalgal axenic cultures were treated for 10 days under controlled conditions with different concentrations (from 0.1 μM to 100 μM) of glufosinate (a non-selective contact herbicide that inhibits glutamine synthase activity, thus disturbing photorespiration, inhibiting photosynthetic carbon assimilation, and generating ammonium excess in plant cells). *S. opoliensis* was found to be a better indicator of adverse effects of glufosinate than *S. acuminatus*. Changes in the ground chlorophyll fluorescence (reflecting light energy harvesting capacity), in cell division rate and in chlorophyll-a content may be early, cost-effective and sensitive markers of herbicide impact on microalgal communities inhabiting polluted water. Our results bring new data concerning the need of selection among related test organisms based on differentiated tolerance, as well as concerning biochemical parameters suitable for evaluation of water pollution impact when organic xenobiotics accumulate in aquatic environments. Thus, the presented results may be applied in optimizing bioindication of water quality using microalgae, and in treatment of wastewater polluted due to agricultural practices.

Keywords: bioindication, chlorophylls, glufosinate, herbicide, water pollution

^a Technical University of Cluj-Napoca, Faculty of Materials and Environmental Engineering, 103-105 Muncii Bd., RO-400641, Cluj-Napoca, Romania.

* Corresponding author: sebastian.plugaru@yahoo.com

^b Babeş-Bolyai University, Faculty of Biology and Geology, 1 M. Kogălniceanu St., RO-400084, Cluj-Napoca, Romania.

^c Technical University of Cluj-Napoca, Faculty of Machine Building, 103-105 Muncii Bd., RO-400641, Cluj-Napoca, Romania

INTRODUCTION

Even though there are many attempts to replace xenobiotic pesticides with environmental-friendly biological compounds (e.g. certain secondary metabolites of plants and micro-organisms), modern agriculture cannot entirely dispense of chemically synthesized herbicides in order to ensure sufficiently high crop production under various conditions in which several weeds compete with cultivated plants for sunlight, for water and inorganic nutrient reserves of the soil. Herbicides are synthetic organic compounds which may persist over time in the aqueous solution of agricultural soils and finally accumulate in continental still waters where they reach concentrations which are highly toxic to all living organisms of the aquatic ecosystems. Planktonic microalgae, as the mostly widespread primary producers in these polluted waters are the main targets of the influence of herbicides, because they live as plants, so their physiological processes are directly damaged by herbicides. Furthermore, their metabolic plasticity and high functional adaptability sequestration, bioconcentration and biotransformation of herbicides, thus algae have a crucial contribution to decontamination of water polluted with organic xenobiotics [1,17].

Among the various herbicides which may inhibit seed germination, cell division, photosynthesis, photorespiration, specific enzyme activities involved in unsaturated fatty acid synthesis, in amino acid synthesis, in production of chlorophylls and carotenoid pigments, or may disturb plant developmental processes by being hormone analogues [19], glufosinate (the ammonium salt of the formerly commercialized phosphinotricine, i. e. ammonium-(3-amino-3-carboxypropyl)-methyl phosphinate) is one of the most largely used non-selective contact herbicides for various crops over the world (e. g. as a crop desiccant for harvesting in case of potato, canola, maize, spring wheat, or directly disposed on the leaves of weed species before the vegetation period of lettuce, beans, pea, grape, apple and other fruit trees). It inhibits the enzymatic activity of glutamine synthase, thus preventing the formation of a universal proteinogenic amino acid and leading to accumulation of toxic amounts of ammonia in plant cells. Finally, it inhibits the peroxisomal phase of photo-respiration in green leaf cells, by feed-back regulation it disturbs both the oxygenase and the carboxylase activities of Rubisco as the key enzyme in carbon dioxide fixation, it blocks photosynthesis and it induces damages in biological membranes, impairing their selective permeability [2]. These cumulated changes lead to the death of the plants which took up the herbicide. For several crop species, glufosinate-tolerant cultivars were created through genetic transformation (mainly by overexpression of the gene encoding for glutamine synthase),

and their agricultural field is systematically treated with the herbicide. Some plants may develop a natural tolerance to glufosinate, based on its biotransformation through N-acetylation [13].

Its influence on biochemical and metabolic parameters of green microalgae living in water ponds surrounded by agricultural terrains is poorly documented in the literature, many experimental data are controversial because of the use of different algal species and local varieties as test organisms and because of differences in experimental conditions and in methods of evaluation [2]. These are the main reasons why we proposed to compare the reactions of two related algal species to different concentrations of glufosinate, and to find some biochemical and metabolic parameters which may reliably indicate water pollution with this largely used herbicide.

RESULTS AND DISCUSSION

Growth rate of microalgal populations, which reflects the relation between formation of new algal individuals by cell division and death of senescent cells, is an important indicator of living conditions that allow a certain rhythm of development, its dynamics being a determinant factor for the efficiency of bioaccumulation and biotransformation of polluting agents during natural decontamination of polluted waters. In the case of *Scenedesmus acuminatus* (which has typically smaller cells than *Sc. opoliensis*), a very small concentration 0.1 μM of the herbicide glufosinate induced a temporary decrease in cell density, which was followed by a recovery of the number of individuals in a unit of water volume (Fig. 1). 1 μM glufosinate caused a longer decay of net reproductive rate, but in eight days it also allowed a recovery of cell density to values comparable with the non-treated control cultures. Exposure to 10 μM glufosinate led to a rapid populational growth inhibition, followed by stabilization at this lower cell density. High concentration of the herbicide (100 μM) exerted a progressive inhibition of algal multiplication, reflected by a gradual decrease of cell number as exposure time got longer. This dynamics of cell density of algal cultures reflects that this alga gives a differential response to different concentrations of the same herbicide dissolved in its aqueous environment.

Scenedesmus opoliensis responded to low concentration of glufosinate (0.1 μM) by a quick decrease in cell density, followed by a transitory recovery, and then by a new phase of decline after four days of exposure (Fig. 2). This reflects that reproduction of this alga is more sensitive to low concentrations of the herbicide in comparison with the formerly presented one, thus being a better indicator for early detection of water pollution with this organic xenobiotic compound of agricultural origin.

Very similar changes in cell density are also induced by exposure to 1 μM glufosinate (rapid inhibition, recovery and another phase of decrement). As herbicide concentration gets as high as 10 μM , cell density decreases sharply during the first days of exposure, then it stabilizes at a lower value, and after four days it registers a further, but moderate and progressive decrement. In contrast, 100 μM glufosinate causes a progressive decay of cell density during several days, followed by the set of a new steady-state at a low net rate of cell multiplication.

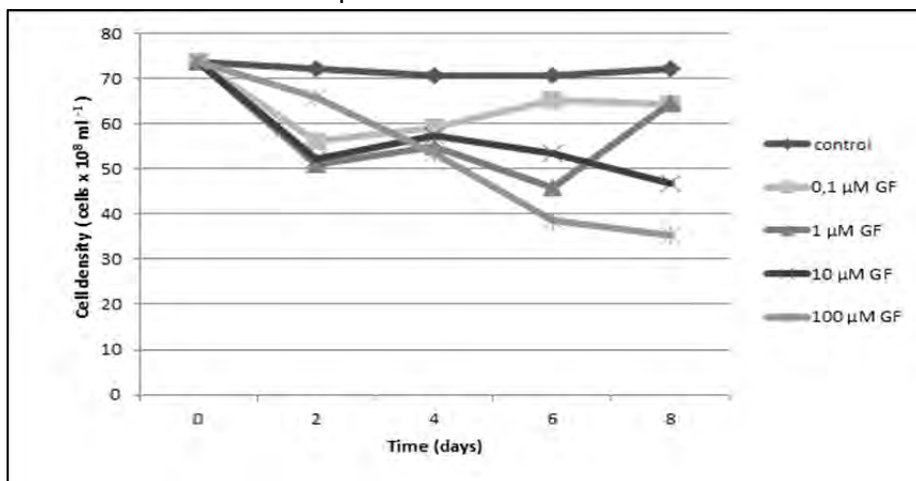


Figure 1. Dynamics of cell density in batch cultures of *Scenedesmus acuminatus* grown for 8 days in the presence of different concentrations of glufosinate (GF, $n = 3$)

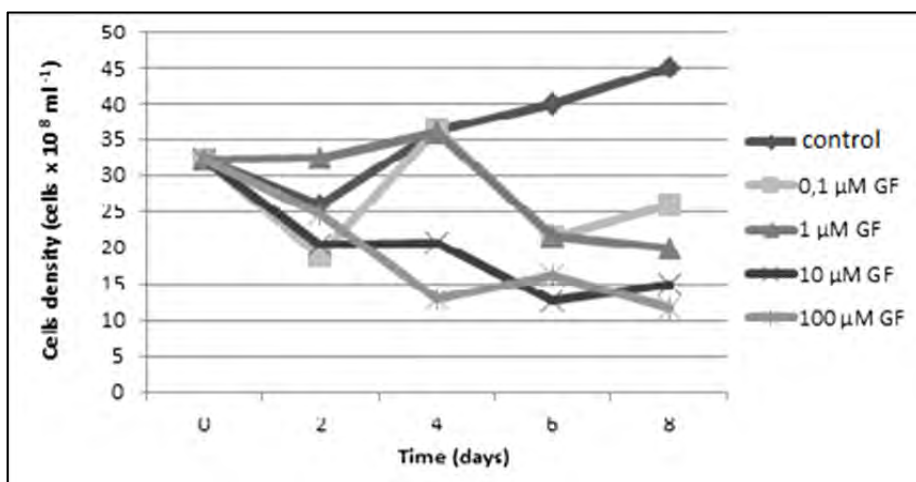


Figure 2. Variation of cell density in batch cultures of *Scenedesmus opoliensis* grown for 8 days in the presence of different concentrations of glufosinate (GF, $n = 3$)

Changes in the cell density of populations of the two algal species reveal different reactions in time to different amounts of the same herbicide, underlining the importance of reliable characterization and comparison of different species and strains during selection of the most suitable algae for indication and bioremediation of water pollution. Species-specific influence of herbicides on algal growth and reproduction were also reported by some authors [4]. Disturbance of cell division rate and induction of early senescence may be related to the indirect effect of glufosinate due to increased levels of ammonia in cell compartments where glutamine synthase is inhibited, and thus ammonium ions cannot be assimilated in glutamic acid [1].

If one compares the final cell density of populations of the two algal species after ten days of exposure to different glufosinate concentrations, without taking into account intermediary changes in cell number at different times of the period of treatment, it can be observed that in the case of *Scenedesmus acuminatus* 0.1 μM , 1 μM and 10 μM glufosinate caused only a moderate decrease in final cell density, the amount of 100 μM being the only one resulting in a more pronounced inhibition of net multiplication rate, while in case of *Scenedesmus opoliensis* all herbicide concentrations led to similar degrees of decrease in populational growth rate (Fig. 3). Extending the incubation time from 1 to 10 days, significantly increased the cell density of *Scenedesmus opoliensis* at the low levels of glufosinate but significantly decreased the cell density of *Scenedesmus acuminatus* at the high levels of glufosinate [20]. The results reflect that while exposure to low amounts of glufosinate is better indicated by *S. opoliensis*, *S. acuminatus* indicates more specifically the deleterious effects of high herbicide concentration after a longer exposure time.

Induced chlorophyll-a fluorescence measurement in the photosynthetic structures is a highly sensitive, accurate and non-damaging method for studying the efficiency of different steps of photochemical conversion of the absorbed light energy, as a prerequisite for sustained primary production of new organic compounds by fixation and reduction of carbon dioxide [5]. It provides information on the operation of the thylakoidal processes which constitute the light reactions of photosynthesis, as the only energy input for all living systems. From among the very numerous chlorophyll fluorescence parameters, which can be recorded or computed under various experimental conditions, we have chosen ground chlorophyll fluorescence (F_0) in dark-preadapted algal cells, on one hand because it is related to the very first steps of light energy harvesting and directional transfer in the photosynthetic pigment antennae, on which all the latter photochemical and assimilatory processes rely, on the other hand because it exhibited variations that are consistent with the impact of different amounts of herbicide in the aquatic environment. F_0 values (expressed as relative fluorescence units which depend on light intensity and on chlorophyll content)

change upon disturbances that occur in the functional organization of light-harvesting pigment-protein complexes that constitute the antennae of photosystem II in thylakoid membranes of chloroplasts, thus reflecting changes in the capacity of chlorophylls to absorb and to transfer light energy. In our cultures of *Scenedesmus acuminatus* the ground value of induced chlorophyll fluorescence exhibited a slight, but statistically significant decrease in the presence of 0.1 μM glufosinate, while higher herbicide amounts caused an increase of F_0 , this being more pronounced upon exposure to 1 μM and to 100 μM glufosinate (Fig. 4). In *Scenedesmus opoliensis* the F_0 was not influenced significantly by low concentrations of the herbicide, but exposure to 10 μM and to 100 μM of glufosinate resulted in a gradual decrease of ground fluorescence values with the increment of herbicide concentration. Thus, as far as F_0 values are concerned, *S. acuminatus* is suitable for early detection of the influence of small herbicide amounts, while *S. opoliensis* is a better indicator of the degree of water contamination with glufosinate if its concentration reaches and exceeds 10 μM . The results suggest that even if glufosinate is not a herbicide which inhibits photosynthesis, its influence on photorespiration and on the carbon assimilation in the Calvin cycle indirectly impairs organization and function of light-harvesting pigment-protein complexes. Accumulation of ammonium ions due to inhibition of glutamine synthase may also affect structure and permeability of thylakoid membranes where the light-harvesting antennae exist [8, 9].

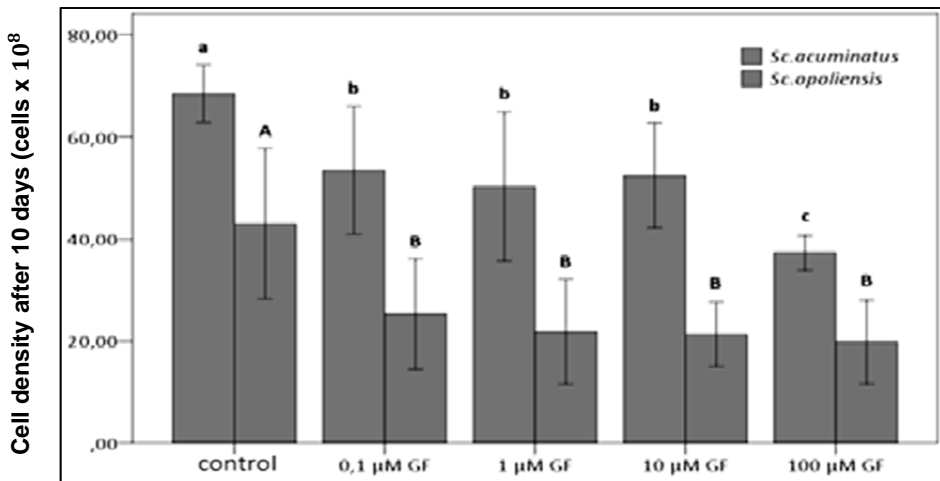


Figure 3. Final cell density in 10-days algal cultures exposed to various concentrations of glufosinate (GF) ($n = 3$, vertical bars represent \pm SD from means, different letters indicate significant differences at $P < 0.05$ between experimental variants of the same species)

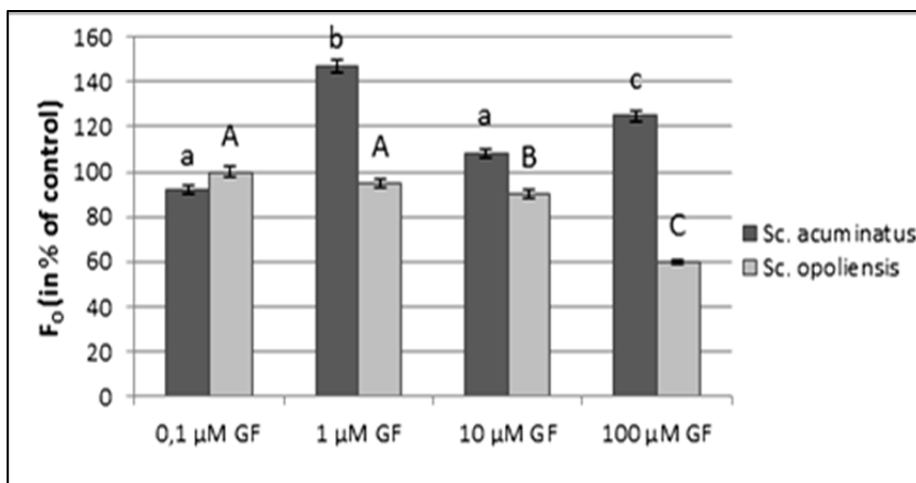


Figure 4. The induced ground fluorescence (F_0) of chlorophylls, expressed as percentage of the control, in the algal cells exposed for one week to different amounts of glufosinate (GF) ($n = 3$, vertical bars represent \pm SD from means, different letters indicate significant differences at $P < 0.05$ between experimental variants of the same algal species)

Ground chlorophyll fluorescence was also used to indicate and to evaluate the influence of other herbicides and water-pollutants on photosynthetic performance of several aquatic plants, but few chemical stress factors were found to significantly affect this parameter in a degree which is consistent with the severity of environmental stress or with the exposure time to water pollutants [6].

Quantity of photosynthetic pigments can be easily determined due to their specific absorption spectra. It varies in a large interval not only during acclimation of plants to different light intensities, but also under the influence of several chemical factors which inhibit steps of their biosynthetic pathway or enhance their catabolism. Because of their fundamental role in selective light-energy harvesting, their quantity is related to the intensity of primary photosynthetic processes in the autotrophy of plants on which primary production relies. Chlorophylls (*a* and *b* types in green algae and in higher plants) are the main light-harvesting pigments, but they are easily photo-oxidized under adverse conditions. Chlorophyll-*b* is always present in smaller amounts than chlorophyll-*a*, and its quantity increases especially during acclimation to low photon flux densities. Carotenoid pigments (carotenes and xanthophylls) are mainly photoprotective molecules with high antioxidative capacity (especially against singlet oxygen, hydroxyl radical and alkyl-hydroperoxyl radicals), their concentration increasing under conditions when energy dissipation is needed in order to protect chlorophylls and other photosynthetic constituents from oxidative damage [7].

In the alga *Scenedesmus acuminatus*, chlorophyll-*a* content expressed on a dry weight basis moderately increased in the presence of 1 μM glufosinate, and slightly decreased when the algal cells were exposed for several days, under constant illumination, to 10 μM glufosinate. Very low and very high concentrations of this herbicide did not induce statistically significant changes in the chlorophyll-*a* content (Fig. 5). Quantity of chlorophyll-*b* exhibited a very similar pattern of variation with chlorophyll-*a*. Overall carotenoid pigment content moderately increased under the influence of 1 μM and 10 μM glufosinate in the aquatic environment. In the case of the species *Scenedesmus opoliensis*, chlorophyll-*a* content increased in the presence of 1 to 100 μM glufosinate (the highest concentration did not cause depletion of this pigment's content as in case of the other alga). The amount of chlorophyll-*b* was augmented only by 1 μM glufosinate, but did not show any correlation with herbicide concentration, thus being not a suitable biochemical marker for water pollution with this compound. Carotenoid pigment content was depleted in similar degrees by the different concentrations of glufosinate, so in the case of this alga carotenoid pigment content may indicate the presence of the herbicide, but not its quantity in the aqueous medium in which the algal cell live (Fig. 6). Our experimental results show that the amount of chlorophyll-*a*, exposed to the cultures of *Sc. Opoliensis* glufosinate is also increased by the 1 μM concentration because of the influence of the herbicide. At the same time, compared to the control as can be seen in *Sc. Acuminatus* cultures (Fig. 6), the treatment with the two largest glufosinate amount (10 μM and 100 μM) does not decrease neither the amount of chlorophyll-*a* and chlorophyll-*b*, nor the carotenoid pigments. Despite the fact that in the case of *Sc. Opoliensis*, the glufosinate-treated cultures did not reduce the amount of photosynthetic pigments in any of the variants, the values of F_0 and F_m mutated to a certain extent impaired the organization of the antenna pigments and the energy transfer was more strongly inhibited.

To defend themselves, the algae supposedly increased the synthesis of photosynthetic pigment molecules.

If we compare variations in photosynthetic pigment content of the two algae, we can conclude that for *S. acuminatus* chlorophyll-*a* content, while in *S. opoliensis* the carotenoid content is a more adequate biochemical marker of water pollution with glufosinate.

The decreased chlorophyll content of plant cells exposed to glufosinate was partly explained by its strong inhibitory effect on synthesis of the chlorophyll precursor, 5-aminolevulinic acid [11]. When green microalgae were exposed to micromolar concentrations of the herbicide, their chlorophyll content (mainly the chlorophyll-*b* concentration) exhibited a significant increase, because impairment of photochemical reactions of photosynthesis on the acceptor side of photosystem II resulted in an enhancement of the light-

harvesting capacity, as algae tried to compensate energy deficiency by increasing the number of light-absorbing molecules [3],[16].

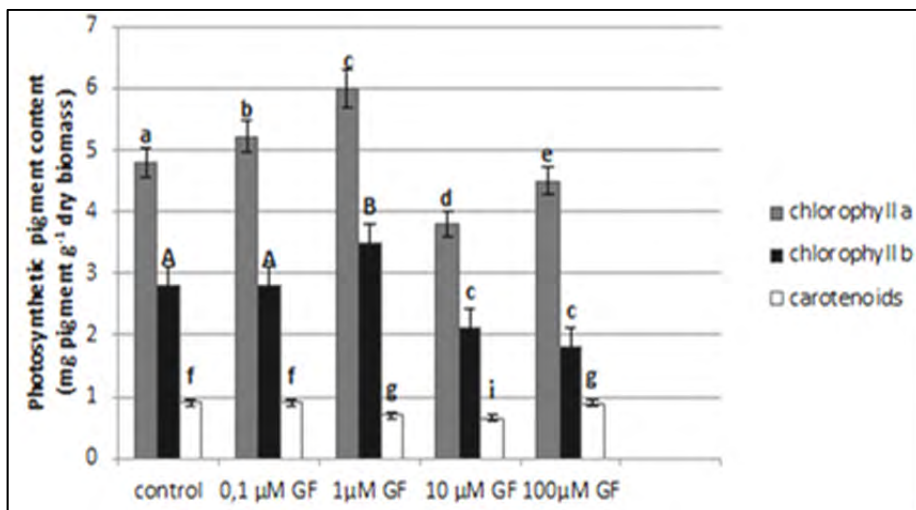


Figure 5. Effects of different concentrations of glufosinate (GF) on the photosynthetic pigment content of the green alga *Scenedesmus acuminatus* (n = 3, vertical bars represent ± SD from means, different letters indicate significant differences at $P < 0.05$ for the same pigment type)

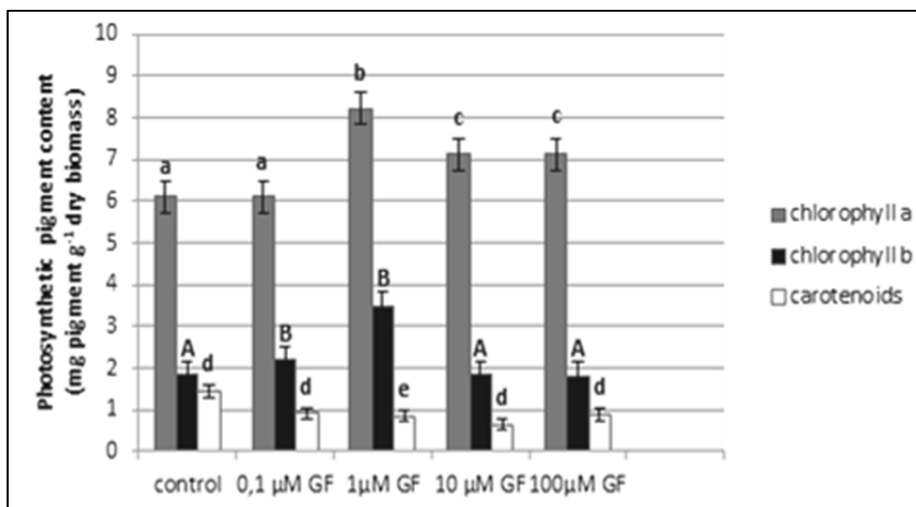


Figure 6. Effects of different concentrations of glufosinate (GF) on the photosynthetic pigment content of the green alga *Scenedesmus opoliensis* (n = 3, vertical bars represent ± SD from means, different letters indicate significant differences at $P < 0.05$ for the same pigment type)

These examples underline the finding that dynamics of different photosynthetic pigments may be differential markers for the influence of various chemical stress factors on plants living in polluted water [12].

CONCLUSIONS

Indicator organisms for water pollution with herbicides and other organic contaminants should be tested at species and intraspecific levels, because even related species, belonging to the same genus and living in similar aquatic environments, may exhibit differential biochemical and functional sensitivity. This is the case of the two *Scenedesmus* species from the freshwater green microalgae: *S. acuminatus* and *S. opoliensis*, the latter being more suitable for bioindication of water pollution with the herbicide glufosinate, considering changes induced in cell division rate, in chlorophyll and carotenoid pigment content of the cells, and in functional organization of the light-harvesting pigment antennae of the photosynthetic apparatus responsible for primary photochemical reactions. Monitoring changes of algal cell number at regular time intervals gives a better discrimination of herbicide impact than evaluation of final cell density after a certain period of exposure. Chlorophyll-*a* content varies in a greater extent under the influence of different herbicide concentrations than chlorophyll-*b* and carotenoid pigment contents do, thus being a better biochemical marker of algal reaction to water pollution with glufosinate. As a continuation of the present research, it is worth considering other biochemical parameters that do not show species-dependent differences, but more generally indicate the concentration- and time-dependent effects of certain water pollutants on the main primary producers of aquatic environments.

EXPERIMENTAL SECTION

Local strains of two green microalgal species, belonging to the same genus and widespread in variously polluted freshwater ponds: *Scenedesmus acuminatus* strain AICB 136 collected from the Tur creek near Cluj-Napoca, and *Scenedesmus opoliensis* strain AICB 141 originating in a pond of Săcălaia, Cluj county [5] were introduced in axenic monoalgal batch cultures, being grown in Bold's basal inorganic nutrient medium [14]. Cell cultures being at the beginning of the stationary phase of their population growth were used for initiation of the experiments. Both algal species were treated for ten days with 0.1 μM , 1 μM , 10 μM , and respectively 100 μM of the herbicide glufosinate [ammonium salt of phosphinothricin, i. e. ammonium-(3-amino-3-carboxy-propyl)-methyl phosphinate, dissolved in the sterile nutrient medium. Control cultures were grown in Bold's basal medium with no addition of herbicide. The initial pH value of all cultures was set to 5.6. The cultures were grown under constant environmental conditions in Certomat BS-1 algal growth

chamber, at a photosynthetically active photon flux density of $130 \mu\text{M photons m}^{-2} \text{ s}^{-1}$, at $22 \text{ }^\circ\text{C}$, with horizontal shaking at 60 rpm [6]. Cultures were set in three repetitions, and measurements were repeated three times.

Variations in the cell density of algal cultures were established with a periodicity of two days by cytometry, using Bürker's cell counter slide and a light microscope. This growth parameter reflects the capacity of microalgae to reproduce by cell divisions, i. e. to modify the number of individuals in a given volume of aqueous solutions[18].

Parameters of the induced chlorophyll-*a* fluorescence were recorded *in vivo* and *in situ* with a photosynthetic efficiency analyzer type fluorimeter (PEA from Hansatech, UK), in homogenized algal cell cultures adjusted to the same cell density, and dark-adapted for 5 minutes before measurement of chlorophyll fluorescence parameters by use of actinic light flashes with different intensities. The ground fluorescence (F_0) and the transitory maximal fluorescence (F_m) values were recorded, and the ratio between the variable and the maximal fluorescence (F_v/F_m , where $F_v = F_m - F_0$) was calculated, this latter being correlated with the potential or maximal quantum yield of photosynthesis under the given developmental and metabolic conditions [7,8,15]. Because from the above-mentioned parameters ground fluorescence was found the most sensitive to the herbicide treatments, only this one was selected for presentation.

Photosynthetic pigments (chlorophyll-*a*, chlorophyll-*b* and carotenoids) were extracted from the algae collected by filtration and dehydrated for three days at $80 \text{ }^\circ\text{C}$. After measurement of dry weight of the algal samples, extraction was performed for two days at room temperature and in darkness with dimethylformamide (5 ml for each algal probe). Photosynthetic pigment content was determined photometrically, based on the absorbance of the algal extracts at wavelengths of 480 nm, 663.8 nm and 646.8 nm [10].

Experimental data were evaluated statistically (in R environment, R Development Core Team 2014), using one-way ANOVA and the post-hoc Tukey HSD test for establishing the significance of differences between treatments (normality of values distribution was established with the Shapiro-Wilk test, while homogeneity of variances was analyzed with Bartlett's test).

REFERENCES

1. C. Aflalo, W. Bing, A. Zarka, S. Boussiba, *Zeitschrift fur Naturforschung - Section C Journal of Biosciences*, **1999**, 54, 49.
2. N. Abdel-Raouf, I. B. M. Ibraheem, O. Hammouda, Eutrophication of River Nile as indicator of pollution. *Al-Azhar Bulletin of Science*, **2003**, 293.
3. O. Aksakal, *Acta Physiologiae Plantarum*, **2013**, 35, 2281.

4. F. Araniti, A. Sorgona, A. Lupini, M. R. Abenavoli, *Allelopathy Journal*, **2002**, 29, 107.
5. N. Dragoş, L. S. Péterfi, L. Momeu, C. Popescu, An introduction to the algae and the culture collection of algae at the Institute of Biological Research Cluj-Napoca, *Cluj University Press*, Cluj-Napoca, **1997**, 197-200.
6. M.C. Falco, A. Tulmann Neto, E.C. Ulian, *Plant Cell Reports*, **2000**, 19, 1188.
7. L. Fodorpataki, S. Barna, H. Deak, B. Kovacs, J. Geraj, B. Holinka, *Analele Universităţii din Oradea, Fasc. Biologie*, **2014**, 21, 19.
8. L. Fodorpataki, A. Márton, T. Csorba, *Contribuţii Botanice*, **2001**, 36, 101.
9. L. Fodorpataki, C. Bartha, Z. G. Keresztes, *Analele Universităţii din Oradea, Fasc. Biologie*, **2009**, 16(1), 51.
10. G. Horvath, M. Droppa, L. Fodorpataki, A. Istokovics, G. Garab, W. Oettmeier, *Proceedings of the National Academy of the USA*, **1996**, 96, 3876.
11. G. S. Johal, D. M. Huber, *European Journal of Agronomy*, **2009**, 31, 144.
12. V. Lozovaya, A. Ulanov, A. Lygin, D. Duncan, J. Widholm, *Planta* **2006**, 224, 1385.
13. F.A. Macias, A. Oliveros-Bastidas, D. Marin, C. Carrera, N. Chinchilla, J.M. G. Molinillo, *Phytochemistry Reviews*, **2008**, 7(1), 179.
14. F. Marva, V. Lopez-Rodas, M. Rouco, M. Navarro, F.J. Torro, E. Costas, A. Flores-Moya, *Aquatic Toxicology*, **2010**, 96(2), 130.
15. N. Mallick, F. M. Mohn, *Ecotoxicology and Environmental Safety*, **2003**, 55, 64.
16. J. Papp, L. Fodorpataki, *Contribuţii Botanice*, **2002**, 37, 231.
17. R. Prado, C. Rioboo, C. Herrero, A. Cid, *Chemosphere*, **2009**, 76, 1440.
18. H. Scragg, A. M. Illman, A. Carden, S. W. Shales, *Biomass and Bioenergy*, **2002**, 23(1), 67.
19. Ulanov, A. Lygin, D. Duncan, J. Widholm, V. Lozovaya, *Journal of Plant Physiology*, **2009**, 167, 978.
20. S. Zhou, Y. Shao, N. Gao, Y. Deng, J. Qiao, H. Ou, J. Deng, *Science of the Total Environment*, **2013**, 463-464, 111.

DETERMINATION OF LETROZOLE, ANASTROZOLE AND EXEMESTANE BY CAPILLARY ZONE ELECTROPHORESIS

AURA RUSU^a, GABRIEL HANCU^{a*}, LAVINIA BERȚA^b,
CAMIL EUGEN VARI^c

ABSTRACT. A new validated capillary zone electrophoresis method was developed for the quantification of three aromatase inhibitors - anastrozole, letrozole and exemestane. After preliminary analysis a sodium tetraborate background electrolyte containing carboxymethyl β -cyclodextrine was selected for the simultaneous determination of the three aromatase inhibitors. 100 mM sodium tetraborate containing 5 mM carboxymethyl β -cyclodextrine as buffer additive, 25 kV applied voltage, 20 mbar/2 s injection pressure and 25°C temperature were selected as optimum parameters for the determination. Analysis was performed in approximately 10 minutes. Validation parameters, including linearity, precision, detection and quantification limits were determined. Our results prove the applicability of capillary zone electrophoresis for the simultaneous determination of the three aromatase inhibitors from pharmaceutical products. The applicability of the optimized method was also tested for biological samples, proving its reliability for the determination of letrozole without any special treatment of the analyzed spiked urine sample and presenting potential for other biological matrices.

Keywords: *aromatase inhibitors, anastrozole, letrozole, exemestan, capillary zone electrophoresis, cyclodextrines*

^a University of Medicine and Pharmacy of Targu Mures, Faculty of Pharmacy, Department of Pharmaceutical Chemistry, 38 Gh. Marinescu str., RO-540139, Targu Mures, Romania.

* Corresponding author gabriel.hancu@umftgm.ro

^b University of Medicine and Pharmacy of Targu Mures, Faculty of Pharmacy, Department of General and Inorganic Chemistry, 38 Gh. Marinescu str., RO-540139, Targu Mures, Romania.

^c University of Medicine and Pharmacy of Targu Mures, Departement of Pharmacology and Clinical Pharmacy, 38 Gh. Marinescu str., RO-540139, Targu Mures, Romania.

INTRODUCTION

Anastrozole (ANA) and letrozole (LET) are nonsteroidal competitive inhibitors of aromatase (Als), the enzyme required for the last step in estrogen synthesis. Exemestane (EXE) is an irreversible aromatase inhibitor with a steroid structure. These drugs are used in the treatment of breast cancer and are administered orally in a daily single dose [1].

ANA is indicated for first-line treatment of postmenopausal women with advanced or metastatic breast cancer, for second-line treatment of postmenopausal patients with advanced breast cancer who have had disease progression following tamoxifen therapy, and for adjuvant treatment of women with early breast cancer. LET is specific for aromatase inhibition, with no additional effects on adrenal corticoid biosynthesis. EXE is a steroid-based aromatase inhibitor approved for the treatment of breast cancer with a mechanism-based inactivator that irreversibly inhibits the enzyme [2]. Although they share a general mechanism of action, the third generation Als produce varying degrees of aromatase inhibition and estrogen suppression [3].

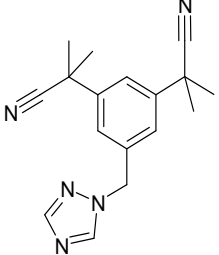
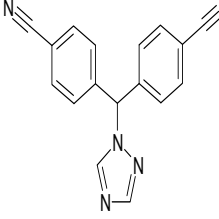
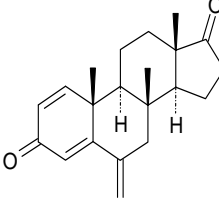
The chemical and physical characteristics of the studied substances are presented in Table 1.

Als are used as *off label* therapy in male infertility following LH deficiency (in morbid obesity and in anabolic steroid induced hypogonadism) [4-6]. Also, ANA, LET and EXE are included in the World Anti-Doping Agency Prohibited List [7]; these drugs are used in combination with anabolic steroids to prevent the onset of gynecomastia by estrogenic excess; aromatase inhibitors are also used by doped athletes as post cycle therapy in order to promote restoration of hypothalamic-pituitary-testicular axis integrity [8,9].

Several capillary electrophoretic methods have been reported for determination of Als in combination with other compounds, mainly micellar electrokinetic capillary chromatographic (MEKC) [17-20]. So far, there is no published electrophoretic method for the simultaneous determination of all three Als selected in this research.

The main objective of this study was to elaborate a new simple, rapid and accessible capillary zone electrophoresis (CZE) method for determination of ANA, LET and EXE, with applications in the determination of the studied substances in pharmaceutical products and biological samples. A simple validated CZE method could also be very useful in analysis of Als counterfeit drugs, used by athletes in doping offenses.

Table 1. Chemical structure and physical properties of ANA, LET and EXE.

Als	Chemical structure	MW	pK_a	Solubility	LogP / Log D	Ref.
ANA		293.36	$pK_a = 2.01$ pK_a for [BH+] = 4.78	freely soluble in methanol, acetone, ethanol, tetrahydrofuran, and very soluble in acetonitrile	Log P 0.77, Log D at pH 7 is 0.77	[10-13]
LET		285.30	pK_a for [BH+] = 3.63 $pK_a = 5.4$ (dibenzonitrile group) pK_a for [BH+] = 4.4 (nitrogen protons in the triazole ring)	freely soluble in dichloromethane; slightly soluble in ethanol; practically insoluble in water	Log P 1.52, Log D at pH 7 is 1.52	[13-15]
EXE		296.41		freely soluble in dimethylformamide; soluble in methanol and ethanol; sparingly soluble in acetonitrile; practically insoluble in water	Log P 3.30, Log D at pH 7 is 03.30	[13,14,16]

RESULTS AND DISCUSSION

Preliminary experiments. At the beginning of determinations we have selected the type of background electrolyte (BGE) by checking the electrophoretic behavior of the analytes using an acidic BGE - phosphoric acid 25 mM and a basic BGE - 25 mM borax. After our preliminary results we selected a 25 mM borax (pH 9.3) as BGE also taking in consideration previous electrophoretic studies [17-21].

Method optimization. Electrophoretic behavior of the selected Als are obvious consequences of their physico-chemical properties. In order to obtain a better resolution of the separation various buffer additives as organic solvents, surfactants, β -cyclodextrines (β -CDs) were tested.

Organic solvents are used in CZE in order to increase solubility of the analytes [20, 22]. Addition of organic solvents (methanol, acetonitrile, n-propanol, dimethylformamide) could not improve the resolution, probably because the selected AIs exhibit very close electrophoretic mobility's that cannot be differentiated by adding a small amount of organic solvent. Moreover, addition of organic solvents increased migration times.

We tried to improve separation by using the most commonly used surfactant, sodium dodecylsulfate (SDS) (20 – 100 mM), an anionic surfactant, in varying concentrations of BGE (25 – 100 mM). Although ANA, LET and EXE are in neutral form in this BGE all three compounds migrated with the same electrophoretic mobility [24].

Because of similarity of chemical structures between ANA and LET we choose to add in BGE a variety of β -cyclodextrines (β -CD) derivatives in order to improve the separation resolution: β -cyclodextrine (MW 1135, native CD), 2-hydroxypropyl β -cyclodextrine (2-HP- β -CD) (MW 1460, neutral derivatized CD), carboxymethyl β -cyclodextrine (CM- β -CD) (MW 1541, anionic CD), and sulfobutyl β -cyclodextrine (SB- β -CD) (MW 2245, anionic CD). Usually, CDs are the most popular chiral selectors used in capillary electrophoresis (CE) or for increasing aqueous solubility, higher dissolution rate and intestinal permeation of drugs [22, 24]. Adding β -CD derivatives to BGE (5 – 15 mM) improved the separation of ANA, LET and EXE. Also, we used dual CD systems (β -CD and CM- β -CD in various concentrations between 5 – 15 mM) containing a neutral CD and a ionized one, and studied their influence on the separation. Due to encouraging results obtained by using β -CD derivatives as BGE additives we tried to combine β -CD derivatives with small concentration of SDS, without improving the analytes separation.

The influence of the most important electrophoretic parameters (BGE concentration and pH, applied voltage, temperature, injection time and pressure) on the separation was studied and the parameters were optimized.

The migration times of the analytes increased with the increase of the BGE concentration, because of the decrease of electroosmotic flow (EOF) with the increase in ionic strength.

In CZE the pH of BGE is very important since affects ionization of the analytes and their electrophoretic mobility. Using MarvinSketch 17.1.2 (ChemAxxon) chemical editor [25] we found that major microspecies of selected AIs are neutral in the range of pH 4 - 13.

We varied the pH of BGE between 8.30 – 10.40 by adding small amounts of 1M NaOH and 1M boric acid without satisfactory results (no improvement of separation under 9.4 values and at pH values greater than 9.4 the migration time are longer and peaks are distorted).

Regarding the influence of applied voltage and system temperature, the migration times decreased with the increase of these parameters, the limiting factors being the Joule heating and the viscosity of BGE which is directly related with temperature. We selected an applied voltage of 25 kV and a temperature of 25°C as optimum parameters.

The migration times were slightly influenced by injection pressure and time; however, injection parameters influenced peak shape and amplitude. Thus, a 20mbar injection pressure and a short injection time (2 seconds) were chosen to avoid peak broadening or splitting.

Thereby, ANA, LET and EXE can be separated with the optimized parameters within 10 minutes (Figure 1). The best separation was obtained using a 100 mM sodium tetraborate containing 5 mM CM- β -CD, 25 kV applied voltage, 20 mbar/2 s injection pressure and 25°C temperature as optimum parameters (Table 2). The confirmation of peaks identity was achieved by comparing migration times of individual analytes and overlaying the UV spectra using the electrophoretic system photodiode detector with the ones obtained from standards.

Table 2. Parameters of ANA, LET and EXE separation by CZE (T - migration time, A - area, H - height, Symm. – symmetry, Res. – resolution, Sel. – selectivity).

Als	T (min)	A (mAU*s)	H (mAU)	Symm.	Width (min)	Plates	Res.	Sel.
ANA	4.871	10.32	2.20	0.80	0.085	17841	-	-
LET	6.040	25.10	6.22	0.17	0.034	168966	11.4	1.24
EXE	8.506	7.03	1.96	0.32	0.037	291505	40.44	1.41

It is known that the electrophoretic mobility is related to charge and mass (μ_{pH} vs. q/M^{α}). Semiempirical methods describe this relation which differ in the α value which is 1/3 in the Stoke's law, and 2/3 in Offord's approach [26]. Molar mass values of the three compounds are very close (Table 1). A notable difference we distinguish on EXE chemical structure which is a steroidal neutral compound. There are published studies related to the complexation of EXE with β -CD derivatives in terms of increased aqueous solubility of drug, higher dissolution rate and intestinal permeation [27-29]. Thereby is very probable that EXE could form a complex more soluble with CM- β -CD from the BGE and that may explain the longest migration time. Although ANA and LET are compounds of high structural similarity, differences also exist in their molecular shape and association capability with CM- β -CD [30]. These properties also influence the electrophoretic mobility.

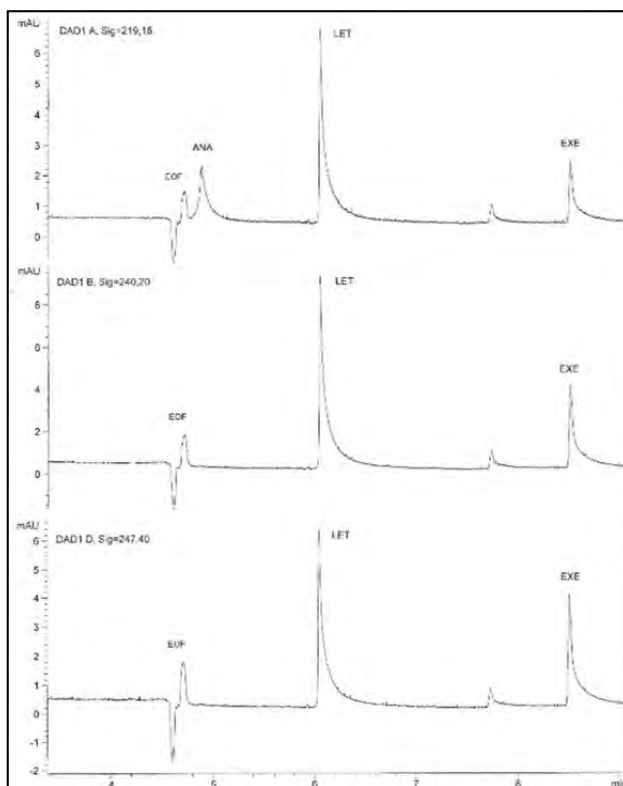


Figure 1. Separation of ANA, LET, and EXE by CZE (working conditions: BGE 100 mM sodium tetraborate + 5 mMCM- β -CD, applied voltage: 25 kV, injection pressure: 20 mbar/ 2 s injection pressure, temperature: 25°C).

Method validation. Our optimized method was validated and validation parameters were calculated. The selected internal standard was ciprofloxacin, a stable fluoroquinolone compound with a good signal in the selected BGE [31].

Specificity. The elaborated method allows the detection of an AIs derivative from a mixture by quantitative measurement of a parameter (area of the obtained signal). The three selected AIs could be quantified without any interference with other present components.

Linearity and detection limits. The linear regression equations were calculated using six concentration levels and three replicates per concentration. Correlation coefficient was over 0.99, which demonstrates a very good linearity of the method. LOD and LOQ were calculated based on the standard deviation of the response and the slope; the residual standard

deviation of a regression line or the standard deviation of y-intercepts of regression lines was used as the standard deviation in accordance with the International Conference on Harmonization (ICH) criteria (Table 3)[32].

Precision. The precision of the method was investigated in repeatability and intermediate precision terms for migration times and peak areas of the three AIs compounds in accordance with ICH criteria [32]. The measurement was performed by six replicate injections of three different concentrations, three consecutive days for all AIs. The results, expressed as RSD values, indicate a good precision (Table 4).

Table 3. Linearity - statistical parameters (T = migration time, A = area).

AIs	Concentration domain ($\mu\text{g}\cdot\text{mL}^{-1}$)	Regression equation	Correlation coefficient	LOD ($\mu\text{g}\cdot\text{mL}^{-1}$)	LOQ ($\mu\text{g}\cdot\text{mL}^{-1}$)
ANA	187.5 - 625	$y = 0.0438x - 3.3156$	0.9908	51.92	173.08
LET	62.5 - 500	$y = 0.1576x - 3.5290$	0.9936	43.40	144.67
EXE	187.5 - 625	$y = 0.0820x - 4.7439$	0.9948	42.54	141.82
Internal standard CIP 187.5 $\mu\text{g}\cdot\text{mL}^{-1}$ (n = 18)				T	A
		Average		7.32	23.43
		SD		0.314	2.47
		RSD%		4.280	10.55

Table 4. Intra-day and inter-day precision of CZE method (T = migration time, A = area).

AIs	Concentration ($\mu\text{g}\cdot\text{mL}^{-1}$)	Intra-day precision (RSD%) n = 6		Inter-day precision (RSD%) n= 18 Days 3	
		T	A	T	A
ANA	625	0.493	6.183	1.661	11.430
	500	0.247	9.174	2.167	7.612
	312.5	0.176	10.012	1.766	11.824
LET	500	0.552	3.443	0.812	14.238
	375	0.243	8.969	0.216	7.080
	187.5	0.220	0.199	0.777	13.179
EXE	625	0.697	5.638	4.714	14.607
	500	0.195	8.610	4.574	8.574
	312.5	0.338	4.290	4.457	10.700

Application to biological samples. In order to verify the applicability of our CZE method in determination of AIs from biological samples we took in consideration the biotransformation of LET. LET is excreted into urine approximately 70% of the administered dose as unchanged ($6.0 \pm 3.8\%$) or as the glucuronide of the major, pharmacologically inactive metabolite carbinole (CGP44645) ($64.2 \pm 22.7\%$) [33,34]. Thus, in a 5 mg administered dose, $0.35 \text{ mg} \pm 0.07\%$ was recovered in the urine [35]. Analytical performance of our CZE was evaluated on spiked urine from healthy volunteers.

Specificity. LET could be quantified from spiked urine samples without any interference with other present components (Figure 2).

Linearity and detection limits. The linearity response and detection limits for spiked with LET urine samples are presented in Table 5.

Table 5. Linearity - statistical parameters.

Als	Conc. domain ($\mu\text{g}\cdot\text{mL}^{-1}$)	Regression equation	Correlation coefficient	LOD ($\mu\text{g}\cdot\text{mL}^{-1}$)	LOQ ($\mu\text{g}\cdot\text{mL}^{-1}$)
LET	50 - 200	$y = 0.3783x - 4.25$	0.9954	12.37	41.23

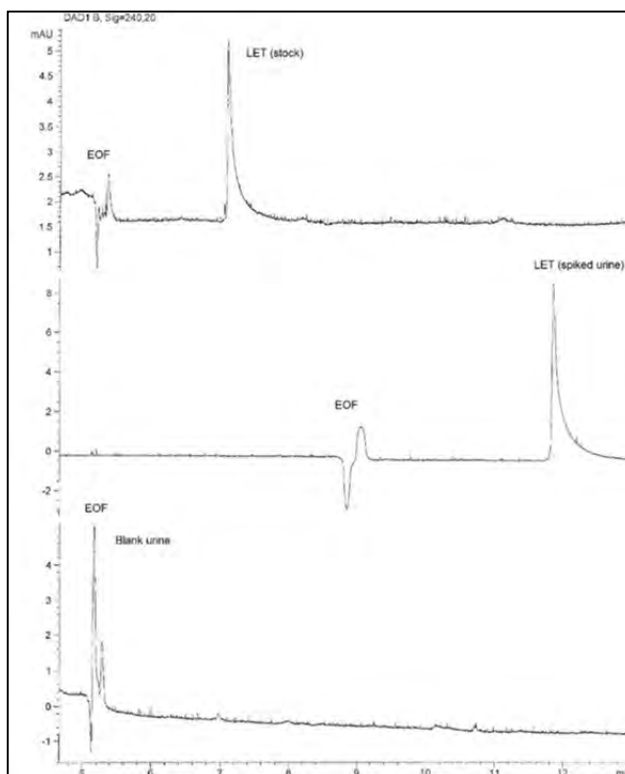


Figure 2. Electrophoregrams of LET from stock solution, spiked urine and blank samples ($200 \mu\text{g mL}^{-1}$) using optimized electrophoretic parameters.

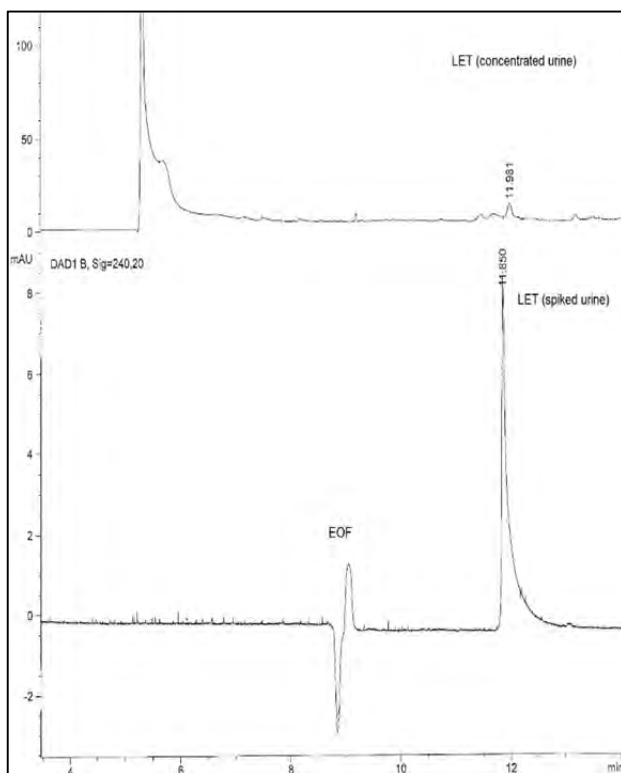
The linear regression equations were calculated using six concentration levels and three replicates per concentration. Correlation was over 0.99, which demonstrates a very good linearity of the method.

Precision. The precision of the method was investigated in repeatability and intermediate precision terms for migration times and peak areas of LET in spiked urine samples (Table 6).

Table 6. Intra-day and inter-day precision of CZE method for determination of LET in spiked urine samples (T - migration time, A - area).

AIs	Concentration ($\mu\text{g}\cdot\text{mL}^{-1}$)	Intra-day precision (RSD%) n = 6		Inter-day precision (RSD%) n= 18 Days 3	
		T	A	T	A
	200	0.489	6.701	0.693	10.707
LET	125	0.528	5.901	0.667	5.309
	75	0.333	5.778	0.474	8.646

Although the results of determination of LET from spiked urine plasma was encouraging, when we tried to quantify the concentration of LET in a concentrated urine clinical sample the method sensibility was too low (Figure 3).

**Figure 3.** Electropherograms of LET from concentrated urine sample and spiked urine samples ($200 \mu\text{g mL}^{-1}$) using optimized electrophoretic parameters.

Regarding determination of selected AIs our results were not satisfactory as respect to selectivity and migration time. Consequently the method requires further improvements regarding both the electrophoretic method and the sample

preparation. Also the spiked plasma samples with EXE electrophoregrams present interferences from plasma components (Figure 4).

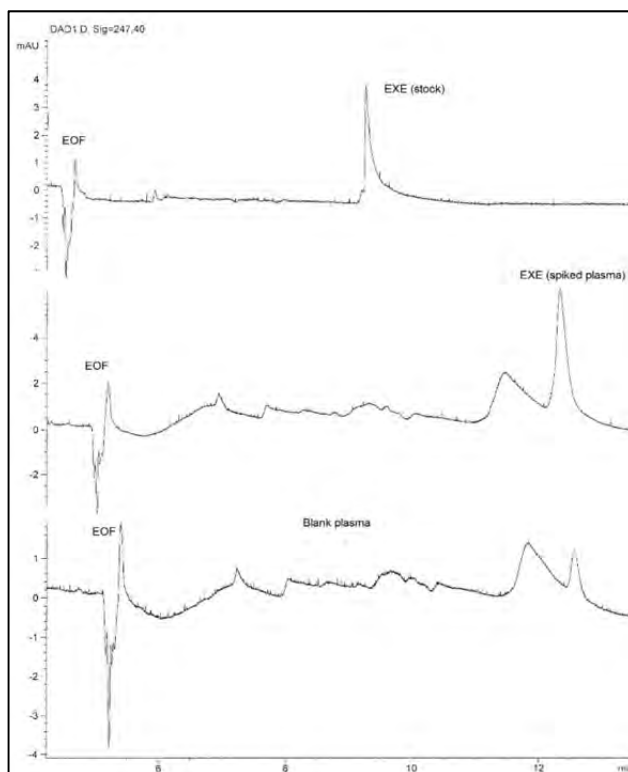


Figure 4. Electrophoregrams of EXE from stock solution, spiked plasma and blank plasma samples (0.67 mg mL^{-1}) using optimized electrophoretic parameters.

Application to Pharmaceutical Formulations. For the determination of ANA and LET from commercial preparations, a total of 20 tablets were weighed and powdered from each commercial product. An equivalent to about 10 mg was weighed accurately and transferred into a 100ml volumetric flask and 50 ml methanol was added. After ultrasonic vibration for 30 minutes, the mixture was diluted to volume with methanol and then filtrated. A concentration of $100 \text{ }\mu\text{g mL}^{-1}$ of substance was set [36]. For determination of EXE a total of 20 tablets were weighed and powdered. An equivalent to about 400 mg was weighed accurately and transferred into a volumetric flask similar to ANA and LET. Additionally a second dilution was necessary to obtain a concentration of $100 \text{ }\mu\text{g mL}^{-1}$.

The amount of AIs labeled claim and standard deviation were calculated (Table 7).

Table 7. Recovery of ANA, LET and EXE from pharmaceutical formulation (average for three replicates).

Comercial product/Producer	Substance	Formulation	Amount (mg)	Recovery (%) \pm SD
Anastrozol/Teva	ANA	Tablets	1	97.64 \pm 4.36
Letrozol/Teva	LET	Tablets	2.5	99.37 \pm 3.49
Exemestan/Actavis	EXE	Tablets	25	97.35 \pm 3.89

Also, our method can be useful in quantifying the three AIs from counterfeit drugs.

CONCLUSIONS

The developed CZE method can be used for separation, identification and quantitative determination for important representatives from AIs class. Our validated CZE method is a simple and reliable, using a particular BGE composed of sodium tetraborate and CM- β -CD as buffer additive. With the new validated CZE method we quantified ANA, LET and EXE from pharmaceutical products; the method can find applicability in the analysis of AIs counterfeit drugs. Our method also present potential to analyze biological samples. We succeed to quantified LET from spiked urine samples without any special treatment, an encouraging step which demonstrate that the method can be improved for analysis of clinical samples.

EXPERIMENTAL SECTION

Materials and reagents. The substances and pharmaceutical products were purchased from the following suppliers: ANA, LET and EXE from Sigma Aldrich, borax from Chemical Company, dodecyl sulfate sodium salt from Merck, β -cyclodextrin (β -CD) Biochemica from AppliChem Panreac, 2-Hydroxypropyl- β -cyclodextrin (2-HP- β -CD) from AppliChem Panreac, carboxymethyl β -cyclodextrine (CM- β -CD) from Sigma Aldrich, sulfobutyl β -cyclodextrinefrom (SB- β -CD) from Cyclolab Ltd., ciprofloxacin hydrochloride (CIP) form Ranbaxy Laboratories Limited, Anastrozol 1 mg and Letrozol 2.5 mg from Teva, Exemestan 25 mg from Actavis. All reagents and solvents were of analytical grade and were obtained from commercial suppliers and used without further purification. The deionized water was prepared with a Milli-Q Direct 8 Millipore system.

CE system. All CE experiments were conducted in an Agilent 1600CE system equipped with diode-array detector, while the results were recorded and processed using Chemstation 7.01 software (Agilent). Separations were performed using uncoated fused-silica capillaries of 60 cm x 50 μm I.D (effective length 52cm) (Agilent). In all measurements hydrodynamic sample injection was used, by injecting the sample at the anodic end of the capillary, with the detector at the cathodic end.

CZE method. A background electrolyte (BGE) containing 25 mM borax at a pH – 9.3 was selected. The detection was carried out in UV at 219 nm, 240 nm, 247 nm and 279 nm, taking into consideration the UV absorption maxima of the studied analytes and internal standard. All experiments were carried out at room temperature. At the beginning of each day the capillary was conditioned with 1 M NaOH (30 min), deionized water (5 min) and BGE (20 min). The capillary was preconditioned before every run with water (1 min) and BGE (2 min). The pH was adjusted using a Terminal 740 (Inolab) pH-meter.

Preparation of stock and standard solutions. The AIs stock solutions were prepared daily by dissolving the substance in methanol at 1 $\text{mg}\cdot\text{mL}^{-1}$ concentration. They were stored in the refrigerator at +4°C, and later diluted to an appropriate concentration.

Urine and plasma sample treatment. Fresh human urine samples and plasma were obtained from different healthy volunteers; a clinical urine sample were provide by a volunteer men (45 years old) who has taken 5 mg of LET then the urine sample was collected after 10 hours. The urine and plasma samples were spiked with LET stock solution, centrifuged (4800 rpm, 10 minutes) and supernatant filtrated (0.45 μm Whatman filter). The clinical sample was concentrated 16 times with a rotary evaporator at 40°C under vacuum, centrifuged (4800 rpm, 10 minutes in a Centurion Scientific Ltd. centrifuge) and supernatant filtrated.

ACKNOWLEDGMENTS

The research was supported by a project funded through Internal Research Grants by the University of Medicine and Pharmacy of Tîrgu Mures, Romania (grant contract no. 17/23.12.2014).

REFERENCES

1. A. Trevor, B. Katzung, S. Masters, M. Knudering-Hall, „Katzung & Trevor's Pharmacology Examination and Board Review”, McGraw-Hill Education, New York, **2012**, chapter 40.
2. J. M. Beale Jr., J. H. Block, „Wilson and Gisvold's Textbook of Organic Medicinal and Pharmaceutical Chemistry”, Lippincott Williams & Wilkins, Philadelphia, **2011**, chapter 25.
3. J. Berry, *Clinical Therapeutics*, **2005**, 27, 167.
4. L. DiGiorgio, H. Sadeghi-Nejad, *Translation Andrology and Urology*, **2016**, 5, 844.
5. S. M. Stephens, A. J. Polotsky, *Seminars in Reproductive Medicine*, **2013**, 31, 251.
6. C. E. Vari, B. E. Ösz, A. Miklos, A. Berbecaru-lovan, A. Tero-Vescan, *Farmacia*, **2016**, 64, 813.
7. WADA publishes 2017 Prohibited List https://www.wada-ama.org/sites/default/files/resources/files/2016-09-29_-_wada_prohibited_list_2017_eng_final.pdf (Accessed 21 April 2017).
8. R. El Osta, T. Almont, C. Diligent, N. Hubert, P. Eschwège, J. Hubert, *Basic and Clinical Andrology*, **2016**, 26, 2.
9. E. Nieschlag, E. Vorona, *European Journal of Endocrinology*, **2015**, 173, R47.
10. S. Budavari, „The Merck index: an encyclopedia of chemicals, drugs, and biologicals”, Whitehouse Station, N.J Merck, **1996**.
11. K. Wellington, D. M. Faulds, *Drugs*, **2002**, 62, 2483.
12. <https://pubchem.ncbi.nlm.nih.gov/compound/2187#section=Top> (Accessed 21 April 2017).
13. J. M. Beale Jr., J. H. Block, „Wilson and Gisvold's Textbook of Organic Medicinal and Pharmaceutical Chemistry”, Lippincott Williams & Wilkins, Philadelphia, **2011**, Appendix.
14. P. D. R. Thomson, „Physicians Desk Reference”, Montvale, NJ, **2006**.
15. M. Pal, S. Dan, B. Ghosh, A. Das, D. Das, T. K. Pal, *Journal of Analytical & Pharmaceutical Research*, **2017**, 4, 00093.
16. https://www.accessdata.fda.gov/drugsatfda_docs/nda/99/20-753_Aromasin_biopharmr_P1.pdf (Accessed 21 April 2017)
17. J. Rodríguez Flores, J. J. Berzas Nevado, G. Castañeda Peñalvo, M. I. Rodríguez Cáceres, *Chromatographia*, **2002**, 56, 283.
18. J. Rodríguez-Flores, A. M. Contento Salcedo, M. J. Villaseñor Llerena, L. Muñoz Fernández, *Electrophoresis*, **2008**, 29, 81.
19. J. Rodríguez Flores, A. M. Salcedo, M. J. Llerena, L. M. Fernández, *Journal of Chromatography A*, **2008**, 1185, 281.
20. J. Rodríguez-Flores, A. M. Contento Salcedo, L. Muñoz Fernández, *Electrophoresis*, **2009**, 30, 624.
21. S. Orlandini, R. Gotti, S. Furlanetto, *Journal of Pharmaceutical and Biomedical Analysis*, **2014**, 87, 290.
22. K. M. M. Al Azzam, B. Saad, „Determination of Drugs using Capillary Electrophoresis”, Lambert Academic Publishing, Saarbrücken, **2012**, chapter 1.

23. G. Hancu, B. Simon, A. Rusu, E. Mircia A. Gyeresi, *Advanced Pharmaceutical Bulletin*, **2013**, 3, 1.
24. T. Loftsson, P. Jarho, M. Másson, T. Järvinen, *Expert Opinion on Drug Delivery*, **2005**, 2, 335.
25. <https://www.chemaxon.com/products/marvin/marvinsketch/> (Accessed 21 April 2017).
26. P. Schmitt-Kopplin, A. Fekete, *Methods in Molecular Biology*, **2008**, 384, 593.
27. B. Yavuz, C. Sarisözen, I. Vural, E. Bilensoy, M. Sumnu, *Journal of Controlled Release*, **2010**, 20, e83.
28. G. Li, F. Li, L. Deng, X. Fang, H. Zou, K. Xu, T. Li, G. Tan, *Steroids*, **2013**, 78, 1148.
29. M. S. I. Shaikh, N. D. Derle, R. Bhamber, *Journal of Applied Pharmaceutical Science*, **2012**, 02, 34.
30. M. F. Wempe, C. M. Buchanan, N. L. Buchanan, K. J. Edgar, G. A. Hanley, M. G. Ramsey, J. S. Skotty, P. J. Rice, *Journal of Pharmacy and Pharmacology*, **2007**, 59, 795.
31. A. Rusu, G. Hancu, G. Völgyi, G. Tóth, B. Noszál, Á. Gyéresi, *Journal of Chromatographic Science*, **2014**, 52, 919.
32. http://www.ich.org/fileadmin/Public_Web_Site/ICH_Products/Guidelines/Quality/Q2_R1/Step4/Q2_R1__Guideline.pdf (Accessed 21 April 2017).
33. C.U. Pfister, A. Martoni, C. Zamagni, G. Lelli, F. De Braud, C. Souppart, M. Duval, U. Hornberger, *Biopharmaceutics & Drug Disposition*, **2001**, 22, 191.
34. http://www.bccancer.bc.ca/drug-database-site/Drug%20Index/Letrozole_monograph_1April2011.pdf (Accessed 21 April 2017).
35. http://www.accessdata.fda.gov/drugsatfda_docs/nda/97/20726_FEMARA%202.5MG_BIOPHARMR.PDF (Accessed 21 April 2017).
36. S.K. Acharjya, P. Mallick, P. Panda, K.R. Kumar, M.M. Annapurna, *Journal of Advanced Pharmaceutical Technology & Research*, **2010**, 1, 348.

REMOVAL OF HYDROGEN SULPHIDE CONTENT FROM BIOGAS BY ATOMIZING OF ALKALI SOLUTION

ÉVA MOLNÁR^{a,*}, DÓRA RIPPEL-PETHŐ^a, GÉZA HORVÁTH^a,
JANKA BOBEK^a, RÓBERT BOCSI^a, ZOLTÁN HODAI^a

ABSTRACT. Our energy requirements increased significant in the last decades. For this reason the potential utilization of renewable energy sources come into view. Biogas is a kind of renewable energy sources. Purification of raw biogas is essential prior to use. Mainly the hydrogen sulfide content of gas is very harmful. It can cause corrosion in compressors and engines. Furthermore sulfur dioxide and sulfur trioxide are formed from hydrogen sulfide due to combustion, which similarly corrosive present of water and toxic like hydrogen sulfide. We examined the hydrogen sulfide absorption from biogas model gas mixtures (CO₂, H₂S, N₂) based on alkali competitive chemisorption technology.

Keywords: *biogas, chemisorption, sodium hydroxide, hydrogen sulphide, carbon dioxide*

INTRODUCTION

Renewable energy produced by biogas technology has a great potential for growth to meet our future energy demands. Furthermore the technology is instrumental in waste management [1-2]. Biogas is generated from organic materials (fats, proteins, carbohydrates) by anaerobic metabolism [1-6]. The character of the used biomass and the applied operational conditions during anaerobic digestion determine the effective composition of the gas [6]. The raw biogas consists of mainly methane (CH₄) and carbon dioxide (CO₂). Additionally small amount of ammonia (NH₃), hydrogen sulfide (H₂S), nitrogen (N₂), oxygen (O₂), carbon monoxide (CO), water (H₂O), siloxanes and halogenated volatile organic compounds (VOCs) are present as impurities in biogas [2; 5-8]. Table 1 shows the chemical composition of raw biogas from different sources [7].

^a *Institute of Chemical and Process Engineering, Department of Chemical Engineering Science, University of Pannonia, H-8200 Veszprém, Hungary.*

* *Corresponding author: molnare@almos.uni-pannon.hu*

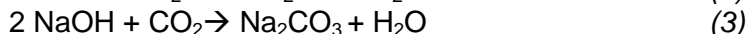
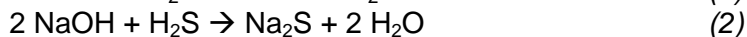
First of all H₂S content should be removed from the raw gas for many reasons. It can cause corrosion in compressors, gas storage and engines, in addition sulfur di- (SO₂) and trioxide (SO₃) are formed duo to combustion, which are similarly hazardous components like H₂S [1-2; 5-10].

Table 1. Chemical composition of raw biogas from different sources [7]

Component	Biogas factory	Sewer factory	Garbage landfill
CH ₄ [% vol.]	60-70	55-65	45-55
CO ₂ [% vol.]	30-40	35-45	30-40
N ₂ [% vol.]	<1	<1	5-15
H ₂ S [ppmv]	10-2000	10-40	50-300
NH ₃ [ppmv]		Trace	
CO [ppmv]		Trace	
O ₂ [ppmv]		Trace	
VOCs [ppmv]		Trace	
H ₂ O [ppmv]		Trace	
Siloxanes [ppmv]		Trace	

Nowadays desulfurization of biogas can be carried out in many ways, for example biological desulphurization, adsorption on impregnated activated carbon, scrubbing in aqueous sodium hydroxide (NaOH) solution or in water (H₂O), addition of iron chloride (FeCl₂) to the bioreactor, membrane separation and so on [1-3; 6-10].

In this paper we deal with H₂S chemisorption in NaOH solution. The reaction time of CO₂ and H₂S with NaOH are different. CO₂ reacts with NaOH solution more slowly than H₂S [11-13]. Based on this fact the chemisorption in NaOH solution is able to work as a selective method for H₂S capture, if the sufficiently short contact time (<1s) is provided. The selectivity is important in order to minimize the consumption of chemicals. Besides it is necessary to ensure the large contact surface and intense contact of gas and absorbent in order that the operation achieves a relatively high efficiency (>50%) [12; 14-16]. During the process stable and undangerous compounds are formed (Equations 1-2-3), such as sodium sulfide (Na₂S) and sodium carbonate (Na₂CO₃) [15; 18].



The mentioned requirement for conditions of operation cannot be achieved by using a classical packed column chemisorber [12-16]. Therefore, spray method was applied for measurements. The objective of

this work was to study the feasibility of technique based on competitive chemisorption of H_2S and CO_2 in NaOH fine spray for biogas purification. If the efficiency of H_2S absorption achieves at least 50% while the alkali excess is less than 10mol NaOH/mol H_2S , we can say that the operation is economic. The primary purpose is to achieve this theoretical limit.

RESULTS AND DISCUSSION

Measurements were performed based on knowledge of general properties of biogas, results of pre-experiments and the application range of experimental apparatus. The experiences of pre-measurements were the follows: the optimal concentration of NaOH solution is influenced by contact time of gas and liquid phases; the molar alkali excess (>1 mol NaOH/mol H_2S) must be provided to achieve effective operation; increase of absorbent volumetric flow rate causes improvement of efficiency of H_2S absorption, however it is limited by the quality of atomization (drop and surface formation) and by the difference between contact time and reaction time requirement.

For the measurements 4 different gas mixture were examined. The applied experimental conditions were: 4 bar pressure; $0,4Nm^3/h$ volumetric gas flow rate; 2% weigh NaOH absorbent concentration; 1-2-3-4-5 cm^3/min volumetric flow rate of NaOH solution. The results of experiments are shown in Figures 1-3.

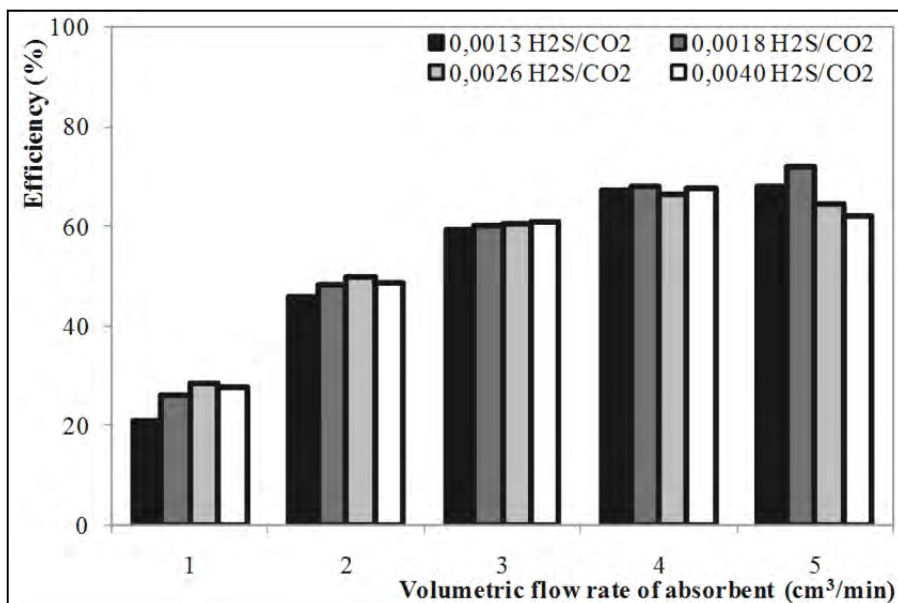


Figure 1. Efficiency of H_2S absorption as a function of absorbent flow rate

The efficiency of absorption system modified between 20 and 72%. Increase of NaOH solution volumetric flow rate caused improvement of efficiency of H₂S absorption, however raising from 4 to 5 cm³/min resulted in clear advance. Striking differences were not observed among the results of test series in Figure 1.

In order to see this process also by economic aspect, efficiency data were represented as a function of molar ratio of NaOH and H₂S (Figure 2).

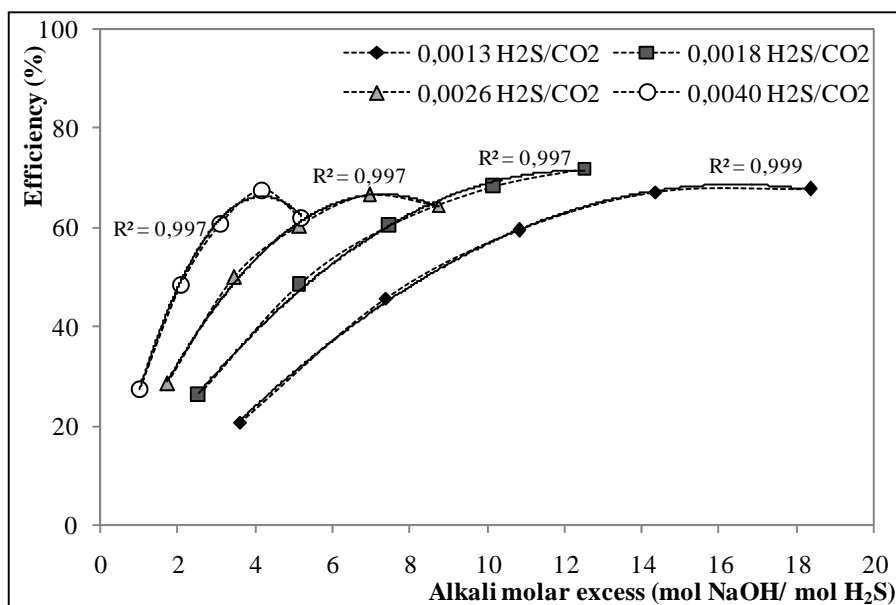


Figure 2. Efficiency of H₂S absorption as a function of alkali molar excess

The system was able to reach 50% efficiency less than 10 mol NaOH/mol H₂S alkali excess by using every gas mixture in the tested range. Namely, according to our expectations the operation was economic and efficient. Second-order polynomial curves can fit on the measuring data ($R^2 \geq 0,997$). The efficiency of H₂S absorption improves with increase of H₂S/CO₂ volumetric ratio. This result can be explained by change of degree of competition. If H₂S/CO₂ volumetric ratio increases, in terms of H₂S the competition will be lower. Furthermore, the probability of encounter of H₂S and NaOH will raise with increase of H₂S/CO₂ ratio. In contrast at the same time the probability of encounter of CO₂ and NaOH will decrease.

Investigation of mass transfer as a function of alkali molar excess was performed as well (Figure 3). To calculate the transfer surface we had to determine the average size of droplets. We assumed Nukiyama-Tanasawa

equation (4 Equation) is capable for this task and the formed droplets are spherical. The number of drops is given by ratio of absorbent volumetric rate and volume of average drop. The transfer surface can be defined by multiplication of quantity of drops and surface of average droplet.

$$D_s = \frac{585}{U_r} \left(\frac{\sigma}{\rho_L} \right)^{0.5} + 597 \left[\frac{\mu_L}{(\sigma \rho_L)^{0.5}} \right]^{0.45} \left(1000 \frac{Q_L}{Q_G} \right)^{1.5} \quad (4)$$

where σ =liquid surface tension (dyne/cm); ρ_L =liquid density (g/cm³); μ_L =liquid viscosity (poise); Q_L =liquid volume flow rate (cm³/sec); Q_G =gas volume flow rate (cm³/sec); U_r =relative velocity between liquid and gas (cm/sec) [19].

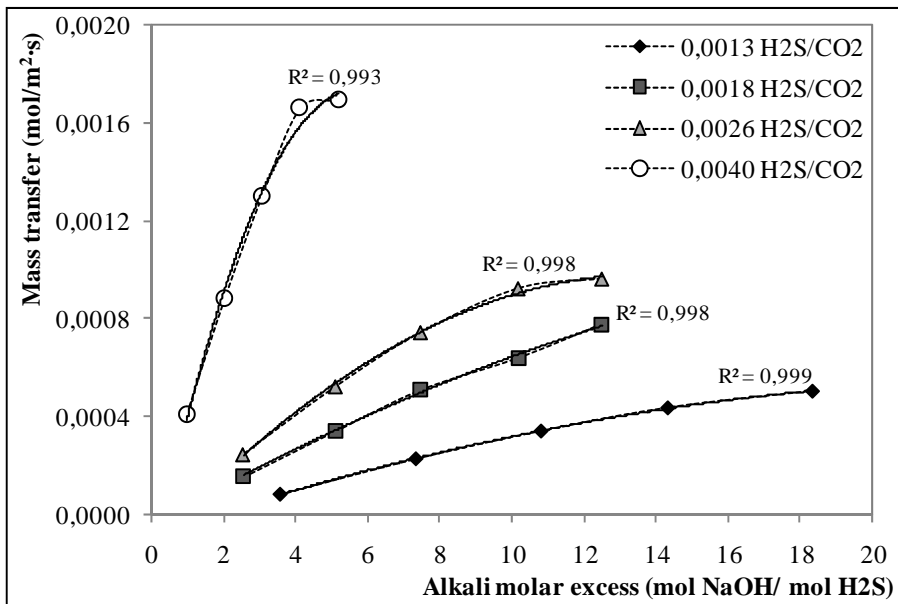


Figure 3. Change of mass transfer as a function of alkali excess

The highest gradient slope of the mass transfer curve was in the case of highest value of H₂S/CO₂ volumetric ratio as a function of NaOH/H₂S molar excess. By using second-order polynomial curves we can follow the change of data series ($R^2 \geq 0,993$). The results can be explained also by the change of degree of competition between H₂S and CO₂.

CONCLUSIONS

The described technique based on competitive chemisorption of H₂S and CO₂ in NaOH fine spray is feasible for biogas purification. The system was able to reach 50% efficiency less than 10mol NaOH/mol H₂S

alkali excess by using every gas mixture in the tested range. The results proves that increase of H₂S/CO₂ volumetric ratio have positive impact on the efficiency of H₂S absorption and the mass transfer of H₂S from gas to liquid phase. This experience can be explained by change of competition degree, and change of probability of encounter of CO₂ and H₂S with NaOH.

EXPERIMENTAL SECTION

Examinations were implemented by use three different compositions of gas mixture (Table 2).

Table 2. Composition of examined gas mixtures

Calculated N ₂ content [% vol.]	Measured CO ₂ content [% vol.]	Measured H ₂ S content [ppmv]	Volumetric ratio of H ₂ S/CO ₂ [-]
62,9520	37,0	480	0,0013
60,9310	39,0	690	0,0018
60,9000	39,0	1000	0,0026
57,4304	42,4	1696	0,0040

Table 3 shows the parameters of operation.

Table 3. Experimental conditions

Pressure [bar]	4
Volumetric gas flow rate [Nm ³ /h]	0,4
Volumetric liquid flow rate [cm ³ /min]	1-2-3-4-5
Concentration of NaOH absorbent [% weigh]	2
Contact time [s]	0,23

The procedure is operated as follows. The NaOH solution is delivered by chemical feeder pump to the experimental appliance. The pre-mixed gas mixture gets into the apparatus from the gas cylinder. The liquid and gas stream encounter in reaction space immediately after the nozzle (Figure 4).

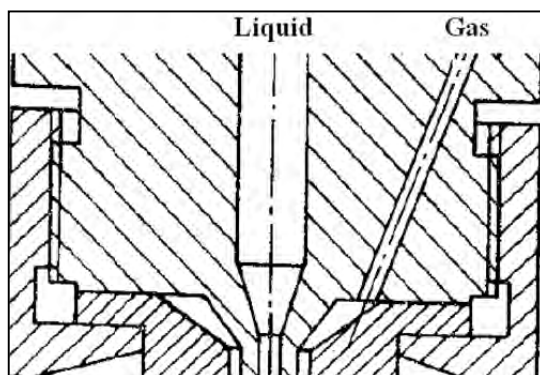


Figure 4. External mixed pneumatic liquid atomizer [20]

The kinetic energy of the gas phase covers the energy required for atomization. After intensive contact of two different phases the phase separation is done by applying mist eliminator. The spent absorbent should be removed periodically from the separation zone by using a tap. The CO₂ (% vol.) and H₂S (ppmv) content of output purified gas is sampled continuous by applying Dräger X-am 7000 gas analyzer [12]. This gas analyzer is able to measure the H₂S level by electrochemical sensor and the CO₂ level by infrared sensor [21].

ACKNOWLEDGMENTS

We are grateful to the MOL for financial supporting this project.

REFERENCES

1. N. Tippayawong, P. Thanompongchart, *Energy*, **2010**, 35, 4531.
2. L. Grazia, *Journal of Cleaner Production*, **2016**, 131, 364.
3. J. Krischan, A. Makaruk, M. Harasek, *Journal of Hazardous Materials*, **2012**, 215-216, 49.
4. S.S. Kapdi, V.K. Vijay, S.K. Rajesh, R. Prasad, *Renewable Energy*, **2005**, 30(8), 1195.
5. S. Qie, L. Hailong, Y. Jinying, L. Longcheng, Y. Zhixin, Y. Xinhai, *Renewable and Sustainable Energy Reviews*, **2015**, 51, 521.
6. E. Ryckebosh, M. Drouillon, H. Vervaeren, *Biomass and Bioenergy*, **2011**, 35, 1633.
7. J. Lasocki, K. Kolodziejczyk, A. Matuszewska, *Polish Journal of Environmental Studies*, **2015**, 24(3), 1427.
8. L. Dubois, D. Thomas, *Chemical Engineering Technology*, **2010**, 33(10), 1601.
9. D. Panza, V. Belgiorno, *Process Safety and Environmental Protection*, **2010**, 88, 420.
10. M. Pawlowska, M. Zdeb, A. Montusiewicz, M. Lebiocka, *Environmental Protection Engineering*, **2009**, 35(3), 157.
11. K. T. Hsieh, R. C. Aiken, *Chemical Engineering Communication*, **1988**, 31, 367.
12. Á. Vágó, D. Rippel-Pethő, G. Horváth, I. Tóth, K. Oláh, *Hungarian Journal of Industrial Chemistry, Veszprém*, **2011**, 39 (2), 283.
13. J. B. Siemak, M. Gelbs, *SPE California Regional Meeting*, **1985**, 13650-MS
14. R. G. Heltz, Al L. Rocklin, *U.S. Patent*, US2747962 A, **1956**.
15. V. Srinivasan, R. C. Aiken, *Fuel Processing Technology*, **1988**, 19, 141.
16. É. Molnár, D. Rippel-Pethő, G. Horváth, Z. Hodai, R. Bocsi, J. Bobek, *Periodica Polytechnica Chemical Engineering*, **2016**, 60(2), 74.

17. E. Bendall, R. C. Aiken, F. Mandas, *AIChE Journal*, **1983**, 29(1), 66.
18. A. L. Kohl, R. B. Nilsen, *Gas Purification*, Houston, Gulf Publishing Company, **1997**.
19. D. S. F. Atkinson, W. Strauss, *Journal of the Air Pollution Control Association*, **1978**, 28(11), 1114.
20. J. Turba, *Carburators*, Műszaki Könyvkiadó, Budapest, Hungary, **1976**.
21. <http://www.draeger.com>

STUDY OF SELECTIVE HYDROGEN SULFIDE ABSORPTION BY COMPARING TWO DIFFERENT ALKALI ABSORBENTS BY USING ATOMIZATION METHOD

ÉVA MOLNÁR^{a,*}, DÓRA RIPPEL-PETHŐ^a, GÉZA HORVÁTH^a,
JANKA BOBEK^a, RÓBERT BOCSI^a, ZOLTÁN HODAI^a

ABSTRACT. Significant part of the energy need of the world is covered by utilization of natural gas. Due to the hydrogen sulphide content of raw gas the natural gas industry has to tackle some serious problems, for example corrosion-, environmental-, economic- and safety engineering problems. Our aim is to develop the selective hydrogen sulfide absorption by using alkali solutions. Experiments were performed in a specially designed atomizing reactor by using potassium- and sodium hydroxide absorbents. During the tests the following parameters have changed: contact time, pressure, volumetric flow rate of gas and liquid, concentration and material quality of absorbents. Three different model gas mixtures were used for measurements; they consist of nitrogen, carbon dioxide and hydrogen sulfide.

Keywords: *selectivity, absorption, hydrogen sulfide, carbon dioxide, sodium hydroxide, potassium hydroxide, atomization*

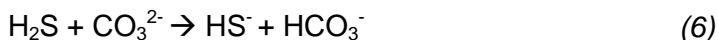
INTRODUCTION

Nowadays several sour gas sweetening methods are known, but only few of these are selective, economic and able to fulfill the environmental regulations [1-7]. The technique based on competitive chemisorptions of hydrogen sulfide (H₂S) and carbon dioxide (CO₂) seems to be a good solution to meet these requirements [5-8]. The removal of H₂S together with other components (for example CO₂) is often costly and not necessary, therefore the demand exist for selective absorption of H₂S from gas mixtures [6; 9]. Absorption in alkali hydroxides is able to work as a

^a *Institute of Chemical and Process Engineering, Department of Chemical Engineering Science, University of Pannonia, H-8200 Veszprém, Hungary.*

* *Corresponding author: molnare@almos.uni-pannon.hu*

selective (for H₂S) method if the appropriate conditions are provided [5-7; 10-12]. It is important that the contact of gas and liquid phase is realized quickly and intensively through large surface. This is necessary because of the difference of reaction time requirements of H₂S and CO₂; furthermore with these conditions the operation can achieve high efficiency [5-7; 11-12]. Atomization methods are widely used in the chemical industry for absorption of gas components [9; 13-14]. The surface and droplet size are very substantial factors in these methods in terms of dissolution [4; 9-10; 13-14]. In addition, there are a lot of conditions which have a significant impact on mass transfer of gas purification in an atomizing apparatus, for example material quality, concentration, density, surface tension, viscosity, volumetric flow rate and pH value of absorbent; composition and flow of gas mixture; contact time and pressure [5; 13-16]. The following pH – dependent (1)-(8) reactions are considered to be important which occur within the alkali hydroxide solutions [10; 16].



In terms of the consumption of caustic and selectivity the reaction (1) and (6) are most desirable and the reaction (2) and (7) are least preferred reactions [10; 16].

RESULTS AND DISCUSSION

Experiments were performed to know the effect of contact time, pressure, gas flow, carbon dioxide content of gas mixtures, material quality, concentration and volumetric flow rate of alkali absorbent in that case if atomization method was used for contact of gas and liquid phases. Efficiency of process was examined as a function of the molar ratio of absorbent and hydrogen sulfide (OH⁻/H₂S molar rate). The molar excess of absorbent is essential to ensure the efficient operation of system. For

economical operation the goal is to maximize the efficiency of H₂S absorption by providing the smallest possible OH⁻/H₂S molar rate.

Impact of contact time and pressure at a constant gas flow rate

The contact time changes together with pressure at a given constant volumetric gas flow rate. As it is known the decrease of contact time favors for H₂S removal and not the CO₂ absorption. The effect of contact time (0,12-0,27s) and pressure (4-10bar) at a constant gas flow rate (0,8Nm³/h) is shown in Figure 1-4 (in these case the concentration of NaOH solutions were 0,25 and 0,50% weigh; KOH solutions were 0,35 and 0,70% weigh).

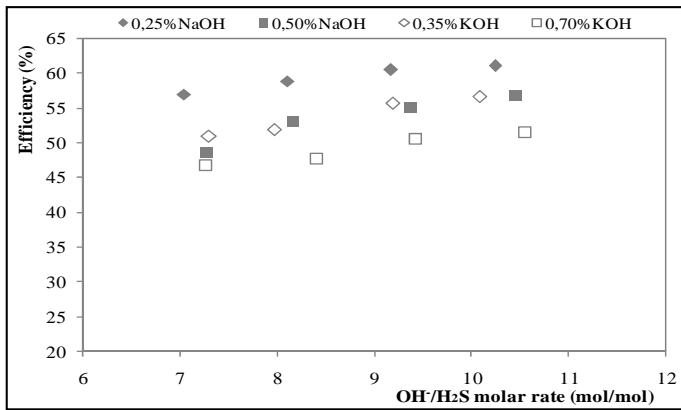


Figure 1. Efficiency of H₂S absorption as a function of the OH⁻/H₂S molar rate (Pressure: 4bar; contact time: 0,12s; gas flow rate: 0,8Nm³/h; CO₂ content of gas mixture: 20% vol.; H₂S content of gas mixture 105ppmv)

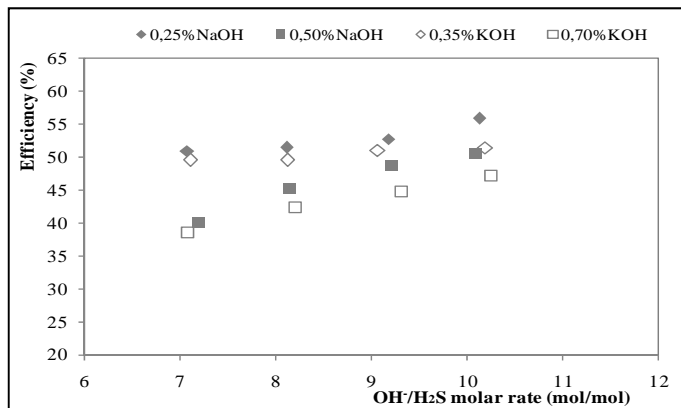


Figure 2. Efficiency of H₂S absorption as a function of the OH⁻/H₂S molar rate (Pressure: 6bar; contact time: 0,17s; gas flow rate: 0,8Nm³/h; CO₂ content of gas mixture: 20% vol.; H₂S content of gas mixture: 105ppmv)

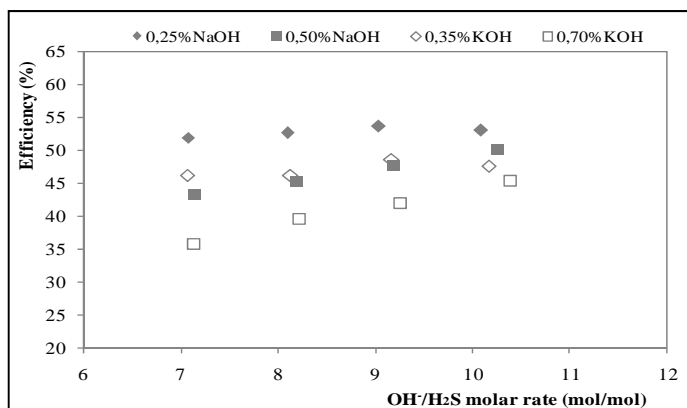


Figure 3. Efficiency of H₂S absorption as a function of the OH-/H₂S molar rate (Pressure: 8bar; contact time: 0,22s; gas flow rate: 0,8Nm³/h; CO₂ content of gas mixture: 20% vol; H₂S content of gas mixture: 105ppmv)

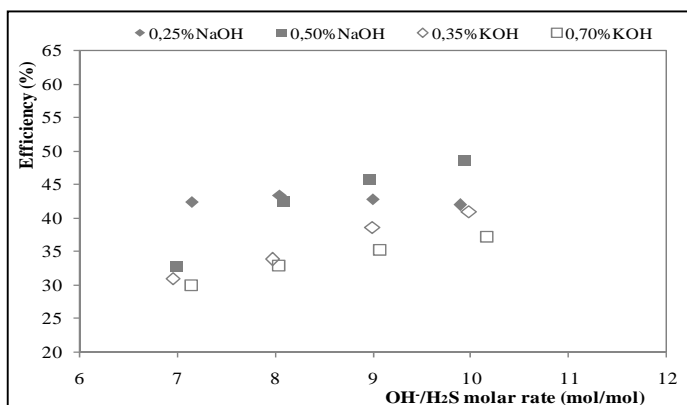


Figure 4. Efficiency of H₂S absorption as a function of the OH-/H₂S molar rate (Pressure 10bar; contact time 0,27s; gas flow rate 0,8Nm³/h; CO₂ content of gas mixture: 20% vol.; H₂S content of gas mixture: 105ppmv)

As seen in Figures 1-4, reduction of pressure and contact time causes improvement in efficiency in the tested range. This is true for all tested absorbents. The efficiency of operating was able to improve up to 20% due to decrease of contact time 0,15s and of pressure 6bar.

Impact of contact time and gas flow rate at a constant pressure

The contact time reduces together with increase of volumetric gas flow rate at a constant pressure. Measurements were executed with two different gas flow rate (0,8 and 1,3Nm³/h). The results are shown in Figure 5.

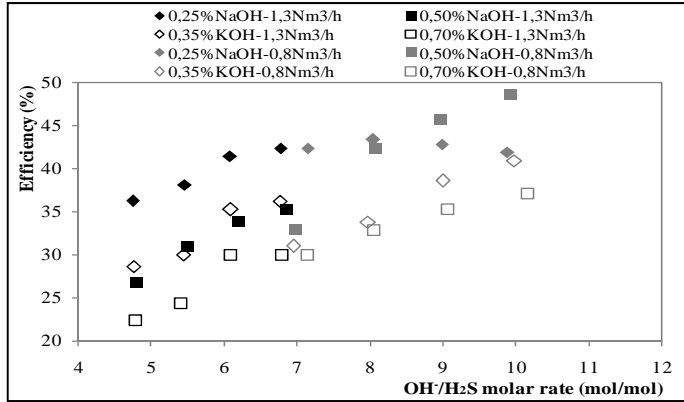


Figure 5. Efficiency of H₂S absorption as a function of the OH⁻/H₂S molar rate (Pressure: 10bar; CO₂ content of gas mixture: 20% vol.; H₂S content of gas mixture: 105ppmv)

The results are easily comparable principally at 7mol OH⁻/mol H₂S ratio. We can see that the higher gas flow rate (1,3Nm³/h) and shorter contact time (0,19s) caused higher efficiency. Also in this case it is proved that reduce of contact time favors for selective H₂S absorption. In this examination the difference of two volumetric gas flow rate was 0,5Nm³/h (this difference in contact time 0,08s) and it can cause up to 5% difference in efficiency.

Impact of CO₂ content

The measurements were performed three different gas mixtures in order to know the effect of CO₂ content. The results are shown in Figure 6 in case of 0,25% weigh NaOH and 0,35% weigh KOH absorbents.

According to Figure 6, 10% CO₂ content was able to cause 50% decrease of efficiency compared to 0% CO₂ even if the contact time is few tenths sec magnitude (0,27s). However, increase of CO₂ content from 10% to 20% did not generate further significant decrease of efficiency. The reason of this experience is that the contact time, the surface, the droplet size and the molar amount of absorbent set a limit to gas absorption. (During measurements the difference of inlet and outlet CO₂ level was below 1% vol.)

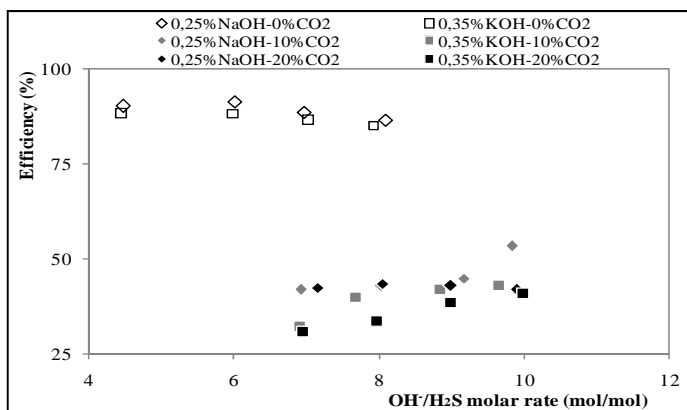


Figure 6. Efficiency of H₂S absorption as a function of the OH⁻/H₂S molar rate (Pressure: 10bar; contact time: 0,27s; gas flow rate: 0,8Nm³/h; H₂S content of gas mixture: 105ppmv)

Impact of absorbent material quality and concentration

Every diagram (Figure 1-6) in this paper presents the effectiveness of two kinds of alkali absorbent in various conditions. Every figure shows that the efficiency results by using the NaOH were better absorbent and not the KOH under experimental conditions. This experience can be explained by the different molar mass of two compounds. KOH has a bigger molar mass (56,1g/mol) compared with NaOH (40,0g/mol). Consequently in case of KOH the particular molar concentration solution will have higher density and also liquid-side resistance. The big liquid-side resistance is a disadvantage in the tested contact time interval. The absorption in a higher density solution belongs to a longer contact- and dissolution time demand. Besides density, viscosity and surface tension of liquid phase determine the work of atomization and for this reason quality of atomization is influenced.

Further measurements were made about liquid-side resistance by using various concentration solutions of alkali absorbents (Figure 1-5). The efficiency of H₂S absorption was better by using the lower concentration of absorbents in almost every tested point. Also this observation supports the previous conclusion about density of absorbent, contact time requirement and liquid-side resistance.

Figure 4 seems to be an extreme case. There are some measuring points, where it can be seen, that applying of the more concentrated absorbent was the more useful in contrast to more dilute one. Therefore, investigation of the created surface and the droplet size is necessary (Table 1).

Investigation of reaction surface and droplet size

The size of droplets and created surface are very important parameters in the efficiency of the H₂S absorption. By using Nukiyama-Tanasawa equation the droplet size can be defined easily, if we are aware of surface tension, density, viscosity and volume flow rate of absorbent, volume flow rate of gas phase and relative velocity between two phases [15]. If we assume that the formed droplets are spherical, also the reaction surface can be defined based on the diameter of droplets and volume flow rate of absorbent. Table 1 shows the surface and droplet size information in case of Figure 4 by using 0,25 and 0,50% weigh NaOH absorbents.

Table 1. Investigation of reaction surface and droplet size on the absorption efficiency (Pressure 10bar; contact time 0,27s; gas flow rate 0,8Nm³/h; CO₂ content of gas mixture: 20% vol.; H₂S content of gas mixture: 105ppmv)

NaOH/H ₂ S molar ratio (mol/mol)	0,25% weigh NaOH			0,50% weigh NaOH		
	Drop size (μm)	Surface (m ²)	Efficiency (%)	Drop size (μm)	Surface (m ²)	Efficiency (%)
7	11	64,3	42	4	79,0	33
8	13	62,6	43	5	76,3	42
9	15	60,6	43	6	75,7	46
10	17	59,0	42	7	74,2	49

Theoretically, the increasing reaction surface and NaOH/H₂S molar ratio have a beneficial effect on efficiency of H₂S absorption. It can be observed that the surface was larger by using 0,50% weigh NaOH absorbent than 0,25% weigh in every single point of tested range. Nevertheless the 0,25% weigh solution was the more efficient absorbent by applying 7mol NaOH/mol H₂S caustic excess. It is also important to notice that the efficiency of operation can be improved over the decrease of surface and increase of drop size. Based on the observations, the following conclusions can be drawn: the efficiency can be increased together with alkali excess not only to reach of the maximum reaction surface; and better efficiency can be achieved by using the lower concentration absorbent even if the reaction surface is smaller because of the less liquid-side resistance and dissolution time requirement.

CONCLUSIONS

As a summary of the experiences the following conclusions can be drawn. The efficiency of H₂S removal improves by reduce of contact time

(0,12-0,27s) because it redounds to selective absorption of H₂S. (The contact time is changeable by pressure or gas flow rate.) If the contact time is such short, it is necessary that the liquid-side resistance should be small. Therefore, it is recommended to use low density, dilute absorbents for the operation. Also, the comparative study of NaOH and KOH showed that the NaOH is the better absorbent in the examined conditions because it has a lighter molar mass. Consequently, in case of KOH the particular molar concentration solution will have higher density and also liquid-side resistance. As it is an atomization method, we have to take into consideration the size of surface and droplets, as well. Theoretically, enhancements of OH⁻/H₂S molar ratio and surface have beneficial effect for efficiency. Improvement of efficiency is feasible not only up to reaching the maximum surface by rise of OH⁻/H₂S alkali excess. In addition, better efficiency can be achieved by using the lower concentration of absorbent even if the reaction surface is smaller at a given OH⁻/H₂S molar ratio. It depends on the difference of droplet- and surface size, and also difference of concentrations of absorbents at constant gas flow rate and pressure. The reason is the less liquid-side resistance and dissolution time requirement. Harmful effect of CO₂ level in gas mixtures is very significant for the efficiency of operation even if the contact time is just few tenths sec magnitude (0,27s). The effect and content of CO₂ do not change directly proportional way because the contact time, the surface, the droplet size and the molar amount of absorbent set a limit to gas absorption.

EXPERIMENTAL SECTION

Examinations were implemented by use of two different concentrations of NaOH and KOH absorbents (Table 2) and three different compositions of gas mixture (Table 3).

Table 2. The concentration and density of absorbents

Concentration of absorbents (mol/dm ³)	Weight% of NaOH solution (% weigh)	Density of NaOH solution (g/cm ³)	Weight% of KOH solution (% weigh)	Density of KOH solution (g/cm ³)
0,06	0,25	1,0011	0,35	1,0015
0,12	0,50	1,0039	0,70	1,0046

Table 3. Composition of gas mixtures

Calculated N ₂ content (% vol.)	Measured CO ₂ content (% vol.)	Measured H ₂ S content (ppmv)
99,9895	0,0	105
89,3895	10,6	105
79,9895	20,0	105

The schematic representation of the experimental apparatus is given in Figure 7.

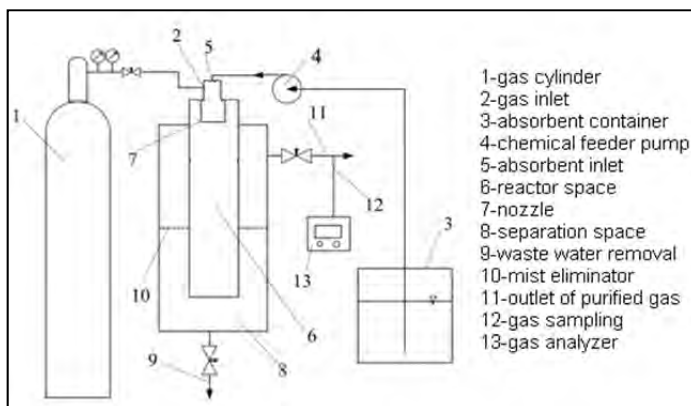


Figure 7. The special experimental appliance [5]

Applying of this special reactor provides the opportunity to minimize the contact time (<1s) between gas and liquid phases. The gas stream atomizes the fed absorbent to droplets through the nozzle. The contact of two different phases is very intensive in the reactor zone. The contacted gas and liquid get from the reactor zone to the separation. In the separation zone the waste absorbent can be removed from the system after the mist eliminator. The CO₂(% vol.) and H₂S(ppmv) content of outlet gas is measured continuous by using Drager X-am 7000 gas analyzer [5].

ACKNOWLEDGMENTS

We are grateful to the MOL for financial supporting this project.

REFERENCES

1. L. Grazia, *Journal of Cleaner Production*, **2016**, 131, 364.
2. R. Álvarez-Cruz, B.E. Sánchez-Flores, J. Torres-González, R. Antano-López, F. Castaneda, *Fuel*, **2012**, 100, 173.
3. N. Tippayawong, P. Thanompongchart, *Energy*, **2010**, 35, 4531.
4. E. Üresin, H. I. Sarac, A. Sarioglan, S. Ay, *Process Safety and Environmental Protection*, **2015**, 94, 196.

5. Á. Vágó, D. Rippel-Pethő, G. Horváth, I. Tóth, K. Oláh, *Hungarian Journal of Industrial Chemistry, Veszprém*, **2011**, 39 (2), 283.
6. É. Molnár, D. Rippel-Pethő, G. Horváth, Z. Hodai, R. Bocsi, J. Bobek, *Periodica Polytechnica Chemical Engineering*, **2016**, 60(2), 74.
7. J. B. Siemak, M. Gelbs, *SPE California Regional Meeting*, **1985**, 13650-MS
8. R. G. Heltz, Al L. Rocklin, *U.S. Patent*, US2747962 A, **1956**.
9. E. Bendall, R. C. Aiken, F. Mandas, *AIChE Journal*, **1983**, 29(1), 66.
10. K. T. Hsieh, R. C. Aiken, *Chemical Engineering Communication*, **1988**, 31, 367.
11. D. Mamrosh, C. Beitler, K. Fisher, S. Stem, *Gas Processing Developments*, **2008**, Special Report, 69.
12. V. Bontozoglou, A. Karabelas, *Industrial and Engineering Chemical Research*, **1993**, 32(1), 165.
13. A. Trupin, A. Couvert, A. Laplanche, A. Paillier, *Chemical Engineering and Processing*, **2008**, 47, 886.
14. Y. Tamhankar, B. King, J. Whiteley, K. McCarley, T. Cai, M. Resetarits, C. Aichele, *Separation and Purification Technology*, **2015**, 156, 311.
15. D. S. F. Atkinson, W. Strauss, *Journal of the Air Pollution Control Association*, **1978**, 28(11), 1114.
16. A. L. Kohl, R. B. Nilsen, *Gas Purification*, Houston, Gulf Publishing Company, **1997**.

STATISTICAL ANALYSIS OF AIR POLLUTION WITH SPECIFIC REGARD TO FACTOR ANALYSIS IN THE CIUC BASIN, ROMANIA

RÉKA KERESZTES^a*, ESZTER RÁPÓ^b

ABSTRACT. In the present study, the changes of the concentration of air pollutants were examined, based on air pollution, meteorological and climatologic data gathered over an interval of two years (2012-2013) by the regional measuring station located in the basin, as well as the sources of the air pollutants were studied with the help of factor analysis. Biomass burning, traffic and photochemistry were characteristic regarding the source of air pollutants. This was also confirmed by the correlations between pollutants. Furthermore, the increasingly busy car traffic in the cold season and the atmospheric stability characteristic for it are also important observations with regard to the sources of air pollutants.

Keywords: *air pollution, factor analysis, air quality, atmospheric stability, environment and human originated ozone sources*

INTRODUCTION

Air pollution is an important factor affecting health and life quality. Road traffic and biomass burning can produce substantial increases in the concentrations of carbon monoxide (CO), nitrogen oxides (NO_x), volatile organic compounds (VOC), particulate matter (PM), sulphur oxides (SO_x), ozone (O₃) [1], [2]. Nitrogen oxides may also cause adverse effects on vegetation and contribute to the formation of secondary inorganic PM and O₃ with associated effects on health, ecosystems and climate [3]. Sulphur dioxide is a precursor in the formation of PM and damages forests and terrestrial ecosystems, affecting the human respiratory system [4]. Carbon

^a Sapiientia Hungarian University of Transylvania, Faculty of Technical and Social Sciences, Piața Libertății nr. 1, 530104, Miercurea Ciuc, Romania.

* Corresponding author: keresztes91@gmail.com

^b Sapiientia Hungarian University of Transylvania, Faculty of Sciences and Arts, Calea Turzii no. 4, RO-400193, Cluj-Napoca, Romania.

monoxide can reduce the oxygen-carrying capacity of blood [5]. In the atmosphere, CO slowly oxidizes into carbon dioxide or ozone [3].

In Europe, emissions of many air pollutants have decreased since the 1970s [3]. Despite regulations, the emission concentrations observed in Romania indicate air pollution levels exceeding European Union standards. In the last few years, air pollution concentrations decreased in Romania too, except PM_{2.5} and VOC [6]. In 2012, the PM_{2.5} concentrations were higher than the target value threshold at several stations in Romania. Furthermore, in Romania there are more than 500 premature deaths a year due to ozone exposure [3]. PM_{2.5} mitigation measures reduced the premature deaths by 5 to 6 premature deaths annually per 10 000 people [7].

The present paper includes an analysis of the above described air pollution variations in the Ciuc basin in 2012 and 2013. Furthermore, air pollution factor analysis has been carried out using the measurements from the monitoring stations.

The Ciuc basin is a bowl-shaped basin in the Eastern Carpathian Mountains, Romania [8], characterized by a special microclimate, with significantly different changes of air pollutant concentrations, in comparison with other regions. In the cold season inversion periods occur and pollutants get trapped in the atmosphere of the basin [9]. Their accumulation causes frequent exceedances of limit values [10]. Emitted air pollutants can cause serious damage not only from the perspective of global warming, but also on the level of local conditions, with regard to the entire environment (e.g. acid rains, respiratory and cancerous diseases, plant ageing, damages of buildings etc) [11].

Solutions to global problems can be mitigated by local solutions, thus the exploration of the air pollution problems in the Ciuc basin can also play a significant role in the development of specific atmosphere protection policies.

RESULTS AND DISCUSSION

Air pollution variations and correlations

In order to decrease the extent of air pollution, the European Union has determined certain limit values in the case of the various pollutants. Air quality data collected in the Ciuc basin between 2012 and 2013 is shown in Table 1 in relation to these values.

Sulphur dioxide: Sulphur dioxide concentrations are almost insignificant, falling within the threshold values determined by the EU. Levels of sulphur dioxide have decreased in most of Europe [12]. The main sources of sulphur dioxide are fossil combustibles, which are less used in the basin.

Table 1. Concentration of pollutants in Ciuc basin during the study period (2012-2013) in relation to the European Union air quality standards set for the protection of human health [13]

		Limit value ($\mu\text{g}/\text{m}^3$)/number of allowed exceedances	Measured concentration ($\mu\text{g}/\text{m}^3$)/number of exceedances	
			2012	2013
SO ₂	annual mean ¹	20	4.5	3.96
	max daily mean	125/3	18.82/0	16.53/0
	max hourly mean	350/24	35.97/0	24.91/0
NO ₂	annual mean	40	7.78	25.96
	max daily mean	200/18	62.61/0	61.99/0
CO	annual mean	not applicable	0.32	0.32
	max 8-h mean	10 000	0.45	4.10
PM ₁₀	annual mean	40	21.35	14.32
	max daily mean	50/35	21.31/0	122.05/13
PM _{2.5}	annual mean ²	25	37.19	28.03
O ₃	annual mean	not applicable	38.36	26.81
	daily max 8-h mean ³	120/25	50.10/0	75.15/0
	max hourly mean ⁴	180	107.92	89.34

¹Protection of vegetation; ²To be met by 2015; ³Target value; ⁴Information threshold

Carbon monoxide: The two annual cycles of air pollution concentrations began to increase at the beginning of November and reached their peaks at the end of January. This observation is best presented by PM₁₀ and CO concentrations (Fig. 1). Biomass burning and traffic emissions significantly increase in the cold season, which have a great impact on air quality. In parallel atmospheric stability prevents the elimination of air pollutants like CO and PM₁₀ from the basin [10], [14]–[18].

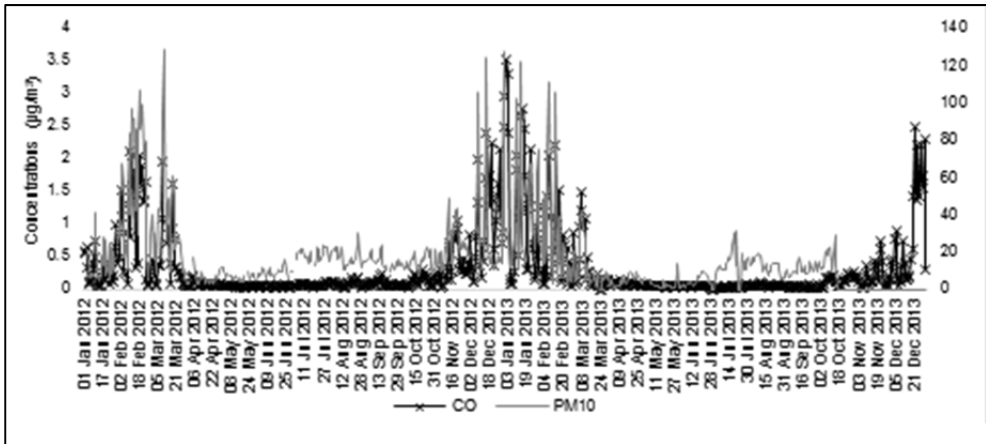


Figure 1. Daily CO and PM₁₀ concentration in 2012-2013 period

Ozone and precursors: The lowest concentrations occurred between April and October (Fig. 2). During the same period, high ozone and precursors (NO₂, NO_x) concentrations show atmospheric stability conditions [14]. The tropospheric ozone was not consumed in reactions with exhaust gas NO and a small quantity was produced photochemically from NO₂. In this period air pollution is accumulated [15].

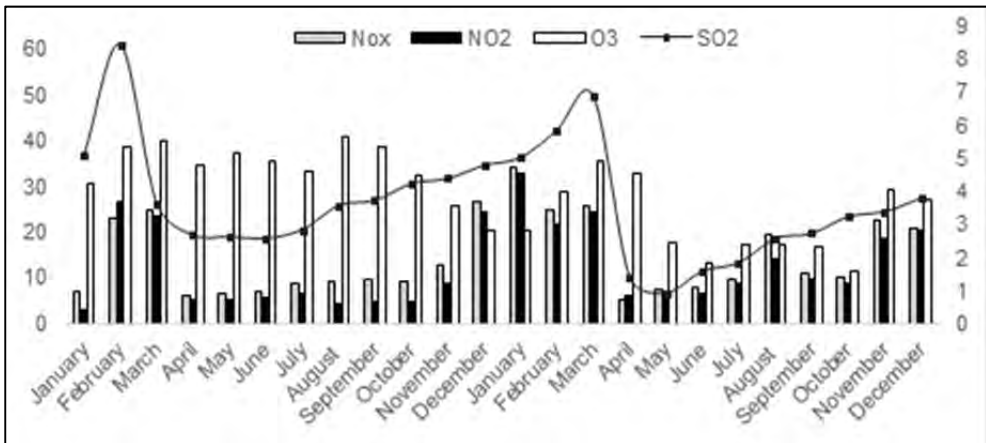


Figure 2. Monthly O₃, NO_x, NO₂ and SO₂ concentration in 2012-2013 periods

High ozone concentrations can cause major diseases, both for humans and to the vegetation. Because of their considerable oxidative effect, they influence the radical reactions of the organisms. In winter, human organisms

are even more prone to illnesses, thus accumulated air polluting ozone is a further stress factor that can cause disease in the human body. As a consequence of the frequent fog (and of the stable atmospheric conditions) in the cold season, pollution remains constantly in the air. The only market-town of the Ciuc basin (Miercurea Ciuc), from an air pollution perspective contributes to poor air quality only in a smaller degree; the climatology and the terrain of the basin are much more the cause of such poor air quality.

Particulate matter: The daily concentrations of PM₁₀ (122.03 µg/m³ in 2013) exceeded the limit value (50 µg/m³), while the annual mean concentration of PM_{2.5} were higher than the limit value (25 µg/m³). The ratios between these PM pollutions are stable, approximately 0.67 and r=0.95 in 2013, but in 2012 no correlations can be observed between PM₁₀ and PM_{2.5}, as these behaved differently in the atmosphere. They differ in size and in time, being present in the atmosphere, under different properties, such as atmospheric distribution and electrostatic character etc.). In the case of PM, we are talking about solid pollutants that can easily be eliminated from the atmosphere by sedimentation. The air pollutants are traffic induced dust and floating dust from the increased biomass burning in the cold season. The quantity of dust from traffic, settles down more easily due to its larger size and lower position, whereas the floating dust originating from smoke at higher altitudes is formed from tinier particles, which are mostly only eliminated from the air by precipitation. Thus, in the stable periods of the cold season, their concentration gets significantly higher, just as the concentration of ozone.

Air pollution correlations

In the case of other air pollutants, significant correlation could be observed in 2012, between CO and NO_x (r=0.938), CO and NO₂ (0.936), NO₂ and NO_x (r=0.992), NO and SO₂ (r=0.585), NO_x and SO₂ (r=0.505), NO₂ and SO₂ (r=0.635), PM₁₀ and SO₂ (r=0.650), and in 2013 between PM₁₀ and CO (r=0.725), SO₂ and CO (r=0.477), NO₂ and NO_x (r=0.908). In the case of correlations of air pollutants with meteorological parameters significant correlations could be observed in 2012 between RH and O₃ (r=-0.766), temperature and CO (r=0.692) temperature and SO₂ (r=-0.560), and in 2013 between RH and O₃ (r=-0.745), temperature and CO (r=0.699), temperature and SO₂ (r=-0.392). The listed correlations are significant at the 0.01 level (2-tailed). These correlations support the reactions that occur in the atmosphere:



The ozone then decays, and redevelops:



During its development, solar radiation with a wavelength of less than 0.41 μm dissociates the nitrogen dioxide into nitric monoxide and atomic oxygen [19]:



Then, atomic oxygen combines with one molecular oxygen in the presence of a third molecule (M), forming ozone:



Due to solar radiation, the newly formed nitrogen dioxide is decomposed again into nitrogen monoxide and atomic oxygen:



The reason of the high correlation between NO_x and NO_2 , respectively CO is a similar source of pollution (traffic) [20]. According to the researchers, the correlation between RH and O_3 results from a shift in the soil moisture-atmosphere coupling regime, because the condition of the photochemical formation of ozone is the oxidation of the carbon-hydrates by the hydroxyl radical (OH), in the presence of nitrogen-oxides (NO_x) and sunlight [21]. The high relative humidity is often associated with fog and rain events. Thus, in both cases drifting ozone is removed from the atmosphere through humid precipitation.

The explanation of the connections between CO and PM_{10} can also be traced back to their common origins, as in both cases biomass burning and traffic can be considered their main originators [6] [22].

Result of the factor analysis

During factor analysis for the sake of more accurate results the hourly series of data from 2012 and 2013 were organised in one data block on which the analysis was carried out. In the case of $\text{PM}_{2.5}$ the measuring station only detects daily data; therefore, this data block was not included in the factor analysis. Factor analysis (FA) summarizes the correlation patterns. According to the results of the analysis in the case of two factors the eigenvalue is higher than in the case of one factor (Table 2). These values are 4.763 and 2.260, while the value of total cumulated variance is 70.234%.

Eigenvalues can be influenced by various factors. The characteristics of highlighted eigenvalues in Table 2 are shown by the component matrix in Table 3.

Factor 1 is composed of NO_x , NO_2 , CO, SO_2 , PM_{10} , and temperature. According to Table 2 their cumulative variation is 47.635%. The highest factor

loadings of NO_x in table 3 reach 0.916, followed by temperature (-0.898), CO (0.896), NO₂ (0.876), PM₁₀ (0.780) and SO₂ (0.700). NO_x is an important indicator of air pollution and is emitted by vehicles, biomass burning and industrial emissions [23]. Statistical analysis shows that a high percentage of CO, NO₂ and PM₁₀ in the atmosphere is emitted from households [16]. The SO₂ is mainly produced from the combustion of fuel containing sulphur, energy production and households [11].

Table 2. Factor analysis and variances

Components	Initial Eigenvalues		
	Total	% of Variance	Cumulative %
1	4.763	47.635	47.635
2	2.260	22.599	70.266
3	0.750	7.504	77.738
4	0.637	6.365	84.103
5	0.509	5.094	89.197
6	0.418	4.180	93.377
7	0.279	2.788	96.164
8	0.210	2.096	98.260
9	0.156	1.562	99.822
10	0.018	0.178	100.000

Extraction Method: Principal Component

Table 3. Component matrix of air quality factor loadings

Pollutants	Factors	
	1	2
NO _x	0.916	0.191
NO ₂	0.876	0.167
O ₃	-0.197	0.830
CO	0.896	0.102
SO ₂	0.700	0.250
PM ₁₀	0.780	0.359
Wind speed	-0.295	0.680
Temperature	-0.898	-0.005
Relative humidity	0.382	-0.760
Solar radiation	-0.421	0.515

Extraction Method: Principal Components.

In conclusion, pollutants of Factor 1 sources are biomass burning and car transport. Biomass smoke contains the oxide of nitrogen, carbon monoxide, oxide of sulfur and particle matter [24].

Factor 2 is characterized by O₃ and meteorological components (wind speed, relative humidity, solar radiation), with a cumulated variance of

22.599%. The O₃ value of the factor is 0.830. Ozone is a secondary pollutant, resulting from photochemical reactions. Because factor 2 is only constituted by ozone, it can be said that factor 2 is the “factor of photochemistry”.

CONCLUSIONS

According to our earlier studies the determinant parameters of the air quality in the Ciuc basin are its relief and the emerging atmospheric conditions (atmospheric stability who induced high inversion periods). The decrease of temperature causes more frequent atmospheric inversions, which prevent the dilution of air pollutants in the basin's atmosphere. These pollutants often accumulate. In the studied period between 2012 and 2013, the limit values defined by the EU were exceeded only by floating dust, still, an established fact is that in the cold season (November-January) the concentrations of air pollutants remain high.

In the Ciuc basin, according to the results of the factor analysis, the formation of pollutants can be classified in two major groups: environmental and anthropogenic. The environmental source strands for the photochemical formation of ozone, whereas the anthropogenic source can be divided into two main components: biomass burning and traffic emissions.

According to our observations, decreasing temperatures cause biomass burning and car traffic emission increase (walking and cycling are more frequent in the summer). In correlation with the above-mentioned fact, more air pollutants are produced, such as the precursors of ozone, from which ozone is created thru photochemistry. With the decreasing temperatures, the frequency of atmospheric stability increases and the concentration of polluting gases and substances increases. This process (the accumulation of air polluting substances) is highly dangerous for human health; and all air polluting gases and substances that accumulate to a degree that exceeds certain limits of concentration can cause numerous diseases.

EXPERIMENTAL SECTION

Sampling

The sampling site is situated in the Ciuc basin, in the shelter of the orographic dam determined by the limitrophic mountain frame of the Eastern Carpathians. The Ciuc basin is similar to a (depressional) groove in which thermal inversions are remarkable [25, 26].

The data of SO₂, NO₂, CO, PM₁₀, PM_{2.5} and O₃ are under observation in the period of January the 1st 2012 and December the 31st 2013, at the Jigodin HR01 background measurement station.

The nitrogen analyser (ME9841B monitor Europe, US EPA, nr. RFNA-1292-090) continuously measured NO, NO₂ and NO_x values, using

chemical luminescent method, while the ozone analyser (ME9810B Monitor Europe, Photometric UV, US EPA, reference no. EQOA-0193-091) measured the O₃ values in the air by the UV absorption techniques. The PM₁₀ were sampled with an Automatic analyser LSPM10 equipped with PM₁₀ and PM_{2.5} impactors, and Low volume gravimetric sampler for PM₁₀/PM_{2.5} - lead analysis (FOX Pump and Sentinel). The CO (carbon monoxide) hourly data were recorded by the MONITOR EUROPE-ML 9830B.

The air temperature values have been sampled by a TS Thermometer sensor with measuring range between -30°C and +50°C installed at standard 2 meter above the ground, and the solar radiation with ORION – Mod SR-S sensor. Regarding data processing we have used values validated by the Environmental Agency, the eventual wrong data have been filtered. The wind speed detector is placed above ten meters of the ground and it can measure wind speed between 0-60 m/s (ORION WS-S anemometer, CUP WHEEL sensor type).

Statistical analysis

The statistical analysis was carried out using IBM SPSS Statistics 22 programme, with the help of which Spearman rank correlation and factor analysis were performed. The latter was only used when we wanted to reveal which parts of the set of variables included common fluctuations.

Factor analysis starts from the pairwise covariance of the variables, searching for factors that doesn't correlate, and whose effects can be summed up, or by using a linear combination of them, "simple" variables can be shown. The number of factors is optimal if it is as small as possible, but this minimal number of factors still represents the pairwise covariance system. Factor weights (factor coefficients in linear combinations) can be deduced as to how close the linear relationship between a given "simple" variable and a factor is. The higher the factor weight, the closer the linear relationship is to the corresponding factor-variable pair, i.e. between the background context (factor) and the part content. An important difference between the main component analysis and between the factor analysis is that during the factor analysis, the meaning of the factors is also searched for.

During factor analysis, the data were rotated using the varimax method. The role of this method is to obtain final eigenvectors with the most representatives of individual sources of variation. The maximum varimax rotation is used to carry out orthogonal rotation, to explain the number characteristics of factors [26].

ACKNOWLEDGMENTS

Particular thanks to the Harghita County Environmental Protection Agency for the meteorological and pollution dates.

REFERENCES

1. Y.-L. Zhang, F. Cao, *Environmental Pollution*, **2015**, 202, 217–219.
2. G. Iorga, C. Balaceanu Raicu, S. Stefan, *Atmospheric Pollution Research*, **2015**, 6, 824–834.
3. C. B. B. Guerreiro, V. Foltescu, F. de Leeuw, *Atmospheric Environmental*, **2014**, 98, 376–384.
4. World Health Organization, “Review of evidence on health aspects of air pollution - REVIHAAP Project”, Technical Report, Copenhagen, **2013**
5. World Health Organization, “Air quality guidelines for Europe”, Regional Office for Europe, Copenhagen, **2000**
6. European Environment Agency, “Romania air pollution country fact sheet — European Environment Agency” **2013**
7. S. T. Turnock, E. W. Butt, T. B. Richardson, G. W. Mann, C. L. Reddington, P. M. Forster, J. Haywood, M. Crippa, G. Janssens-Maenhout, C. E. Johnson, N. Bellouin, K. S. Carslaw, D. V. Spracklen, *Environmental Research Letters*, **2016**, 11.
8. A. Kristó, *Csiki Zöld Füzetek*, **1994**, 7–26.
9. S. Petres, A. Korodi, R. Keresztes, R. Szép, *Applied and Environmental Geophysics*, accepted manuscript, will be published in **2017**
10. R. Szép, R. Keresztes, G. Deák, F. Toba, M. Ghimpusian, E. M. Craciun, *Revista de Chimie* **2016**, 67, 639.
11. European Environment Agency, „Human health - Climate Change”, **2015**
12. World Health Organization, “Air Quality Guidelines: Global Update 2005: Particulate Matter, Ozone, Nitrogen Dioxide, and Sulfur Dioxide”, **2006**
13. ***European Commission, Air quality standard, **2017**, <http://ec.europa.eu/environment/air/quality/standards.htm>
14. R. Szép, L. Mátyás, R. Keresztes, M. Ghimpusian, *Revista de Chimie* **2016**, 67, 205.
15. R. Szép, L. Mátyás, *Carpathian Journal Earth Environmental Science*, **2014**, 9, 241.
16. R. Szép, R. Keresztes, C. Lucian, *Revista de Chimie-Bucharesti*, **2016**, 67, 3, 408.
17. R. Szép, R. Keresztes, A. Korodi, Sz. Tonk, *Revista de Chimie*, accepted manuscript
18. R. Szép, R. Keresztes, A. Korodi, Sz. Tonk, *Revista de Chimie* accepted manuscript
19. T. Nishanth, N. Ojha, M.K.S. Kumar, M. Naja, *Atmospheric Environmental*, **2011**, 45, 1752–1758.
20. R. Szép, R. Keresztes, A. Korodi, Sz. Tonk, *Revista de Chimie* **2016**, 67, 4, 639.
21. Y. X. Wang, *Journal Geophys. Research*, **2004**, 109.
22. A. B. Tawfik, A. L. Steiner, *Atmospheric Environmental*, **2013**, 72, 50.
23. P. Saide Peralta, “Aerosol predictions and their links to weather forecasts through online interactive atmospheric modeling and data assimilation”, Theses Dissertation, **2013**
24. R. Szép, R. Keresztes, Sz. Tonk, A. Korodi, *Revista de Chimie*, **2016**, 97, 10, 1914.
25. O. Bogdan, E. Niculescu, “Aspecte climatice specifice ale depresiunilor Giurgiu, Ciuc, Braşov”, in *Factori și procese pedogenetice din zonă temperată*, **2004**, 3–115.
26. E. Wu, S.-L. Kuo, *Atmosphere*, **2013**, 4, 349.

A NOVEL PHENYLALANINE AMMONIA-LYASE FROM *KANGIELLA KOREENSIS*

ANDREA VARGA^a, ZSÓFIA BATA^{b, d}, PÁL CSUKA^{b, d}, DIANA MONICA BORDEA^a, BEÁTA G. VÉRTESSY^{c, d}, ADRIANA MARCOVICI^e, FLORIN DAN IRIMIE^a, LÁSZLÓ POPPE^{* a, b}, LÁSZLÓ CSABA BENCZE^{* a}

ABSTRACT. This study describes the cloning of the gene encoding a novel phenylalanine ammonia-lyase from *Kangiella koreensis* (KkPAL) into pET19b expression vector. Optimization of protein expression and purification conditions yielded 15 mg pure soluble protein from one liter of *E. coli* culture. Enzymatic activity measurements of the ammonia elimination reaction from different natural aromatic amino acids proved the protein to be a phenylalanine ammonia-lyase. The isolated protein showed remarkably high, 81.7 °C melting temperature, making it especially suitable for biocatalytic applications.

Keywords: phenylalanine ammonia-lyase, *Kangiella koreensis*, protein expression, optimization

INTRODUCTION

The use of enzymes as biocatalysts for the preparation of chemicals has received steadily increasing attention over the past few years and found significant applications in many areas, especially in the synthesis of

^a Babeş-Bolyai University, Faculty of Chemistry and Chemical Engineering, Arany János str. 11, RO-400028, Cluj-Napoca, Romania.

^b Department of Organic Chemistry and Technology, Budapest University of Technology and Economics, Műegyetem rkp. 3, H-1111 Budapest, Hungary.

^c Department of Biotechnology and Food Sciences, Budapest University of Technology and Economics, Szt. Gellért tér 4, H-1111 Budapest, Hungary.

^d Institute of Enzymology, Research Centre for Natural Sciences of Hungarian Academy of Sciences, Magyar tudósok körútja 2, H-1117 Budapest, Hungary.

^e Clinical, Pharmacology and Pharmacokinetics Department, Terapia SA, Fabricii str. 124, RO-400632 Cluj-Napoca, Romania.

* Corresponding authors: cslbencze@chem.ubbcluj.ro; poppe@mail.bme.hu;

pharmaceutical and fine chemical targets. [1] Microbial sources received significant attention in the development of enzymes for research or industrial purposes, as microbes can be produced economically in short fermentation time and using inexpensive media. [2]

The natural role of phenylalanine ammonia-lyases (PALs) is the catalysis of non-oxidative ammonia elimination from L-phenylalanine (L-Phe), to form (*E*)-cinnamic acid,[3] as part of the phenylpropanoid synthesis pathway in case of plants, and to form secondary metabolites in fungi and bacteria. [4] Structurally, PALs resemble to phenylalanine 2,3-aminomutases (PAMs),[5] tyrosine 2,3-aminomutases (TAMs),[6] tyrosine ammonia-lyases (TALs),[7] and histidine ammonia-lyases (HALs). [8] All of these enzymes rely on the protein-derived electrophilic prosthetic group, 3,5-dihydro-4-methylidene-5*H*-imidazol-5-one (MIO), that forms autocatalytically from an XSG triade which contains usually Ala-Ser-Gly active site residues. [9]

Synthetic applications are based mostly on the reverse reaction of PAL, as the stereoselective ammonia addition results in the formation of enantiopure unnatural L-amino acids from the corresponding acrylates. [10] However, PALs as biocatalysts in these reactions must withstand as high as 6M ammonia concentrations to achieve high conversions. PALs of marine origin – especially PAL from *Idomarina loihiensis* (IPAL) – were capable of catalyzing the ammonia addition with high activity at elevated ammonia and substrate concentrations. [11] Alternatively, enzyme immobilization proved to be a successful strategy for prolonging the lifetime of PALs as biocatalysts. [12]

In frame of our general interest to clone thermotolerant and stable PALs as efficient biocatalysts focusing on enzymes of marine and extremophile origin, herein we describe the molecular cloning, expression and purification of a novel PAL from a marine bacterium *Kangiella koreensis* (KkPAL). [13]

RESULTS AND DISCUSSION

Identification of KkPAL

Prokaryotic MIO enzymes are about 150-200 residues shorter than the MIO enzymes from eukaryotes, as the eukaryotic ones contain an additional shielding domain at their C-terminus (**Table 1**). The shorter bacterial enzymes tend to be more stable than the ones of eukaryotic origin.

Table 1. Comparison of six typical MIO enzymes.

	Uniprot code	Seq. length	Seq. identity [14]
<i>Kangiella koreensis</i> PAL	C7R9W9	516	100%
<i>Idomarina loihiensis</i> PAL	Q5QXE5	515	66%
<i>Anabaena variabilis</i> PAL	Q3M5Z3	567	28%
<i>Petroselinum crispum</i> PAL	P24481	716	22%
<i>Rhodobacter sphaeroides</i> TAL	Q3IWB0	523	29%
<i>Pseudomonas putida</i> HAL	P21310	510	27%

Proteins encoded in extremophile organisms, similarly to their host organisms, are adapted to their living conditions. Thus, enzymes isolated from thermophilic or marine organisms are expected to function efficiently at high temperatures and salt concentrations, respectively. A recently identified PAL from *Idomarina loihiensis* (*IIPAL*) [15] showed promising results in the production of optically active phenylalanine derivatives. [11] A bioinformatics based search using Blastp in the NCBI Non-redundant protein sequence database identified the *KkPAL* sequence to be 66% identical to *IIPAL* (**Table 1**). Thus, it was expected that *KkPAL* could be a stable and efficient biocatalyst for the synthesis of optically active phenylalanine analogues.

Comparison of the active site residues of *KkPAL* with *IIPAL* and two further MIO enzymes (**Table 2**) showed that all catalytic residues and residues in the carboxylate binding region of the active site were conserved. However, the aromatic binding region of the active site of *KkPAL* appeared to be different, as at position 90 in *KkPAL*, a histidine was found instead of leucine within the mesophilic PALs (*AvPAL* and *PcPAL*). Automated annotation of the sequence database assigned HAL function to the *KkPAL* sequence due to the characteristic histidine residue at position 90. However, phenylalanine at position 89 renders the aromatic binding pocket of the active site more “PAL-like” (**Table 2**). Based on sequence similarity, we hypothesized that amongst the natural aromatic amino acids, this enzyme will be the most active in the ammonia elimination reaction from phenylalanine.

Histidine to phenylalanine mutations of the adjacent residue (residue 89 in **Table 2**.) enhanced the PAL activity of the tyrosine ammonia-lyase from *Rhodobacter sphaeroides* (*RsTAL*), and decreased significantly the TAL activity. [16] The presence of a hydrogen bond forming residue, histidine at the aromatic binding pocket of *KkPAL* suggested a possible tyrosine ammonia-lyase activity and probable substrate promiscuity towards other natural aromatic amino acids.

Table 2. Sequence alignment of active site residues^a in six typical MIO enzymes

	60	66	86	90	149	153	202	283	316
<i>KkPAL</i>	IYGVTTGYG	..LHLTRFHGCGL	..V	ASGDLT	..MNGTAV	..QDRYSIR	..NDNPI		
<i>IiPAL</i>	IYGVTTGYG	..IHLTRFHGCGL	..V	ASGDLT	..MNGTAV	..QDRYSIR	..NDNPI		
<i>AvPAL</i>	IYGVTSFGF	..TNLVWFLKTGA	..I	ASGDLV	..MNGTAV	..QDRYSIR	..TDNPL		
<i>PcPAL</i>	SYGVTTGFG	..KELIRFLNAGI	..I	ASGDLV	..MNGTAV	..QDRYALR	..NDNPL		
<i>RsTAL</i>	VYGLTTGFG	..ANLVVHLLASGV	..V	ASGDLT	..VNGTSA	..QDAYSLR	..TDNPV		
<i>PpHAL</i>	AYGINTGFG	..RSLVLSHAAGI	..V	ASGDLA	..LNGTQA	..QDPYSLR	..SDNPL		

^a Active sites residues are colored by their locations and roles. Residues directly involved in catalysis are shown in green. Residues forming the hydrophobic binding pocket (binding of the aromatic group) are shown in orange and residues found at the hydrophilic part (carboxylate binding) of the binding pocket are shown in blue.

Molecular cloning of *KkPAL*

The gene encoding *KkPAL* was codon optimized for better expression in *E. coli* and synthesized. The synthetic *KkPAL* gene was cloned in pUC57 production vector and later sub-cloned into the pET19b expression vector. Restriction sites for *NdeI*, *NcoI* and *BamHI* were added to the protein coding sequence allowing directional cloning into the expression vector. Primers detailed in **Table 3** (*KkPAL*_forward and *KkPAL*_reverse primers) were used to amplify the synthetic gene from the pUC57 cloning vector, followed by restriction cloning to the expression vector using *NdeI* and *BamHI* enzymes and T4 DNA ligase. The pET19b vector contains an *N*-terminal His₁₀-tag attached through enterokinase cleavage site to the inserted sequence, facilitating protein purification.

Table 3. Primers used for amplification of *KkPAL* gene and for the colony PCR

Primers	Sequences	T _m (°C)
<i>KkPAL</i> _forward primer	5'CTAGATAATACCATGGGCCATATG3'	62
<i>KkPAL</i> _reverse primer	5'CCGATTATGGATCCTTAGTTAGC3'	62
T7-promoter_forward primer	5'AATACGACTCACTATAGGGGAATTG3'	54
T7-terminator_reverse primer	5'TGCTAGTTATTGCTCAGCGG3'	55

Colony PCR verified the successful insertion of the DNA encoding *KkPAL* to the pET19b vector. This convenient high-throughput method determines the presence or absence of the inserted DNA sequence by a standard PCR process, from individual colonies obtained after the ligation reaction. Vector specific T7-promoter forward and T7-terminator reverse oligonucleotides (**Table 3**) served as primers for the PCR reactions. Sequencing of plasmid DNA, isolated from the colonies with positive colony PCR reactions, ascertained the cloning results.

Optimization of the overexpression of *KkPAL*

Variation of the host cell strain, growth temperature and inducer concentration influence the overexpression levels of the target protein. Strategy for optimization and the identified optimal conditions for *KkPAL* overexpression are detailed in the next section.

E. coli is the most commonly used bacterial host for recombinant protein production. It has become the most popular expression platform, as it is easy to manipulate genetically, inexpensive to culture, and its expression is rapid. [17] *E. coli* strain Rosetta(DE3)pLysS enables low background expression, and expresses T7 lysozyme suppressing basal T7 RNA polymerase expression, reducing translation of the pET recombinants in the absence of inducer. Hence, we choose Rosetta(DE3)pLysS as host strain for expression of *KkPAL*.

Optimization of the inducer concentration

Induction of the *lac* promoter expresses the target genes in pET systems. Naturally, this promoter is induced by the lactose metabolite allolactose. However, in practice the non-degradable IPTG (isopropyl β -D-1-thiogalactopyranoside) is employed, instead of lactose. Varying the concentration of IPTG regulates the expression of the target protein. Lowering the IPTG concentration may reduce the protein expression level, thereby increasing the solubility of aggregation prone protein. Although at the cost of increased expression time and lower protein yield. [18]

Protein expression levels of recombinant *KkPAL* as a function of various inducer concentrations were evaluated in liquid cultures. Upon achieving exponential growth phase (OD at 600 nm ~ 0.6), cultures were induced with five different concentrations of IPTG between 0 mM and 0.5 mM and expression proceeded for 3 h at 37 °C (**Figure 1**). *KkPAL* expression occurred already at 0.1 mM IPTG (60 kDa band Lane **3**), and inducer concentration above 0.1 mM enhanced *KkPAL* production (Lanes **4-6**). However, further increase of the IPTG concentration above 0.2 mM (Lane **4**) did not increase *KkPAL* expression (Lanes **5,6**). As later experiments showed, the protein expressed in a soluble form, therefore the IPTG concentration was set to 0.2 mM.

*Effect of expression temperature on the overexpression of *KkPAL**

The optimum temperature for *E. coli* growth is 37 °C, and several studies reported 37 °C as the best temperature for maximum protein production as well. [19] On the other hand, other studies showed that not

only the rate of expression, but the culturing temperature affects the proper folding of recombinant proteins. [20] Lowering the expression temperature leads to slower growth of bacteria and reduces the rate of protein production, hence decreasing the risk of aggregation of target protein. In addition, most of the proteases express much less activity at lower temperatures. Thus, degradation of the target proteins at lower temperatures are much less pronounced. [21,22]

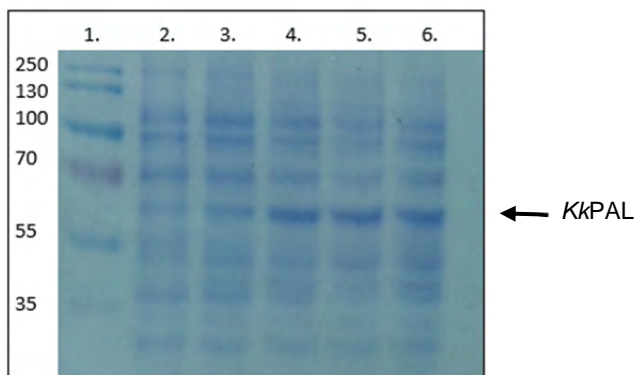


Figure 1. SDS-PAGE showing the effect of various IPTG concentrations on the expression of *KkPAL* (after 4 h at 37 °C). Samples in the lanes: **1:** protein ladder, **2:** control (0 mM IPTG), **3:** induction with 0.1 mM IPTG, **4:** induction with 0.2 mM IPTG, **5:** induction with 0.3 mM IPTG, **6:** induction with 0.5 mM IPTG.

Intermittent optical densitometry (OD) measurements at 600 nm evaluated the effect of growth temperature on the expression of *KkPAL* after induction. Initially, the cell cultures were incubated at 37 °C. After the density of cells reached $OD_{600} \sim 0.4$ (approx. 2-3 h), the temperature was reduced (to 20, 25 or 30 °C). To allow cultures to adjust to the temperature change, protein production was only induced 30 minutes after decreasing the temperatures. The density of the cells was monitored as a function of time (**Figure 2**).

Due to the reduced incubation temperature, the protein synthesis rate was slower at 20 °C than at 25 or 30 °C and longer induction times were necessary for cells growth. At higher expression temperatures (25 or 30 °C), the protein synthesis was faster and the stationary phase was reached after 8 h, compared to 14 h at 20 °C. After post-induction, the cells were harvested by centrifugation, followed by sonication and the crude protein mixture in the lysate was purified by metal affinity chromatography on Ni-NTA resin. The maximum yield, 15 mg L⁻¹ purified enzyme, was obtained at 25 °C expression temperature. The optimal post-induction time on the expression of *KkPAL* was 12-14 h.

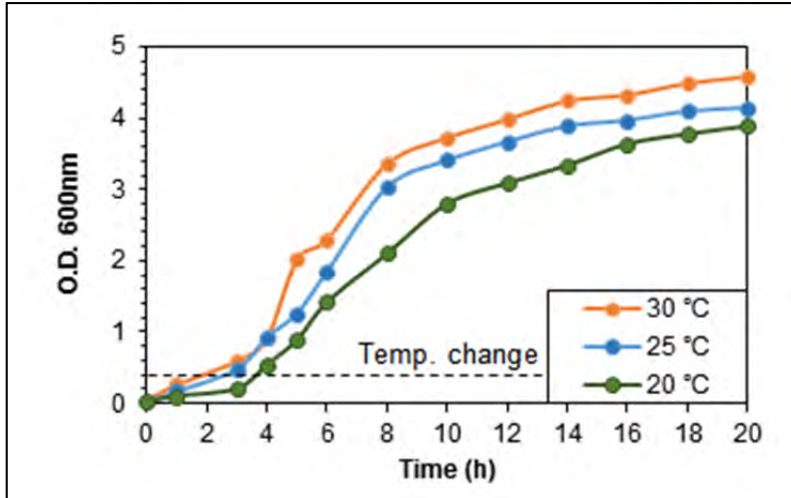


Figure 2. Growth curves of *E. coli* Rosetta(DE3)pLysS containing the pET19b-*KkPAL* plasmid, at 20, 25 and 30 °C in LB medium.

Purification

Purification using Ni-NTA chromatography

Ni-NTA chromatography is a rapid and easy purification technique for recombinant proteins carrying a His-tag at either the *N*- or *C*-terminus. The N atoms of the imidazole rings of the His-tag residues form complexes with the unoccupied coordination sites of the immobilized nickel ions. [23]

In the pET19b vector, a His₁₀-tag at the *N*-terminus is fused to the target proteins, which is longer than the usual His₆-tag. Lengthening the His-tag increases the affinity of the enzyme to the Ni-NTA resin. Consequently, higher imidazole concentrations were required to elute the bounded enzyme from the resin (from 250 mM up to 500 mM). [24] We observed, that *KkPAL* activity decreased after elution from the Ni-NTA column probably due to prolonged exposure to high imidazole concentration. In order to eliminate this effect, we tested 250, 350, 450, 500 mM imidazole concentrations for protein elution. The best result was obtained by elution with 350 mM imidazole, resulting in a protein solution which gave a single band on the SDS-PAGE (**Figure 3**, Lane 2), indicating high purity of the target enzyme.

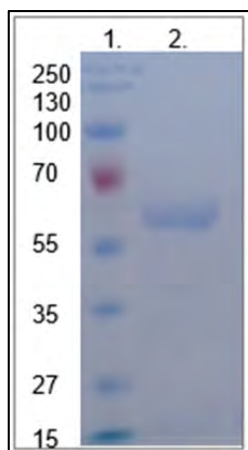


Figure 3. Purification of *KkPAL* with Ni-NTA chromatography. Lane 1: protein ladder, Lane 2: fraction eluted from Ni-NTA with 350 mM imidazole. Samples were prepared as described in the experimental section.

Characterization of *KkPAL*

Enzyme activity measurements

PAL activity was assayed both in the ammonia elimination and in the ammonia addition reactions. The enzyme activity in the ammonia elimination reaction was determined spectrophotometrically by monitoring the formation of (*E*)-cinnamic acid. Conversions after 16 h obtained by HPLC analysis characterize the enzyme activity in the ammonia addition reaction. [25] In **Table 4** the specific activity and the conversion of the reaction catalyzed by *KkPAL* were compared with the corresponding properties of the well-studied *PcPAL*. Contrary to our expectations, *PcPAL* had better catalytic activity in the addition as well as in the elimination reactions.

Table 4. Specific activities in the ammonia elimination and the conversion in the addition reactions measured for *KkPAL* and *PcPAL*.

Enzyme	Elimination reaction	Addition reaction
	Specific activity ^a [$\mu\text{mol min}^{-1} \text{mg}^{-1}$]	Conversion ^b [%]
<i>KkPAL</i>	0.063	3.9
<i>PcPAL</i>	1.08	77.2

^a Specific activity measured at 30 °C, with 5 mM L-phenylalanine at pH 8.5 in 100 mM TRIS buffer.

^b Conversion measured after 16 h at 30°C, with 5 mM (*E*)-cinnamic acid and 6 M ammonium-carbonate, pH 10.

KkPAL catalyzed ammonia elimination also from L-tyrosine, however at a slower rate compared to phenylalanine. The spectrophotometric assays could not detect ammonia elimination from histidine and tryptophan, corroborating with the sequence based annotation of the protein as phenylalanine ammonia-lyase.

Thermal stability

The nanoDSF differential scanning fluorimetry technique is able to analyze the conformational stability and colloidal stability (aggregation behavior) of proteins under different thermal and chemical conditions. The conformational stability of a protein is described by the unfolding transition midpoint T_m ($^{\circ}\text{C}$), which is the point at which half of the protein is unfolded. The truly label-free nanoDSF method monitors the intrinsic fluorescence of tryptophans in proteins, which relies on the close surrounding of the given tryptophan and changes upon thermal unfolding. Maximum values in the change of the first derivate of the fluorescent signal define the melting temperature of the protein.

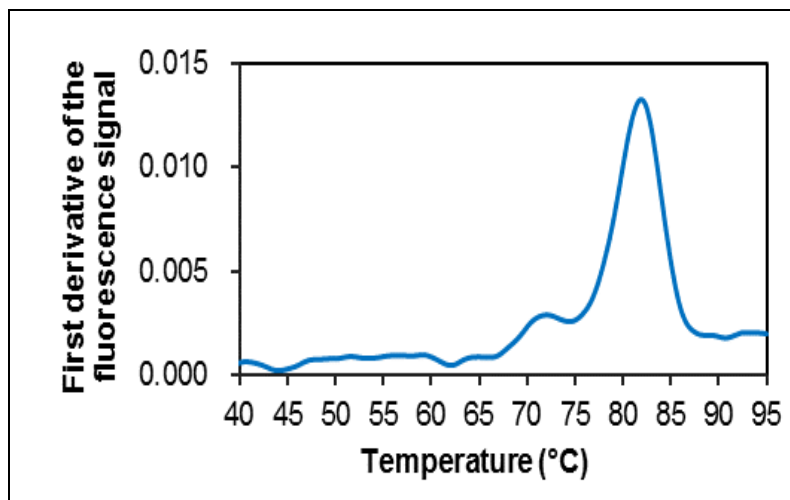


Figure 4. Thermal unfolding curve of *KkPAL* obtained by nanoDSF measurement

The *KkPAL* exhibited outstanding thermal stability, as its melting temperature was 81.7 $^{\circ}\text{C}$ (**Figure 4**). This melting temperature is 10 $^{\circ}\text{C}$ higher than that of the eukaryotic *PcPAL*, 71 $^{\circ}\text{C}$.

CONCLUSIONS

Different experimental conditions were examined for the expression and purification of *KkPAL* in order to obtain the enzyme in high yield and high purity. After optimization of IPTG concentration, post-induction temperature on the expression and the imidazole concentration in the purification steps, 15 mg L⁻¹ of high purity protein was obtained. For production of *KkPAL* the induction level with an IPTG concentration of 0.2 mM was sufficient, followed by 12-14 h post-induction incubation at 25 °C. During the purification of the His₁₀-tagged protein on Ni-NTA column, a reduction of the imidazole concentration from 500 mM to 350 mM improved the stability of the resulted enzyme.

Activity measurements showed that the newly cloned *KkPAL* was less active in the ammonia elimination and addition reactions than the most frequently used *PcPAL*, but the melting temperature of this novel PAL from a marine bacterium exceeded that of the eukaryotic protein by about 10 C.

The hydrophobic binding pocket *KkPAL*, similarly to *IIPAL* is a hybrid between the typical motifs found in TALs and HALs. In agreement with our sequence-based annotation, *KkPAL* showed the highest activity towards phenylalanine amongst the aromatic amino acids. Nevertheless, residue patterns at the hydrophobic region of the binding pocket and the recently reported F137V *PcPAL* with expanded substrate range,[26] suggest that site directed mutagenesis could enhance activity towards other aromatic amino acids.

EXPERIMENTAL SECTION

All reagents were purchased from Sigma-Aldrich, unless otherwise specified.

Synthesis and cloning of *KkPAL* gene

The gene of the *Kangiella koreensis* PAL (Uniprot code: C7R9W9, encoding 735 AA – **Table 5**) was optimized to the codone usage of *E. coli*. The 1538 bp long synthetic gene was produced by Genscript in pUC57 vector. At the end of the gene, restriction sites of *NdeI*, *NcoI* and *BamHI* restriction enzymes were introduced for directional cloning into the pET19b expression vector (**Figure 5**).

Table 5. Amino acid and DNA sequences of recombinant *wt-KkPAL*

Amino acid sequence of <i>KkPAL</i>	Nucleotide sequence of the gene
<p>MTDTKTNITFGHSSLTIEQICQLAKG NATAKLNSAPEFKHKIDQGDPIKEL LREDGVIYGVTTGYGDSVTPVPVQD THELPLHLTRFHCGLGSI FSAHTR AILATRLASLSQYSGVSWSLQLLE LLLQKDI LPRIPEEGSVGASGLDLP SYVAALIGEREVLKYGTQPTPEQVF KSLGIKPIITLQPKGLAIMNGTAVMT ALACLAFQRADYLTQLCSKRITSLCSI ALQNSAHFDELLFSVKHPGQNVVA AWIRDDLNHYKHPRNSDRLQDRYSIR CAPHIIGALKDAMPWMRQTIETELMS ANDNPIIDGAGQHVHLHGHPYGGHIA MVMDSMKTGIANLADLMDRQMLLVD SKFNGLPNNLSAASEQRRLPHNGFK AVQIGVSAWTAELKLTMPASVFSRS TECHNQDKVSMGTIAARDCLRLIDLIT EQVAASIMAAQTAVTLRIKQSQLDK SSLSDGVLSTLEQVFEHFLVSEDPRP LEHELRFHVALIQEQHWSTYAN</p>	<p>5' AATACCATGGGCCATATGATGACCGACACAAAACCAACATCACCTTCGGTCACTCTTCTCTGACCA TCGAACAGATCTGCCAGCTGGCTAAAGGTAACGCTACCGCTAAACTGAACCTCTCGCGAATTTAAAC ACAAATCGAACAGGCTGCTGACTTCATCAAAGAAGCTGCTGCGTGAAGACGGTGTATCTACGGTGTTA CCACCGGTTACGGTACTCTGTTACCACCCCGGTTCCGGTTCAGGACACCCACGAACCTGCCGCTGCACC TGACCCGTTTCCACGGTTCGGCTCGGGTCTATCTTCTCTGCTGAACACACCCGCTGCTATCTGGGTA CCCGCTCGGCTTCTCTGCTCAGGGTACTCTGGTGTTCCTGGTCTCTGCTGCAGCAGCTGGAAGTCTG TGCTGCAGAAAGACATCTGCCCGGTATCCCGGAAGAAGGTTCTGTTGGTCTTCTGGTGACCTGACCC CGCTGCTTACGTGCTGCTGCTGATCGGTGAAGCTGAAAGTCTGTACAAAGGTGACAGCCAGCCGA CCGAACAGGTTTTCAAATCTCGGGTATCAAAACCGATCACCCCTGACGCGGAAGAAGGTTCTGGTATCA TGAAACGTACGGCTGTTATGACCGCTCGGCTGCTGCTGCTGCTGCTGCTGCTGCTGCTGCTGCTGCTGCT TGTGCTCTCGTATCACCTCTCTGTGCTCTATCGCTCTGCAGGTAACCTGCTCACTTCGACGAACTGC TGTCTCTGTTAAACCGCACCCGGTCAAGAACAGGTTGCTGCTTGGATTCTGACGACCTGAACCACT ACAACACCCGCTAACTCTGACCGTCTGCAGGACCTACTCTATCCGTTGGCTCCGCACATCATCG GTGCTCTGAAAGACGCTATGCCGPGGATGCGTCAGACCATCGAAACCGAAGTGAAGTCTGCTAAGCACA ACCCGATCATCGAGGCTGCTGGTCAGCAGCTCTGACAGGTTGCTCACTCTACGGTGGTCACATCGGTA TGGTATGGACTCTATGAAAACCGGTATCGCTAACCTGGCTGACCTGATGGACCGTCAAGTGGCTCTGC TGGTTCGACTCTAAATTCACACACGGTCTGCCGAACACCTGCTGCTGCTCTGTAACAGCGTCTGTCGC TGAACACCGTTTCAAAGCTGTTCCAGATCGGTGTTTCTGCTGGACCGCTGAAGCTCTGAAACTGACCA TGCCGGCTTCTGTTTCTCTGTTCTACCGAATGCCACAACAGGACAAAAGTTTCTATGGGTACGATCG CTGCTCGTGACTGCCTGCGTATCCTGGACCTGACCGAACAGGTTGCTGCTGCTCTCTGATGGCTGCTA CCCAGGCTGTTACCCTGCGTATCAAACAGTCTCAGCTGGACAAATCTTCTCTGCTGACGGTGTCTGCT CTACCCCTGGAACAGGTTTTCGAACACTTCGAACCTGGTTCGAAAGCCGTCCTGGAACACGAACTGC GTCACTTCGTTGCTCTGATCCAGAACAGCACTGGTCTACCTACGCTAACTAAGGATCCATA 3'</p>

Cleavage sites of the restriction enzymes: *NcoI* : **CCATGG**, *NdeI* : **CATATG**, *BamHI* : **GGATCC**

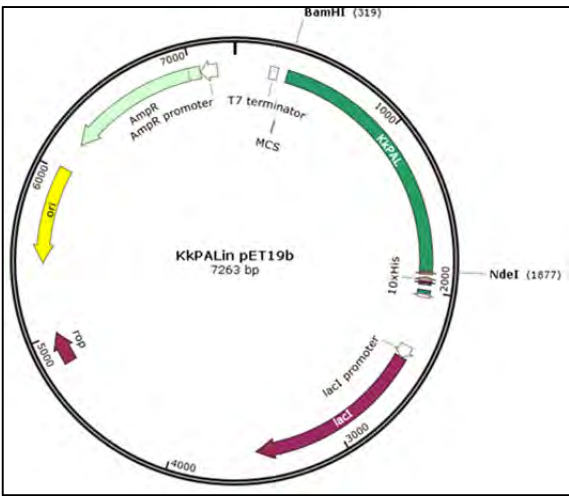


Figure 5. Vector map of the pET19b-*KkPAL* construct.

PCR reaction for amplification of the gene

The PCR reactions with a total volume of 50 μL consisted of 90 ng of DNA template (plasmid containing the gene of *KkPAL*), 1 μM of each of the primers, 200 μM dNTP (ThermoFischer) and 2.5 units of *Phu Hot-Start DNA polymerase* (ThermoFischer). The PCR cycles were initiated at 95 $^{\circ}\text{C}$ for 3 min to denature the template DNA, followed by 35 amplification cycles (95 $^{\circ}\text{C}$ for 30 s, 57 $^{\circ}\text{C}$ for 30 s and 72 $^{\circ}\text{C}$ for 3 min). The PCR cycles were finished with a final extension step at 72 $^{\circ}\text{C}$ for 15 min.

The PCR products were further purified, using the *DNA Clean & ConcentratorTM-25 Kit*, by Zymo research. The purified PCR products and the recipient circular pET19b vector were digested with *NdeI* and *BamHI* restriction enzymes (ThermoFischer), at 37 $^{\circ}\text{C}$ for 1 h and then 40 μL (approx. 2 μg) of each digested DNA was purified by agarose gel electrophoresis. The DNA bands were cut out from the agarose gel. The recipient plasmid and insert at a molar ratio 1:3 were co-extracted using *Gen Elute Gel Extraction Kit* (Genomed) and afterwards ligated in presence of T4 DNA ligase (ThermoFischer) at 22 $^{\circ}\text{C}$ for 1 h.

Transformation in *E. coli* cells

For the transformation of plasmid DNA into *E. coli* XL1-Blue (for plasmid amplification) and Rosetta(DE3)pLysS (for expression) the heat shock method was used. Thawing the chemically competent bacterial cells (50 μL) on ice for 15 min, 1-2 μL of plasmid DNA was added followed by incubation for 20 min on ice. The heat shock was performed by incubating the sample at 42 $^{\circ}\text{C}$ for 45 s, and on ice for further 2 min. 400 μL LB media was added and the cells were grown at 37 $^{\circ}\text{C}$ for 1 h. In case of XL1-Blue transformation the transformed bacteria were plated on LB agar-plates containing tetracycline (30 $\mu\text{g mL}^{-1}$) and carbenicillin (50 $\mu\text{g mL}^{-1}$). In case of Rosetta(DE3)pLysS transformation carbenicillin (50 $\mu\text{g mL}^{-1}$) and chloramphenicol (30 $\mu\text{g mL}^{-1}$) were used. pET19b encodes the resistance gene for ampicillin, however carbenicillin was used for selection, due to its higher stability. Agar plates were incubated overnight at 37 $^{\circ}\text{C}$, forming single colonies of bacteria bearing the plasmid encoding the recombinant protein.

Colony PCR reaction

The PCR reactions with a total volume of 20 μL consisted of 10 μL *Dream Tag Green Master Mix* (ThermoFischer), 1 μM each of the primers

(**Table 3**), one colony of DNA template and 8 μL of ddH₂O. The PCR cycles were initiated at 95°C for 3 min to denature the template DNA, followed by 40 amplification cycles. Each amplification cycle consisted of 95°C for 3 min, 57°C for 30 s and 72 C for 1 min 30 sec. The PCR cycles were finished with a final extension step at 72°C for 15 min. The PCR reactions were analyzed by agarose gel electrophoresis. Presence of the amplified ~1500 bp product indicated colonies where insertion of the gene was successful.

Expression of the recombinant *KkPAL*

The recombinant *KkPAL* carrying *N*-terminal (His)₁₀-tag was overexpressed in *E. coli* host cells Rosetta(DE3)pLysS. For the expression step, a colony of the transformed plasmid was grown overnight at 37°C in 50 mL of Luria-Bertani (LB) medium containing carbenicillin (50 $\mu\text{g mL}^{-1}$) and chloramphenicol (30 $\mu\text{g mL}^{-1}$). A 0.5 L of LB medium was inoculated with 1 v/v% of the overnight culture and grown at 37°C until the optical density at 600 nm (OD₆₀₀) reached 0.4, after which the temperature was reduced to 20, 25 and 30°C. To induce protein production varying concentrations of IPTG was added to the cells at OD₆₀₀ of 0.6-0.7. In the expression phase the culture was shaken at 180 rpm for 16 h.

Purification of *KkPAL*

All protein purification steps were performed at 4 C. Cells were harvested by centrifugation (25 min, 5000 \times g) and resuspended in 50 mL lysis buffer (150 mM NaCl, 50 mM TRIS (2-amino-2-(hydroxymethyl)propane-1,3-diol) pH 7.5) supplemented with DNase, RNase, Lysosyme and EDTA-free protease-inhibitor cocktail. Further, the cells were lysed by sonication and cell debris was removed by centrifugation (12000 \times g, 30 min).

The His-tagged *KkPAL* was separated from other proteins in the supernatant by Ni-NTA-agarose column. After loading the sample, the column was washed with low salt buffer, (50 mM HEPES (4-(2-hydroxyethyl)piperazine-1-ethanesulfonic acid), 30 mM KCl pH 7.5 4V; V= resin volume) high salt buffer (50 mM HEPES, 300 mM KCl pH 7.5, 2V), and low salt buffer (2-4V) again. The low salt buffer supplemented with 25 mM imidazole removed the non-specifically bound contaminating proteins. Low salt buffer supplemented with varying amounts (between 250-500 mM) imidazole eluted the *KkPAL* from the column.

The resulting eluate was dialyzed against 100 mM TRIS-buffer (pH 8.0) for 5 h at 4 C. The purity of the resulting fractions was verified by SDS-

PAGE analysis on a 12% SDS-PAGE. After dialysis the fractions containing purified protein were concentrated by centrifugal ultrafiltration with Amicon filter units. The concentration of the purified protein was determined by the Bradford method.

Enzyme activity measurements

Elimination reactions. Activity of *KkPAL* in the ammonia elimination reaction was determined spectrophotometrically by monitoring the formation of the conjugated acrylic acid product. The measurements were performed at 30 °C for 5 min with 5 mM L-phenylalanine, in the presence of 0.3 μM enzyme in 0.1 M TRIS-buffer (pH 8.5). Phenylalanine ammonia-lyase activity was determined by measuring the formation of (*E*)-cinnamic acid at 290 nm for 10 min, using quartz cuvettes of 1 mL. Histidine ammonia-lyase activity was determined as the rate of urocanate formation measured spectrophotometrically at 277 nm. The conversion of L-tyrosine to *p*-coumarate followed at 310 nm, determined the tyrosine ammonia-lyase activity. Tryptophan ammonia-lyase activity was measured by the rate of indole 3-acrylic acid formation at 315 nm.

Addition reactions. Into the solution of (*E*)-cinnamic acid (5 mM) in 6 M NH₃, pH 10 (adjusted with CO₂), *KkPAL* or *PcPAL* (0.6 μM) was added and the reaction mixtures were shaken at 300 rpm, at 30 °C. After 16 h samples (50 μL) were taken from the enzymatic reaction mixtures, quenched by adding an equal volume of MeOH, vortexed and centrifuged (13000 rpm, 2 min). The supernatant was filtered through a 0.22 μm membrane filter and used directly for HPLC analysis.

Conversions were determined on *Phenomenex Gemini NX-C-18* column, using as mobile phase: NH₄OH buffer (0.1 M, pH 8.5): MeOH 90:10 to 61:39 in 12 min and 1 mL min⁻¹ flow rate. Conversions were calculated from peak area integrations with use of appropriate response factors. [25]

Thermal stability assay

The thermal stability of the enzyme was determined by nanoDSF. The capillaries were filled with the 0.125 mg mL⁻¹ (2 μM) *KkPAL* in 100 mM TRIS-buffer pH 8.5 and placed onto the capillary tray of the *Prometheus NT.48, NanoTemper Technologies*. Melting curves were measured by heating the samples by 1 °C min⁻¹ increment from 20 °C to 95 °C.

ACKNOWLEDGMENTS

Financial support for project NEMSyB, ID P37_273, Cod MySMIS 103413 funded by the Romanian Ministry for European Funds, through the National Authority for Scientific Research and Innovation (ANCSI) and co-funded by the European Regional Development Fund, Competitiveness Operational Program 2014-2020 (POC), Priority axis 1, Action 1.1 is gratefully acknowledged. LCB thanks for the financial support from the Romanian National Authority for Scientific Research and Innovation, CNCS-UEFISCDI, project number PN-II-RU-TE-2014-4-1668. BGV and LP thank the support from COST Action CM1303 (SysBiocat).

REFERENCES

- [1] B. M. Nestl, S. C. Hammer, B. A. Nebel, B. Hauer, *Angewandte Chemie, International Edition* **2014**, *53*, 3070–3095.
- [2] J. L. Barredo, *Microbial Enzymes and Biotransformations*. **2005**, Humana Press, Totowa.
- [3] D. S. Hodgins, *Journal of Biological Chemistry* **1971**, *246*, 2977–2985.
- [4] M. Petersen, J. Hans, U. Matern in *Annual Plant Reviews*, 2nd ed., Vol. 40, *Biochemistry of Plant Secondary Metabolism* (Ed.: M. Wink), Wiley-Blackwell, **2010**, 182–257.
- [5] L. Feng, U. Wanninayake, S. Strom, J. Geiger, K. D. Walker, *Biochemistry* **2011**, *50*, 2919–2930.
- [6] a) S. D. Christenson, W. Liu, M. D. Toney, B. Shen, *Journal of the American Chemical Society* **2003**, *125*, 6062-6063; b) C. V. Christianson, T. J. Montavon, S. G. Van Lanen, B. Shen, S. D. Bruner, *Biochemistry* **2007**, *46*, 7205–7214.
- [7] J. A. Kyndt, T. E. Meyer, M. A. Cusanovich, J. J. Van Beeumen, *FEBS Letters* **2002**, *512*, 240–244.
- [8] a) L. Givot, T. A. Smith, R. H. Abeles, *Journal of Biological Chemistry* **1969**, *244*, 6341–6353; b) R. B. Wickner, *Journal of Biological Chemistry* **1969**, *244*, 6550–6552.
- [9] T. F. Schwede, J. Rétey, G. E. Schulz, *Biochemistry* **1999**, *38*, 5355–5361.
- [10] L. Poppe, Cs. Paizs, K. Kovács, F.D. Irimie, B.G. Vértessy in *Methods in Molecular Biology*, Vol. 794 (Eds.: L. Pollegioni, S. Servi), **2012**, 3–19. Humana Press, Totowa.
- [11] F.B.J. van Assema, N. Sereinig (DSM0). WO 2008/031578, **2008** and PCT/EP 2007/007945, **2007**.
- [12] a) D. Weiser, L.C. Bencze, G. Bánóczy, F. Ender, R. Kiss, E. Kókai, A. Szilágyi, B.G. Vértessy, O. Farkas, C. Paizs, L. Poppe, *ChemBioChem*, **2015**, *16*, 2257–2402; b.) J. H. Bartha-Vári, M. I. Tosa, F.D. Irimie, D. Weiser, Z.

- Boros, B. G. Vértessy, Cs. Paizs, L. Poppe, *ChemCatChem* **2015**, *7*, 1122–1128; c.) F. Ender, D. Weiser, B. Nagy, L.C. Bencze, C. Paizs, P. Pálovics, L. Poppe, *Journal of Flow Chemistry* **2016**, *6*, 43–52.
- [13] C. Han, J. Sikorski, A. Lapidus, M. Nolan, T. Glavina Del Rio, H. Tice, J. F. Cheng, S. Lucas, F. Chen, A. Copeland, N. Ivanova, K. Mavromatis, G. Ovchinnikova, A. Pati, D. Bruce, L. Goodwin, S. Pitluck, A. Chen, K. Palaniappan, M. Land, L. Hauser, Y. J. Chang, C. D. Jeffries, P. Chain, E. Saunders, T. Brettin, M. Göker, B. J. Tindall, J. Bristow, J. A. Eisen, V. Markowitz, P. Hugenholtz, N. C. Kyrpides, H. P. Klenk, J. C. Detter, *Standards in Genomic Sciences*, **2009**, *1*, 226–233.
- [14] Söding J, *Bioinformatics*, **2005**, *21*, 951–960.
- [15] S. Hou, J. H. Saw, K. S. Lee, T. A. Freitas, C. Belisle, Y. Kawarabayasi, S. P. Donachie, A. Pikina, M. Y. Galperin, E. V. Koonin, K.S. Makarova, M. V. Omelchenko, A. Sorokin, Y. I. Wolf, Q. X. Li, Y. S. Keum, S. Campbell, J. Denery, S. Aizawa, S. Shibata, A. Malahoff, M. Alam, *Proceedings of the National Academy of Sciences USA*, **2004**, *101*, 18036–18041.
- [16] G. V. Louie, M.E. Bowman, M. C. Moffitt, T. J. Baiga, B. S. Moore, J. P. Noel, *Chemistry & Biology* **2006**, *13*, 1327–1338.
- [17] F. Baneyx, *Current Opinion in Biotechnology*, **1999**, *10*, 411–421.
- [18] J. Sambrook, D. W. Russell, *Molecular Cloning a Laboratory Manual. 3rd Edition*, New York: Cold Spring Harbor Laboratory Press; **2001**.
- [19] H. M. Sadeghi, M. Rabbani, E. Rismani, F. Moazen, F. Khodabakhsh, K. Dormiani, Y. Khazaei, *Research in the Pharmaceutical Science*, **2011**, *6*, 87–92.
- [20] R. Y. Li, C. Y. Cheng. *Journal Bioscience and Bioengineering*, **2009**, *107*, 512–515.
- [21] A. Vera, N. Gonzalez-Montalban, A. Aris, A. Villaverde, *Biotechnology and Bioengineering*, **2007**, *96*, 1101–1106.
- [22] J. A. Vasina, F. Baneyx, *Protein Expression and Purification* **1997**, *9*, 211–218.
- [23] J. Crowe, H. Dobeli, R. Gentz, E. Hochuli, D. Stiber, K. Hence, *Methods in Molecular Biology*, **1994**, *31*, 371–387.
- [24] T. Tanaka, M. Kubota, K. Samizo, Y. Nakajima, M. Hoshino, T. Kohno, E. Wakamatsu, *Protein Expression and Purification*, **1999**, *1*, 207–212.
- [25] A. Varga, G. Bánóczy, B. Nagy, L. C. Bencze, M. I. Toşa, Á. Gellért, F. D. Irimie, J. Rétey, L. Poppe C. Paizs, *RSC Advances*, **2016**, *6*, 56412–56420.
- [26] L. C. Bencze, A. Filip, G. Bánóczy, M. I. Toşa, F. D. Irimie, Á. Gellért, L. Poppe, C. Paizs, *Organic & Biomolecular Chemistry*, **2017**, *15*, 3717–3727.